

Synthesis and structural characterization of new transition metal alkynylamidinates

Dissertation

zur Erlangung des akademischen Grades

Doktor rerum naturalium

(Dr.rer.nat.)

von:

M.Sc. Sida Wang

Geboren am 24. März. 1989 in Dalian, China

Genehmigt durch die Fakultät für Verfahrens- und Systemtechnik
der Otto-von-Guericke-Universität Magdeburg

Promotionskommission:

Prof. Dr. rer. nat. habil. Frank T. Edelmann, Gutachter

Prof. Dr. rer. nat. Dietmar Stalke, Gutachter

Prof. Dr.-Ing. Andreas Seidel-Morgenstern, Vorsitz

eingereicht am:

27.09.2019

Promotionskolloquium am:

13. Feb. 2020

Table of Contents

Abbreviations	
Abstract	
Introduction.....	1
1.1 Transition metal amidinate chemistry.....	1
1.1.1 Amidine and amidinate ligands	1
1.1.2 Cyclopropylethynyl and dimethylaminopropynyl substituents	5
1.1.3 Synthetic routes to amidinate complexes of transition metals.....	6
1.1.4 Coordination modes of amidinate ligands in transition metal complexes	7
1.2 The developments and applications of transition metal amidinate complexes.....	11
1.2.1 Amidinate complexes in catalysis.....	11
1.2.2 Amidinate complexes in materials science	12
1.3. Motivation.....	13
Results and discussion	16
2.1. Lithium cyclopropylethynylamidinates	16
2.2. Synthesis and structural characterization of new lithium and potassium amidinates	21
2.2.1. New lithium dimethylaminopropynylamidinates	21

2.2.2. New potassium cyclopropylethynylamidates	25
2.3. Synthesis and structural characterization of transition metal bis(amidinate) complexes	29
2.4. Synthesis and structural characterization of transition metal tris(amidinate) complexes	39
2.5. Synthesis and structural characterization of transition metal amidinates with short M-M contacts	55
2.5.1. A dichromium complex containing bridging <i>N,N'</i> -di- <i>iso</i> -propylpropynylamidinate ligands	55
2.5.2. Dimolybdenum complexes containing bridging acetate ligands and <i>N,N'</i> -di- <i>iso</i> -propylpropynylamidinate or <i>N,N'</i> -dimethylaminopropynylamidinate ligands	60
2.6. Synthesis and structural characterization of dichlorido-bis(cyclopropylalkynylamidine) transition metal complexes	68
2.7. The discovery of oxygen-centered variants of transition metal amidinate complexes	73
Summary	80
Experimental section.....	88
Crystal data and refinement details.....	110

Abbreviations

Me	methyl group (CH ₃)
Et	ethyl group (CH ₂ CH ₃)
ⁱ Pr	<i>iso</i> -propyl group (CH(CH ₃) ₂)
^t Bu	<i>tert</i> -butyl group (C(CH ₃) ₃)
R	alkyl or other organic groups
Cy	cyclohexyl group (<i>c</i> -C ₆ H ₁₁)
Ph	phenyl group
Ar	aromatic group
THF	tetrahydrofuran
Et ₂ O	diethyl ether
DME	1,2-dimethoxyethane
NMR	nuclear magnetic resonance
MS	mass spectrometry
IR	infrared
δ	chemical shift
ppm	parts per million
s	singlet
d	doublet
t	triplet
<i>et al.</i>	and others
<i>e. g.</i>	for example
DphBz	diphenylbenzamidinato
AMD	acetamidinato
DTolF	[(<i>p</i> -tol)-NC(H)N(<i>p</i> -tol)]
DPhF	[(phenyl)-NC(H)N(phenyl)]

Abstract

The aim of this Ph.D. work was mainly to synthesize new transition metal amidinate complexes and to investigate their structures. First of all, the introduction of this thesis includes a brief description of the main synthetic approaches and coordination modes of amidine and amidinate ligands. In addition, an overview of the developments and applications of transition metal amidinate complexes is given. A series of lithium cyclopropylethynylamidates $\text{Li}[c\text{-C}_3\text{H}_5\text{-C}\equiv\text{C-C}(\text{NR})_2]\cdot\text{THF}$ (**1**: R = *i*Pr, **2**: R = Cy), lithium dimethylaminopropynylamidates $\text{Li}[(\text{CH}_3)_2\text{N-CH}_2\text{-C}\equiv\text{C-(NR}_2)]\cdot\text{THF}$ (**4**: R = *i*Pr, **5**: R = Cy), potassium cyclopropylethynylamidates $\text{K}[c\text{-C}_3\text{H}_5\text{-C}\equiv\text{C-C}(\text{NR})_2]\cdot\text{THF}$ (**6**: R = *i*Pr, **7**: R = Cy), and transition metal amidinate complex are the main result of this Ph.D. thesis. Most of the previously reported lithium amidinates are dimers. However, an unexpected unsolvated homoleptic complex of lithium cyclopropylethynylamidinate $\text{Li}[c\text{-C}_3\text{H}_5\text{-C}\equiv\text{C-C}(\text{NR})_2]_4$ (**3**: R = *i*Pr) was obtained in *n*-pentane. The results of transition metal amidinate complexes are subdivided into five subtitles. New transition metal bis- and tris-amidinate complexes were obtained by metathesis reactions of anhydrous transition metal halides with **1-2** and **4-7**. Dichromium and dimolybdenum complexes containing bridging amidinate ligand with short M–M quadruple bonds were prepared by the reaction of anhydrous CrCl_2 with **1** in a 1:2 ratio and quadruple bonded dimolybdenum complex $[\text{Mo}_2(\mu\text{-OAc})_4]$ as starting material with two or four equivalents of **1** and **6**, respectively. In the course of this work, bis(cyclopropylalkynylamidine) transition metal dichloride complexes were occasionally observed and structurally characterized. Moreover, a series of an oxygen-centered variant of transition metal amidinate complexes were obtained by the transition metal amidinate complexes exposed to the air and moisture. All these complexes were thoroughly investigated by NMR, MS, IR spectroscopy, as well as elemental analyses and X-ray crystallography.

Zusammenfassung

Hauptziel dieser Dissertation war die Synthese und Strukturaufklärung neuer Amidinat-Komplexe von Übergangsmetallen. In der Einleitung der Arbeit werden die wichtigsten Synthesemethoden und Koordinationsweisen von Amidinen und Amidinat-Liganden vorgestellt, ebenso wie ein Überblick über die Entwicklung und Anwendungen von Übergangsmetall-Amidinat-Komplexen. Eine Reihe von Lithium-cyclopropylethynylamidinaten $\text{Li}[\text{c-C}_3\text{H}_5\text{-C}\equiv\text{C-C}(\text{NR})_2]\cdot\text{THF}$ (**1**: $\text{R} = \textit{iPr}$, **2**: $\text{R} = \text{Cy}$), Lithium-dimethylaminopropinylamidinaten $\text{Li}[(\text{CH}_3)_2\text{N-CH}_2\text{-C}\equiv\text{C-C}(\text{NR})_2]\cdot\text{THF}$ (**4**: $\text{R} = \textit{iPr}$, **5**: $\text{R} = \text{Cy}$), Kalium-cyclopropylethynylamidinaten $\text{K}[\text{c-C}_3\text{H}_5\text{-C}\equiv\text{C-C}(\text{NR})_2]\cdot\text{THF}$ (**6**: $\text{R} = \textit{iPr}$, **7**: $\text{R} = \text{Cy}$), und Übergangsmetall-Amidinat-Komplexen sind wichtige Ergebnisse dieser Promotionsarbeit. Die meisten bisher beschriebenen Lithiumamidinate sind Dimere. Durch Kristallisation aus *n*-Pentan konnte unerwartet der unsolvatisierte, homoleptische Komplex $\text{Li}[\text{c-C}_3\text{H}_5\text{-C}\equiv\text{C-C}(\text{NR})_2]_4$ (**3**) erhalten werden. Die Ergebnisse mit Übergangsmetall-Amidinat-Komplexen gliedern sich in fünf Abschnitte. Neue Bis- und Tris(amidinat)-Komplexe von Übergangsmetallen wurden durch Metathesereaktionen von wasserfreien Übergangsmetallhalogeniden mit **1-2** und **4-7** erhalten. Dichrom- und Dimolybdän-Komplexe mit verbrückenden Amidinat-Liganden und kurzen M–M Vierfachbindungen wurden durch Reaktionen von wasserfreiem CrCl_2 mit **1** im Molverhältnis 1:2 bzw. von $[\text{Mo}_2(\mu\text{-OAc})_4]$ mit zwei oder vier Äquivalenten **1** und **6** synthetisiert. Im weiteren Verlauf der Arbeit wurden neue Bis(cyclopropylalkinylamidin)metalldichlorid-Komplexe dargestellt und strukturell charakterisiert. Durch Zutritt von Luft und Feuchtigkeit entstanden aus den Übergangsmetall-Amidinat-Komplexen verschiedene Sauerstoff-zentrierte Folgeprodukte. Alle neuen Komplexverbindungen wurden mittels NMR- und IR-Spektroskopie, Massenspektrometrie, Elementaranalysen sowie Einkristall-Röntgenstrukturanalysen umfassend charakterisiert.

Chapter 1

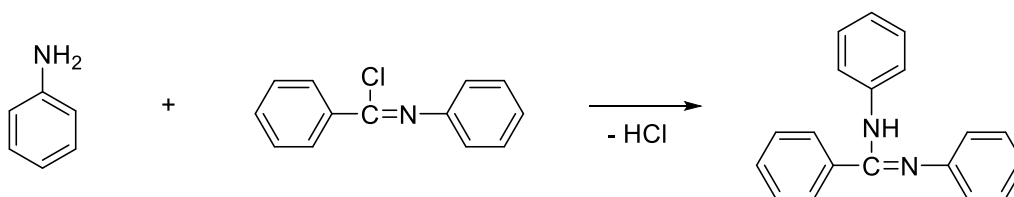
Introduction

1.1 Transition metal amidinate chemistry

With the continuous development of organic chemistry, transition metals are increasingly involved in organic reactions. Since the discovery of ferrocene in 1951, research on cyclopentadienyl and transition metals came into a boom, and a large number of important results have been gained [1]. Designing and synthesizing ligands with unique structures and characteristics is one of the long-term goals of the field of organometallic and coordination chemistry. In the last three decades, many chemists have turned their attention to a variety of ligands coordinated by nitrogen and oxygen atoms. Seeking alternatives to cyclopentadienyl ligands have led to the recent revival of anionic *N*-chelating donor ligands in various fields of organometallic and coordination chemistry. In these alternate ligands, the highly versatile and readily available amidinate anions $[\text{RC}(\text{NR}')(\text{NR}'')]^-$ play a major role and have been widely employed as ligands in transition metal and main group chemistry [2-4]. Since the carbon-nitrogen bond in amidinate can be flexibly regulated to meet the requirements of coordination with various metal elements, the reports of metal amidinate complexes have increased year by year, mainly in the aspects of synthesis and catalytic properties [3].

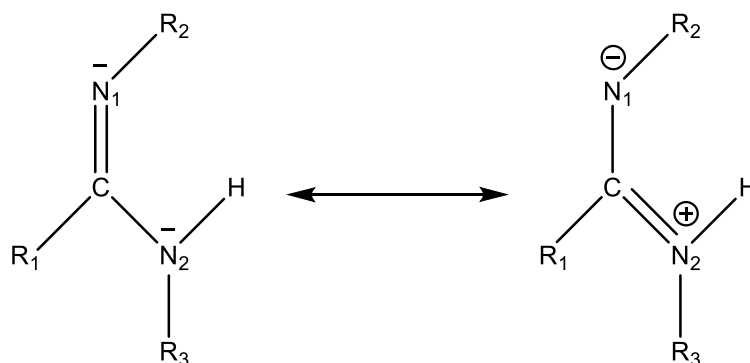
1.1.1 Amidine and amidinate ligands

Amidines, first synthesized by Gerhardt [5] in 1858 by the reaction of aniline with *N*-phenylbenzimidyl chloride (Scheme 1), are more basic than amides and are one of the strongest uncharged/unionized bases [6, 7] to form stable salts with acids.



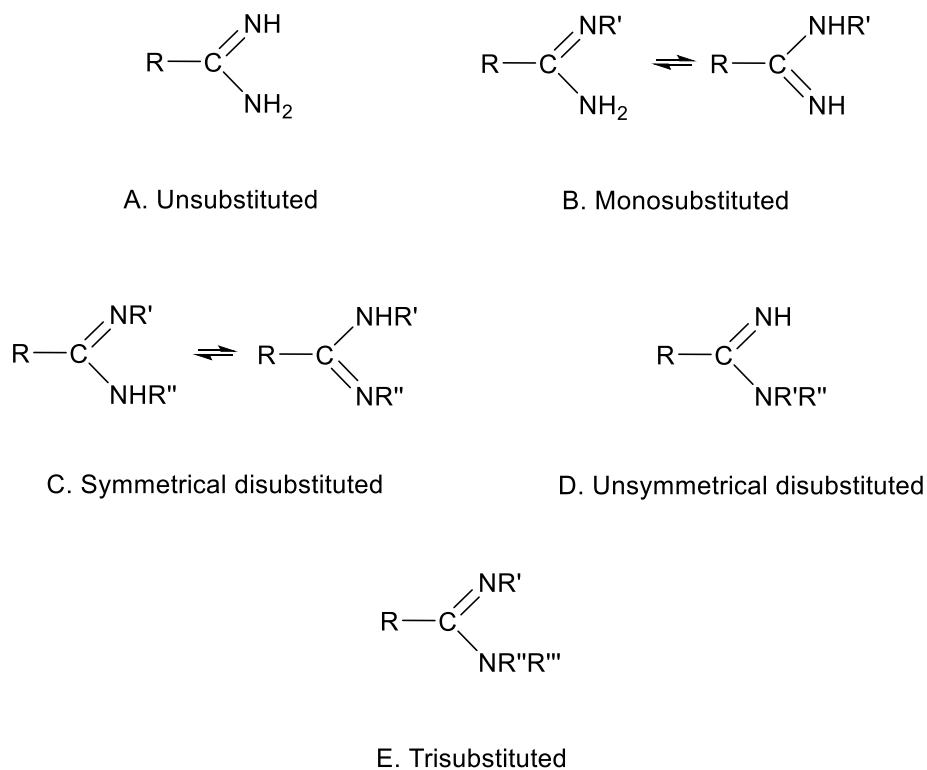
Scheme 1. Synthesis of an amidine by the reaction of aniline with *N*-phenylbenzimidyl chloride.

Amidines are a group of organic chemical compounds that can be formally described as carboxylic acid derivatives with ammonia or primary amines. The general structural formula is $R_1-C(=NR_2)-NHR_3$ in the *anti*-configuration, where R_1 , R_2 , and R_3 are organic substituents, and *anti* represents the N_1R_2 and N_2R_3H groups relatively disposed about the $C=N_1$ bond, and anti to that of R_1 and H about the $C-N$ bond (Scheme 2) [8, 9]. The N_1 or N_2 in amidine can share with their lone pair of electrons, followed by the formation of the resonated structure. The simplest amidine is formamidine, $HC(=NH)-NH_2$.



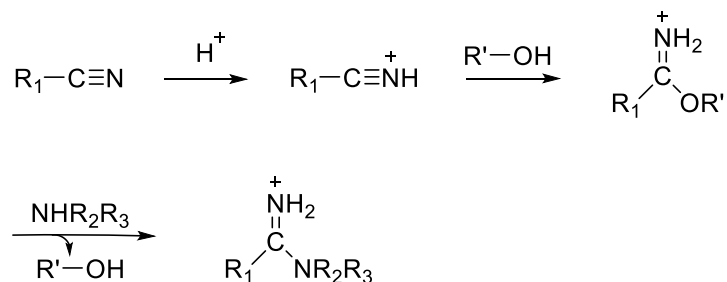
Scheme 2. The formation of the resonated structure in amidines.

Depending on the number and distribution of substituents at the nitrogen atom, amidines can be classified into five general types (Scheme 3) [10].



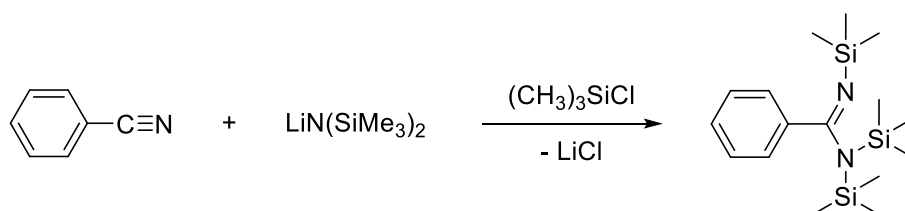
Scheme 3. Five general types of amidines.

The reactivity and fascinating coordination modes of amidines make them valuable as ligands in metal complexes. Amidines and their derivatives are widely used as antibiotics, diuretics, antiphlogistic drugs, and important intermediates of organic synthesis [11-14]. With the expansion and in-depth study of amidine's applications, the research on their synthesis method has attracted considerable attention. One of the most prevalent synthetic approaches for the preparation of amidines is the Pinner reaction named after the first describer Adolf Pinner in 1877 [15]. The Pinner reaction refers to the partial solvolysis of a nitrile with gaseous HCl in a mixture of anhydrous chloroform and alcohol producing the iminoester hydrochloride (Pinner salt), which may react further with ammonia or an amine to form an amidine [16, 17]. A general reaction mechanism is illustrated herein in Scheme 4.



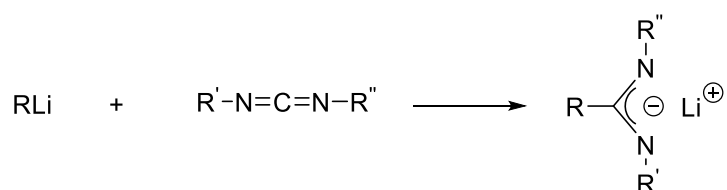
Scheme 4. Synthesis of amidines by Pinner reaction.

In 1973, with the discovery of *N,N,N'*-tris(trimethylsilyl)benzamidine $\text{PhC}(=\text{NSiMe}_3)[\text{N}(\text{SiMe}_3)_2]$ by Sanger et al. the amidine complexes story has begun. The reaction of benzonitrile with lithium bis(trimethylsilyl)amide followed by the treatment of chlorotrimethylsilane is shown in Scheme 5 [18].



Scheme 5. Synthesis of *N,N,N'*-tris(trimethylsilyl)benzamidine.

There are two types of amidinate anions, the C_1 -symmetric ligands ($\text{R}' \neq \text{R}''$) and C_2 -symmetric ligands ($\text{R}' = \text{R}''$), respectively. Also notable is that C_2 -symmetric ligands are the relatively common type. The reaction of carbodiimides with organolithium reagents can be carried out under mild conditions in high yield and mainly used in this thesis (Scheme 6).



Scheme 6. Synthesis of lithium amidinates.

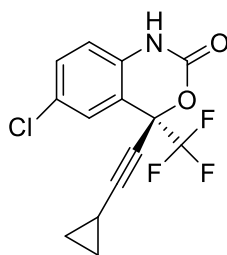
Due to the different organic substituents R and R' present at the nitrogen atom, the steric and electronic properties of these *N,N'*-chelating substituents can be easily modified, thereby allowing fine-tuning of the chemical properties of the resulting metal complexes [19]. Furthermore, the preparation of amidinate anions usually uses commercially available or readily prepared starting materials. In conclusion, these excellent properties of amidinate anions make them almost as versatile as the cyclopentadienyl ligands [20].

1.1.2 Cyclopropylethynyl and dimethylaminopropynyl substituents

C-Alkynyl-substituted amidinate ligands as a potentially useful variation of the amidinate theme are becoming more and more important in lanthanide and d-transition metal chemistry. Alkynylamidinates have attracted considerable attention due to their diverse applications in biological and pharmacological systems, such as a special group of alkynylamidinates be useful antitussives [21]. Moreover, the alkynylamidinates are well established as valuable reagents for the preparation of many of heterocycles [21]. Recently, a series of reactions of rare earth metals with lithium cyclopropylethynylamidinates have been developed in our research group [22-25].

The cyclopropyl group was chosen because of the well-known electron-donating ability of this substituent to an adjacent electron-deficient center, which would provide a rare chance to electronically influence the amidinate ligand system rather than altering only its steric demand [26]. But beyond that, an antiretroviral medication Efavirenz (EFV) is used to treat and prevent HIV/AIDS, which is chemically described as (*S*)-6-chloro-(cyclopropylethynyl)-1,4-dihydro-4-(trifluoromethyl)-2*H*-3,1-benzoxazin-2-one (Scheme 7) and is on the World Health Organization's List of Essential Medicines. It shows an aspect of the practical importance of cyclopropylalkynyl substituents. In the course of an ongoing investigation of transition metal amidinates, lithium cyclopropylethynylamidinates were used as starting materials in this Ph.D. thesis.

Another potential functional group used in this work is the dimethylamino substituent. There is some practical importance of metal complexes with *N*-amino-amidinate ligands used as precursors for producing functional layers by gas-phase deposition. Very prominent examples are CVD (chemical vapor deposition), MO-CVD (metal organic chemical vapor deposition) and ALD (atomic layer deposition). Also, the complexes can be used as catalysts for olefin hydroamination and olefin polymerization [27]. In this Ph.D. work, for the first time, both alkynyl and dimethylamino group functionalized amidinates were successfully synthesized.



Scheme 7. The structural formula of (*S*)-6-chloro-(cyclopropylethynyl)-1,4-dihydro-4-(trifluoromethyl)-2*H*-3,1-benzoxazin-2-one, Efavirenz (EFV).

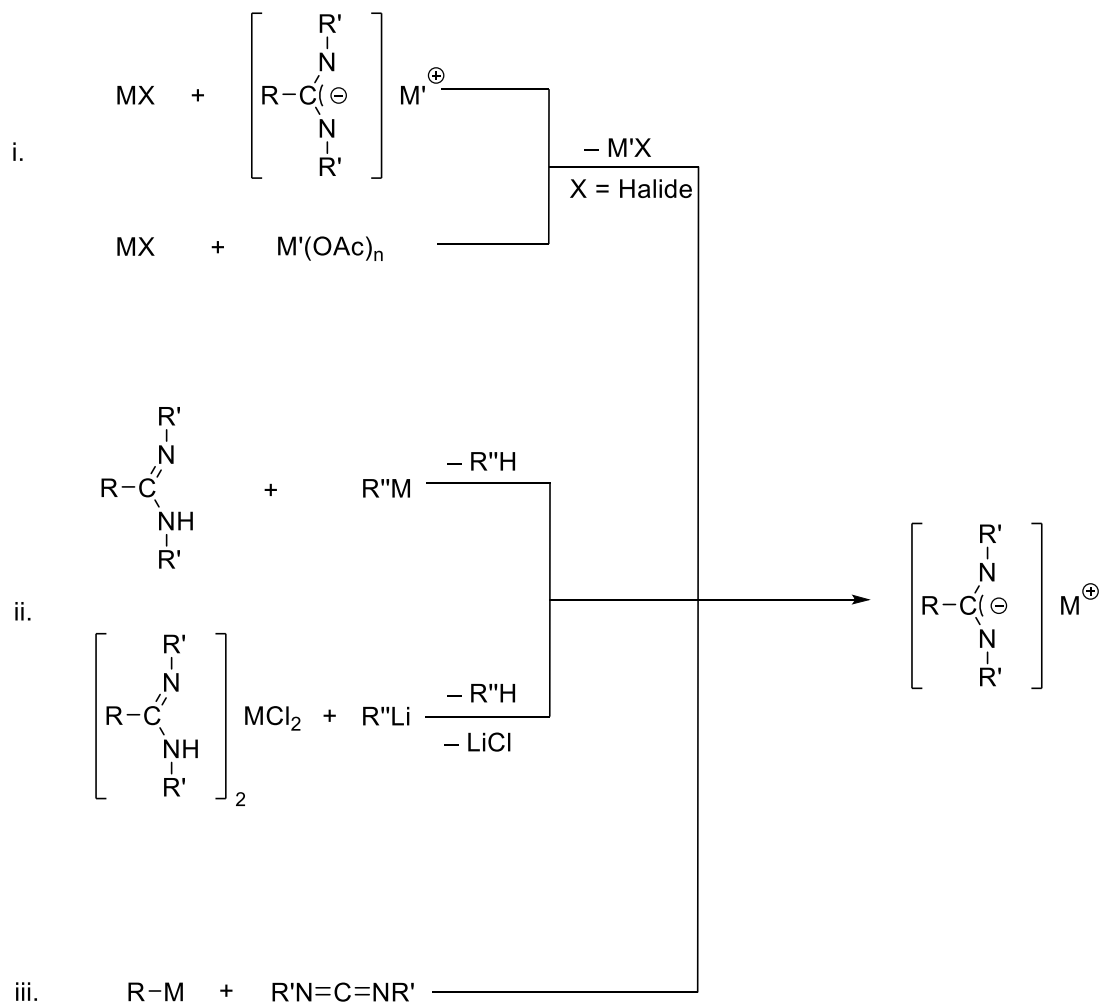
1.1.3 Synthetic routes to amidinate complexes of transition metals

There has been significant interest in the amidinate complexes over the past three decades because amidinate ligands can form metal complexes with a large number of metal elements in the periodic table. Transition metal amidinate complexes can be prepared by various synthetic routes. The most prevalent of them include (Scheme 8) [28-33]:

- i. Salt metathesis reaction between anhydrous transition metal halides and amidinates of alkali or alkaline-earth metals. Some transition metal acetates can also be used as starting materials for salt metathesis.
- ii. The amidinate metal alkyl complexes can be obtained directly by the corresponding alkane elimination reactions of amidines with metal alkyls. A variant of this

method is deprotonation of amidine transition metal complexes with the aid of an organolithium reagent.

- iii. Under mild conditions, insertion of a carbodiimide into existing metal-carbon bonds is a clean and direct route to amidinate transition metal complexes.

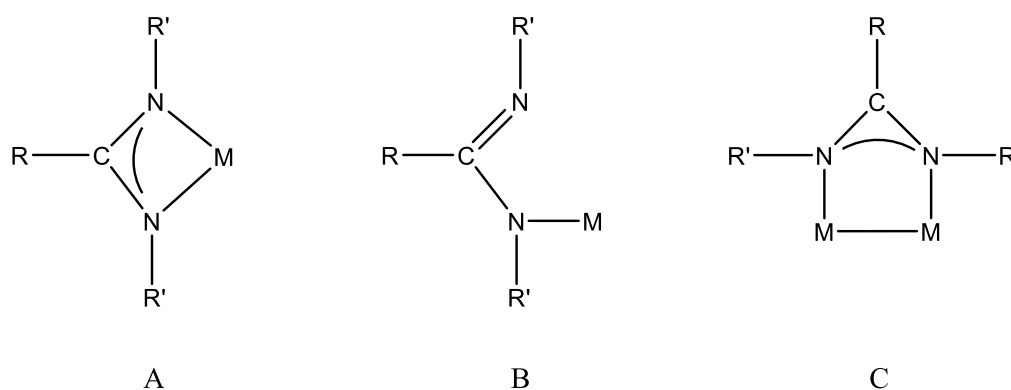


Scheme 8. Most prevalent synthetic routes of transition metal amidinate complexes.

1.1.4 Coordination modes of amidinate ligands in transition metal complexes

For the amidinate ligands, complexes of many transition metals, lanthanides, and main group elements have been reported. The common coordination modes of amidinate ligands are shown in Scheme 9 [34]. This ligand shows rich coordination chemistry in which both chelating and bridging coordination modes can be achieved. By far the most

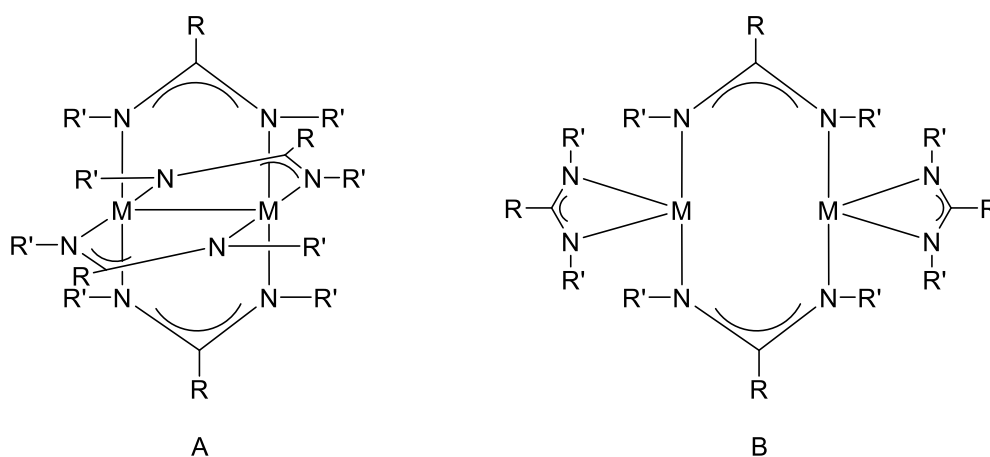
often found chelating ($\kappa N, \kappa N$) type is coordination (**A**), symmetric with two similar M–N and C–N bonds. The small size of the four-membered chelate ring results in a relatively small N–M–N bite angle (typically 63–65°). On the contrary, only a few examples of monodentate (κN) coordination (**B**) are reported. This type of bonding mainly is formed for amidinates containing sterically encumbering substituents on the nitrogen or carbon atoms such as $[M\{C_6H_3(CH_2NMe_2)_{2-2,6}\}(dptf)]$ ($dptf = p\text{-MeC}_6\text{H}_4\text{N}=\text{CHNC}_6\text{H}_4\text{-Me-}p$, $M = \text{Pd}$ or Pt), $MCl_2(HDTolF)_2$ ($HDTolF = N, N'\text{-Di}(p\text{-tolyl})\text{formamidine}$, $M = \text{Fe}$ or Co) [35-41]. The bridging coordination mode (**C**) is also very common in transition metal chemistry. The Group 11 metals copper, silver, and gold strongly tend to form dinuclear complexes containing two amidinate bridging ligands [34].



Scheme 9. Common coordination modes of amidinate and guanidinate ligands.

Moreover, the bridging coordination mode is often found in dinuclear transition metal complexes with short metal–metal distances. The majority of these complexes were found in the class of “paddlewheel-complexes” or “lantern-complexes” with the general formula $M_2(\text{amidinate})_4$ in Scheme 10 (A). In some cases, three amidinates bridge two metal centers such as $[Cr_2\text{-}\{Ar^{Xyl}NC(H)NAr^{Xyl}\}_3]$ ($Ar^{Xyl} = 2,6\text{-C}_6\text{H}_3(\text{CH}_3)_2$), which exhibited the shortest metal–metal bond length of 1.739(9) Å [42]. Meanwhile, Cr(II), and Mo(II) complexes were often observed in this class of complexes with short metal–

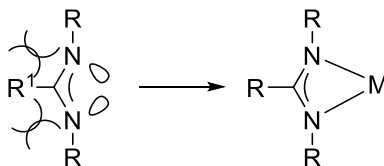
metal bond lengths and classified as quadruple bonds, while the other metals such as the Fe–Fe bond length 2.462(2) Å in $\text{Fe}_2(\mu\text{-DPhF})_4$ (HDPHF = *N,N'*-diphenylformamidine) [43] is much longer than that of Cr(II), and Mo(II) complexes. The research of these charming complexes has been conducted mainly by Cotton and Murillo et al. [43-58]. It is shown in Scheme 10 (B) that both bridged and chelating amidinate ligands can also exist simultaneously in one complex [43, 59-61]. Comparing lantern complex (A) and dinuclear complex (B) in Scheme 10, another significant difference is the long metal–metal separation such as 3.124(1) Å in $[\text{Fe}_2(\mu\text{-DPhBz})_2(\eta^2\text{-DphBz})_2]$ (HDPHBz = *N,N'*-diphenylbenzamidine) [43], which precludes the formation of any iron–iron bond.



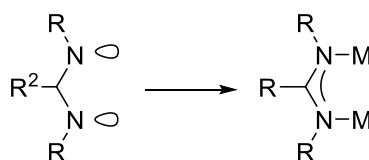
Scheme 10. Lantern (paddlewheel) complex (A) and dinuclear complex (B) with a combination of bridging and chelating amidinates.

The advantages of these ligands, in addition to being readily available, are the ability to modify their carbon and nitrogen substituents to adjust their space requirements over a wide range. To some extent, changes in the substituents on carbon or nitrogen allow the spatial requirements of the anion to be adjusted within a certain range to affect the electronic properties. Meanwhile, the substituents on the carbon and nitrogen atoms of amidinate have a large effect on the coordination properties of the amidinate ligand. Large substituents on the carbon atoms in the NCN unit, such as *t*-butyl groups, will

promote the position of the substituent at the nitrogen atom toward the metal center to facilitate chelation rather than bridging coordination (Scheme 9) [39, 62-65]. However, the most important thing is that, unlike "flat" carboxylate and carbamate anions, amidinate ligands can be described as "steric cyclopentadienyl equivalents" [34].



R¹ Large substituent, Chelating mode of amidinate ligand



R² Small substituent, Bridging mode of amidinate ligand

Scheme 11. Effect of different size substituents on coordination properties.

1.2 The developments and applications of transition metal amidinate complexes

In the past three decades, the field of transition metal amidinate chemistry has witnessed tremendous growth. A large number of transition metal amidinate complexes have been synthesized, and various applications in catalysis and materials science are beginning to emerge.

1.2.1 Amidinate complexes in catalysis

Seeking new homogeneous Ziegler-Natta catalysts for the polymerization of olefins has always been a topic of constant concern. In recent years, the structure of active catalysts has gradually expanded from conventional metallocenes to include nitrogen-based ligands. The amidinate $[\text{RC}(\text{NR}')_2]^-$ ligands can be considered as “steric cyclopentadienyl equivalents,” and the steric and electronic properties that are easily modified have led to their popularity in coordination chemistry and catalysis. The first patent application on the use of olefin polymerization catalysis with transition metal amidinates was from the work of Edelman and co-workers in cooperation with BASF [66]. There are two principal aspects in the use of transition metal complexes in polymerization catalysis, one is for simple olefins and non-conjugated α,ω -dienes polymerization, and the other is for polar monomer polymerization and involving styrene and conjugated dienes. The vast majority of published transition metal amidinate catalysts in the polymerization of ethylene, α -olefins, and non-conjugated dienes are from group 4 of the periodic table and have proven to be efficient catalysts, even with high stereoregularity in some cases [34, 67-75]. With the increasing reports on the use of group 4 $[\text{RC}(\text{NR}')_2]$ complexes in olefin polymerization, publications and patents on the use of other transition metal amidinate complexes have begun to emerge. Due to the fact that neutral group 3 and cationic group 4 amidinate complexes are isoelectronic, the group 3 elements attract a great deal of attention. Both Y(III)

amidinate and the analogous guanidinate complexes exhibit varying degrees of catalytic activity in the polymerization of ethylene [76, 77], and the study of sterically hindered mono-amidinate complexes is of great interest [78-80]. Most of the amidinate complexes of group 5 and group 6 elements have been reported in the literature, but the use of olefin polymerization is more focussed on Ta(V) and Cr(III) [75]. Compared with early transition metals, the use of late transition metals in olefin polymerization is limited and still in its infancy, with only examples of copper and nickel [81-83]. In the literature on the polymerization of polar monomers, Ti(IV) and Cu(II) or Cu(I) amidinate complexes can be used for the controlled polymerization of carbodiimides [83, 84].

In recent years, people's awareness of environmental protection has been continuously enhanced, and research on environmentally friendly biomaterials instead of petrochemical materials has begun to attract much attention. Among the many biodegradable biomaterials, polylactic acid is the most promising environmentally friendly material. At present, the relatively mature polylactic acid production process is done by ring-opening polymerization of lactide. In transition metal amidinate complexes, Y(III) and Fe(III) amidinate complexes have been studied in the context of ring-opening polymerization (ROP) of lactide [85, 86].

1.2.2 Amidinate complexes in materials science

Amidinate transition metal complexes are not only used in the field of homogeneous catalysis but also material sciences. Atomic Layer Deposition (ALD) is a thin film deposition technique currently used for making highly conformal thin films as a key process in the fabrication of semiconductor devices and as a set of tools for synthesizing nanomaterials [87-89]. The thin film is grown on a substrate by exposing its surface in a sequential, self-limiting manner to alternate gaseous species, typically called precursors. Recently, ALD processes have been extensively studied, especially for

metal oxides, metal nitrides, and elemental metals [90, 91]. Due to good volatility, high thermal stability and high reactivity, some amidinates of Ti, V, Mn, Fe, Co, Ni, Cu have been reported to be suitable as precursors for the ALD or MOCVD of transition metals and metal oxides [34, 60, 92-94]. For a good MOCVD precursor, the most important property is sufficient volatility over a wide temperature range between evaporation and decomposition. However, the volatility of the amidinate transition metal complexes can be adjusted by changing the amidinate substituents.

Most precursors are very sensitive to oxygen/air and must be volatile and do not decompose, thus placing certain restrictions on the substrates that may be used. At the same time, the process of ALD is very slow and it is known that this is its main limitation. By far, ALD is commonly used to produce substrates for microelectronics and nanotechnology, so a thick atomic layer is not desired. The sensitivity and precision of the device are very beneficial for the field of microelectronics and nanotechnology to produce small and effective semiconductors [95, 96]. There is no doubt that the chemistry of transition metal amidinates and related complexes has great potential and looks forward to continued exciting results and applications in the coming years.

1.3. Motivation

Based on the recent work in our group, Sroor et al. have reported the synthesis and spectroscopic properties of a series of lithium cyclopropylethynylamidinates, which are readily accessible on a large scale using commercially available starting materials [97]. Subsequently, these ligands have been employed for the preparation of new di- and trivalent lanthanide complexes by our research group in recent years [22-25]. However, reactions of transition metals with these lithium cyclopropylethynylamidinates were not performed. To understand the reactivity of lithium cyclopropylethynylamidinates with transition metals, two of the lithium cyclopropylethynylamidinates reported by Sroor et al. were used for synthesizing transition metal amidinate complexes. Designing new

ligands with alkynyl groups at the central C atom is of continuing interest, while alkynylamidines of the composition $\text{RC}\equiv\text{C}-\text{C}(=\text{NR}')(\text{NR}')$ have a wide range of applications in organic synthesis and biological and pharmacological systems [98-102]. In this Ph.D. work, for the first time, both alkynyl and dimethylamino group functionalized amidinates were successfully synthesized. Lithium amidinates have been shown to be common and important starting materials in the metal halide metathesis reaction, while the heavier alkali metal amidinates are relatively less studied. The first potassium propiolamidinate, $\text{K}[\text{Ph}-\text{C}\equiv\text{C}-\text{C}(\text{N}^i\text{Pr})_2]$, was prepared by our group in 2010, referring to Dröse et al. report [103]. In potassium amidinates and guanidates, symmetric double chelate coordination generally prefers a coordination mode with the contribution of the π -electron system [104]. Meanwhile, larger potassium ions provide more space for ligand coordination, and the tendency of potassium to interact with aromatic groups provides the possibility of new structural motifs [105, 106]. Moreover, the insolubility of the potassium halide by-product increases in THF, which generally contributes to the post-reaction treatment [107]. To understand the reactivity of potassium amidinates with transition metals, for the first time, two potassium cyclopropylethynylamidinates were successfully synthesized.

The homoleptic lanthanide amidinates are widely used as homogeneous catalysts and as valuable precursors in materials science and nanotechnology [108]. In the meanwhile, more and more publications and patents on the use of transition metal amidinates have begun to emerge which were described in detail in the last section. Synthesis, structural characterization, and catalytic activity of lanthanide cyclopropylethynylamidinate complexes have been studied by our research group in recent years [22-26]. However, the study of transition metals with lithium cyclopropylethynylamidinate has not yet started. In this Ph.D. work, such an attempt was made not only for lithium cyclopropylethynylamidinate but also for lithium dimethylaminopropynylamidinates and potassium cyclopropylethynylamidinates. For that purpose, a series of transition metal amidinate complexes were successfully synthesized, which will be outlined in

the following chapter. The transition metal amidinate complexes in this Ph.D. work can be divided into five categories by the difference in molecular structure, bis- and tris(amidinate) complexes, dichromium and dimolybdenum complexes with short M-M contacts, dichloridobis(amidine) complexes, and the oxygen-centered variant of amidinate complexes.

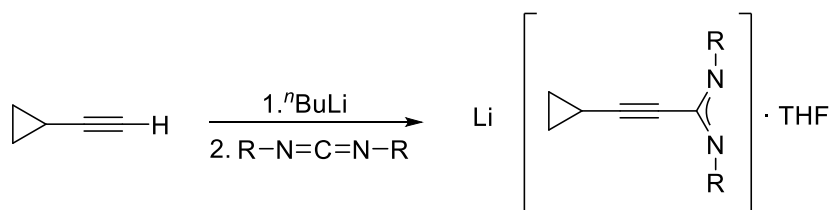
Chapter 2

Results and discussion

2.1. Lithium cyclopropylethynylamidates

Among the anionic heteroallylic ligands, the amidates and guanidates are extremely versatile ligands for the preparation of a wide range of transition metal, main group, and f-block derivatives [2, 109]. In 2013, Sroor et al. have reported the synthesis and spectroscopic properties of a series of lithium cyclopropylethynylamidates and complexes of lanthanide metals [97]. To understand the reactivity of lithium cyclopropylethynylamidates with transition metals, two of the lithium cyclopropylethynylamidates reported by Sroor et al. were used for synthesizing new transition metal amidinate complexes.

Lithium amidates **1** and **2**, $\text{Li}[c\text{-C}_3\text{H}_5\text{-C}\equiv\text{C-C}(\text{NR})_2]\cdot\text{THF}$ (**1**: R = *i*Pr **2**: R = Cy), were synthesized according to the published procedures in our research group [97]. As shown in Scheme 12, **1** and **2** were prepared by *in situ* deprotonations of a solution of commercially available cyclopropylacetylene in the presence *n*-butyllithium followed by treatment with either *N,N'*-di-*iso*-propylcarbodiimide or *N,N'*-dicyclohexylcarbodiimide to yield lithium amidates **1** and **2** as white solids. Compared to the prior mentioned procedure, a complete reaction was ensured by slightly modified experimental parameters (e.g., longer reaction times), and the yields (**1**: 85% and **2**: 87%) were improved.



1: R = *i*Pr, 85% yield

2: R = Cy, 87% yield

Scheme 12. Synthesis of lithium cyclopropylethynylamidinates **1** and **2**.

Both lithium amidinates **1** and **2** are moisture-sensitive compounds which are freely soluble in THF and moderately soluble in the non-polar solvent *n*-pentane. THF solutions of lithium amidinates **1** and **2** were stored at $-25\text{ }^{\circ}\text{C}$ in a freezer to give colorless crystals [97]. Compared to the dimeric ladder-type molecular structures of lithium amidinates **1** and **2**, an unexpected molecular structure of lithium amidinate **3**, $\text{Li}[c\text{-C}_3\text{H}_5\text{-C}\equiv\text{C-C}(\text{N}^i\text{Pr})_2]_4$, was obtained by recrystallization of lithium amidinate **2** from *n*-pentane (Figure 2) as very moisture-sensitive, colorless, prismatic crystal (70% yield). The lithium amidinate **3** was characterized by X-ray diffraction, NMR, IR, and mass spectroscopy as well as elemental analyses.

The IR spectra of lithium amidinates **1** and **3** showed characteristic bands at 2216 cm^{-1} and 1593 cm^{-1} which can be assigned to $\text{C}\equiv\text{C}$ stretching vibrations, and the $\text{C}=\text{N}$ bond stretching vibration in the NCN units of amidinate ligands, respectively [97, 103, 110]. The elemental analysis of lithium amidinate **3** was not consistent with the proposed formulation. The possible reason is that since lithium amidinate **3** is very sensitive to moisture; **3** cannot be maintained in a stable state during the measurement, and thus hydrolysis and decomposition reactions occurred at the same time. However, the mass spectrum of lithium amidinate **3** showed a molecular ion peak at m/z 793.

NMR measurements of all the amidinate related complexes in this Ph.D. thesis were carried out in THF- d_8 . The ^1H NMR spectrum of lithium amidinate **3** reveals five signals in the region of 0–4 ppm. The signal corresponding to the protons of the *isopropyl* groups showed doublets at $\delta = 0.98$ ppm [$\text{CH}(\text{CH}_3)_2$] and septet at $\delta = 3.78$ ppm [$\text{CH}(\text{CH}_3)_2$]. The three remaining signals were observed at $\delta = 0.65$ ppm and 0.79 ppm (CH_2 , $c\text{-C}_3\text{H}_5$) and at $\delta = 1.37$ ppm (CH , $c\text{-C}_3\text{H}_5$) as multiplets, respectively, which can be assigned to the cyclopropyl group. Compared to the ^1H NMR of **1**, the only difference is that two THF ligand signals [**1**: $\delta = 3.22\text{--}3.29$ ppm (m, 4H, THF), $\delta = 1.37\text{--}1.45$ ppm (m, 4H, THF)] are missing in **3** (Figure 1) [97]. The ^{13}C NMR data of **3** is very similar to that of **1**, only two signals corresponding to the THF ligand were not observed [**1**: $\delta = 67.1$ (THF), 26.3 (THF) ppm] [97].

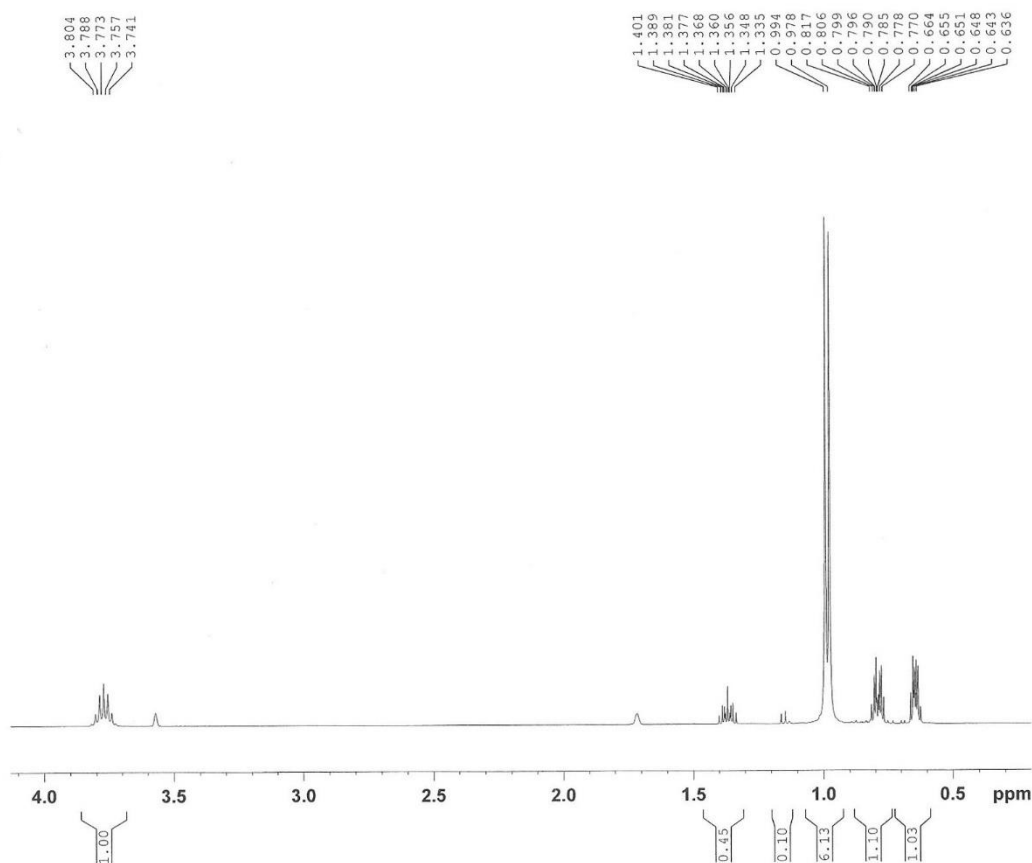


Figure 1. ^1H NMR spectrum (400 MHz, THF- d_8 , 25 °C) of lithium amidinate **3**.

The molecular structure of lithium amidinate **3** is displayed in Figure 2. Selected bond lengths and angles are given in Table 1. Lithium amidinate **3** crystallizes in the triclinic space group $P\bar{1}$ containing one complex molecule in the asymmetric unit. Each of the lithium ions is coordinated to four nitrogen atoms of NCN units viz., two nitrogen atoms of one amidinate ligand, two nitrogen atoms of another two different amidinate ligands, respectively.

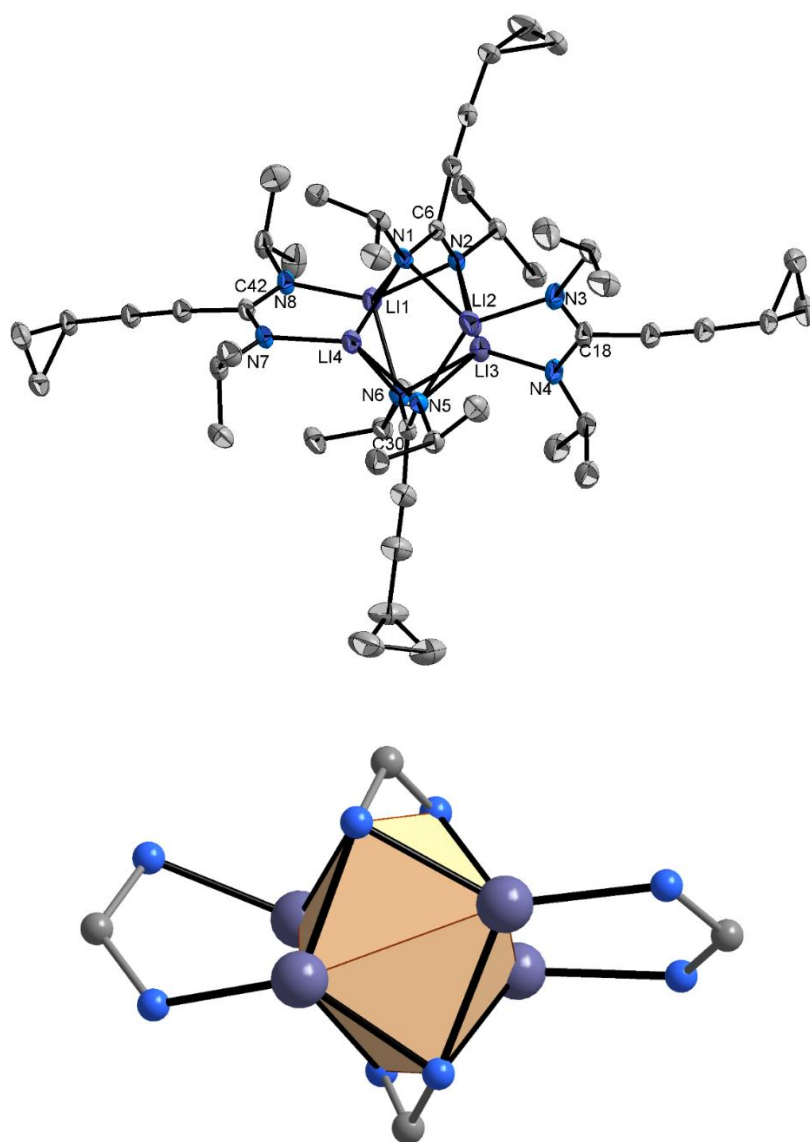


Figure 2. Molecular structure of $\{\text{Li}[c\text{-C}_3\text{H}_5\text{-C}\equiv\text{C}-(\text{N}^i\text{Pr})_2]\}_4$ (**3**) (top) in the crystalline state. Thermal ellipsoids with 50% probability, H atoms omitted for clarity. Representation of the coordination spheres of the Li atoms in **3** (bottom).

In Figure 2, two amidinate ligands on either side are combined with a centrally heterocubane-type cluster consisting of four nitrogen and four lithium atoms in alternating corners. In the central structural unit, the two four-membered metallacycle rings are almost planar [N(1)–Li(2)–N(5)–Li(4) $-3.1(1)^\circ$, N(2)–Li(3)–N(6)–Li(1) $5.4(1)^\circ$]. The four groups of C–N bonds lengths in lithium amidinate **3** are in a narrow range of 1.326 to 1.339 Å, thus indicating π -electron delocalization over the N–C–N fragments. In Table 1, the bond lengths and angles of lithium amidinate **3** are typical for related lithium amidinate **1**. Compared to **1**, the range of N–Li–N bond angles in lithium amidinate **3** is slightly larger and the maximum bond angle of N–Li–N is increased to $143.2(2)^\circ$. The reason can be attributed to the difference in the molecular structures. Compared to lithium amidinates **1** and **2**, these two previously reported lithium amidinates are dimeric ladder-type molecular structures in the solid-state [97]. In fact, regarding most previously reported lithium amidinate structures, the dimeric structure is a common feature of such compounds [111-113].

Table 1. Selected bond lengths (Å) and bond angles ($^\circ$) for lithium amidinates **1** and **3**

Compound	1	3
Bond lengths and angles		
Li–N (min) ^a	1.975(3)	1.963(3)
Li–N (max) ^b	2.336(4)	2.356(4)
N–Li–N	63.2(1)–126.9(2)	62.4(1)–143.2(2)

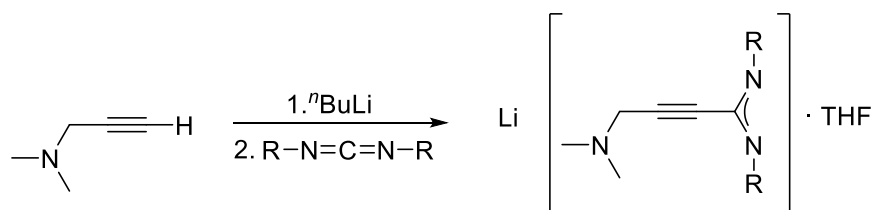
^a minimum bond length. ^b maximum bond length.

2.2. Synthesis and structural characterization of new lithium and potassium amidinates

2.2.1. New lithium dimethylaminopropynylamidinates

Designing new ligands with alkynyl groups at the central C atom is a continuing interest, while alkynylamidines of the composition $RC\equiv C-C(=NR')(NR')$ has a wide range of applications in organic synthesis and biological and pharmacological systems [98-102]. Dimethylamino substituents were used in this Ph.D. because of some practical importance of metal complexes with *N*-amino-amidate ligands used as precursors for producing functional layers and catalysts for olefin hydroamination and polymerization [27]. In this Ph.D. work, for the first time, both alkynyl and dimethylamino groups functionalized amidinates were successfully synthesized.

Using the straightforward reaction shown in Scheme 13, two new lithium dimethylaminopropynylamidinates, $Li[(CH_3)_2N-CH_2-C\equiv C-(NR)_2]\cdot THF$ (**4**: R = *i*Pr, **5**: R = Cy) were prepared by *in situ* deprotonations of commercially available starting material 3-dimethylamino-1-propynyl with *n*-butyllithium followed by addition of either *N,N'*-di-*iso*-propylcarbodiimide or *N,N'*-dicyclohexylcarbodiimide. The solution was concentrated in vacuum to a small volume and stored at $-25\text{ }^\circ\text{C}$ to obtain colorless, block-like single crystals of lithium amidinates **4** and **5** in good yield (79%) and yield (84%), respectively. Both THF adducts **4** and **5** were fully characterized by spectroscopic methods (NMR, IR, and MS) and elemental analyses, as well as structurally characterized by single-crystal X-ray diffraction.



4: R = *i*Pr, 79% yield

5: R = Cy, 86% yield

Scheme 13. Synthesis of lithium dimethylaminopropynylamidinates **4** and **5**.

The IR spectra of two new lithium amidinates **4** and **5** show two characteristic very strong bands at 1502 and 1506 cm^{-1} which can be assigned to the C=N bond stretching vibration in the NCN units of amidinate ligands [97, 103, 110]. However, the signals of C≡C stretching vibrations are not identifiable in both cases. Compared to the strong band at 2216 cm^{-1} in the IR spectrum of **3**, only a weak band was observed at 2121 cm^{-1} in that of **5**. Meanwhile, a medium band around 2791 cm^{-1} corresponding to the stretching vibrations of the C–N bond could be assigned to the Me₂N units. Elemental analysis values for C, H, and N of lithium amidinates **4** and **5** were consistent with the proposed formulation, showing that **4** and **5** lose the THF of crystallization upon drying. The molecular ion peaks of **4** and **5** were not observed in the EI mass spectra. However, the peak at m/z 208 (3) in **4** could be assigned to fragment $[M - \text{Li}]^+$ and the peak at m/z 206 (1) in **5** could be assigned to fragment $[M - \text{Li} - \text{Cy}]^+$.

The ¹H NMR spectra of lithium amidinates **4** and **5** showed four well-resolved signals in the region of 0–4 ppm, respectively, as detailed in Table 2. Compared to the NMR spectra of **1** and **2**, Li[*c*-C₃H₅–C≡C–C(NR)₂].THF (**1**: R = *i*Pr **2**: R = Cy), two characteristic coordinated THF signals are missing because the coordinated THF of the test samples were removed in the drying process. The ¹³C NMR spectra of **4** and **5** confirmed the formulation as unsolvated homoleptic complexes and reported in Table 3. Compared to the signal of the acetylenic carbon atoms bearing a cyclopropyl

substituent ($c\text{-C}_3\text{H}_5\text{-C}\equiv\text{C}$) of lithium amidinates **1** and **2** (**1**: 97.1, **2**: 96.9 ppm), the resonances corresponding to the acetylenic carbon atom attached to a dimethyl-amino substituent ($\text{CH}_2\text{-C}\equiv\text{C}$) were observed to shift to a lower field at 78.2 and 78.5 ppm, respectively. Notably, the difference can be attributed to the electron-donating ability of the cyclopropyl group to the adjacent electron-deficient center [97, 114]. Meanwhile, the signal of the acetylenic carbon atom ($\text{CH-C}\equiv\text{C}$) is in good agreement with the reported ^{13}C NMR spectrum of cyclopropyl-2-propionic acid, $c\text{-C}_3\text{H}_5\text{-C}\equiv\text{C-COOH}$ ($\delta = 68.1$ and 96.8 ppm) [115].

Table 2. ^1H NMR spectra of lithium dimethylaminopropynylamidinates **4–5**.

$\delta(\text{ppm})$ Comp.	CH_2 , NCH_2C	CH_3 , $(\text{CH}_3)_2\text{N}$	CH , $i\text{Pr}$	CH , Cy	CH_3 , $i\text{Pr}$	CH_2 , Cy
4	3.40	2.55	3.87	–	1.01	–
5	3.41	2.28	–	3.46	–	1.11–1.78

Table 3. ^{13}C NMR spectra of lithium dimethylaminopropynylamidinates **4–5**.

$\delta(\text{ppm})$ Comp.	NCN	$\text{C}\equiv\text{C-C}$	$\text{CH}_2\text{-C}\equiv\text{C}$	$\text{CH}(\text{CH}_3)$ CH , Cy	$\text{CH}(\text{CH}_3)_2$ CH_2 , Cy	$\text{CH}_2\text{-}$ $\text{C}\equiv\text{C}$	$(\text{CH}_3)_2\text{N}$
4	156.6	88.5	78.2	49.9	27.0	48.7	44.2
5	156.5	87.9	78.5	58.8	38.4, 26.3	48.7	44.3

Figure 3 and Figure 4 depict the molecular structures of the lithium amidinates **4** and **5**, while crystallographic details are listed in Table 14 and Table 16. **4** and **5** crystallized in the triclinic space group $P\bar{1}$ (**4**) and monoclinic space group $P2_1/c$ (**5**) with one complex molecule in the asymmetric unit, respectively. The lithium ions are coordinated to the two nitrogen atoms of one amidinate ligand, one nitrogen atom of the other amidinate, and the oxygen atom of the THF ligand. In both cases, the crystal structure determinations revealed the presence of a ladder-type dimeric structure, which

is the most characteristic structural motif of most previously characterized lithium amidinates [26]. The dimers have a centrosymmetric structure with a strictly central planar four-membered Li_2N_2 ring. The C–N bond lengths in the amidinate NCN unit of lithium amidinate **4** are in a narrow range of 1.319(1) to 1.335(2) Å, and that of lithium amidinate **5** is in the range of 1.326(2) to 1.337(1) Å. The narrow range of C–N bond lengths indicates π -electron delocalization over the NCN unit of lithium amidinates **4** and **5**. Meanwhile, the C–N bond length of **4** and **5** in the NCN units are characteristic of a 1,3-diazaallylic system. Generally, the bite angles of amidinate ligands are small and restricted in the range of 63–65° by the geometry of the amidinate backbone. The range of N–Li–N bite angles in lithium amidinates **4** and **5** is fully consistent with this rule [N(1)–Li(1)–N(2) 65.4(7) and N(1A)–Li(1A)–N(2A) 65.4(7)° (**4**); N(1)–Li(1)–N(2) 65.3(1) and N(1A)–Li(1A)–N(2A) 65.4(1)° (**7**)]. Comparing the bond lengths and angles of **1**, **2**, and **4**, **5**, the data are in good agreement with similar structures of lithium amidinates [26, 62, 109, 111, 113, 116–119].

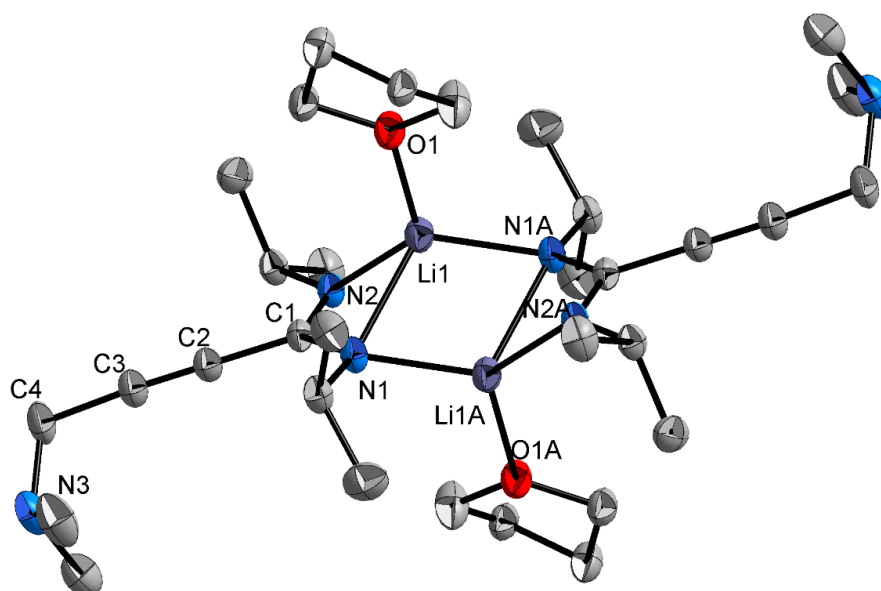


Figure 3. Molecular structure of $[\text{Li}\{(\text{CH}_3)_2\text{N}-\text{CH}_2-\text{C}\equiv\text{C}-(\text{N}^i\text{Pr})_2\}\cdot\text{THF}]_2$ (**4**) in the crystalline state. Thermal ellipsoids with 50% probability, H atoms omitted for clarity.

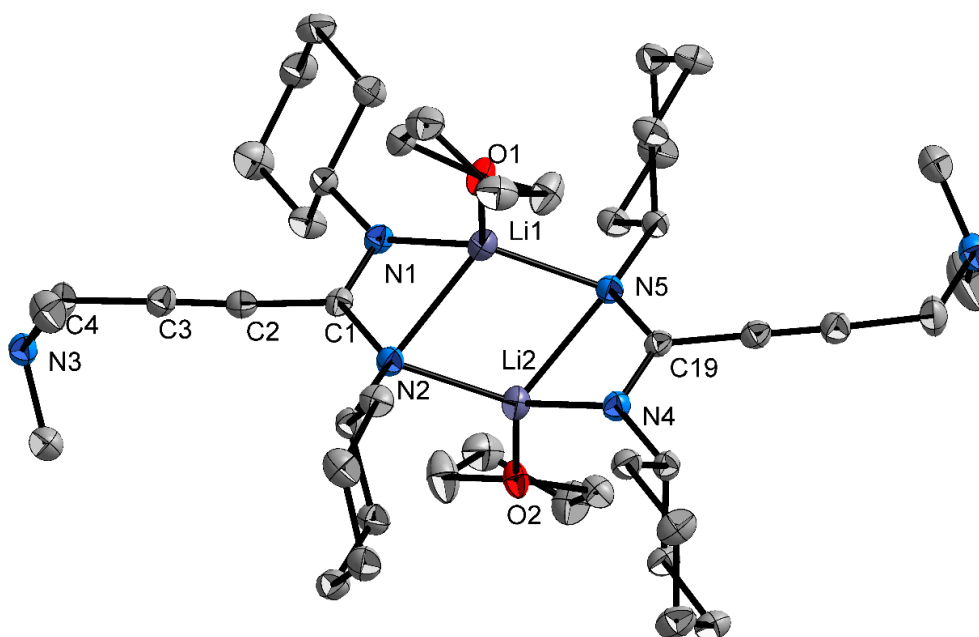
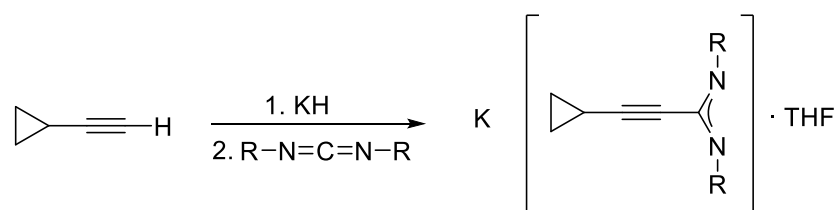


Figure 4. Molecular structure of $\{\text{Li}[(\text{CH}_3)_2\text{N}-\text{CH}_2-\text{C}\equiv\text{C}-(\text{NCy})_2]\cdot\text{THF}\}_2$ (**5**) in the crystalline state. Thermal ellipsoids with 50% probability, H atoms omitted for clarity.

2.2.2. New potassium cyclopropylethynylamidinates

Lithium amidinates are common and important starting materials in the metal halide metathesis reaction, while the heavier alkali metal amidinates are relatively less studied. One characteristic of heavier alkali metals is the increased tendency of the π -coordination mode, which is often observed in other complexes with nitrogen ligands [112, 120]. With the increasing number of lithium and potassium diazaallylic species reported, the related sodium reagents were rarely mentioned. It is presumably due to limited synthetic advantage over an easier to handle lithium analogue or the increased insolubility of potassium halide by-products relative to sodium halides, which typically assists reaction workup [107]. To understand the reactivity of potassium amidinates with transition metals, for the first time, two potassium cyclopropylethynylamidinates were successfully synthesized.

As illustrated in Scheme 14, potassium hydride was used as deprotonation reagent instead of *n*BuLi as for **1** and **2**, $\text{Li}[c\text{-C}_3\text{H}_5\text{-C}\equiv\text{C-C}(\text{NR})_2]\cdot\text{THF}$ (**1**: R = *i*Pr **2**: R = Cy). Two new potassium cyclopropylethynylamidates, $\text{K}[c\text{-C}_3\text{H}_5\text{-C}\equiv\text{C-C}(\text{NR})_2]\cdot\text{THF}$ (**6**: R = *i*Pr, **7**: R = Cy) were synthesized in a straightforward manner by nucleophilic addition of potassium cyclopropylacetylide to *N,N'*-di-*iso*-propylcarbodiimide or *N,N'*-dicyclohexylcarbodiimide. The starting material $[c\text{-C}_3\text{H}_5\text{-C}\equiv\text{C}]\text{K}$ was obtained by *in situ* deprotonation of cyclopropylacetylene using potassium hydride. The solvent was removed in vacuum affording moisture-sensitive white solids of **6** and **7** in 82% and 76% isolated yield, respectively.



6: R = *i*Pr, 78% yield

7: R = Cy, 80% yield

Scheme 14. Synthesis of potassium cyclopropylethynylamidates **6** and **7**.

Unfortunately, attempts to recrystallize the products from various solvents such as THF, toluene, DME, *n*-pentane, and mixtures thereof over a range of temperatures (from -20 °C to room temperature) have not succeeded in obtaining single crystals suitable for X-ray diffraction.

The IR spectra of potassium amidates **6** and **7** showed a significant band at about 2210 cm^{-1} , which could be assigned to $\text{C}\equiv\text{C}$ stretching vibrations [103]. Another characterized band could be assigned to the stretching vibration of the delocalized NCN unit of amidate moieties, which were observed at 1693 cm^{-1} as a medium band and at 1634 cm^{-1} as a strong band, respectively [97, 103, 110]. Meanwhile, a medium and

a strong band observed at 2863 and 2957 cm^{-1} (**6**), 2849 and 2920 cm^{-1} (**7**) could be attributed to the C–H valence vibrations of the *isopropyl* and *cyclohexyl* groups, respectively. Elemental analysis values for C, H, and N of the potassium amidinates **6** and **7** were consistent with the proposed formulation, showing that **6** and **7** keep the THF of crystallization (coordinated THF) upon drying. The molecular ion peak of **6** was observed in the EI mass spectrum. However, the mass spectrum of **7** showed only fragments such as a peak at m/z 208 (3) which could be assigned to the molecular ion without the potassium ion [*c*-C₃H₅-C≡C-C(NCy)₂]⁺.

The ¹H and ¹³C NMR spectroscopic data of potassium amidinates **6** and **7** were in good agreement with that of **1** and **2** are collected in Table 4 and Table 5. In the ¹³C NMR spectra of **6** and **7**, the signal corresponding to the carbon of NCN unit and the carbon (CH–C≡C) are slightly shifted to a higher field (compared to that of **1** and **2**) from 157.0 to 153.6 ppm and 97.1 to 94.7 ppm, respectively. On the contrary, the signal corresponding to the carbon (C≡C–C) is inconspicuously shifted to a lower field from 69.0 to 70.5 ppm. This trend was also found in the ¹³C NMR spectra of recently reported lithium and potassium propiolamidinates Li[PhC≡C–C(NCy)₂].THF and K[PhC≡C–C(N^{*i*}Pr)₂] [26, 103]. The signals corresponding to the carbons of the NCN unit in lithium and potassium propylamidinates were observed at $\delta = 159.3$ and 153.6 ppm and carbons directly bonded to the amidinate group were observed at $\delta = 94.4$ and 91.5 ppm, as well as the carbons bearing the phenyl group, which appeared at $\delta = 82.4$ and 84.3 ppm, respectively. The main reason is that the potassium amidinates are more ionic, while the lithium amidinates have more covalent Li–N bonds. The different substituents (Cy and ^{*i*}Pr) at the nitrogen atoms of the NCN unit do not affect the result.

Table 4. ^1H NMR spectra of lithium and potassium cyclopropylethynylamidates **1-2** and **6-7**.

$\delta(\text{ppm})$ Comp.	$\text{CH}, c\text{-C}_3\text{H}_5$	$\text{CH}_2, c\text{-C}_3\text{H}_5$	$\text{CH}, i\text{Pr}$	CH, Cy	$\text{CH}_3, i\text{Pr}$	CH_2, Cy
1	1.36	0.65–0.79	3.77	–	0.98	–
2	1.31	0.77	–	3.32	–	1.01–1.67
6	1.33	0.75	3.71	–	0.95	–
7	1.30	0.77	–	3.28	–	1.01–1.69

Table 5. ^{13}C NMR spectra of lithium and potassium cyclopropylethynylamidates **1-2** and **6-7**.

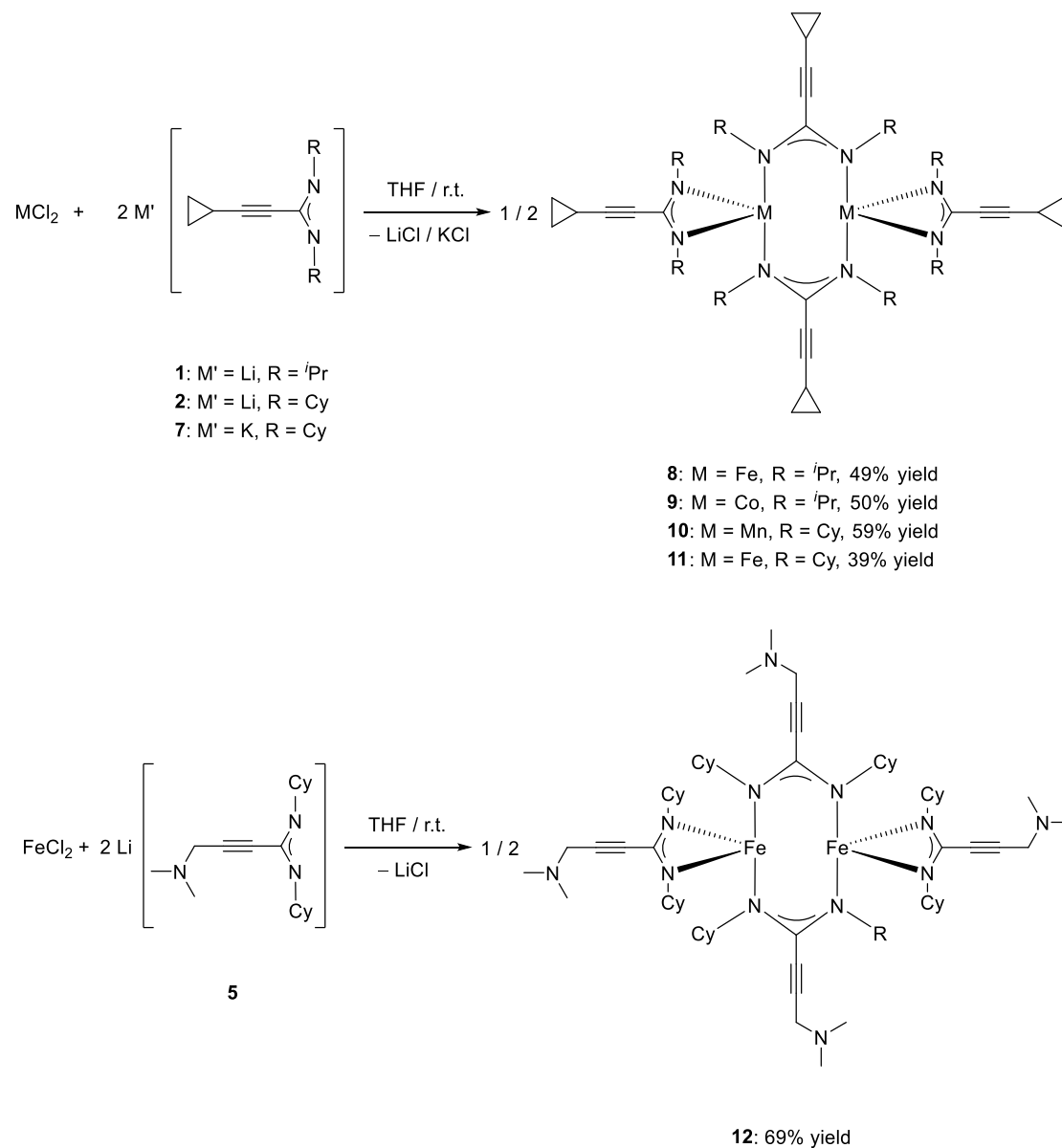
$\delta(\text{ppm})$ Comp.	NCN	$\text{CH}-\text{C}\equiv\text{C}$	$\text{C}\equiv\text{C}-\text{C}$	$\text{CH}(\text{CH}_3)_2$ CH, Cy	$\text{CH}(\text{CH}_3)_2$ CH_2, Cy	$\text{CH}_2,$ $c\text{-C}_3\text{H}_5$	$\text{CH},$ $c\text{-C}_3\text{H}_5$
1	157.0	97.1	69.0	49.8	26.8	8.9	0.4
2	157.0	96.9	69.3	59.0	38.0, 27.1	9.1	0.4
6	153.8	95.2	70.4	49.3	27.4	9.1	0.5
7	153.6	94.7	70.5	59.2	38.5, 27.3	9.4	0.5

2.3. Synthesis and structural characterization of transition metal bis(amidinate) complexes

Recently, a series of lithium cyclopropylethynylamidates, $\text{Li}[c\text{-C}_3\text{H}_5\text{-C}\equiv\text{C-C}(\text{NR})_2]$ [$\text{R} = {}^i\text{Pr}, \text{Cy}$] has been employed for the preparation of new complexes of divalent lanthanide by F. Sroor et al. in our research group [22-26]. Moreover, the lanthanide bis(cyclopropylethynylamidate) were found to exhibit a catalytic activity towards C–C and C–N bond formation (as extremely active precatalysts for the guanylation of *p*-phenylenediamine with *N,N'*-diisopropylcarbodiimide) [24, 25]. To study the influence of transition metals on the molecular structure of amidinate complexes, a series of transition metal amidinate complexes were successfully synthesized and be outlined in this section. Manganese(II), iron(II), and cobalt(II) chloride were used as starting materials; for instance, iron is attractive for applications in catalysis because it is cheap and non-toxic.

As described in Scheme 15, five new transition metal bis(amidinate) complexes $[\text{M}_2\{\mu\text{-}c\text{-C}_3\text{H}_5\text{-C}\equiv\text{C-C}(\text{NR})_2\}_2\{\eta^2\text{-}c\text{-C}_3\text{H}_5\text{-C}\equiv\text{C-C}(\text{NR})_2\}_2]$ (**8**: $\text{M} = \text{Fe}$, $\text{R} = {}^i\text{Pr}$; **9**: $\text{M} = \text{Co}$, $\text{R} = {}^i\text{Pr}$; **10**: $\text{M} = \text{Mn}$, $\text{R} = \text{Cy}$; **11**: $\text{M} = \text{Fe}$, $\text{R} = \text{Cy}$), and $[\text{Fe}_2\{\mu\text{-(CH}_3)_2\text{N-CH}_2\text{-C}\equiv\text{C-C}(\text{NCy})_2\}_2\{\eta^2\text{-(CH}_3)_2\text{N-CH}_2\text{-C}\equiv\text{C-C}(\text{NCy})_2\}_2]$ (**12**) were obtained by metathesis reactions of anhydrous transition metal halides with two equivalents of lithium cyclopropylethynylamidates $\text{Li}[c\text{-C}_3\text{H}_5\text{-C}\equiv\text{C-C}(\text{NR})_2]\cdot\text{THF}$ (**1**: $\text{R} = {}^i\text{Pr}$, **2**: $\text{R} = \text{Cy}$), potassium cyclopropylethynylamidate $\text{K}[c\text{-C}_3\text{H}_5\text{-C}\equiv\text{C-C}(\text{NCy})_2]\cdot\text{THF}$ (**7**), and lithium dimethylaminopropynylamidinate $\text{Li}[(\text{CH}_3)_2\text{N-CH}_2\text{-C}\equiv\text{C-C}(\text{NCy})_2]\cdot\text{THF}$ (**5**) in THF, respectively. The 1:2 reaction mixture were stirred overnight at room temperature and afforded complexes **8–12** in moderate to good yields (**8**: 49%, **9**: 50%, **10**: 59%, **11**: 39%, **12**: 69%). The title compounds were isolated from *n*-pentane solution as unsolvated, exceedingly air- and moisture-sensitive, colored crystals (**8**: yellow prism-like, **9**: yellow-green plate-like, **10**: yellow prism-like, **11**: orange block-like, **12**: brown block-like). The dimeric nature and the connectivity of the transition

metal bis(cyclopropylethynylamidinate) complexes **8–12** were determined by single-crystal X-ray diffraction. These compounds were fully characterized by NMR, IR, and MS methods, as well as elemental analyses.



Scheme 15. Synthesis of transition metal bis(amidinate) complexes **8–12**.

The IR spectra of complexes **8–11** showed characteristic medium bands in the range of 1593–1606 cm^{-1} and a very strong band observed at 1603 cm^{-1} in the IR spectrum of **12**, which can be attributed to the C=N bond stretching vibration in the NCN units of amidinate ligands [110]. The C≡C bond stretching vibrations were observed as medium

bands in the range of 2217–2225 cm^{-1} in the IR spectra of **8–11**, while that of **12** was observed at 2218 cm^{-1} as weak band and consistent with **5** (2121 w cm^{-1}) [103]. Compared to the IR spectra of the lithium amidinates **1**, **2**, and **5** and potassium amidinate **7**, the C=N bond stretching vibration in the NCN units and C≡C bond stretching vibration were observed as strong or very strong bands. Several bands with intensities from medium to very strong observed in the range of 2848–2966 cm^{-1} could be assigned to the C–H valence vibrations of the *isopropyl* substituents and cyclohexyl groups. Elemental analysis values for C, H, and N of complexes **8–12** were in good agreement with the proposed formulation. The molecular ion peaks were not observed in the EI mass spectra of **8–12** and exhibited only fragments. The peak at m/z 705 in the mass spectrum of **8** could be assigned to the fragment $[M - 4 \textit{iPr}]^+$, while the peak at m/z 593 in the mass spectrum of **9** could be assigned to the fragment $[M - 3 \textit{iPr} - 4(c\text{-C}_3\text{H}_5)]$. In the case of complexes **10** and **11**, the peaks at m/z 667 and 595 could be assigned to $[M - 3(c\text{-C}_3\text{H}_5\text{-C}\equiv\text{C}) - 4\text{Cy}]^+$ and $[M - 2\{c\text{-C}_3\text{H}_5\text{-C}\equiv\text{C-C}(\text{NCy})_2\} - \text{Cy}]^+$, respectively. In the mass spectrum of complex **12**, the peak observed at m/z 931 could be assigned to the molecular ion without four cyclohexyl groups $[M - 4\text{Cy}]^+$.

All the bis(amidinate) transition metal complexes reported in this Ph.D. work are paramagnetic, so the full interpretation of NMR spectra is complicated or impossible. In general, the strongly paramagnetic nature of Mn^{2+} , Fe^{2+} and Co^{2+} ions prevented the measurement of interpretable NMR spectra, whereas the NMR spectrum of complex **11** could be obtained to produce the only meaningful data in this series of transition metal bis(amidinate) complexes. THF- d_8 was found to be a suitable solvent for measuring the NMR spectra of these homoleptic complexes **8–12**. The ^1H NMR spectrum of complex **11** showed resonances in the region of 0–8 ppm and displayed several well-resolved signals. The protons of the cyclopropyl group of amidinate ligands were observed as multiplets at $\delta = 0.80$ ppm (CH_2 , $c\text{-C}_3\text{H}_5$) and 1.43 ppm (CH , $c\text{-C}_3\text{H}_5$). The signals appearing at $\delta = 3.21$ (CH_2 , Cy) and 4.27 (CH , Cy) ppm as multiplets, as well as in the range of 3.36–3.56 (CH , Cy) ppm as broad singlets can be assigned to the cyclohexyl

groups. Compared to the potassium amidinate **7**, $\text{K}[c\text{-C}_3\text{H}_5\text{-C}\equiv\text{C-C}(\text{NCy})_2]\cdot\text{THF}$, the protons signals of **11** are shifted to lower magnetic field and showed no indication of the presence of THF ligands which is in agreement with the formulation. In the ^{13}C NMR spectrum, the signals corresponding to the carbon atoms of the cyclopropyl group of **11** were observed at $\delta = 0.3$ (CH) and $\delta = 9.2$ (CH_2) ppm. The signals corresponding to the carbon atoms (CH_2) of the cyclohexyl group appeared at $\delta = 52.0$ and 56.7 ppm shifted around 20–30 ppm to lower field compared to the potassium amidinate **7**, and the carbon atoms (CH) of the cyclohexyl group were observed at $\delta = 66.7$ ppm (lower field compared to the potassium amidinate **7**). The signals observed at $\delta = 60.4$, and 94.6 ppm (higher field compared to **7**) could be assigned to the carbon atoms ($\text{C}\equiv\text{C-C}$ and $\text{CH-C}\equiv\text{C}$), respectively. The signals appearing at $\delta = 140.8$ could be assigned as the carbon atoms of the NCN units which are shifted to a higher field (compared to **7**). This difference in the presence of NMR shifts between **7** and **11** can be attributed to the paramagnetic nature of the Fe^{2+} ion.

It was found that the homoleptic bis(amidinate) complexes **8**, **9** and **10**, **11** exhibit isotopic molecular structures, respectively. Figure 5 displays the molecular structure of complex **8** as a characteristic example, and similar structural features occur in the other four transition metal bis(amidinate) complexes **9–12** (Figure 7 and Figure 8). Complex **12** shows a similar molecular structure to **11** except that the substituents at the carbon atoms in the NCN units changed from 3-dimethylamino-1-propynyl to cyclopropylacetylene. The additional nitrogen donor group does not contribute to metal coordination.

Complexes **8** and **9** crystallize in the monoclinic space group $C2/c$ with one complex molecule in the asymmetric unit. However, complexes **10** and **11** crystallize in the same space group with one complex molecule and a half *n*-pentane molecule in the asymmetric unit, respectively. Complex **12** crystallizes in the monoclinic space group $P2_1/c$ with one complex molecule in the asymmetric unit. Complexes **8–12** exist as a

four-coordinate, dimeric complex in which transition metal atoms are coordinated by both one η^2 -amidinate ligand and two bridging $\mu, \eta^1: \eta^1$ -amidinate ligands. In complex **8**, the average Fe–N bonds length of bridging amidinate ligands is 2.058(1) Å, which is slightly shorter than that observed in the terminal chelating ligand (2.110(1) Å). In Table 6, the M–N bond lengths in the isotopic molecular structures (complexes **8**, **9**, and **10**, **11**, respectively) are proportional to the atomic radius (Mn > Fe > Co). Comparing the M–N bond lengths in three iron(II) bis(amidinate) complexes **8**, **11**, and **12**, the M–N bond lengths are elongated by the substituent at the nitrogen atoms in the NCN units changed from *isopropyl* to *cyclohexyl* groups [**8**: 2.109(1), 2.058(1) Å; **11**: 2.168(2), 2.063 (2) Å], and shortened by the substituent at the carbon atom in the NCN units changed from 3-dimethylamino-1-propynyl to cyclopropylethynyl [**11**: 2.168(2), 2.063 (2) Å; **12**: 2.099(2), 2.063(3) Å]. Therefore, a bulkier substituent at nitrogen or carbon atoms in the NCN units of the amidinate moiety probably leads to a longer M–N bond lengths. The Fe–N bond lengths in the iron bis(amidinate) complexes **8**, **11**, and **12** are in the range of 2.047(1) to 2.150(2) Å are slightly shorter than that [in the range of 2.065(3) to 2.186(3) Å] in the similar iron bis(amidinate) complex $\text{Fe}_2(\mu\text{-DPhBz})_2(\eta^2\text{-DPhBz})_2$ (DPhBz = diphenylbenzamidinato) [43]. The Mn–N bond lengths in manganese bis(amidinate) complex **10** are in the range of 2.107(2) to 2.195(2) Å, which is similar to another manganese bis(amidinate) complex $\{(\text{CyNCHNCy})\text{Mn}\}_2(\mu\text{-CyNCHNCy})_2$ [2.104(2) to 2.193(2) Å]. In complex **8**, the coordination environment around the iron atoms can be described as a distorted tetrahedral arrangement. The distorted tetrahedral arrangement is characterized by N(1)–Fe–N(3) 104.8(5), N(2')–Fe–N(1) 132.8(1), N(3)–Fe–N(4) 69.9(1), N(4)–Fe–N(2') 105.7(1)°, respectively. Compared to complex **8**, the coordination environments of the metal atoms in **9–12** adopt a similar arrangement as in **8**. The N–M–N angles of the complexes **9–12** are in the range of **9**: 65.0(1) to 131.1(1)°, **10**: 62.1(8) to 125.5(8)°, **11**: 63.5(1) to 127.7(7)°, and **12**: 64.0(1)° to 127.7(7)°, respectively. The narrow range of C–N bond lengths in complexes **8–12** indicates the negative charge delocalization

within the NCN units [**8**: 1.325(2) to 1.333(2), **9**: 1.323(2) to 1.331(2), **10**: 1.325(3) to 1.333(3), **11**: 1.320(2) to 1.337(2), **12**: 1.325(4) to 1.331(4)]. According to the torsion angles [Fe–N(1)–C(1)–N(2) 34.4(2), Fe–N(2)–C(1)–N(1) 34.4(2), Fe'–N(2)–C(1)–N(1) 34.4(2), Fe'–N(1)–C(1)–N(2) 41.8(2), Fe'–N(2)–C(1)–N(1) 41.8(2)^o] in complex **8**, the N–C–N backbones of bridging amidinate ligands are not coplanar with the two metal centers (the same structural features occur in complexes **9–12**). It is severely skewed to allow the distortion necessary to accommodate the long intermetallic distance.

Table 6. Selected bond lengths [Å] for bis(amidinate) transition metal complexes **8–12** [$M_2\{\mu\text{-}c\text{-}C_3H_5\text{-}C\equiv C\text{-}C(NR)_2\}_2\{\eta^2\text{-}c\text{-}C_3H_5\text{-}C\equiv C\text{-}C(NR)_2\}_2$] (**8**: M = Fe, R = ⁱPr; **9**: M = Co, R = ⁱPr; **10**: M = Mn, R = Cy; **11**: M = Fe, R = Cy), [$Fe_2\{\mu\text{-}(CH_3)_2N\text{-}CH_2\text{-}C\equiv C\text{-}C(NCy)_2\}_2\{\eta^2\text{-}(CH_3)_2N\text{-}CH_2\text{-}C\equiv C\text{-}C(NCy)_2\}_2$] (**12**).

Bond lengths [Å]	8	9	10	11	12
M–N (ave. η^2 -amidinate ^a)	2.109(1)	2.079(1)	2.168(2)	2.128(2)	2.099(2)
M–N (ave. μ -amidinate ^b)	2.058(1)	2.026(1)	2.139(2)	2.063(2)	2.063(3)

^aAverage M–N bond lengths of two amidinates in chelating coordination. ^bAverage M–N bond lengths of two amidinates in bridging coordination.

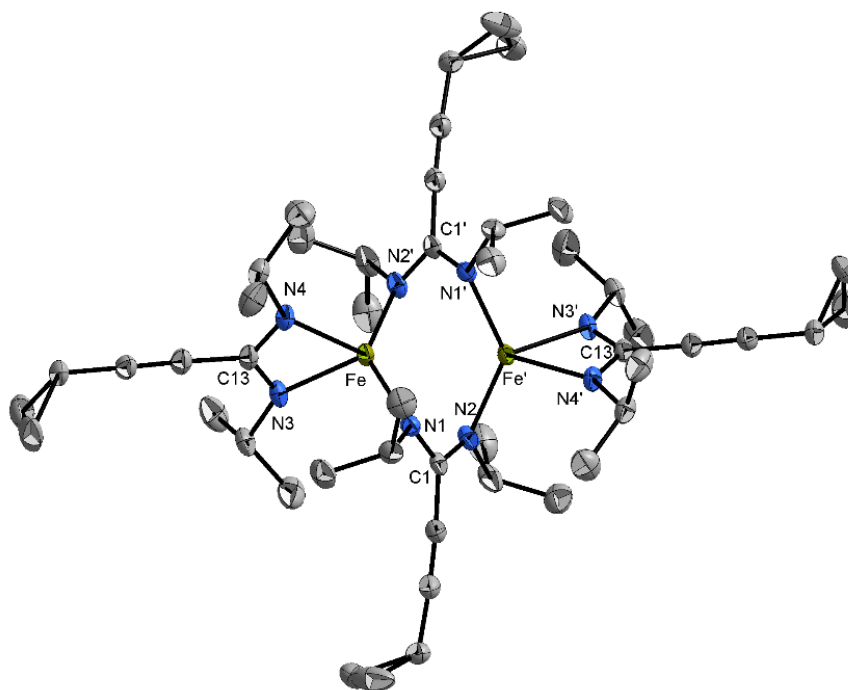


Figure 5. Molecular structure of $[\text{Fe}_2\{\mu\text{-}c\text{-C}_3\text{H}_5\text{-C}\equiv\text{C-C}(\text{N}^i\text{Pr})_2\}_2\{\eta^2\text{-}c\text{-C}_3\text{H}_5\text{-C}\equiv\text{C-C}(\text{N}^i\text{Pr})_2\}_2]$ (**8**) in the crystalline state. Thermal ellipsoids with 50% probability, H atoms omitted for clarity.

The Fe...N interaction at a distance of 2.949(1) Å (Fe–N2 and Fe'–N2') shown in Figure 6 is too long to be considered as a fully bonded interaction but too short to be just a van der Waals interaction. The existence of the longest bond length of up to 290 pm (C–C) was claimed in a dimer of two tetracyanoethylene dianions [121, 122]. The relatively long Fe–Fe distance of 3.001(6) Å in **8** as compared to 2.462(2) Å found in the $\text{Fe}_2(\mu\text{-DPhF})_4$, DPhF = [(phenyl)-NC(H)N(phenyl)], indicates that there is no Fe–Fe bond formation in this dimer. A similar observation (3.124(1) Å) was also made in the analogous iron bis(amidinate) complex $\text{Fe}_2(\mu\text{-DPhBz})_2(\eta^2\text{-DPhBz})_2$ (DPhBz = diphenylbenzamidinato) [43]. Similarity, the nonbonded M–M distances in the complexes **9–12** are also rather long and outside the bonding range [**9**: 3.057(4), **10**: 3.161(5), **11**: 3.072(6), **12**: 2.939(1) Å]. The absence of a long Mn–Mn distance in **10** is typical and also appeared in previously published manganese bis(amidinate) complexes such as $[\{(\text{CyNCHNCy})\text{Mn}\}_2(\mu\text{-CyNCHNCy})_2]$ (3.170(6) Å) [59].

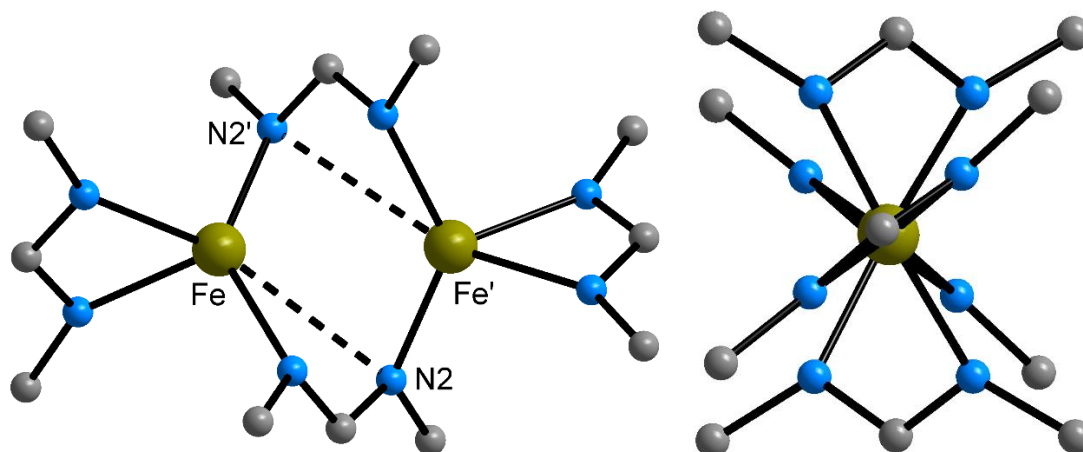


Figure 6. Representation of the coordination spheres of the Fe atoms in complex **8**: viewed perpendicularly to the Fe–Fe vector (left) and viewed along the Fe–Fe vector (right).

Metal amidinate complexes in the oxidation state +2 occur in either monomeric or dimeric form. Normally, metals with smaller ionic radii (Co, Ni) are monomeric. Larger metals (Fe, Mn) give monomeric structures only with the bulkier *tert*-butyl-substituted amidinates, while the less bulky *isopropyl*-substituted amidinates formed dimers (compared to the *tert*-butyl substituents, cyclohexyl-substituted amidinate is less bulky) [60]. However, the molecular structure of cobalt bis(amidinate) complex **9** (Figure 7), $[\text{Co}_2\{\mu\text{-}i\text{-C}_3\text{H}_5\text{-C}\equiv\text{C-C}(\text{N}^i\text{Pr})_2\}_2\{\eta^2\text{-}i\text{-C}_3\text{H}_5\text{-C}\equiv\text{C-C}(\text{N}^i\text{Pr})_2\}_2]$, was observed as a dimeric form. Compared to the previously published monomeric cobalt amidinate complex, $[\text{Co}(^i\text{Pr-MeAMD})_2]$ (AMD = acetamidinato), the substituents (methyl group) at the carbon atoms in the NCN units were less bulky than that of **9** (cyclopropylethynyl group). It seems like the carbon atom substituents in the NCN unit also have a steric influence on the structures of the resulting metal compounds. Bulkier substituents at carbon atom in the NCN units hinder the formation of the monomeric structures, but bulkier substituents at the nitrogen atoms in the NCN units promote it.

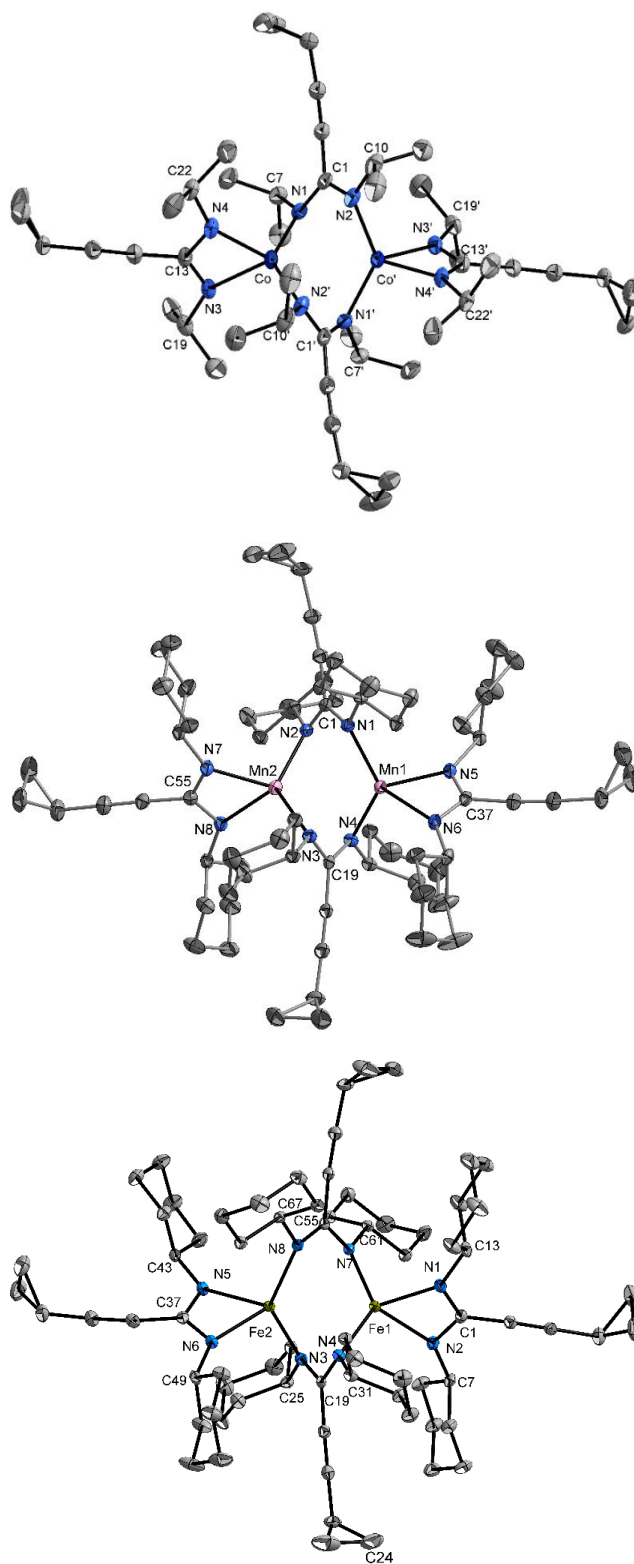


Figure 7. Molecular structures of $[M_2\{\mu\text{-}c\text{-}C_3H_5\text{-}C\equiv C\text{-}C(NR)_2\}_2\{\eta^2\text{-}c\text{-}C_3H_5\text{-}C\equiv C\text{-}C(NR)_2\}_2]$ (**9**: M = Co, R = *i*Pr; **10**: M = Mn, R = Cy; **11**: M = Fe, R = Cy) in the crystalline state. Thermal ellipsoids with 50% probability, H atoms omitted for clarity.

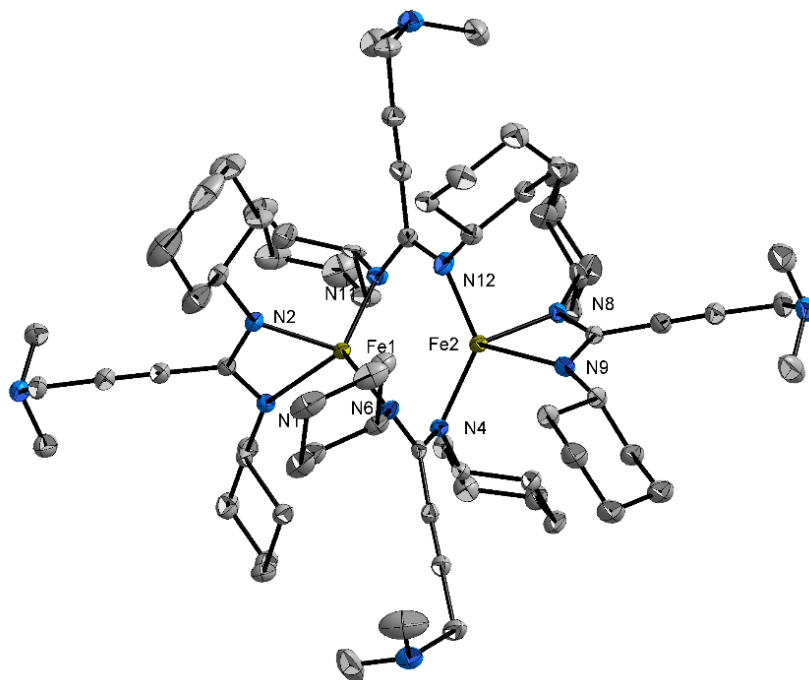


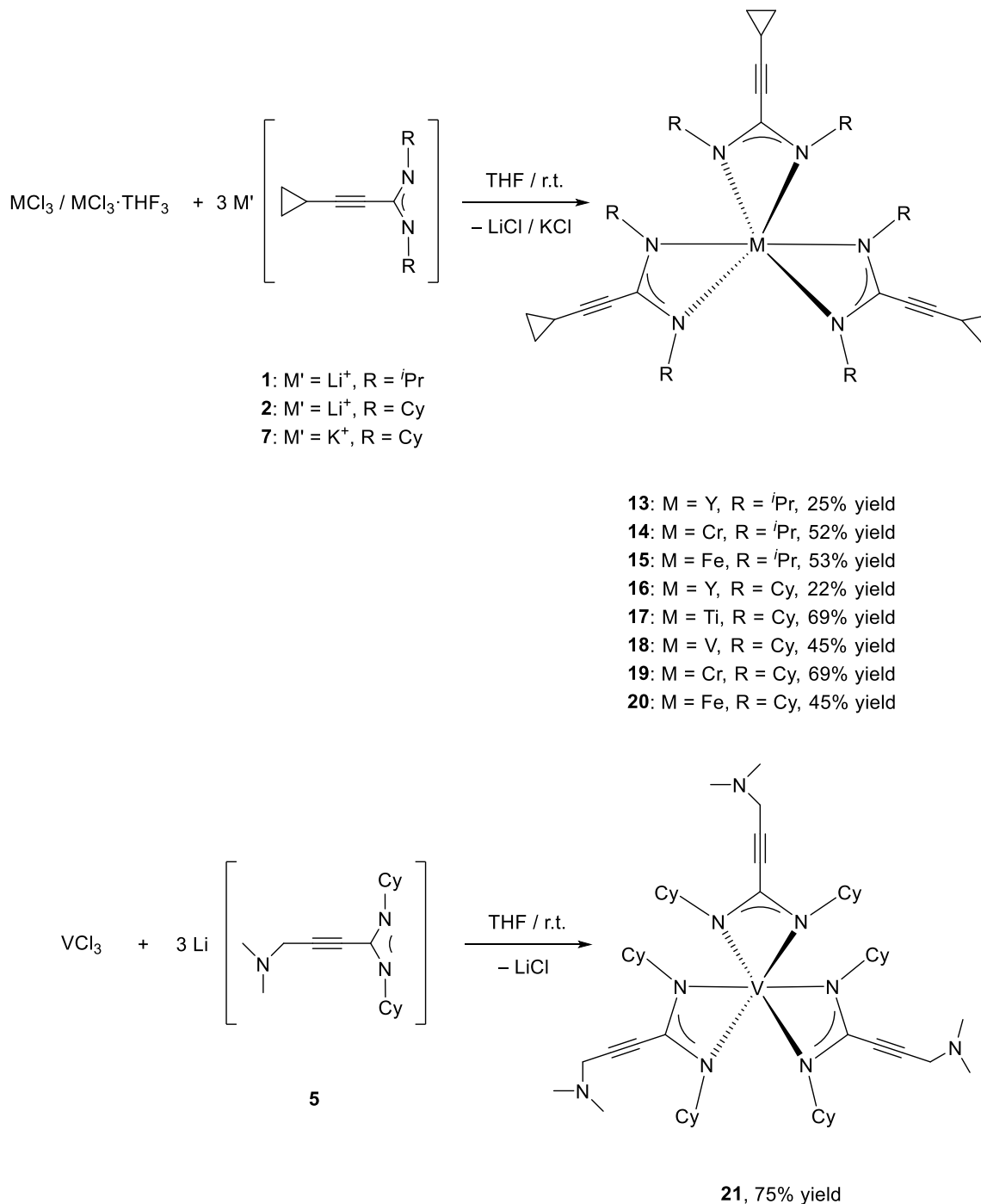
Figure 8. Molecular structure of $[\text{Fe}_2\{\mu\text{-(CH}_3)_2\text{N-CH}_2\text{-C}\equiv\text{C-C(NCy)}_2\}_2\{\eta^2\text{-(CH}_3)_2\text{N-CH}_2\text{-C}\equiv\text{C-C(NCy)}_2\}_2]$ (**12**) in the crystalline state. Thermal ellipsoids with 50% probability, H atoms omitted for clarity.

2.4. Synthesis and structural characterization of transition metal tris(amidinate) complexes

Bidentate amidinate ligands provide volatile, thermally stable, homoleptic compounds with a wide range of transition metals with oxidation states of 1, 2 and 3, which were found reactive enough to be used as vapor sources for the ALD of pure transition metal films [60]. After a series of dinuclear complexes were successfully synthesized in the previous section, the study of transition metal tris(amidinate) complexes is a continuous interest in this Ph.D. work. In the course of this work, the propensity of these amidinate ligands to form tris-chelated species has been noted repeatedly despite the resulting seemingly formidable steric crowding and formation of relatively strained four-membered rings.

Scheme 16 illustrate the the reactions of anhydrous transition metal halides MCl_3 ($M = Y, Cr$ and Fe) and solvated transition metal halides $MCl_3 \cdot S_3$ ($M = Ti$ and $V, S = THF$) with three equivalents of lithium or potassium amidinates **1**, **2**, **5** and **7**, $Li[c-C_3H_5-C\equiv C-C(NR)_2] \cdot THF$ (**1**: $R = iPr$, **2**: $R = Cy$), $Li[(CH_3)_2N-CH_2-C\equiv C-C(NCy)_2] \cdot THF$ (**5**), and $K[c-C_3H_5-C\equiv C-C(NCy)_2] \cdot THF$ (**7**), respectively. The reactions were carried out in THF and stirred at room temperature to obtain a series of *isopropyl*- or *cyclohexyl*-substituted homoleptic transition metal tris(cyclopropylethynylamidinate) complexes, $[M\{c-C_3H_5-C\equiv C-C(N^iPr)_2\}_3]$ (**13**: $M = Y$, **14**: $M = Cr$ **15**: $M = Fe$), $[M\{c-C_3H_5-C\equiv C-C(NCy)_2\}_3]$ (**16**: $M = Y$, **17**: $M = Ti$, **18**: $M = V$, **19**: $M = Cr$, **20**: $M = Fe$), and a vanadium(III) tris(dimethylaminopropynylamidinate) complex $V[\{(CH_3)_2N-CH_2-C\equiv C-C(NCy)_2\}_3]$ (**21**). The products **13–21** were isolated from *n*-pentane solution as unsolvated, exceedingly air- and moisture-sensitive complexes (yttrium(III) and iron(III) tris(amidinate) complexes **13**, **15**, **16**, and **20** are only moisture-sensitive) in the form of block-like (**13–15**, and **17–20**) or plate-like (**16**) colored crystals (**13**: colorless, **14**: pale pink, **15**: black, **16**: colorless, **17**: black, **18**: red, **19**: brown, **20**: blue, **21**: brown).

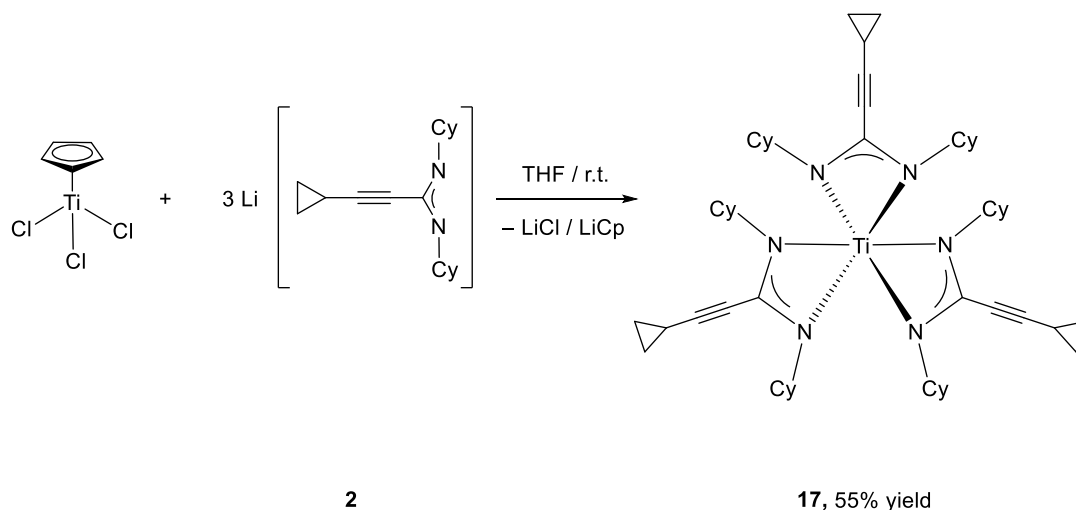
Complexes **13–20** were isolated in low yields of 22–25% to moderate yields of 45–53%, while the yield of **21** is very good at 75%.



Scheme 16. Synthesis of transition metal tris(cyclopropylethynylamidinate) complexes **13–21**.

It is worth mentioning that the first-row transition metal halides scandium(III) chloride was also used as starting material in this series of studies. Unfortunately, the data quality did not allow a full structure refinement. Therefore, the halide of yttrium as a heavier homolog of scandium was used as starting material, and two complexes **13**, and **16** were successfully obtained. The molecular structures of the trivalent transition metal amidinate complexes **12–21** were determined by single-crystal X-ray diffraction and fully characterized by NMR, IR, and MS, as well as elemental analyses.

The synthesis method of complex **17** requires some comment, **17** can also be carried out by a different reaction, as shown in Scheme 17. Complex **17** was prepared in THF by the treatment of trichloro(cyclopentadienyl)-titanium(IV) and lithium amidinate **2** in a 1:3 molar ratio. The THF solution was stirred for 3 hours at room temperature, and the resulting dark red reaction mixture was dried in vacuum. The residue was extracted with *n*-pentane (20 mL) to give a clear, deep red solution. Black block-like crystals were obtained at $-30\text{ }^{\circ}\text{C}$ after 5 days. By changing to the starting material trichloro(cyclopentadienyl)titanium(IV), the yield decreased slightly from 69% to 55%.



Scheme 17. Reaction of trichloro(cyclopentadienyl)titanium(IV) with lithium cyclopropylethynylamidinate **2**.

The IR spectra of complexes **13–21** showed medium bands at 2221–2219 cm^{-1} , which can be assigned to the $\text{C}\equiv\text{C}$ stretching vibration [103]. Characteristic antisymmetric valence vibration attributable to the $\text{C}=\text{N}$ bond in the NCN units were observed in the range of 1598–1647 cm^{-1} as medium bands [110]. Also notable is that the complexes **13–15** with *isopropyl* substituents at the nitrogen atoms in the NCN units are always showing one strong and two medium intensity bands in the range of 2863–2867 (m) and 2926–2929 (m), as well as 2958–2965(s) cm^{-1} , which could be assigned to the C–H valence vibrations of the *isopropyl* substituents. Meanwhile, the IR spectra of the complexes **16–21** with cyclohexyl groups at the nitrogen atoms in the NCN units are always showing one very strong and one strong band in the range of 2848–2849 (s) and 2921–2924 (vs) cm^{-1} , respectively, which are attributable to the C–H valence vibrations of the cyclohexyl groups. Compared to the IR spectrum of lithium amidinate **5** (2791 m cm^{-1}), a medium band at 2823 (m) cm^{-1} could be assigned to the C–H bond stretching vibration in the Me_2N unit in the IR spectrum of **21**. Elemental analysis values for C, H, and N of complexes **13–21** were in good agreement with the proposed formulation. The molecular ion peaks of complexes **16** and **21** were observed in the EI mass spectra, whereas the other complex showed only fragments. In the mass spectrum of **13**, the peak observed at m/z 274 can be assigned to the molecule ion fragment $[M - 2(c\text{-C}_3\text{H}_5\text{-C}\equiv\text{C}) - 6^i\text{Pr}]^+$. The peaks at m/z **15**: 433, **18**: 667 in the mass spectra of complexes **15** and **18** can be assigned to the molecule ion without three cyclopropylethynyl groups $[M - 3(c\text{-C}_3\text{H}_5\text{-C}\equiv\text{C})]^+$. The peak observed at m/z 612 of complex **17** can be attributed to the molecular ion misses three cyclohexyl groups $[M - 3\text{Cy}]^+$. The peak at m/z 433 (**14**) and 593 (**19**) could be attributed to the molecular ion without a cyclopropylamidinate unit $[M - \{c\text{-C}_3\text{H}_5\text{-C}\equiv\text{C-C}(\text{NR})_2\}]^+$ (**14**: R = *i*Pr; **19**: R = Cy). The mass spectrum of **20** showed a peak at 831 $[M - c\text{-C}_3\text{H}_5]^+$, which can be assigned to the molecular ion without a cyclopropyl group.

Most of the transition metal tris(amidinate) complexes reported in this Ph.D. work are paramagnetic (except the yttrium(III) complexes **13** and **16**), and full interpretation of the NMR spectra is complicated. The NMR spectra of **13** and **16** are in good agreement with that of **1** and **2**. THF ligand signals are missing in the NMR spectra of **13** and **16**, which is consistent with the molecular structures. In Figure 9, the signals corresponding to the protons of cyclopropyl were observed at $\delta = 0.74$ and 0.89 ppm (CH_2 , $c-C_3H_5$) and $\delta = 1.45$ ppm (CH , $c-C_3H_5$) which are shifted to a lower field compared to that of **1** [$\delta = 0.65$ and 0.74 ppm (CH_2 , $c-C_3H_5$) and $\delta = 1.36$ ppm (CH , $c-C_3H_5$)]. However, the signals of protons ($CH(CH_3)_2$) of *isopropyl* were observed at $\delta = 3.63$ ppm, which is shifted to a higher field (**1**: $\delta = 3.77$). Despite the paramagnetic nature of the transition metal ions, while the NMR spectra of the complexes **14**, **15**, **17** and **19** were measured and discussed. Deuterated tetrahydrofuran was found to be a suitable solvent for measuring the NMR spectra of these homoleptic complexes. The 1H NMR spectrum of complexes **14**, **15**, and **19** could not be analyzed, and that of complex **17** showed resonances in a region 0 to 3 ppm and displayed several resolved signals. The signal of protons (CH_2 , Cy) of the cyclohexyl groups of amidinate ligand appeared in the range of 1.01–1.89 ppm, whereas the signal corresponding to the protons (CH , Cy) was not observed. The signal of protons (CH and CH_2) of the cyclopropyl groups were observed at $\delta = 1.35$ ppm as overlapped resonances and at $\delta = 0.68$ and 0.83 ppm (CH_2 , $c-C_3H_5$) as multiplet. The ^{13}C NMR spectra of complexes **14**, **15**, **17**, and **19** are collected in Table 7. The signal corresponding to the carbon atoms of the NCN unit was only observed in complex **14** ($\delta = 139.6$ ppm) and was shifted to a higher field compared to lithium amidinate ligand **1**. The signals corresponding to the carbon atoms bearing amidinate ligand ($C\equiv C-C$) found for **14** ($\delta = 67.1$) and **17** ($\delta = 65.0$ ppm) were not observed in complexes **15** and **19**, and the signal corresponding to the carbon atoms (CH , Cy) was only observed in complex **19**.

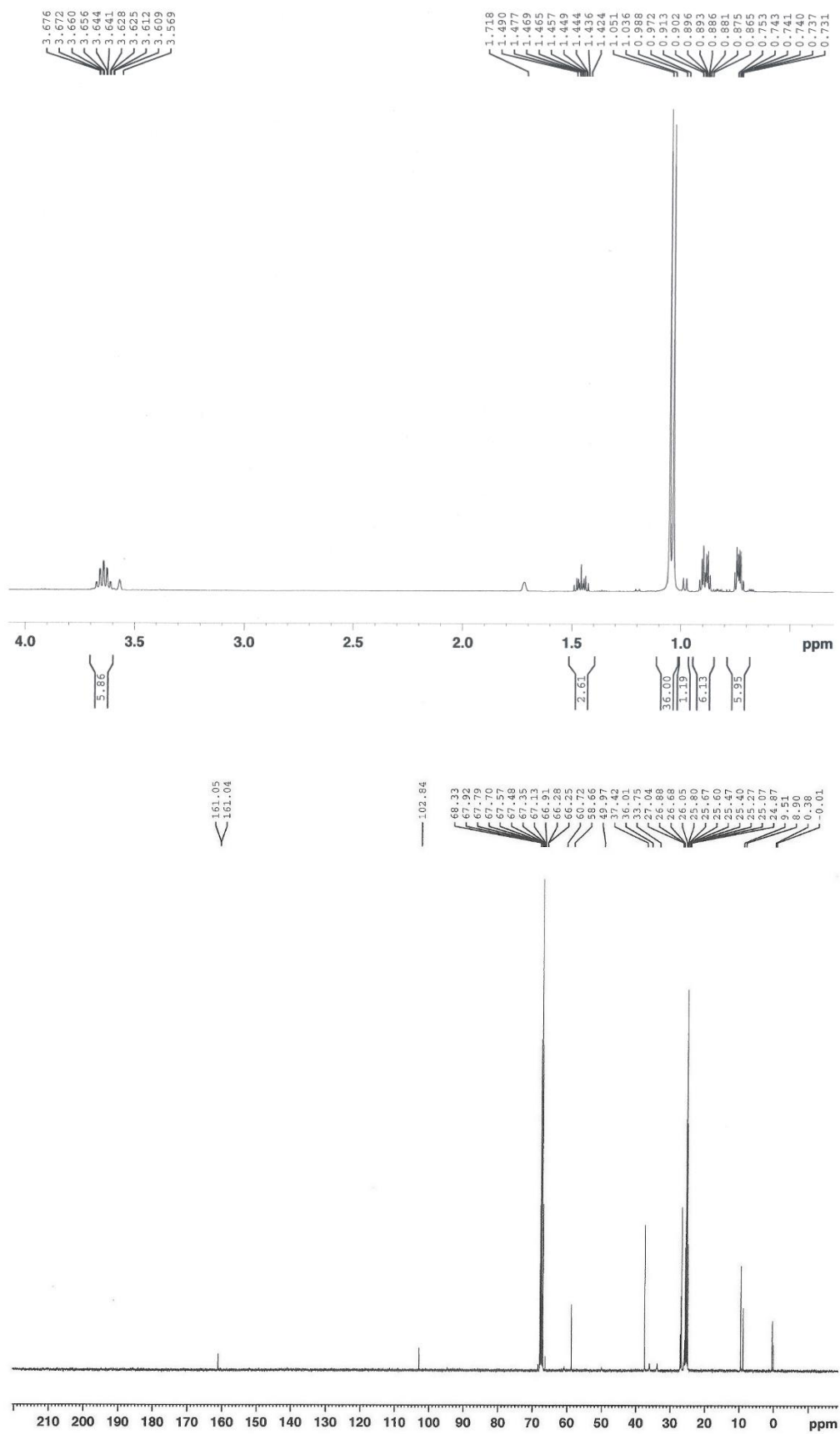


Figure 9. NMR spectrum (400 MHz, THF-*d*₈, 25 °C) of **13**.

Table 7. ^{13}C NMR data of the complexes $[\text{M}\{c\text{-C}_3\text{H}_5\text{-C}\equiv\text{C-C}(\text{NR})_2\}_3]$ **14**: M = Cr, R = ^iPr ; **15**: M = Fe, R = ^iPr ; **17**: M = Ti, R = Cy; **19**: M = Cr, R = Cy;).

Comp. δ (ppm)	14	15	17	19
CH, $c\text{-C}_3\text{H}_5$	-0.9	0.0	0.0	0.0
CH ₂ , $c\text{-C}_3\text{H}_5$	8.9	8.8	8.9	8.9
CH-C \equiv C	93.6	90.9, 105.1	94.8	95.0
C \equiv C-C	67.1	-	65.0	-
CH, ^iPr	42.2, 52.9	49.0	-	-
CH ₃ , ^iPr	25.3, 22.9	24.5	-	-
CH, Cy	-	-	-	50.5, 60.8
CH ₂ , Cy	-	-	27.6, 24.2, 28.1	26.3, 33.8, 35.9
NCN	139.6	-	-	-

It was found that all nine homoleptic transition metal tris(amidinate) complexes **13–21** exhibit very similar molecular structures. The molecular structure of the complex **13**, $[\text{Y}\{c\text{-C}_3\text{H}_5\text{-C}\equiv\text{C-C}(\text{N}^i\text{Pr})_2\}_3]$, is shown in Figure 11 as a characteristic example of the complexes **13–15** which have *isopropyl* substituents at the nitrogen atoms in the NCN unit of the amidinate ligands. An illustration of the complexes **14** and **15** (Figure 11) shows a high degree of structural similarity to complex **13**.

Complexes **13**, **14**, and **15** crystallized from *n*-pentane in the triclinic space group $P\bar{1}$ with one complex molecule in the asymmetric unit, respectively. In complex **13**, the central Y^{3+} ion is coordinated by three chelating cyclopropylethynylamidinate ligands $[c\text{-C}_3\text{H}_5\text{-C}\equiv\text{C-C}(\text{N}^i\text{Pr})_2]$ in a distorted octahedral fashion, and the N–Y–N bond angles are in the range of 57.5(9) to 154.2(9)°. The coordination environment of **14**, and **15** adopts a similar arrangement as in **13**, while the N–M–N bond angles (**14**: M = Cr, **15**: M = Fe) are in the range of 64.5(6) to 163.9(7) and 63.5(6) to 162.7(6)°, respectively.

The effective shielding of the central metal atom by six *isopropyl* groups prevents the coordination of additional solvent molecules [103]. In complexes **13–15**, the three groups of four-membered rings MNCN (**13**: M = Y, **14**: M = Cr, **15**: M = Fe) are essentially planar with the central metal atom (torsion angles **13**: $-0.9(2)$ to $-2.5(2)^\circ$, **14**: $-2.6(1)$ to $3.0(1)^\circ$, **15**: $-1.4(1)$ to $3.0(1)^\circ$). As shown in Table 8, the Y–N bond lengths are in a very narrow range of 2.346(3) to 2.380(3) Å, while the Cr–N and Fe–N bond lengths are in the range of 2.039(2) to 2.088(2) and 2.068(2) to 2.125(2) Å, respectively. These values are in good agreement with those of previously reported tris(amidinate) complexes, e.g., Y[(Ph–C≡C–C(N^{*i*}Pr)₂)₃], M(DPhF)₃, and M(DtolF)₃ (M = Cr, Fe) [123, 124]. However, yttrium is similar to the lanthanide elements in nature. These the average Ho–N bond length of the complex [Ho{*c*-C₃H₅–C≡C–C(N^{*i*}Pr)₂}₃] is 2.356 Å is also consistent with that of **13** [22]. The average N–C–N angles of complexes **13–15** are 116.7(3)°, 113.1(2)°, and 113.9(2)°, respectively. The M–N bond length of complex **13** is longer than **14** and **15**, while the average N–C–N angle of **13** is also larger than that of **14** and **15**. Therefore, the trend of shorter metal-ligand bond lengths associated with smaller chelating angles is qualitatively evident here [123]. The C–N bond lengths within the chelating N–C–N unit of complexes **13–15** are essentially equal and their average values are 1.330(4), 1.324(3), and 1.327(3) Å, respectively. The equal bond lengths confirm the existence of the negative charge delocalization in the NCN units.

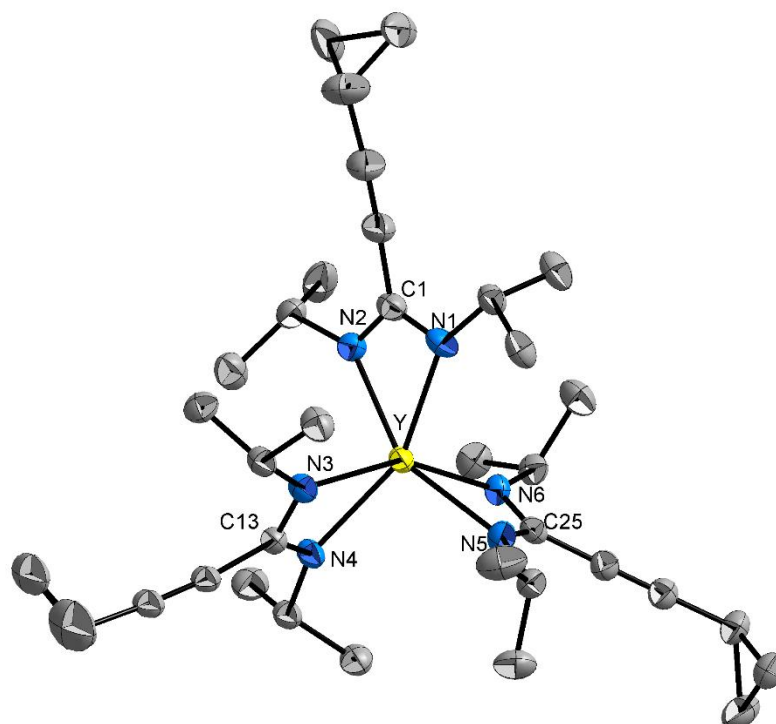


Figure 10. Molecular structure of $[Y\{c\text{-}C_3H_5\text{-}C\equiv C\text{-}C(N^iPr)_2\}_3]$ (**13**) in the crystalline state. Thermal ellipsoids with 50% probability, H atoms omitted for clarity.

Table 8. Selected bond lengths [\AA] and angles [$^\circ$] for compounds **13–15** $[M\{c\text{-}C_3H_5\text{-}C\equiv C\text{-}C(N^iPr)_2\}_3]$ **13**: $M = Y$, **14**: $M = Cr$, **15**: $M = Fe$.

Compound	13	14	15
Bond lengths and angles			
M–N(1)	2.346(3)	2.068(2)	2.119(2)
M–N(2)	2.358(3)	2.074(2)	2.107(2)
M–N(3) ^a	2.336(3)	2.039(2)	2.125(2)
M–N(4) ^a	2.380(3)	2.088(2)	2.068(2)
M–N(5) ^a	2.341(3)	2.045(2)	2.114(2)
M–N(6) ^a	2.340(3)	2.078(2)	2.093(2)
N–C–N (avg) ^b	116.7(3)	113.1(2)	113.9(2)

^aFor better comparison, the atom labels of **14** and **15** are consistent with **13** in Table 8. ^bAverage values for bond lengths and angles refer to the statistical weighted means of the corresponding prior values.

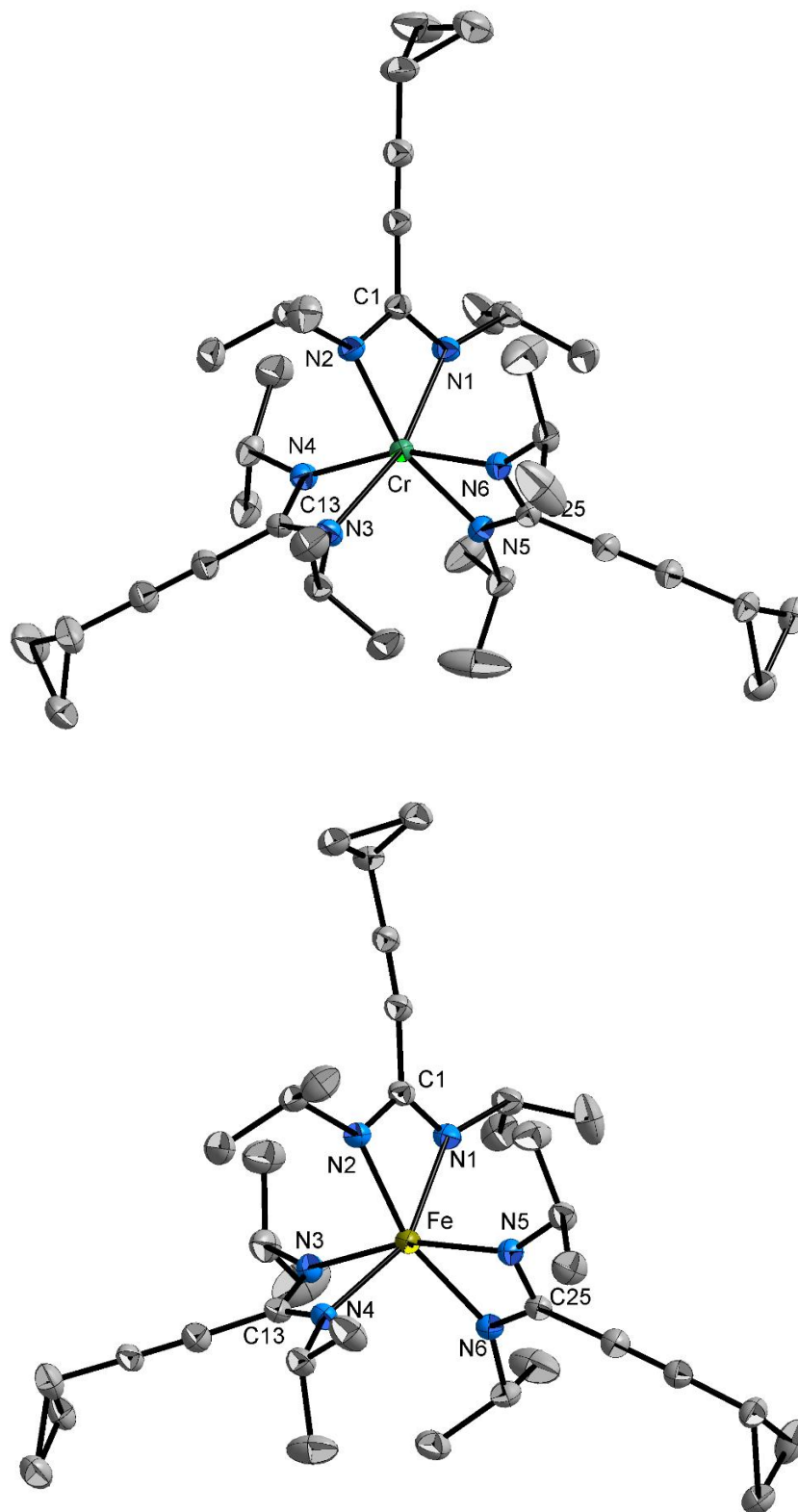


Figure 11. Molecular structures of $[\text{Cr}\{c\text{-C}_3\text{H}_5\text{-C}\equiv\text{C-C}(\text{N}^i\text{Pr})_2\}_3]$ (**14**) and $[\text{Fe}\{c\text{-C}_3\text{H}_5\text{-C}\equiv\text{C-C}(\text{N}^i\text{Pr})_2\}_3]$ (**15**) in the crystalline state. Thermal ellipsoids with 50% probability, H atoms omitted for clarity.

Table 9. N–M–N bond angles (°) for complexes **13–16**, **19** and **20** [M{*c*-C₃H₅–C≡C–C(N^{*i*}Pr)₂}₃] **13**: M = Y, **14**: M = Cr, **15**: M = Fe, [M{*c*-C₃H₅–C≡C–C(NCy)₂}₃] **16**: M = Y, **19**: M = Cr, **20**: M = Fe.

Compound Bond angles	13	14	15	16	19	20
N(1)–M–N(2)	57.5(9)	64.5(6)	63.5(6)	57.3(1)	64.9(7)	63.9(7)
N(1)–M–N(3) ^a	103.2(9)	105.5(7)	99.4(7)	104.7(1)	102.4(8)	101.2(8)
N(1)–M–N(4) ^a	155.0(9)	163.9(7)	154.6(7)	152.8(1)	162.9(8)	159.3(8)
N(1)–M–N(5) ^a	101.8(9)	100.1(7)	103.9(7)	106.9(1)	102.2(8)	103.3(8)
N(1)–M–N(6) ^a	100.6(1)	92.1(7)	93.5(6)	97.3(1)	93.5(8)	96.2(8)
N(2)–M–N(3) ^a	97.1(8)	91.6(6)	92.9(6)	95.2(1)	92.2(8)	93.5(8)
N(2)–M–N(4) ^a	106.2(8)	101.8(7)	96.9(7)	101.0(1)	103.1(8)	101.9(7)
N(2)–M–N(5) ^a	152.2(1)	161.9(7)	162.5(6)	155.3(1)	162.2(8)	160.2(8)
N(2)–M–N(6) ^a	104.3(9)	104.6(7)	103.1(6)	102.7(9)	102.4(8)	101.3(8)
N(3)–M–N(4) ^a	57.3(8)	64.7(7)	63.9(6)	57.8(1)	64.7(7)	63.3(7)
N(3)–M–N(5) ^a	106.6(9)	102.2(6)	101.5(7)	108.2(1)	102.9(8)	104.2(8)
N(3)–M–N(6) ^a	154.2(9)	160.1(7)	162.7(6)	157.1(1)	161.9(8)	160.9(8)
N(4)–M–N(5) ^a	99.1(9)	94.7(7)	98.4(7)	99.1(1)	91.9(8)	94.1(8)
N(4)–M–N(6) ^a	102.2(9)	100.1(7)	107.2(7)	104.1(1)	101.3(8)	101.5(8)
N(5)–M–N(6) ^a	57.9(9)	64.8(7)	63.9(6)	57.8(9)	64.8(8)	63.7(8)

^aFor better comparison, the atom labels of **14** to **20** are consistent with **13** in Table 9.

The molecular structure of the complex **16**, [Y{*c*-C₃H₅–C≡C–C(NCy)₂}₃], shown in Figure 12, is a characteristic example of the complexes **16–20** with cyclohexyl groups at the nitrogen atoms in the NCN unit. The molecular structures of complexes **17–20** together with the atom labeling are shown in Figure 14. The crystal structure of vanadium(III) tris(dimethylaminopropynylamidinate) complex **21** contains four symmetry-independent molecules together in the asymmetric unit, and only one

position is shown in Figure 14 for clarity. However, the poor quality and insufficient X-ray analyses data of **21** cannot afford more details about the structure features.

The complexes **16–20** crystallize in the monoclinic space group $P2_1/c$ with one complex molecule in the asymmetric unit, respectively. For the complexes **16–20** with cyclohexyl substituents, the same conclusion can be drawn that the central atoms M^{3+} (**16**: $M = Y$, **17**: $M = Ti$, **18**: $M = V$, **19**: $M = Cr$, **20**: $M = Fe$) are in a distorted octahedral fashion. Table 9 lists the N–M–N bond angles of complexes **13–20**, which should have values of either 90 or 180° in an ideal octahedral arrangement. Selected bond lengths and angles of complexes **17** and **18** are summarized in Table 37 and Table 39, which will not be repeated here. Compared to the N–M–N bond angles of the yttrium tris(amidinate) complex **13** in Table 9, only minor differences are found in the N–M–N bond angles between them [**13**: 57.3(8) to 155.0(9), **16**: 57.3(1) to 157.1(1)°]. Therefore, the substituents (**13**: iPr and **16**: Cy) at the nitrogen atoms of complexes **13** and **16** do not influence the N–M–N bonds angles. The same conclusion can be drawn for the chromium tris(amidinate) complexes (**14**: iPr and **19**: Cy) and iron tris(amidinate) complexes (**15**: iPr and **20**: Cy), suggesting that different substituents (Cy and iPr) at the nitrogen atoms of NCN unit do not affect the molecular structure of tris-(amidinate) transition metal complexes. The molecule is formally distorted from octahedral toward trigonal prismatic coordination with dihedral angles of (**16**: 84.5 to 87.5, **17**: 84.4 to 88.3, **18**: 88.1 to 88.5, **19**: 89.1 to 89.2, **20**: 84.5 to 87.5°) between NMN planes (**16**: $M = Y$, **17**: $M = Ti$, **18**: $M = V$, **19**: $M = Cr$, **20**: $M = Fe$).

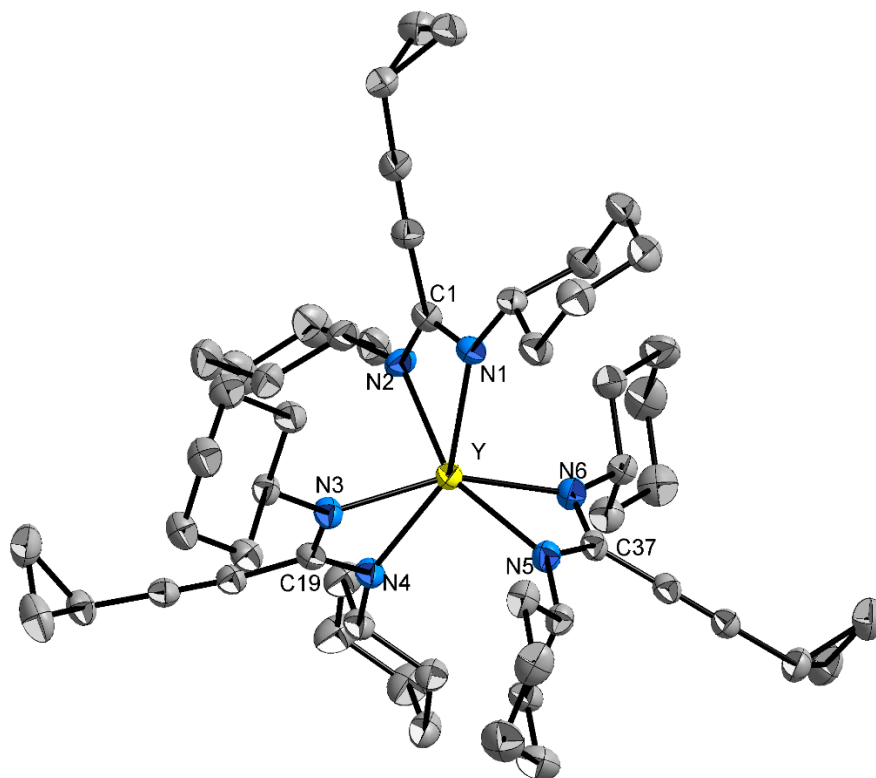


Figure 12. Molecular structure of $[Y\{c\text{-C}_3\text{H}_5\text{-C}\equiv\text{C-C}(\text{NCy})_2\}_3]$ (**16**) in the crystalline state. Thermal ellipsoids with 50% probability, H atoms omitted for clarity.

In Table 10, the average M–N bond lengths and chelating angles for the NCN unit of complexes **16**, **19**, and **20** are essentially identical to those found in complexes **13**, **14**, and **15**. Meanwhile, complexes **16–20** with cyclohexyl substituents at the nitrogen atoms in the NCN unit of amidinate ligands show similar behavior. The amidinate ligands are further removed from the metal center, while the angle is permitted to expand [123]. Therefore, the change in the substituent from *isopropyl* to cyclohexyl groups would not be expected to change the molecular structure and the electronic properties of the ligand in a significant manner. Similarly, the mean Ti–N and V–N bond lengths and the bite angle of the chelating η^2 -amidinate ligand are in good agreement with those of previously reported tris(amidinate) complexes, e.g. $[\text{Ti}(\text{Pr-MeAMD})_3]$ and $[\text{V}(\text{Pr-MeAMD})_3]$ [60]. The narrow range of C–N bond lengths in complexes **16–20** indicates electron delocalization in the NCN framework, which is consistent with that of complexes **13–15** [**16**: 1.319(4) to 1.341(4), **17**: 1.316(4) to

1.331(4), **18**: 1.325(4) to 1.342(4), **19**: 1.318(3) to 1.330(3), **20**: 1.324(3) to 1.331(3) Å].

Table 10. Selected bond lengths [Å] and angles [°] for compounds **16–20**.

	16	17	18	19	20
M–N(1) ^a	2.330(3)	2.166(3)	2.063(2)	2.051(2)	2.069(2)
M–N(2) ^a	2.368(3)	2.105(3)	2.094(2)	2.066(2)	2.135(2)
M–N(3) ^a	2.349(3)	2.105(3)	2.100(2)	2.061(2)	2.106(2)
M–N(4) ^a	2.350(3)	2.130(3)	2.099(2)	2.067(2)	2.117(2)
M–N(5) ^a	2.348(3)	2.118(3)	2.109(2)	2.073(2)	2.107(2)
M–N(6) ^a	2.345(3)	2.152(3)	2.060(2)	2.049(2)	2.107(2)
M–N (avg) ^b	2.348(3)	2.129(3)	2.088(2)	2.061(2)	2.107(2)
N–C–N (avg) ^b	116.5(3)	114.4(3)	113.1(2)	112.9(2)	113.5(2)

^aFor better comparison, the atom labels of **16** to **20** are consistent with **16** in Table 10. ^bAverage values for bond distances and angles refer to the statistical weighted means of the corresponding prior values.

Figure 13 shows a plot of the trend in metal-nitrogen bond lengths in M(III) tris(cyclopropylethynylamidinate) complexes (**17**: M = Ti, **18**: M = V, **14** and **19**: M = Cr, **15** and **20**: M = Fe) proceeding across the first transition series. It is found that the d⁵ system of iron(III) complexes **15** and **20** have longer metal-nitrogen bond lengths than those of chromium(III) and vanadium(III) complexes **14**, **18**, and **19**, respectively. The reason can be attributed to the absence of crystal field stabilization energy (CFSE) for the high-spin electronic configuration. This result is consistent with the previously published trend in metal-nitrogen bond lengths in M(III) tris(chelated) formamidinato complexes [123].

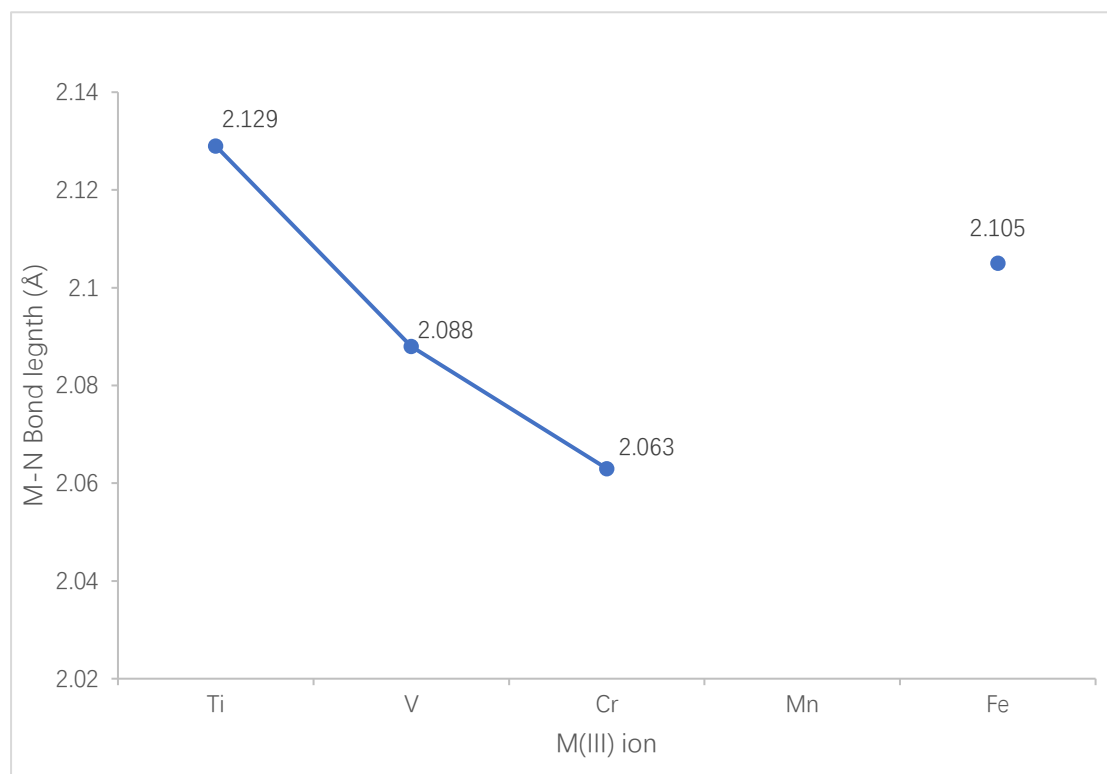


Figure 13. Plot of the trend in metal-nitrogen bond lengths in M(III) tris(cyclopropylethynylamidinate) complexes (**17**: M = Ti, **18**: M = V, **14** and **19**: M = Cr, **15** and **20**: M = Fe) proceeding across the first transition series.

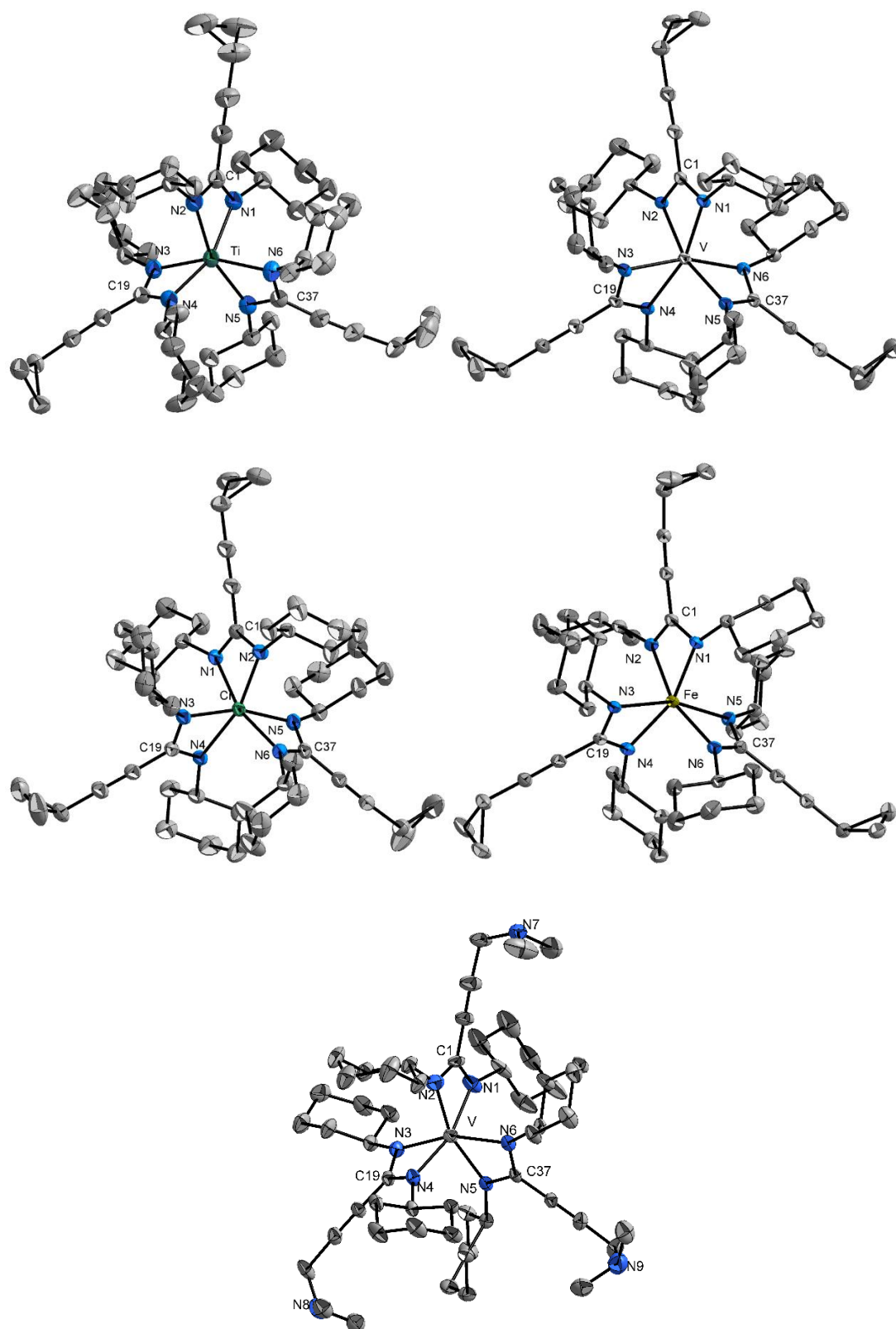


Figure 14. Molecular structures of $[M\{c\text{-C}_3\text{H}_5\text{-C}\equiv\text{C-C}(\text{NCy})_2\}_3]$ (**17**: $M = \text{Ti}$, **18**: $M = \text{V}$, **19**: $M = \text{Cr}$, **20**: $M = \text{Fe}$) and $\text{V}\{[(\text{CH}_3)_2\text{N-CH}_2\text{-C}\equiv\text{C-C}(\text{NCy})_2\}_3\}$ (**21**) in the crystalline state. Thermal ellipsoids with 50% probability, H atoms omitted for clarity.

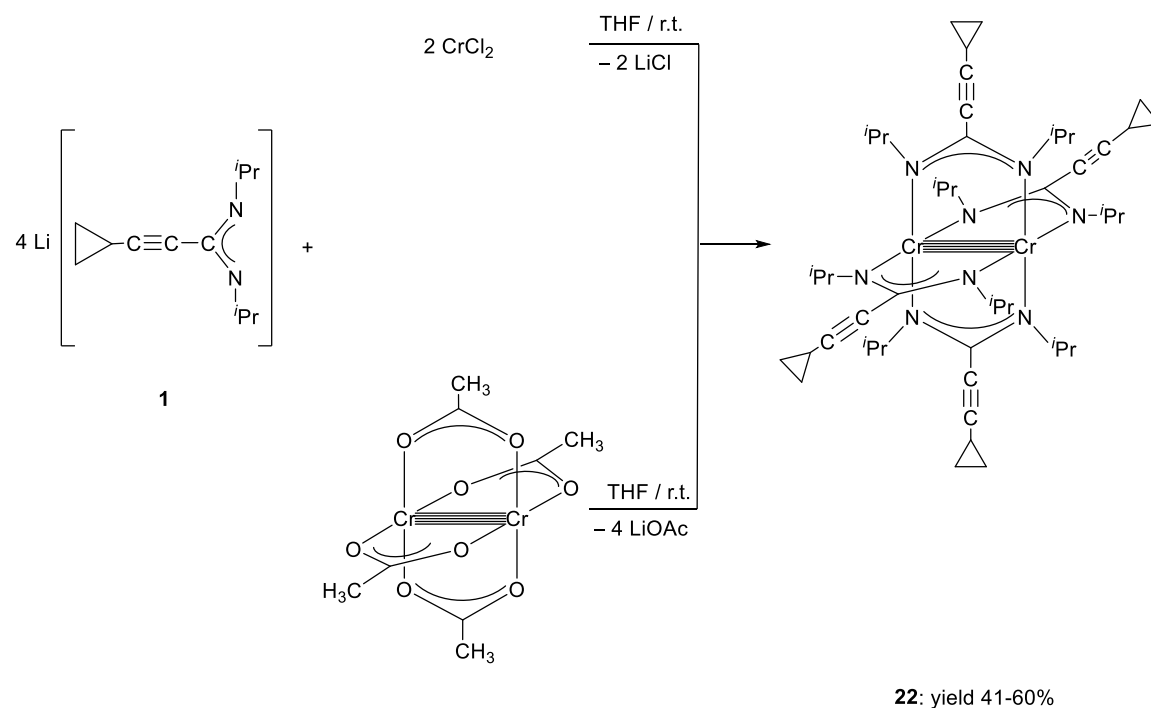
2.5. Synthesis and structural characterization of transition metal amidinates with short M-M contacts

In recent decades, the study of short metal-metal bonds in stabilizing compounds has gained widespread interest. It is known that Group 6 transition metals are capable of forming metal-metal bonds of high formal bond orders [125]. Historically, the chemistry of Cr–Cr multiple bonds began with the preparation of a nearly diamagnetic dichromium(II) species supported by a three-center chelating ligand reported by Hein and Tille in the early 1960s [126]. Meanwhile, a great deal of excellent research has been done on the quadruply bonded dimolybdenum complexes, which are often referred to as paddle-wheel complexes from a shape point of view [127]. The remarkable ability of an amidinate ligand is to construct the bridging mode of coordination which could be useful to build up the dinuclear complexes containing metal-metal multiple bonds. Four chromium and molybdenum amidinate complexes with short M-M contact were successfully synthesized in this Ph.D. work.

2.5.1. A dichromium complex containing bridging *N,N'*-di-*iso*-propylpropynylylamidinate ligands

As described in Scheme 18, the 1:2 reaction of anhydrous chromium(II) chloride and lithium amidinate **1**, $\text{Li}[\textit{i-c-C}_3\text{H}_5\text{-C}\equiv\text{C-C}(\text{N}^i\text{Pr})_2]\cdot\text{THF}$, was carried out in THF solution. The reaction mixture was stirred overnight at room temperature and afforded a new unsolvated exceedingly air- and moisture-sensitive dichromium complex, $[\text{Cr}_2\{\mu\text{-}\textit{i-c-C}_3\text{H}_5\text{-C}\equiv\text{C-C}(\text{N}^i\text{Pr})_2\}_4]$, (**22**). The complex **22** was isolated from *n*-pentane solution in the form of orange, rod-like crystals in a moderate yield of 41%. Notable is that the complex **22** was also obtained by treating lithium amidinate **1** with a different starting material, anhydrous chromium(II) acetate $[\text{Cr}_2(\mu\text{-OAc})_4]$, in a 4:1 molar ratio (Scheme 18) and the yield was increased from 41 to 60%. The product structure was confirmed by X-ray crystallography. The complex **22** was determined by single-crystal

X-ray diffraction and fully characterized by spectroscopic methods (NMR, IR, and MS) and elemental analyses. The molecular structure of complex **22** together with the atom labelling is shown in Figure 16.



Scheme 18. Reactions of anhydrous chromium(II) chloride CrCl_2 and chromium(II) acetate $[\text{Cr}_2(\mu\text{-OAc})_4]$ with lithium cyclopropylethynylamidinate **1**, respectively.

The IR spectrum of complex **22** showed a medium absorption band at 2220 cm^{-1} , which could be assigned to the $\text{C}\equiv\text{C}$ stretching vibration [103], while another very strong band observed at 1506 cm^{-1} is attributable to the $\text{C}=\text{N}$ bond stretching vibration in the NCN units of the amidinate ligands [110]. Meanwhile, three medium intensity bands observed in the range of $2867\text{--}2964\text{ cm}^{-1}$ could be assigned to $\text{C}\text{--}\text{H}$ valence vibrations of the *isopropyl* substituents. Elemental analysis values for C, H, and N of **22** were in good agreement with the proposed formulation. The molecular ion peak of **22** was observed in the EI mass spectrum at m/z 869.

The ^1H NMR spectrum of **22** showed resonances in the region of 0 to 4 ppm and displayed several well-resolved signals. The protons corresponding to the cyclopropyl groups of the amidinate ligand were observed as multiplets in the range of 0.76–0.89 ppm (CH_2 , $c\text{-C}_3\text{H}_5$) and 1.42–1.53 ppm (CH , $c\text{-C}_3\text{H}_5$), respectively. The protons assigned to the *isopropyl* groups of **22** appeared at $\delta = 0.98$ ppm [$\text{CH}(\text{CH}_3)_2$] as a broad singlet and at $\delta = 3.75$ ppm [$\text{CH}(\text{CH}_3)_2$] as a singlet, respectively. The ^{13}C NMR spectrum of **22** showed the signals corresponding to the carbon atoms of the cyclopropyl group at $\delta = 0.6$ (CH) and $\delta = 8.2$ ppm (CH_2), respectively. The signal of carbon atoms (CH) of the *isopropyl* group appeared at $\delta = 24.4$ ppm and CH_2 at $\delta = 51.7$ ppm, respectively. The acetylenic carbon atom which is attached to the amidinate group appeared at $\delta = 96.9$ ppm ($\text{CH-C}\equiv\text{C}$) and the other acetylenic carbon atom was observed at $\delta = 72.6$ ppm ($\text{C}\equiv\text{C-C}$). The signal observed at $\delta = 156.3$ ppm could be assigned to the carbon atom of the NCN unit.

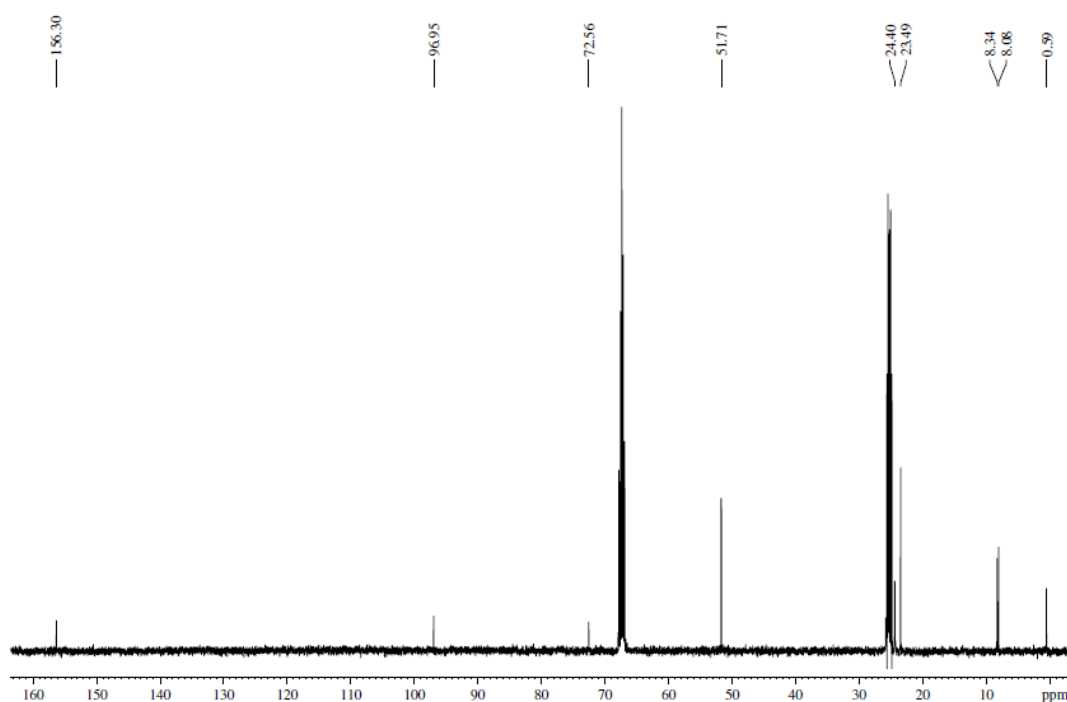


Figure 15. ^{13}C NMR spectrum (400 MHz, $\text{THF-}d_8$, 25 °C) of $[\text{Cr}_2\{\mu\text{-}c\text{-C}_3\text{H}_5\text{-C}\equiv\text{C-C}(\text{N}^i\text{Pr})_2\}_4]$ (**22**).

Complex **22** crystallizes in the monoclinic space group $P2_1/c$ with one complex molecule in the asymmetric unit. In Figure 16, **22** shows a well-known paddle-wheel structure, which is a typical dimeric arrangement of quadruple-bonded $\text{Cr}(\text{amidinate})_2$ units. The molecular structure of **22** is formed by a chromium–chromium unit bridged by four cyclopropylethynylamidinate groups. Each chromium atom is bonded to the nitrogen atoms of four amidinate ligands with μ_2 -interactions. Each of the two donor atoms of one amidinate ligand is combined with two metal centers to form a five-membered ring. The Cr–N bond lengths [Cr(1)–N(1) 2.078(4), Cr(1)–N(3) 2.043(4), Cr(1)–N(5) 2.070(4), Cr(1)–N(7) 2.046(4) Å] are normal and compare well with those of the previously reported quadruply bonded dichromium complex [$\{\text{CyN}-\text{C}(\text{H})-\text{NCy}\}_2\text{Cr}_2$ (2.03(1) to 2.06(1) Å) [58]. In the NCN units of the amidinate ligands, the narrow range of the C–N bond lengths [1.320(6) to 1.344(6) Å] confirms the existence of the negative charge delocalization. The coordination environment around each chromium atom can be regarded as square planar [N(1)–Cr(1)–N(3) 91.9(2)°, N(1)–Cr(1)–N(5) 171.1(1)°, N(1)–Cr(1)–N(7) 87.9(2)°, N(2)–Cr(2)–N(4) 91.5(2)°, N(2)–Cr(2)–N(6) 171.1(1)°, N(2)–Cr(2)–N(8) 87.8(2)°] with the chromium atom slightly elevated above the plane defined by the four nitrogen atoms [Cr(2)–Cr(1)–N(7) 94.3(1), Cr(1)–Cr(2)–N(8) 94.5(1)].

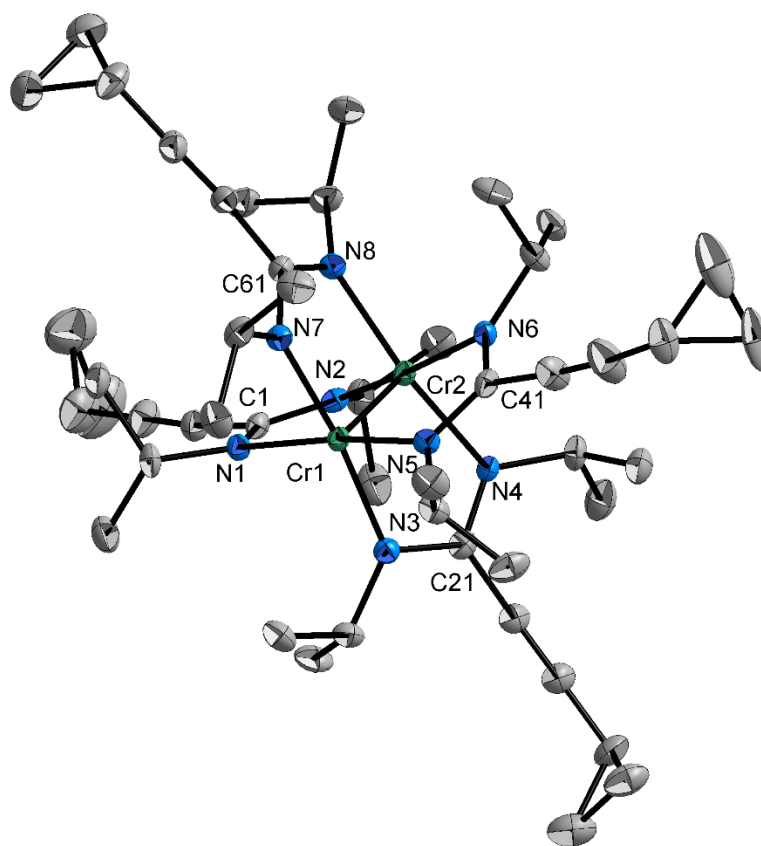


Figure 16. Molecular structure of $[\text{Cr}_2\{\mu\text{-}c\text{-}\text{C}_3\text{H}_5\text{-C}\equiv\text{C-C}(\text{N}^i\text{Pr})_2\}_4]$ (**22**) in the crystalline state. Thermal ellipsoids with 50% probability, H atoms omitted for clarity.

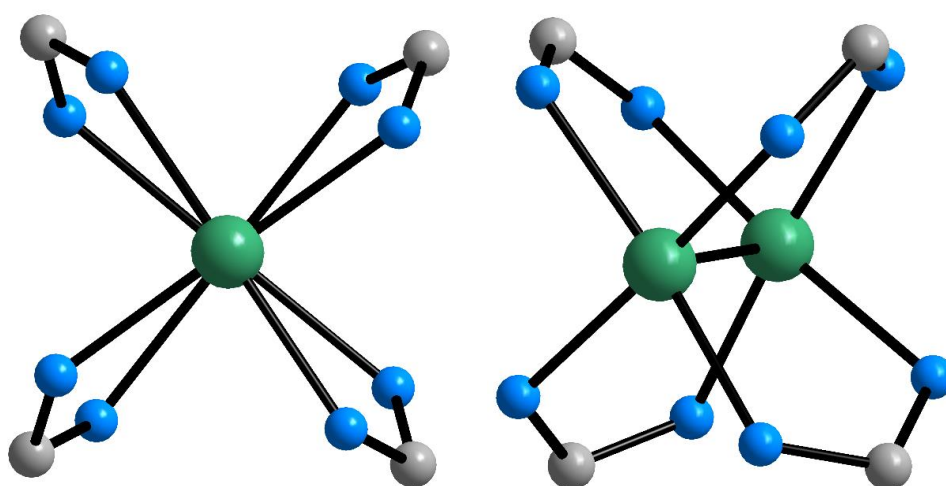
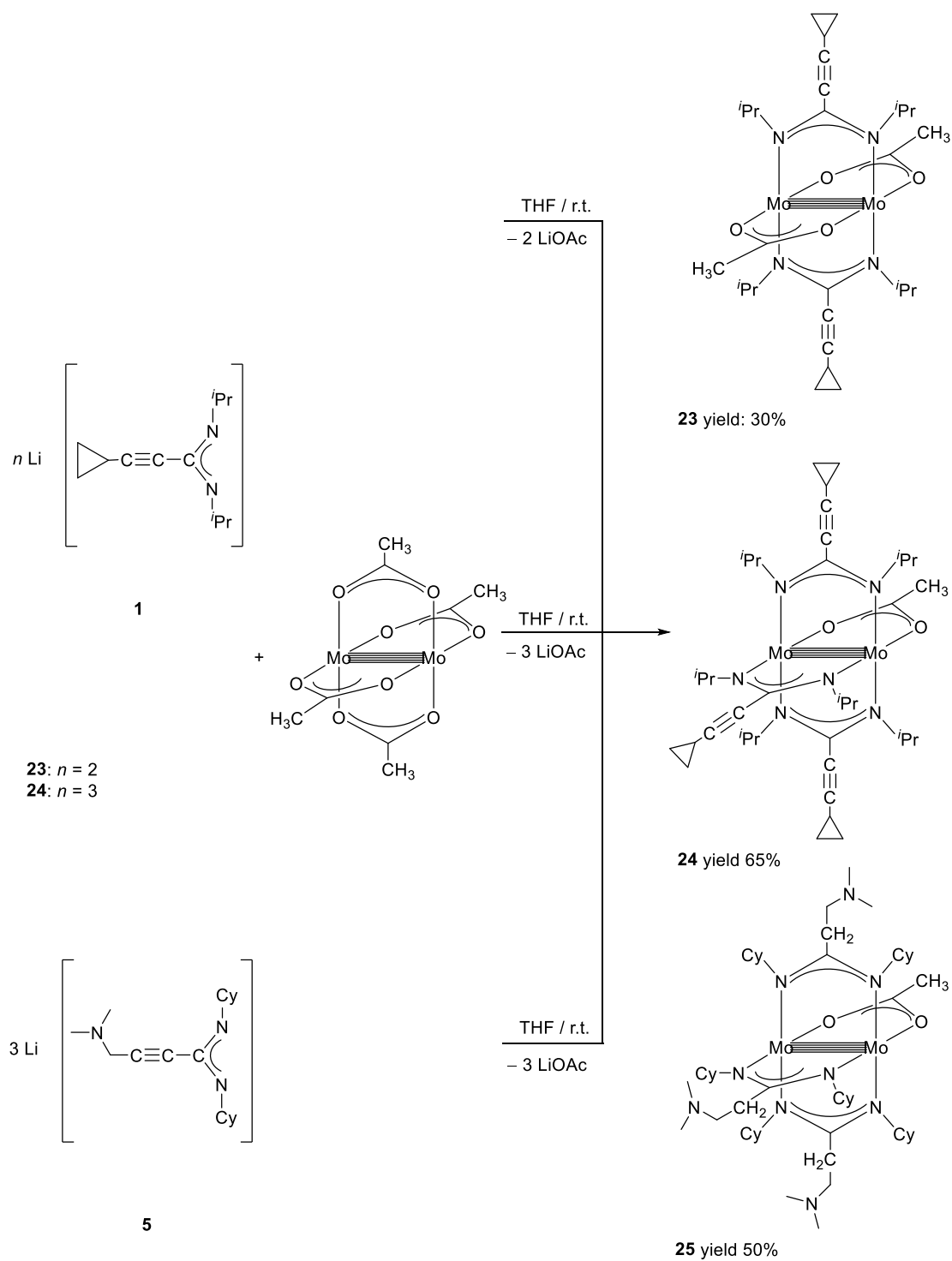


Figure 17. Representation of the coordination sphere of the Cr atoms in complex **22** viewed diagonally to the Cr–Cr vector (right) and viewed along the Cr–Cr vector (left).

For the paddle-wheel complexes, the Cr–Cr bond lengths vary over a range of more than 0.7 Å. The shortest is 1.828 (2) Å for Cr₂(2-oxyphenyl)₄, whereas Cr–Cr bond lengths of 2.4 Å or more are commonly found in dichromium complex with axial ligands such as complex [Cr₂{(2-xylyl)-NCMeO}₄]₂·2THF (2.221(3) Å) [128, 129]. The presence of ligands in axial positions lengthens the Cr–Cr bond lengths [57]. Generally, Cr–Cr bond lengths of less than 2.0 Å are known as “super short”. The Cr–Cr bond length of unsolvated complex **22** is 1.889(1) Å, which belongs to the family of the quadruple-bonded dichromium complexes with a super short intermetallic contact such as complex [{CyN–C(H)–NCy}₂Cr]₂ (1.913(3) Å) [58]. In rare cases, the bridging ligand is not the only interaction employed for stabilizing of the quadruply-bonded dichromium unit, e.g. [Cr{^tBuNC(CH₃)Net}₂]₂ (1.960(1) Å). Each chromium atom in the complex [Cr{^tBuNC(CH₃)Net}₂]₂ is bonded to the nitrogen atoms of one amidinate ligand in a terminal, chelating η²-fashion and to the nitrogen atoms of two amidinate ligands with μ-interactions [130].

2.5.2. Dimolybdenum complexes containing bridging acetate ligands and *N,N'*-di-*iso*-propylpropynylamidinate or *N,N'*-dimethylaminopropynylamidinate ligands

Using the straightforward reaction shown in Scheme 19, the reaction of molybdenum(II) acetate [Mo₂(μ-OAc)₄] with two or three equivalents of lithium amidinate **1** Li[*c*-C₃H₅–C≡C–C(N^{*i*}Pr)₂]₂·THF, and three equivalents of lithium amidinate **5** Li[(CH₃)₂N–CH₂–C≡C–(NCy)₂]₂·THF was carried out in THF, respectively. After the reaction mixture was stirred overnight at room temperature, three paddle-wheel mixed-ligands with quadruply bonded dimolybdenum complexes were obtained, [*trans*-Mo₂(μ-OAc)₂{μ-*c*-C₃H₅–C≡C–C(N^{*i*}Pr)₂}]₂ (**23**), [Mo₂(μ-OAc){μ-*c*-C₃H₅–C≡C–C(N^{*i*}Pr)₂}]₃ (**24**), and [Mo₂(μ-OAc){μ-(CH₃)₂N–CH₂–C≡C–C(NCy)₂}]₃ (**25**). The complexes **23–25** were isolated from *n*-pentane solution as unsolvated complexes (**23**, **24**: orange, block-like, **25**: yellow, plate-like) in moderate yields of 30% (**23**), 40% (**24**), and 45% (**25**).



Scheme 19. Reactions of $[\text{Mo}_2(\mu\text{-OAc})_4]$ with lithium cyclopropylethynylamidinate **1** in molar ratios 1:2 and 1:3, and **5** in ratio 1:3.

It may also be noted that the reaction of molybdenum(II) acetate with lithium amidinates **1** and **5** were also carried out in a 1:4 molar ratio in THF. However, the products also possess a paddle-wheel skeleton bearing three amidinate ligands and one acetate ligand as the same as **24** and **25**. The molecule structures of **23–25** were determined by single-crystal X-ray diffraction. The high air- and moisture-sensitive complexes were fully characterized by NMR, IR, and MS, as well as elemental analyses.

The IR spectra of complexes **23–25** showed a strong and two medium bands of the C=N stretching vibration in the range of 1529 to 1570 cm^{-1} , which can be assigned to the delocalized π -bond in the NCN unit [110]. Medium bands observed at 2216 cm^{-1} (**23**), 2227 (**24**) cm^{-1} can be attributed to the C \equiv C vibration [103]. However, the band corresponding to the C \equiv C stretching vibration is not observed in the IR spectrum of **25**. Each of the complexes **23–25** has four bands from intensity strong to weak (**23**: 2963 m, 2945 m, 2921 m, 2865 m cm^{-1} ; **24**: 2972 m, 2933 w, 2873 w, 2718 w cm^{-1} ; **25**: 2922 s, 2850 s, 2827 m, 2767 m cm^{-1}), which could be assigned to the C–H valence vibrations of the *isopropyl* or *cyclohexyl* substituents in **23** and **24**, or the Me₂N unit in **25**. Elemental analysis values for C, H, and N of complexes **23** and **24** were in good agreement with the proposed formulation, whereas that of **25** was not consistent with the proposed formulation. The possible reason is that since **25** is very sensitive to moisture, cannot be maintained in a stable state during the measurement, and thus hydrolysis and decomposition reactions occurred at the same time. The mass spectrum of **23** showed a peak at m/z 822, which can be assigned to the molecular ion without three hydrogen atoms $[M - 3H]^+$, while the molecular ion peak of **24** was well observed in the EI mass spectrum. It is worth noting that one peak observed at m/z 692 in **23** is equivalent to the molar mass of **24**. The mass spectrum of **25** showed a similar situation to the case of **24**. The peak observed at m/z 887 can be assigned to the fragment of **25**, $[M - (\text{CH}_3)_2\text{N}-\text{CH}_2-\text{C}\equiv\text{C}-\text{C}(\text{NCy})_2 + \text{OAc}]^+$, which is described as one amidinate ligand was replaced by one acetate ligand of the molecular ion. Through this data and

molecular structure features of the molecule structure of these two complexes, there could be a possibility that ligands exchanged in the mass spectrometer of **24** and **25**.

Due to the diamagnetic nature of the $(\text{Mo})_2^{4+}$ fragment in **23–25**, the NMR spectra of **23–25** can be obtained and compared to the NMR spectra of lithium amidinates **1** and **5**. The ^1H NMR spectra of **23** and **24** reveal several well-resolved signals in the region of 0 – 5 ppm, which are slightly shifted to lower magnetic field compared to lithium amidinate **1**. The signal of the *isopropyl* group hydrogen atoms of **23** and **24** were observed as doublets ($\text{CH}(\text{CH}_3)_2$, **23**: $\delta = 0.76$ ppm; **24**: $\delta = 0.85$ ppm) and septets ($\text{CH}(\text{CH}_3)_2$, **23**: 4.57 ppm; **24**: 4.55 ppm) with a coupling constant of 7.0 Hz, respectively. Multiplets in the range of 0.83–0.94 ppm (**23**) and 0.78–0.93 ppm (**24**) (CH_2 , *c*- C_3H_5), as well as 1.54–1.62 ppm (**23**) and 1.55–1.59 ppm (**24**) (CH , *c*- C_3H_5), can be assigned to the five protons in the cyclopropyl group. The signals of the acetate methyl protons (acetate- CH_3) were observed as singlets at $\delta = 1.08$ ppm and $\delta = 1.16$ ppm. The ^{13}C NMR data of the lithium amidinate **1** and complexes **23** and **24** are collected in Table 11. By comparison, the signals of the carbon atoms in the NCN unit appeared at $\delta = 148.5$ ppm in complex **23** and $\delta = 147.6$ and 148.4 ppm in complex **24** (higher field compared to lithium amidinate **1**, $\delta = 157.0$ ppm). The signal corresponding to the carbon atoms (CH) of the *isopropyl* group were observed at $\delta = 53.4$ (**23**) and 53.8, 54.2 (**24**) ppm, which were also shifted to a lower field compared to lithium amidinate **1** ($\delta = 49.8$ ppm). Also notable is that the ^{13}C NMR spectrum of complex **24** showed two separate signals for every carbon atom (Figure 19). Compared to the ^{13}C spectrum of complex **23** (Figure 18), there are two chemically different amidinate ligands in **24**, one *trans* to the acetate and two *cis* to acetate. In other words, there are two different carbon atoms in amidinate ligands corresponding to two different spatial position amidinate ligands.

Table 11. ^{13}C NMR data of lithium amidinate $\text{Li}[c\text{-C}_3\text{H}_5\text{-C}\equiv\text{C-C}(\text{N}^i\text{Pr})_2]\cdot\text{THF}$ (**1**) and complexes $[\text{Mo}_2\{\mu\text{-OAc}\}_2(\mu\text{-}c\text{-C}_3\text{H}_5\text{-C}\equiv\text{C-C}(\text{N}^i\text{Pr})_2)_2]$ (**23**) and $[\text{Mo}_2(\mu\text{-OAc})\{\mu\text{-}c\text{-C}_3\text{H}_5\text{-C}\equiv\text{C-C}(\text{N}^i\text{Pr})_2\}_3]$ (**24**).

	1	23	24
CH, <i>c</i> -C ₃ H ₅	0.4	0.3	0.4, 0.5
CH ₂ , <i>c</i> -C ₃ H ₅	8.9	8.7	8.8, 9.1
CH(CH ₃) ₂	26.8	24.8	23.2, 24.0
CH(CH ₃) ₂	49.8	53.4	53.8, 54.2
C≡C-C	69	68.6	69.7, 70.5
CH-C≡C	97.1	95.6	94.3, 95.2
NCN	157.0	148.5	147.6, 148.4
acetate-CH	—	48.8	53.7
acetate-CH ₃	—	25.6	24.5

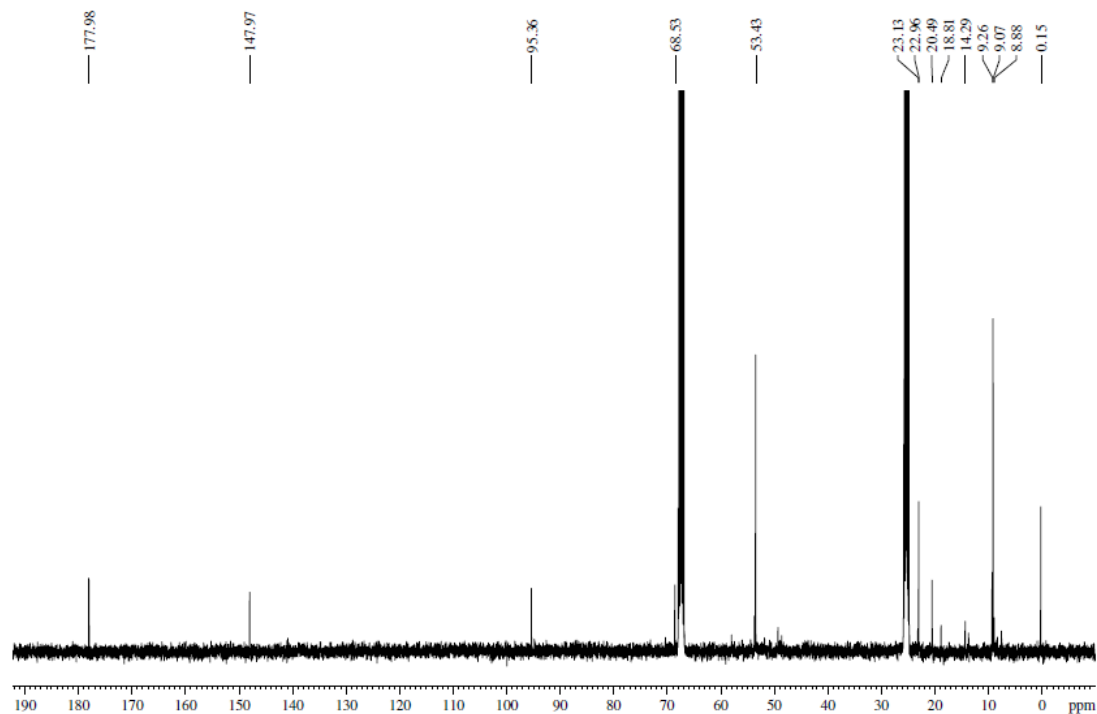


Figure 18. ^{13}C NMR spectrum (400 MHz, THF-*d*₈, 25 °C) of $[\text{Mo}_2(\mu\text{-OAc})_2\{\mu\text{-}c\text{-C}_3\text{H}_5\text{-C}\equiv\text{C-C}(\text{N}^i\text{Pr})_2\}_2]$ (**23**).

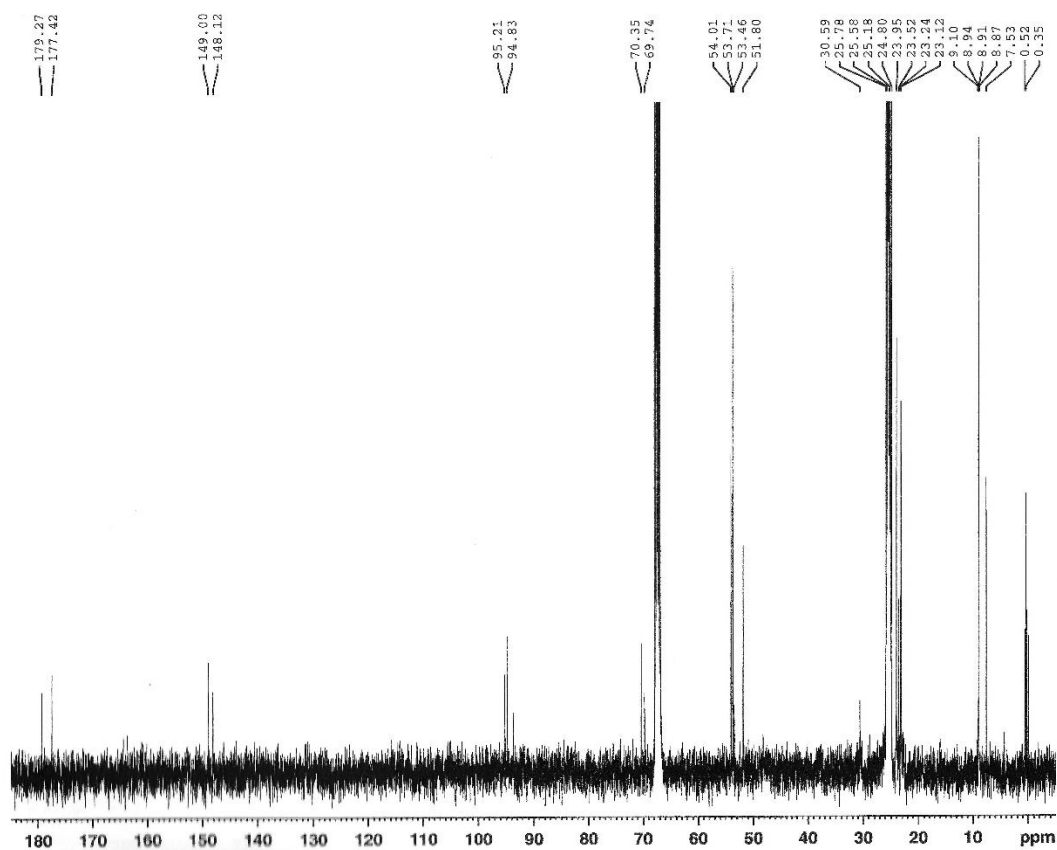


Figure 19. ^{13}C NMR spectrum (400 MHz, $\text{THF-}d_8$, 25 °C) of $[\text{Mo}_2(\mu\text{-OAc})\{\mu\text{-}c\text{-C}_3\text{H}_5\text{-C}\equiv\text{C-C}(\text{N}^i\text{Pr})_2\}_3]$ (**24**).

The very similar molecular structures of **23–25** together with the atom labelling are shown in Figure 20. As in the case of complex $[\text{Fe}_2\{\mu\text{-(CH}_3)_2\text{N-CH}_2\text{-C}\equiv\text{C-C}(\text{NCy})_2\}_2\{\eta^2\text{-(CH}_3)_2\text{N-CH}_2\text{-C}\equiv\text{C-C}(\text{NCy})_2\}_2]$ (**12**), the additional nitrogen donor in Me_2N units also does not contribute to metal coordination in complex **25**. Complexes **23–25** crystallize in the triclinic space group $P\bar{1}$ (**23**, and **25**) and the monoclinic space group $P2_1/c$ (**24**) with one complex molecule in the asymmetric unit, respectively. X-ray diffraction studies on the complexes **23–25** showed a well-known paddle-wheel structure, a typical dimeric arrangement of dimolybdenum complexes with a quadruple bond. The molecular structure of **23** consists of two molybdenum atoms which are spanned by two bridging acetate ligands and two bridging amidinate ligands in a *trans*

arrangement. However, **24** and **25** contain three acetate ligands and one amidinate ligand with μ_2 -interactions. One of the three amidinate ligands is located in the plane of the acetate ligand, and the other two amidinate ligands are located in mutually *trans* positions. The Mo–Mo bond lengths in the complexes **23–25** (**23**: 2.076(1), **24**: 2.076(8), **25**: 2.086(5) Å) are in a narrow range and consistent with the nature of a Mo–Mo quadruple bond (2.06 to 2.17 Å) [127]. Similar to the dichromium complexes, a longer Mo–Mo bond length also occurs in quadruple bonded dimolybdenum complexes having axial ligands such as $\text{Mo}_2[\{(2,6\text{-xylyl})\text{N}\}_2\text{CCH}_3](\text{CH}_3\text{CO}_2)_2\cdot 2\text{THF}$ [2.107(1) Å] [32]. In the complex **23**, the Mo–N bond lengths are in the range of 2.123(3) to 2.127(3) Å, whereas, there are two distinctly different Mo–N bond lengths in **24** and **25**. In **24**, the Mo–N bond lengths [Mo(1)–N(5) 2.103(5) Å, Mo(2)–N(6) 2.099(5) Å] *trans* to the acetate oxygens are slightly shorter than the other two Mo–N bond lengths [Mo(1)–N(2) 2.122(5) Å, Mo(2)–N(1) 2.131(5) Å, Mo(1)–N(3) 2.137(4) Å, Mo(2)–N(4) 2.137(4) Å]. Compared to **24**, the Mo–N bond lengths that are *trans* to the acetate oxygen in **25** are almost identical [**25**: Mo(1)–N(1) 2.098(3) Å, Mo(2)–N(2) 2.114(3) Å] and slightly shorter than the other four Mo–N bond lengths [**25**: 2.134(4) to 2.144(3) Å]. The bond lengths of Mo–O in **23** are in the range of 2.105(2) to 2.121(2) Å, which is slightly shorter than those of Mo–N (2.123 to 2.127 Å). However, the Mo–O bond lengths in **24** and **25** are longer than the Mo–N bond length. For the previously published complexes $\text{Mo}_2(\text{ambt})_3(\text{CH}_3\text{CO}_2)\cdot 2\text{THF}$ (ambt = the anion of 2-amino-4-methylbenzothiazole) and $[\text{Mo}_2(\mu\text{-OAc})\{\mu\text{-(NPh)}_2\text{CMe}\}_3]$ it was suggested that the increase in the Mo–O(OAc) bond lengths was a manifestation of a *trans* effect in the molecule [32, 131]. The long Mo–O bond lengths in **24** and **25** together with the shortening of the Mo–N bond lengths in the amidinate ligand *trans* to the acetate ligand further support that the *trans* effect plays a role in these species. These structural features mentioned above are similar to those of $[\text{Mo}_2(\mu\text{-OAc})_2\{\mu\text{-(NSiMe}_3)_2\text{CPh}\}_2]$ and $[\text{Mo}_2(\mu\text{-OAc})_2(\{\mu\text{-(N}^i\text{Pr)}_2\text{CMe}\}_2)]$, as well as $[\text{Mo}_2(\mu\text{-OAc})\{\mu\text{-(N}^i\text{Pr)}_2\text{CMe}\}_3]$ and $[\text{Mo}_2(\mu\text{-OAc})\{\mu\text{-(NPh)}_2\text{CMe}\}_3]$ [132-134].

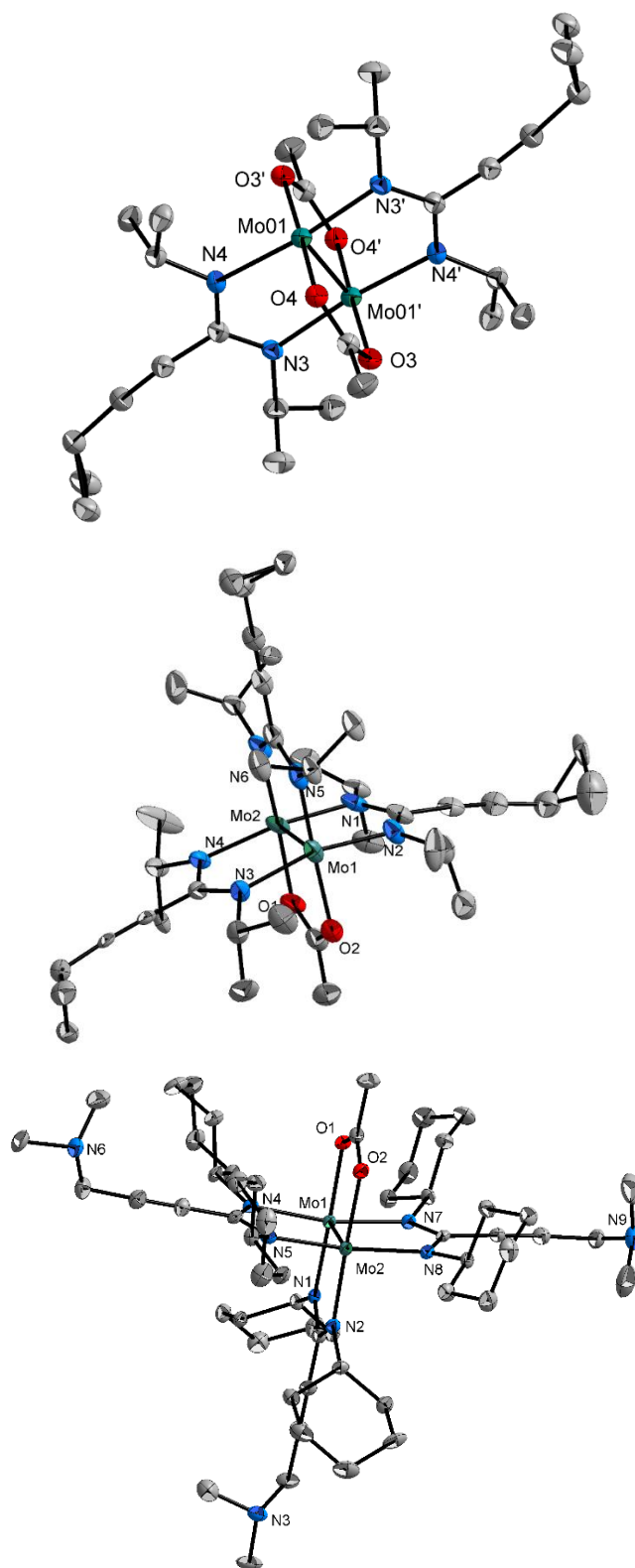


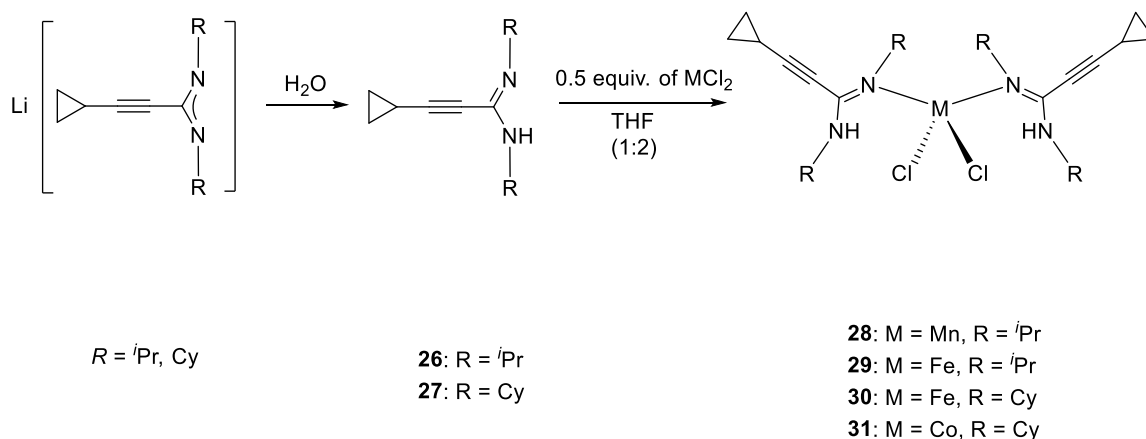
Figure 20. Molecular structures of $[\text{Mo}_2(\mu\text{-OAc})_2\{\mu\text{-}i\text{-C}_3\text{H}_5\text{-C}\equiv\text{C-C}(\text{N}^i\text{Pr})_2\}_2]$ (**23**), $[\text{Mo}_2(\mu\text{-OAc})\{\mu\text{-}i\text{-C}_3\text{H}_5\text{-C}\equiv\text{C-C}(\text{N}^i\text{Pr})_2\}_3]$ (**24**), and $[\text{Mo}_2(\mu\text{-OAc})\{(\text{CH}_3)_2\text{N-CH}_2\text{-C}\equiv\text{C-C}(\text{NCy})_2\}_3]$ (**25**) in the crystalline state. Thermal ellipsoids with 50% probability, H atoms omitted for clarity.

2.6. Synthesis and structural characterization of dichlorido-bis(cyclopropylalkynylamidine) transition metal complexes

In the course of this Ph.D. work, a series of hydrolysis products **28–31** of the composition $MCl_2[c-C_3H_5-C\equiv C-C(NR)(NHR)]$ ($M = Mn, Fe, Co$; $R = iPr, Cy$) were occasionally observed and structurally characterized, which contain the neutral amidines $c-C_3H_5-C\equiv C-C(NR)(NHR)$ as new ligands. Neutral amidines are highly versatile ligands in coordination chemistry in their own right and valuable starting materials for metal and non-metal amidinates [3, 135]. Therefore, the deliberate synthesis of two new cyclopropylalkynylamidines **26** and **27**, $c-C_3H_5-C\equiv C-C(NR)(NHR)$ ($R = iPr, Cy$) as well as the preparation and structural characterization of four first-row transition metal complexes were reported in this section.

The title compounds were first discovered “serendipitously” when studying reactions of anhydrous metal(II) chlorides MCl_2 ($M = Mn, Fe, Co$) with 2 equiv. of the lithium cyclopropylethynylamidinates, $Li[c-C_3H_5-C\equiv C-C(NR)_2]$ ($R = iPr, Cy$) in THF solution (refer to the corresponding chapter). Occasionally, small amounts of well-formed crystals were obtained, which turned out by X-ray diffraction studies to be the aforementioned hydrolysis products $MCl_2[c-C_3H_5-C\equiv C-C(NR)(NHR)]$ ($M = Mn, Fe, Co$; $R = iPr, Cy$). As illustrated in Scheme 20, the lithium amidinate intermediates were then carefully hydrolyzed to afford the neutral amidines $[c-C_3H_5-C\equiv C-C(NR)(NHR)]$ (**26**: $R = iPr$, **27**: $R = Cy$) in > 70% isolated yields. Both compounds form yellow oils, which were characterized by the usual set of spectroscopic techniques (MS, 1H NMR, ^{13}C NMR, IR) and their elemental analyses. With the free amidines in hand, the complexes with first-row transition metals could easily be prepared by treatment of metal(II) chlorides MCl_2 ($M = Mn, Fe, Co$) with 2 equiv. of either **26** and **27** in THF solution. The manganese(II) complex **28** $MnCl_2[c-C_3H_5-C\equiv C-C(N^iPr)(NH^iPr)]$, as well as the two iron(II) complexes $FeCl_2[c-C_3H_5-C\equiv C-C(N^iPr)(NH^iPr)]$ (**29**) and

$\text{FeCl}_2[\text{c-C}_3\text{H}_5\text{-C}\equiv\text{C-C}(\text{NCy})(\text{NHCy})]$ (**30**), form colorless crystals, while the cobalt(II) complex **31** is blue. The molecular structures of the divalent transition metal complexes **28–31** were determined by single-crystal X-ray diffraction and fully characterized by IR and MS, as well as elemental analyses.



Scheme 20. Formation of complexes **28–31** starting by hydrolysis of lithium amidinates **1** and **2**.

In the IR spectra of amidines **26** and **27**, the bands observed in the region above ca. 3100 cm^{-1} could be assigned to the $\nu(\text{N-H})$ vibrations, while strong bands around 1600 cm^{-1} were characteristic for the C=N double bond in the amidines [**26**: 1606 (vs, C=N), **27**: 1626 (m, C=N)]. In the far-infrared region (400 to 50 cm^{-1}), the M-Cl bands [**28**: 279 (vs, Mn-Cl), **29**: 211 (vs Fe-Cl), **30**: 198 (vs, Fe-Cl), **31**: 292 (vs, Co-Cl)] could be assigned by comparison with literature values [136, 137] and IR spectra of the respective anhydrous metal(II) chlorides, MCl_2 ($M = \text{Mn}, \text{Fe}, \text{Co}$; for details see the experimental section). The compositions of all four products were confirmed by elemental analyses. The molecular ion peaks of complex **28–31** were not observed in the EI mass spectra. However, several readily interpretable peaks corresponding to typical fragments can be assigned. The peaks observed at m/z 433 (**28**), and 432 (**29**) can be attributed to the molecular ion misses one chlorine and one *iso*-propyl group of the amidine ligand. The peak observed at m/z 363 of complex **30** and the peak at m/z

402 of complex **31** can be assigned to the fragments $[M - c\text{-C}_3\text{H}_5\text{-C}\equiv\text{C-C}(\text{NCy})(\text{NHCy}) - \text{Cl}]^+$ (**30**) and $[M - c\text{-C}_3\text{H}_5\text{-C}\equiv\text{C-C}(\text{NCy})(\text{NHCy})]^+$ (**31**), respectively.

Complexes **28** and **29** crystallize isotypically in the orthorhombic space group $Fdd2$. The molecular structures together with the atom labelling are shown in Figure 21 and Figure 22. The metal atom is situated on a crystallographic twofold screw axis and is surrounded by two symmetry-equivalent chlorido ligands and two symmetry-equivalent amidine ligands. The latter is attached to the metal atom in a monodentate κN mode *via* the non-protonated nitrogen atom (N1). The crystal structures of $\text{FeCl}_2[c\text{-C}_3\text{H}_5\text{-C}\equiv\text{C-C}(\text{NCy})(\text{NHCy})]_2$ (**30**) and $\text{CoCl}_2[c\text{-C}_3\text{H}_5\text{-C}\equiv\text{C-C}(\text{NCy})(\text{NHCy})]_2$ (**31**) are isotypic in the monoclinic space group $P2_1/c$. In this case, the two amidine ligands are not symmetry-equivalent, but the molecular structures resemble those of complexes **28** and **29**.

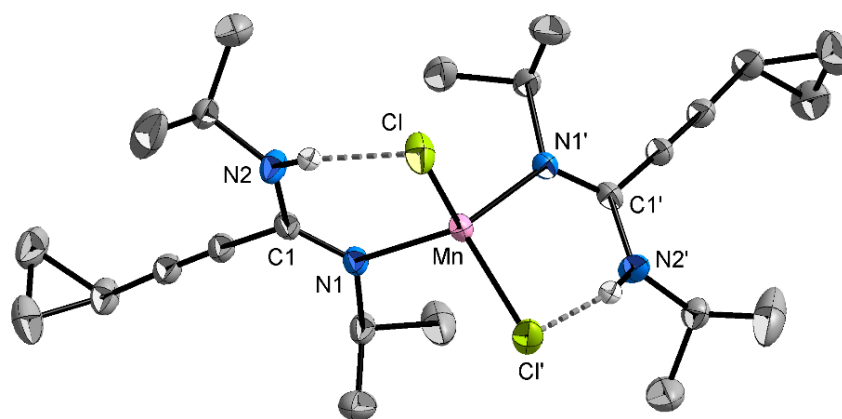


Figure 21. Molecular structure of $\text{MnCl}_2[c\text{-C}_3\text{H}_5\text{-C}\equiv\text{C-C}(\text{N}^i\text{Pr})(\text{NH}^t\text{Pr})]_2$ (**28**) in the crystalline state. Thermal ellipsoids with 50% probability, H atoms omitted for clarity.

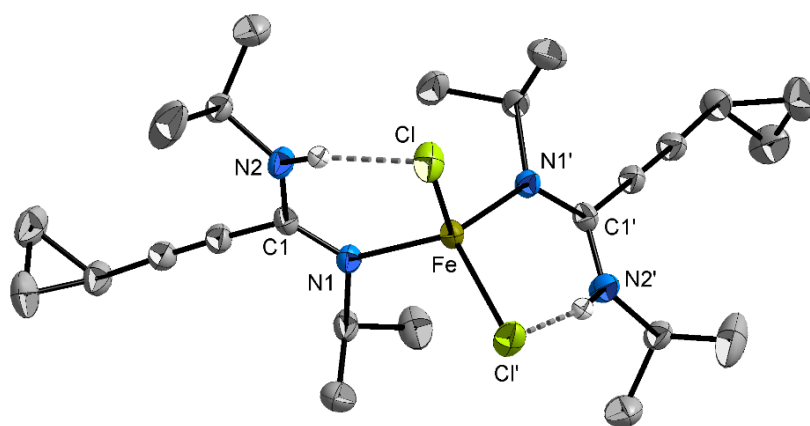


Figure 22. Molecular structure of $\text{FeCl}_2[\text{c-C}_3\text{H}_5\text{-C}\equiv\text{C-C}(\text{N}^i\text{Pr})(\text{NH}^t\text{Pr})_2$ (**29**) in the crystalline state. Thermal ellipsoids with 50% probability, H atoms omitted for clarity.

Complex **30** represents a rare example of a complex of tetra-coordinated manganese(II) with nitrogen ligands, while a larger number of the corresponding iron(II) and cobalt(II) complexes are known. The Mn–N bond length in complex **30** is 2.160(2) Å and therefore comparable to the literature data [138, 139]. In the iron complexes, the Fe–N distances are very similar at 2.088 (3) Å (**29**), and 2.073(2)–2.079(2) Å (**30**). These values are in the range of Fe–N bond lengths usually observed in MCl_2L_2 -type complexes, where L is a ligand with an sp^2 -hybridized nitrogen donor [140-142]. The same is true for the cobalt complex **31**, having Co–N bond lengths of 2.041(2) and 2.043(2) Å [141-143]. The set of C–N bond lengths within the NCN group of the amidine ligands is virtually equal in complexes **28–31**, including one formal C=N double bond at 1.309(2)–1.315(4) Å, and one formal C–N single bond at 1.337(4)–1.340(2) Å. The small difference between single- and double-bond length may indicate some degree of delocalization of the π -electron density. The observed values are consistent with other metal complexes having metal-coordinated amidine moieties [103, 144-148].

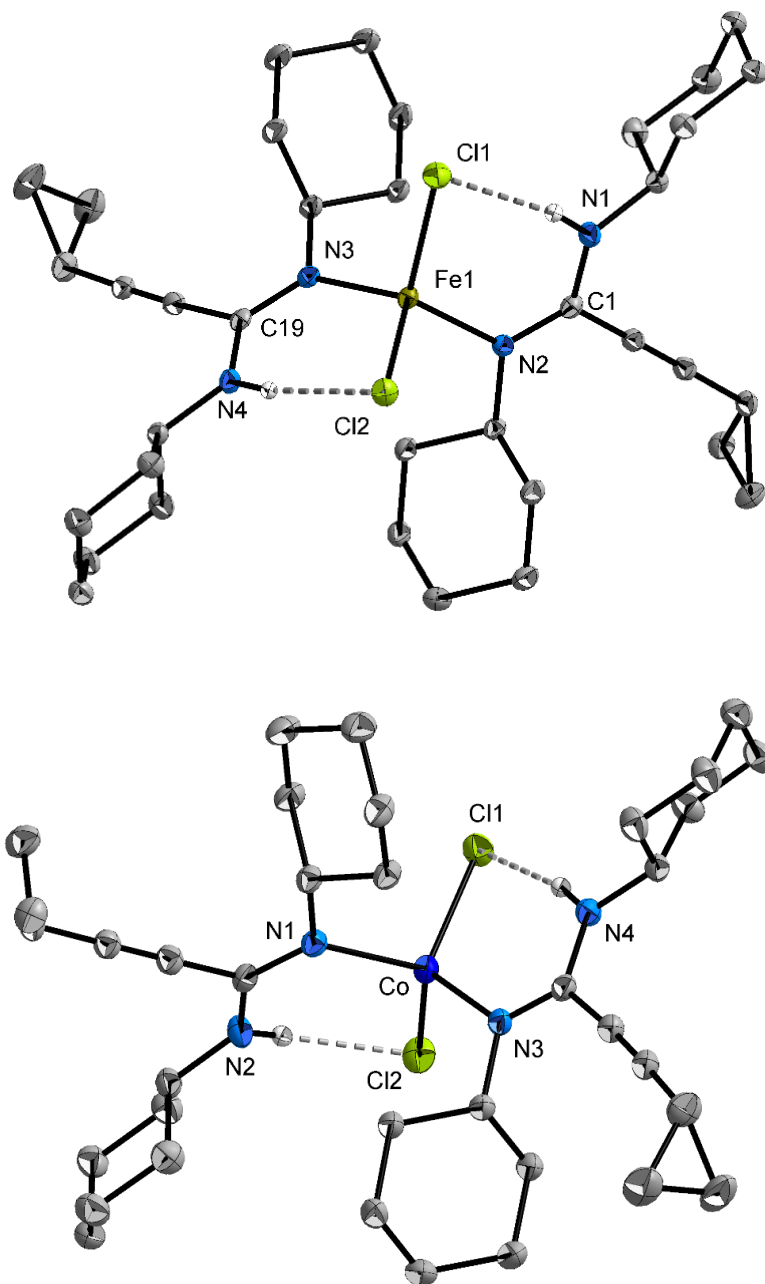


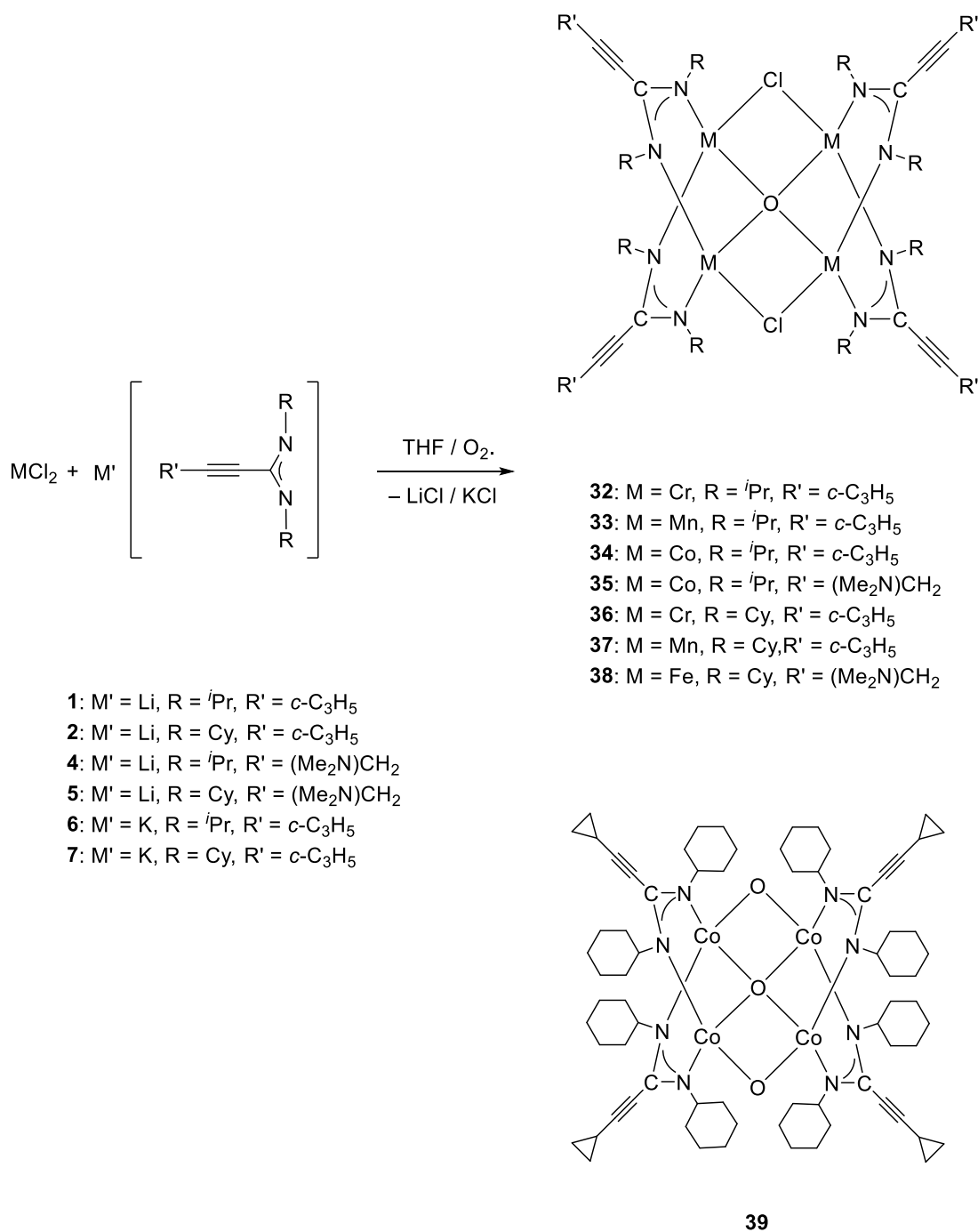
Figure 23. Molecular structures of $\text{FeCl}_2[\text{c-C}_3\text{H}_5\text{-C}\equiv\text{C-C}(\text{NCy})(\text{NHCy})]_2$ (**30**) and $\text{CoCl}_2[\text{c-C}_3\text{H}_5\text{-C}\equiv\text{C-C}(\text{NCy})(\text{NHCy})]_2$ (**31**) in the crystalline state. Thermal ellipsoids with 50% probability, H atoms omitted for clarity.

2.7. The discovery of oxygen-centered variants of transition metal amidinate complexes

The original intention of this part of the work was to synthesize transition metal bis(amidinate) complexes and M–M amidinates complexes with short contacts (M = Cr, Mn, Fe, and Co). Occasionally two different colored crystals green: $(\mu_4\text{-O})[\text{Cr}\{c\text{-C}_3\text{H}_5\text{-C}\equiv\text{C-C}(\text{N}^i\text{Pr})_2\}]_4\text{Cl}_2$ (**32**), orange: $\text{Cr}_2[\mu\text{-}c\text{-C}_3\text{H}_5\text{-C}\equiv\text{C-C}(\text{N}^i\text{Pr})_2]_4$, (**22**) were simultaneously observed in the reaction of anhydrous chromium(II) chloride and lithium amidinate **1** in a ratio 1:1. At that time, it was realized that there might be two crystals with completely different structures. Subsequently, the single-crystal X-ray diffraction confirmed this conjecture. The complex **32** was prepared with the hope that it might have a “normal” structure as **22**, a well-known paddle-wheel structure. However, the molecular structure of **32** is an oxygen-centered amidinate complex. Other than that, the significant oxophilic nature makes the transition metal amidinate complexes very sensitive to water and air. Therefore, the problem of the occasional occurrence of oxygen in the crystalline compounds studied by X-ray diffraction is not new, as was previously shown for $[\{\text{Mn}(\text{CyNCHNCy})_2\}_2(\mu\text{-O})]_2\cdot 2\text{THF}$ [59].

As illustrated in Scheme 21, a series of the unexpected oxygen-centered variants of transition metal amidinate complexes were occasionally discovered when treating a THF solution of anhydrous metal halides [Cr(II), Mn(II), Fe(II), Co(II)] with lithium amidinates $\text{Li}[c\text{-C}_3\text{H}_5\text{-C}\equiv\text{C-C}(\text{NR})_2]\cdot\text{THF}$ (**1**: R = *i*Pr, **2**: R = Cy), $\text{Li}[(\text{CH}_3)_2\text{N-CH}_2\text{-C}\equiv\text{C-(NR)}_2]\cdot\text{THF}$ (**4**: R = *i*Pr, **5**: R = Cy) and potassium amidinates $\text{K}[c\text{-C}_3\text{H}_5\text{-C}\equiv\text{C-C}(\text{NR})_2]\cdot\text{THF}$ (**6**: R = *i*Pr, **7**: R = Cy) in a 1:1 molar ratio. The mixtures were stirred overnight at room temperature and exposed to air for 5 min to afford a series of new oxygen-centered transition metal amidinates $(\mu_4\text{-O})\{\text{M}[c\text{-C}_3\text{H}_5\text{-C}\equiv\text{C-C}(\text{N}^i\text{Pr})_2]\}_4\text{Cl}_2$ (**32**: M = Cr, **33**: M = Mn, **34**: M = Co), $(\mu_4\text{-O})\{\text{M}[c\text{-C}_3\text{H}_5\text{-C}\equiv\text{C-C}(\text{NCy})_2]\}_4\text{Cl}_2$ (**36**: M = Cr, **37**: M = Mn), $(\mu_4\text{-O})\{\text{M}[(\text{Me})_2\text{N-C}\equiv\text{C-C}(\text{N}^i\text{Pr})_2]\}_4\text{Cl}_2$ (**35**: M = Co, **38**: M = Fe), and $(\mu_4\text{-O})(\mu_2\text{-$

$O)_2\{Co[(Me)_2N-C\equiv C-C(N^iPr)_2]\}_4Cl_2$ (**39**). These complexes were isolated as air- and moisture-sensitive colored crystals, (**32**: green, **33**: red, **34**: black, **35**: black, **36**: green, **37**: yellow, **38**: orange, **39**: blue) by extraction and recrystallized from in *n*-pentane solution at $-5\text{ }^\circ\text{C}$.



Scheme 21. Formation of oxygen-centered transition metal amidinate complexes **32–39**.

The structures of the complexes **32–36** and **38** were confirmed by single-crystal X-ray diffraction, although the data quality did not allow for full structure refinement. However, the data of complexes **37** and **39** are good enough to be published and discussed in this section. Complex **39** was characterized by IR, MS, and elemental analyses. The molecular structures of complexes **37** and **39** along with the atomic numbering scheme are shown in Figure 24 and Figure 25, respectively.

The IR spectrum of complex **39** showed a medium absorption band of the C=N bond stretching vibration at 1604 cm^{-1} , which is consistent with the delocalized π -bond of the NCN unit [110]. A weak band at 2223 cm^{-1} and two bands observed at 2922 (vs) and 2849 (vs) cm^{-1} can be attributed to the C–H valence vibrations of the cyclohexyl substituents, respectively. These IR bands of **39** are consistent with the IR data of lithium amidinate **7**. The mass spectrum of **39** exhibited only fragments of the molecular ion. The peak observed at m/z 271 can be assigned to the fragment $[\text{c-C}_3\text{H}_5\text{-C}\equiv\text{C-C}(\text{NCy})_2]^+$. The elemental analyses data of **39** are in good agreement with the expected structure. Due to the paramagnetic nature of the transition metal ions, NMR spectra of the complexes **37** and **39** could not be obtained.

Complex **37** crystallizes in the monoclinic $C2/c$ group with one complex molecule in the asymmetric unit. The centrosymmetric dimeric complex **37** is a characteristic example of these series of oxygen-centered transition metal amidinates complexes. Complex **37** consists of four manganese atoms which are in a distorted tetrahedral coordination [O(1)–Mn(1)–N22 $102.5(7)$, O(1)–Mn(1)–N2_1 $106.8(6)$, N2_2–Mn(1)–N2_1 $116.7(8)$, O(1)–Mn(1)–Cl(2) $93.3(6)$, N2_2–Mn(1)–Cl(2) $119.8(6)$, N2_1–Mn(1)–Cl(2) $113.5(6)^\circ$]. Each of the manganese atoms are linked together by chlorine atoms [Mn(1)–Cl(2) $2.450(9)$, Mn(2)–Cl(1) $2.454(1)\text{ \AA}$] and two bridging N,N' -dicyclohexylpropynamidinate anions [Mn(1)–N2_2 $2.098(2)$, Mn(1)–N2_1 $2.119(2)$, Mn(2)–N11 $2.088(2)$, Mn(2)–N1_2 $2.094(2)\text{ \AA}$], as well as a central oxygen atom [Mn(1)–O(1) $2.019(2)$, Mn(2)–O(1) $2.015(2)$]. In the central structural unit, there are

two planar four-membered rings which are bonded to the central oxygen atom [Mn(1)–Cl(2)–Mn(3)–O(1) 0.0(5), Mn(2)–O(1)–Mn(4)–Cl(1) 0.0(5)°]. The dihedral angle between the two planes Mn(1)–Cl(2)–Mn(3)–O(1) and Mn(2)–O(1)–Mn(4)–Cl(1) is 19.9(2)°. Each of the four amidinate ligands bridges two manganese atoms and adopts the usual three-center chelating coordination in which the N–C–N array is deviated approximately 30° from coplanarity with the Mn–Mn vector [Mn(2)–N1_1–C1_1–N2_1 –6.7(2), Mn(1)–N2_1–C1_1–N1_1 –31.7(3)°]. The coordination of the nitrogen donor atoms is distorted trigonal planar [Mn(2)–N(11)–C(71) 122.4(1), Mn(2)–N(11)–C(11) 115.8(2), C(71)–N(11)–C(11) 121.8(2); Mn(1)–N(21)–C(131) 116.8(2), Mn(2)–N(21)–C(11) 124.8(2), C(11)–N(21)–C(131) 117.6(2)°]. The molecular structure features of the complex **39** are very similar to that of **37**. The only difference between them is that two chlorine atoms of **37** are replaced by two oxygen atoms in **39**. Therefore, the Co(II) ions in the central unit are partially oxidized to Co(III). Similar to **37**, there are two nearly planar four-membered rings in **39** [O(1)–Co(4)–O(3)–Co(2) –0.5(1), O(2)–Co(3)–O(1)–Co(1) –1.7(1)°]. The dihedral angle between these two planes is 12.3(8)°, which is smaller than that of **37**. An inspiration obtained by the structural features of **39**, there is a possibility of Cr(II), Mn(II), and Fe(II) complexes **30–38** to be partially oxidized from +2 to +3. If so, this series of oxygen-centered variants of transition metal amidinate complexes **32–38** can further react with oxygen to obtain a similar complex as in **39**.

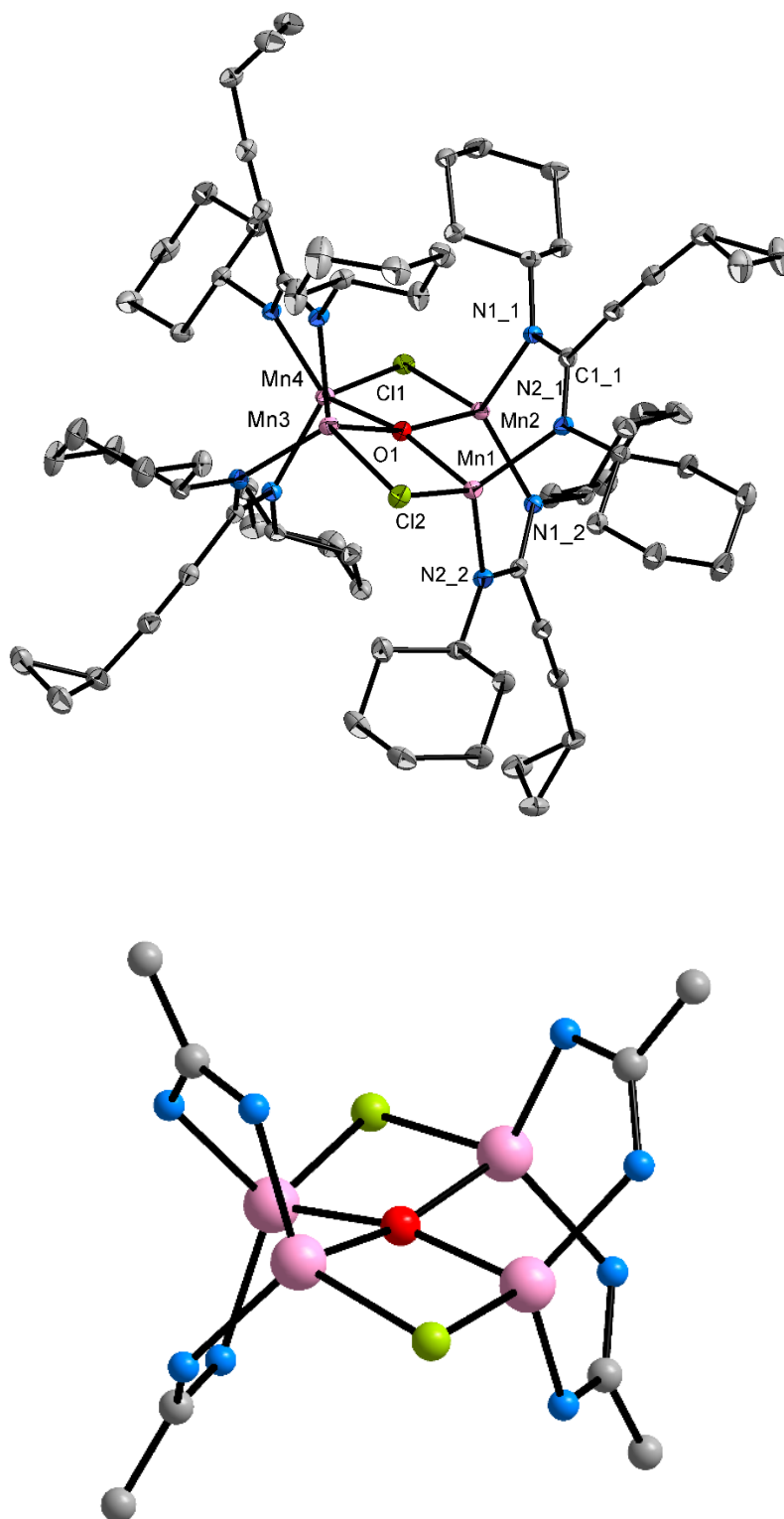


Figure 24. Molecular structure of $(\mu_4\text{-O})\{\text{Mn}[c\text{-C}_3\text{H}_5\text{-C}\equiv\text{C-C}(\text{NCy})_2]\}_4\text{Cl}_2$ (**37**) in the crystalline state. Thermal ellipsoids with 50% probability, H atoms omitted for clarity. (top). Representation of the coordination sphere of the manganese atoms in **37** (bottom).

In the very beginning of this work, two differently colored crystals (**32**: green and **22**: orange) were simultaneously observed in one Schlenk flask. Through the obvious color change, it can be easily distinguished from their oxygen-free counterpart. Meanwhile, the source of the oxygen contamination of these complexes is a confusing issue. The synthesis of complexes **32–39** were carried out under strictly anhydrous conditions. However, it is difficult to completely exclude oxygen from conventional Schlenk vessels, as traces may come from glass or even from commercial oxygen-free protective gas. Moreover, the water contamination of the alkyllithium solution could lead to the formation of hydroxides, but there is no evidence of hydroxide formation, so molecular oxygen is more likely to be a contaminant than moisture. However, it should be emphasized that complex **32** is a secondary product, so the main product is still complex **22** [149].

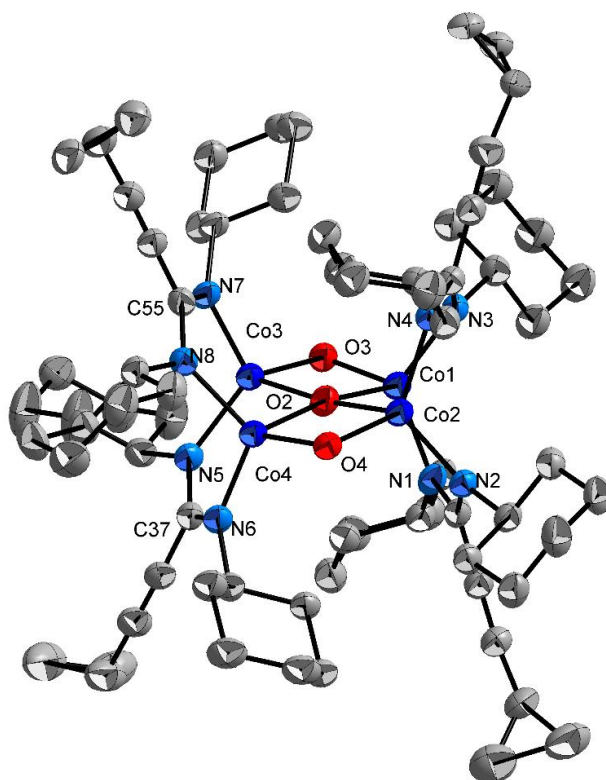


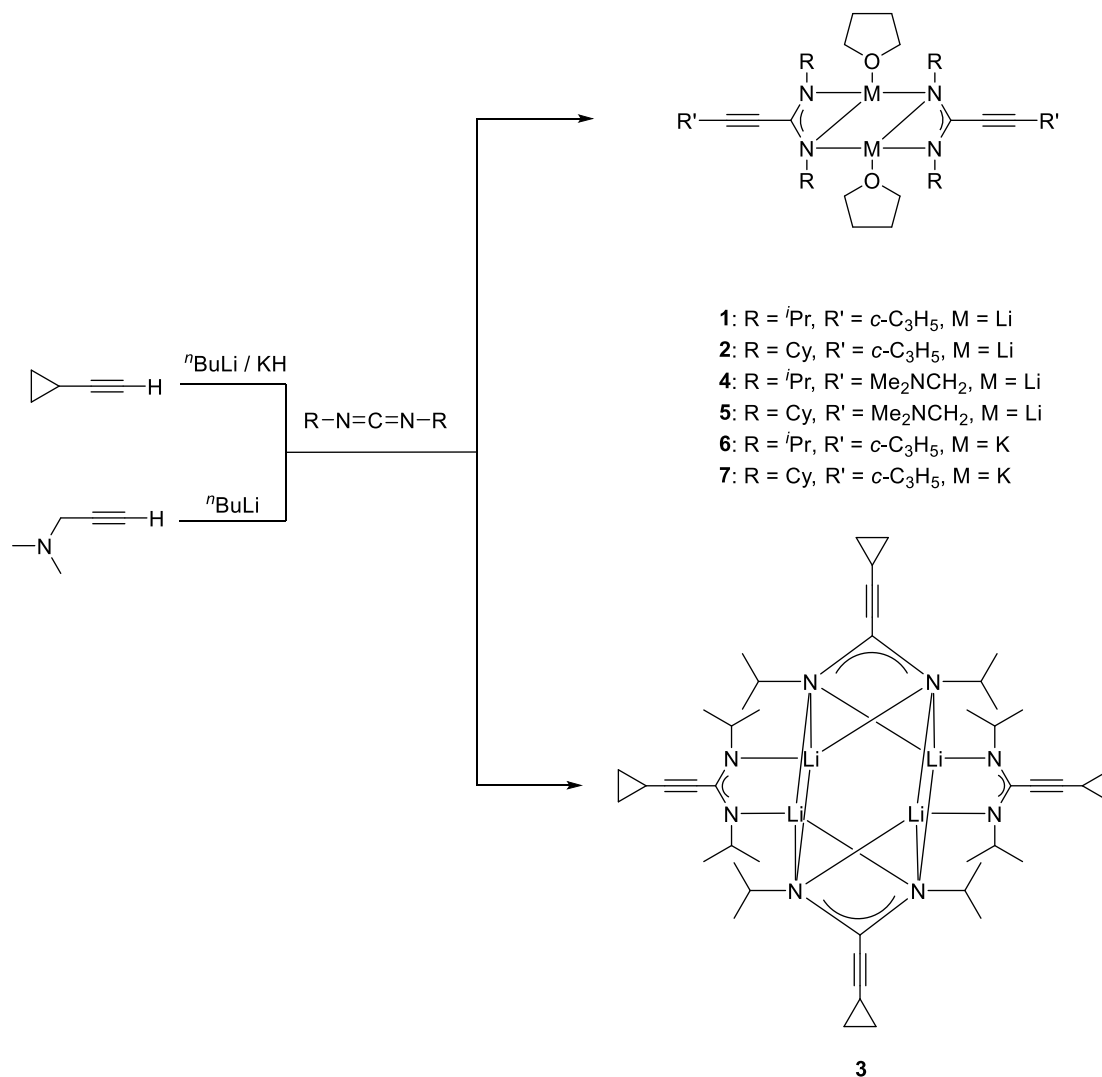
Figure 25. Molecular structure of $(\mu_4\text{-O})(\mu_2\text{-O})_2\{\text{Co}[c\text{-C}_3\text{H}_5\text{-C}\equiv\text{C-C}(\text{NCy})_2]\}_4$ (**39**) in the crystalline state. Thermal ellipsoids with 50% probability, H atoms omitted for clarity.

Furthermore, these oxygen-centered variants of transition metal amidinate complex may have some reactivity of the transition metal oxo complex due to the addition of oxygen atoms, such as acid-base reactions, oxygen atom transfer and hydrogen atom substitution [150, 151]

Chapter 3

Summary

Synthesis and structural characterization of transition metal amidinate complexes was the main goal of this Ph.D. thesis. In the initial stage, a series of lithium and potassium amidinates were prepared as starting materials (Scheme 22). First of all, two lithium cyclopropylethynylamidinates $\text{Li}[c\text{-C}_3\text{H}_5\text{-C}\equiv\text{C-C}(\text{NR})_2]\cdot\text{THF}$ (**1**: $\text{R} = i\text{Pr}$, **2**: $\text{R} = \text{Cy}$) were prepared according to the published procedures [97]. During repeating the synthesis of $\text{Li}[c\text{-C}_3\text{H}_5\text{-C}\equiv\text{C-C}(\text{N}^i\text{Pr})_2]\cdot\text{THF}$, an unexpected complex $\{\text{Li}[c\text{-C}_3\text{H}_5\text{-C}\equiv\text{C-C}(\text{N}^i\text{Pr})_2]\}_4$ (**3**) was obtained by using *n*-pentane as the solvent. In an attempt to prepare new starting materials, an investigation of alkynylamidinate complexes derived from dimethylaminopropyne was carried out. Two new lithium dimethylaminopropynylamidinates **4** and **5**, $\text{Li}[(\text{CH}_3)_2\text{N-CH}_2\text{-C}\equiv\text{C-C}(\text{NR})_2]\cdot\text{THF}$ (**4**: $\text{R} = i\text{Pr}$, **5**: $\text{R} = \text{Cy}$), were prepared similarly to **1** and **2** wherein the commercially available starting material 3-dimethylamino-1-propynyl was used instead of cyclopropylethynyl. Due to the decreased solubility of the potassium chloride relative to the lithium chloride in THF, which generally aids in post-reaction treatment, potassium amidinates as starting materials were great interest in this Ph.D. work. For the first time, two potassium cyclopropylethynylamidinates, $\text{K}[c\text{-C}_3\text{H}_5\text{-C}\equiv\text{C-C}(\text{NR})_2]\cdot\text{THF}$ (**6**: $\text{R} = i\text{Pr}$, **7**: $\text{R} = \text{Cy}$), were successfully synthesized similarly to **1** and **2**.

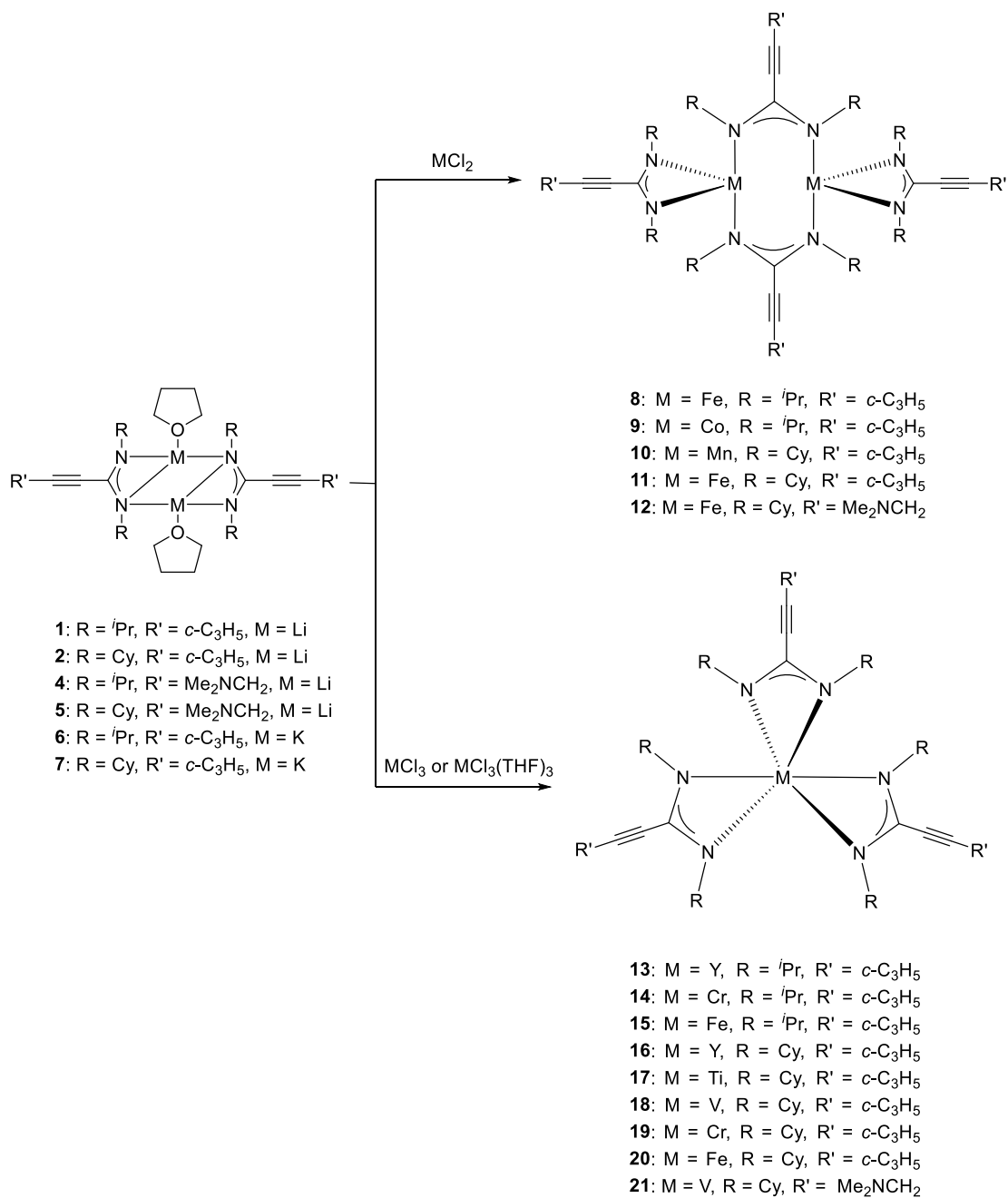


Scheme 22. Synthesis of lithium and potassium amidinates **1–6**.

As illustrated in Scheme 23, reactions of anhydrous transition metal halides MCl_2 ($\text{M} = \text{Mn, Fe, Co}$) with two equivalents of lithium cyclopropylethynylamidinate **1** and **2** or potassium cyclopropylethynylamidinate **7** afforded a series of new transition metal bis(cyclopropylethynylamidinate) complexes $[\text{M}_2\{\mu\text{-}c\text{-C}_3\text{H}_5\text{-C}\equiv\text{C-C}(\text{NR})_2\}_2\{\eta^2\text{-}c\text{-C}_3\text{H}_5\text{-C}\equiv\text{C-C}(\text{NR})_2\}_2]$ (**8**: $\text{M} = \text{Fe}$, $\text{R} = \textit{i}\text{Pr}$; **9**: $\text{M} = \text{Co}$, $\text{R} = \textit{i}\text{Pr}$; **10**: $\text{M} = \text{Mn}$, $\text{R} = \text{Cy}$; **11**: $\text{M} = \text{Fe}$, $\text{R} = \text{Cy}$). All four homoleptic bis(cyclopropylethynylamidinate) complexes were found to exhibit very similar molecular structures. Dinuclear complexes with a combination of bridging and chelating amidinate are a well-known structural type of such complexes of transition elements [152]. Moreover, a new iron

bis(dimethylaminopropynylamidinate) complex, $[\text{Fe}_2\{\mu\text{-(CH}_3)_2\text{N-CH}_2\text{-C}\equiv\text{C-C(NCy)}_2\}_2\{\eta^2\text{-(CH}_3)_2\text{N-CH}_2\text{-C}\equiv\text{C-C(NCy)}_2\}_2]$ (**12**), was successfully synthesized by treating lithium dimethylaminopropynylamidinate **4** with two equiv. of anhydrous iron(II) chloride in THF. X-ray diffraction analysis of **12** showed that the additional nitrogen donor group does not contribute to metal coordination.

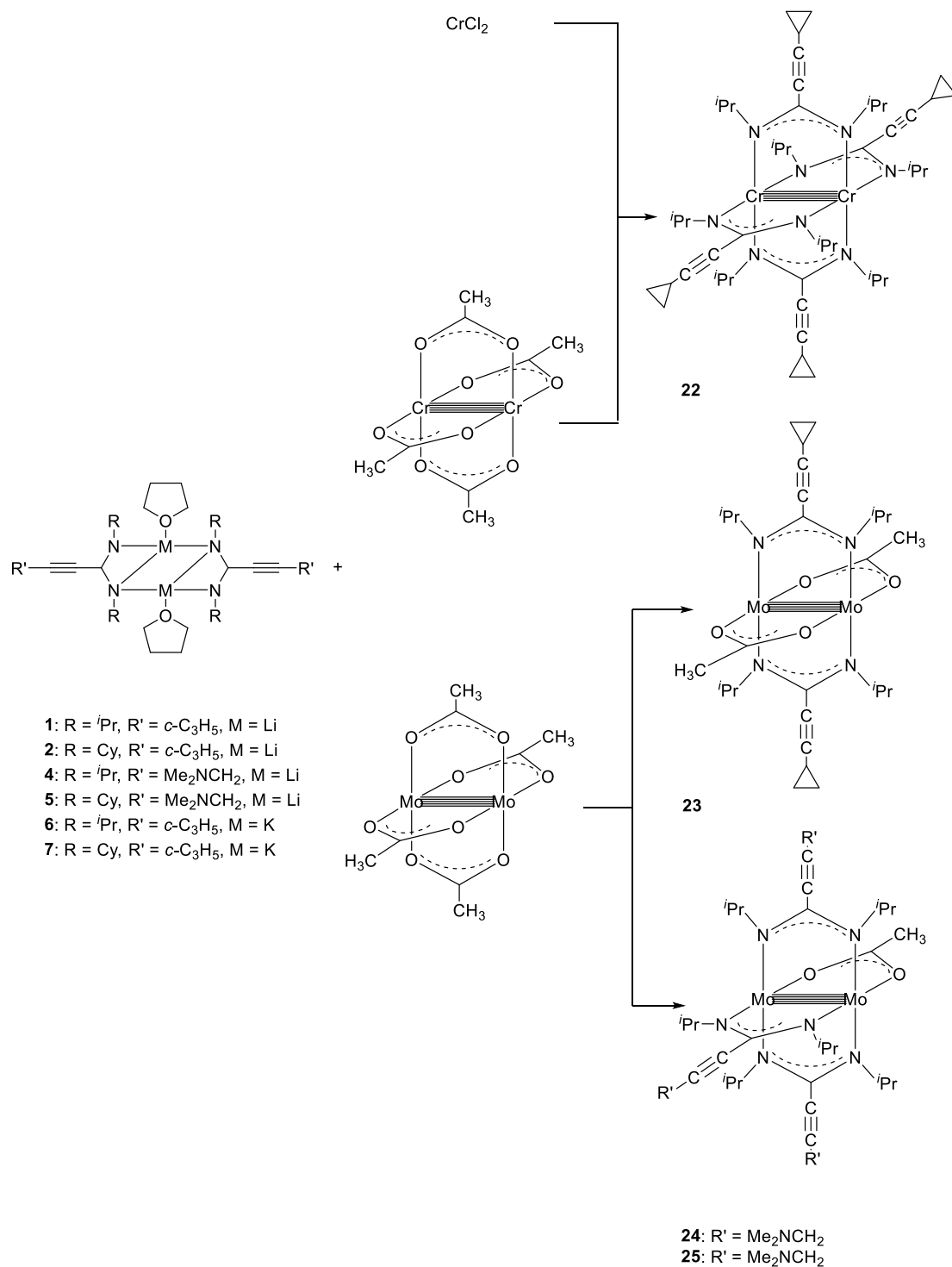
Transition metal tris(cyclopropylethynylamidinate) complexes, $[\text{M}\{c\text{-C}_3\text{H}_5\text{-C}\equiv\text{C-C(N}^i\text{Pr)}_2\}_3]$ (**13**: M = Y, **14**: M = Cr **15**: M = Fe), and $[\text{M}\{c\text{-C}_3\text{H}_5\text{-C}\equiv\text{C-C(NCy)}_2\}_3]$ (**16**: M = Y, **17**: M = Ti, **18**: M = V, **19**: M = Cr, **20**: M = Fe), were prepared by reaction of anhydrous transition metal halides MCl_3 (M = Y, Cr and Fe) or solvated transition metal halides $\text{MCl}_3\cdot\text{THF}_3$ (M = Ti and V) with three equivalents of lithium amidinates **1**, **2** or **7**. The Ti(III) compound **17** could also be prepared by using a different starting material, trichloro(cyclopentadienyl)titanium(IV), with lithium amidinate **2** in a 1:3 molar ratio, whereby the yield was slightly decreased (55%). Similarly, vanadium tris(dimethylaminopropynylamidinate) complex **21** was prepared by the reaction of anhydrous vanadium(III) chloride and lithium amidinate **1** in THF in a 1:3 molar ratio. NMR, IR, and MS, as well as elemental analyses confirmed the molecular structure of **21** is similar to complexes **13–20**.



Scheme 23. Synthesis of transition metal bis- and tris(amidinate) complexes.

The investigation of amidinate complexes with short M–M contacts is always considered to be of significant interest. A new dichromium complex, $[\text{Cr}_2\{\mu\text{-}c\text{-C}_3\text{H}_5\text{-C}\equiv\text{C-C}(\text{N}^i\text{Pr})_2\}_4]$ (**22**), containing bridging amidinate ligand was prepared in a similar way as the transition metal bis(amidinate) complexes **8–12** (Scheme 24). The 1:2 reaction of anhydrous CrCl_2 and lithium amidinate **1** was carried out in THF. As expected, complex **22** belongs to the family of quadruple-bonded dichromium complexes with a short intermetallic contact. A remarkable ability of the amidinate ligand is to construct the bridging mode of coordination which could be useful to build up the dinuclear complexes containing metal–metal multiple bonds.

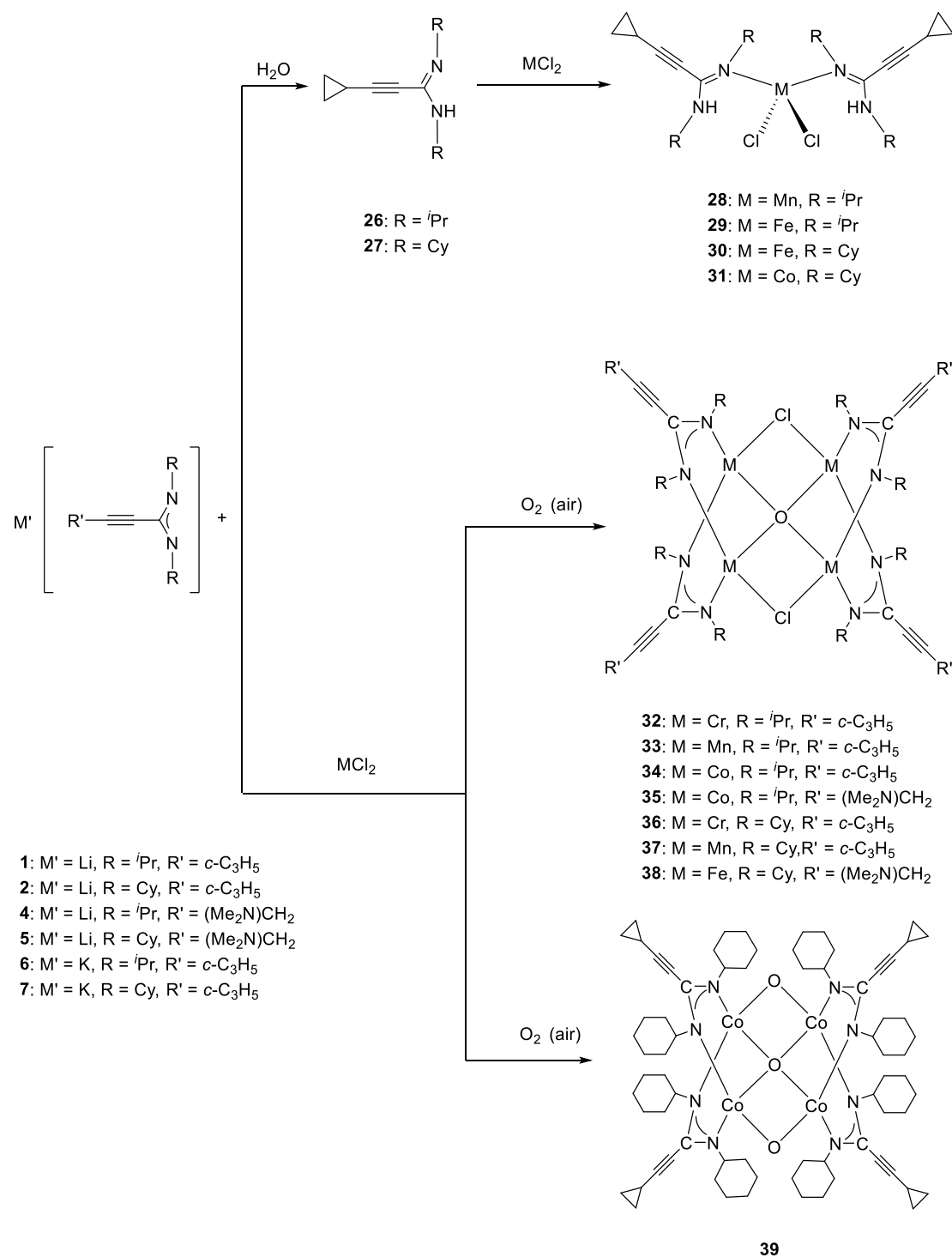
The heavier group 6 transition metal molybdenum also plays a decisive role which is capable of forming metal-metal bonds of high formal bond orders. Reactions of the quadruply bonded dimolybdenum complex $[\text{Mo}_2(\mu\text{-OAc})_4]$ with two or four equivalents of lithium amidinate **1**, $\text{Li}[c\text{-C}_3\text{H}_5\text{-C}\equiv\text{C-C}(\text{N}^i\text{Pr})_2]$, were carried out in THF. The resulting mixed-ligand quadruply bonded dimolybdenum complexes, $[\text{Mo}_2(\mu\text{-OAc})_2\{\mu\text{-}c\text{-C}_3\text{H}_5\text{-C}\equiv\text{C-C}(\text{N}^i\text{Pr})_2\}_2]$ (**23**) and $[\text{Mo}_2(\mu\text{-OAc})\{\mu\text{-}c\text{-C}_3\text{H}_5\text{-C}\equiv\text{C-C}(\text{N}^i\text{Pr})_2\}_3]$ (**24**) are shown in Scheme 24. The complexes show a well-known paddle-wheel structure, a typical dimeric arrangement of quadruply-bonded dichromium complexes. Another dimolybdenum complex, $[\text{Mo}_2(\mu\text{-OAc})\{(\text{CH}_3)_2\text{N-CH}_2\text{-C}\equiv\text{C-C}(\text{NCy})_2\}_3]$ (**25**), was prepared by treating lithium dimethylaminopropynylamidinate **4** with three equiv. of dimolybdenum complex $[\text{Mo}_2(\mu\text{-OAc})_4]$ in a similar way as in complexes **23** and **24**. However, the additional nitrogen donor group does not contribute to metal coordination.



Scheme 24. Synthesis of chromium and molybdenum amidinate complexes with short M–M contacts.

In the course of this work, hydrolysis products $MCl_2[c-C_3H_5-C\equiv C-C(NR)(NHR)]$ (**28**: $M = Mn$, $R = iPr$; **29**: $M = Fe$, $R = iPr$; **30**: $M = Fe$, $R = Cy$; **31**: $M = Co$, $R = Cy$) were occasionally observed and structurally characterized, which contain the neutral amidines $c-C_3H_5-C\equiv C-C(NR)(NHR)$ (**26**: $R = iPr$, **27**: $R = Cy$) as new ligands. The lithium amidinate **1** and **2** were carefully hydrolyzed by treating with a small amount of distilled water to afford neutral amidines **26** and **27** in a deliberate manner.

Moreover, a series of oxygen-centered transition metal amidinate complexes were obtained during the work on synthesis of transition metal bis(amidinate) complexes and M–M amidinates complexes with short contacts by careful exposure to air. The reaction of $CrCl_2 \cdot (THF)_2$ and lithium amidinate **1** was carried out in a ratio 1:1 in THF. The X-ray diffraction analysis of the complexes $(\mu_4-O)[Mn\{c-C_3H_5-C\equiv C-C(NCy)_2\}]_4Cl_2$ (**37**) and $(\mu_4-O)(\mu_2-O)_2[Mn\{c-C_3H_5-C\equiv C-C(NCy)_2\}]_4$ (**39**) showed two oxygen-centred variants of transition metal amidinates. Compared to complex **37**, two chlorine atoms of **37** are replaced by two oxygen atoms in **39**, indicating that the cobalt(II) ions in **39** were partially oxidized to cobalt(III).



Scheme 25. Synthesis of complexes **28–31** starting by hydrolysis of lithium amidinates **1** and **2** and formation of oxygen-centered transition metal amidinate complexes **32–39**.

Chapter 4

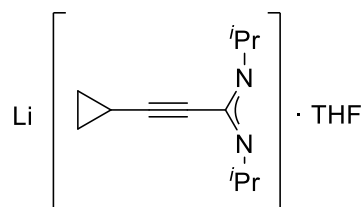
Experimental section

General

All reactions were carried out in oven-dried or flame-dried glassware in an inert atmosphere of dry argon employing standard Schlenk and glovebox techniques. The solvent THF was distilled from sodium/benzophenone in a nitrogen atmosphere before use. *n*-Butyllithium (1.6 M in hexanes) was purchased from Sigma-Aldrich. ^1H NMR (400 MHz) and ^{13}C NMR (100.6 MHz) spectra were recorded in THF- d_8 solution using a Bruker DPX 400 spectrometer at 298 K. Chemical shifts are referenced to tetramethylsilane. IR spectra were measured with a Bruker Vertex 70V spectrometer equipped with a diamond ATR unit between 4000 cm^{-1} and 50 cm^{-1} . The relative intensities of the absorption bands are given as very strong (vs), strong (s), middle (m), weak (w), and shoulder (sh). Mass spectra (EI, 70 eV) were recorded with a MAT 95 apparatus. Microanalyses of the compounds was performed using a Vario EL cube apparatus from Elementar Analysensysteme GmbH.

Preparation of $\text{Li}[c\text{-C}_3\text{H}_5\text{-C}\equiv\text{C-C}(\text{N}^i\text{Pr})_2]\cdot\text{THF}$ (1)

A THF (80 mL) solution of cyclopropylacetylene (4.2 mL, 50 mmol) was cooled to $-20\text{ }^\circ\text{C}$ and treated slowly with *n*-butyllithium (31.3 mL, 50 mmol, 1.6 M solution in



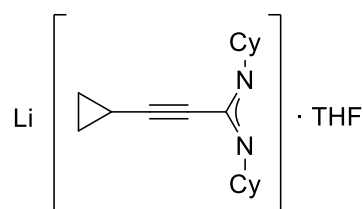
hexanes). After 15 min, to the resultant colorless solution was added *N,N'*-di-*iso*-propylcarbodiimide (7.8 mL, 50 mmol) and stirred for 30 min at $-30\text{ }^\circ\text{C}$. The reaction mixture was then warmed to r.t. and stirred for 2 h. THF

was removed in vacuum to a volume of *ca.* 20 mL and an analytical sample was obtained by crystallization from THF at $-25\text{ }^\circ\text{C}$ for 1 day. The solvent was decanted with a cannula and the resulting product was dried under reduced pressure to afford **1**

as colorless crystals. Yield: 12.7 g (85%). Mp. 115 °C (dec.). Elem. anal. calcd. for $C_{16}H_{27}LiN_2O$ ($M = 270.34$ g/mol): C 71.09, H 10.07, N 10.36; found: C 70.78, H 10.26, N 11.14%. **IR** (ATR): $\nu = 3677$ w, 3209 w, 3097 m, 3016 s, 2961 vs (ν C–H), 2865 s (ν C–H), 2609 s, 2216 s (ν C \equiv C), 1593 s (ν NCN), 1385 s, 1332 m, 1170 m, 1134 s, 1052 m, 964 s, 918 m, 871 w, 840 w, 812 m, 729 w, 716 s, 687 m, 663 w, 529 m, 507 s, 436 m cm^{-1} . **1H NMR** (400 MHz, THF- d_8 , 25 °C): $\delta = 3.77$ (sept, 2H, $CH(CH_3)_2$), 3.60 (m, 4H, α -THF), 1.75 (m, 4H, β -THF), 1.36 (m, 1H, CH , c - C_3H_5), 0.98 (d, 12H, $CH(CH_3)_2$), 0.79 (m, 2H, CH_2 , c - C_3H_5), 0.65 (m, 2H, CH_2 , c - C_3H_5) ppm. **^{13}C NMR** (100.6 MHz, THF- d_8 , 25 °C): $\delta = 157.0$ (NCN), 97.1 ($CH-C\equiv C$), 69.0 ($C\equiv C-C$), 67.1 (α -THF), 49.8 ($CH(CH_3)_2$), 26.8 ($CH(CH_3)_2$), 26.3 (β -THF), 8.9 (CH_2 , c - C_3H_5), 0.4 (CH , c - C_3H_5) ppm. **MS** (EI, 70 eV): m/z (rel. int. %) = 191 (7) [$M - Li(THF)$] $^+$, 149 (12) [$M - Li(THF) - c$ - C_3H_5] $^+$, 72 (100) [THF] $^+$.

Preparation of $Li[c-C_3H_5-C\equiv C-C(NCy)_2]\cdot THF$ (**2**)

In a fashion similar to the preparation of **1**, but adding *N,N'*-dicyclohexylcarbodiimide (10.3 g, 50 mmol) in a THF (80 mL) solution of cyclopropylacetylene (4.2 mL, 50



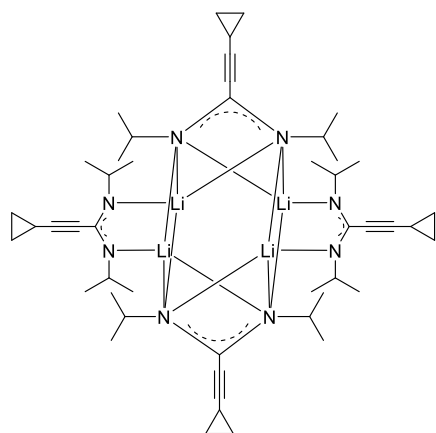
mmol). An analytical sample was obtained by crystallization from THF at -25 °C for 1 day. The solvent was decanted with a cannula and the resulting product was dried under reduced pressure to afford **2** as colorless

crystals. Yield: 15.2 g (87%). Mp. 165 °C (dec.). Elem. anal. calcd. for $C_{22}H_{35}LiN_2O$ ($M = 350.47$ g/mol): C 75.39, H 10.07, N 7.99; found: C 74.50, H 10.33, N 7.77%. **IR** (ATR): $\nu = 3677$ w, 3438 w, 3090 m, 3010 m, 2925 vs (ν C–H), 2849 vs (ν C–H), 2659 w, 2589 w, 2219 s (ν C \equiv C), 1951 w, 1599 s (ν NCN), 1501 vs, 1447 s, 1425 m, 1358 s, 1341 s, 1306 m, 1254 m, 1241 m, 1181 m, 1068 s, 1056 s, 1029 m, 969 vs, 918 m, 898 s, 887 s, 857 m, 842 m, 812 m, 796 w, 785 w, 713 s, 672 m, 544 w, 497 m, 476 w, 451 w, 433 w, 417 w, 403 w cm^{-1} . **1H NMR** (400 MHz, THF- d_8 , 25 °C): $\delta = 3.69$ (m, 4H, α -THF), 3.32 (m, 2H, CH , Cy), 1.75 (m, 4H, β -THF), 1.01 – 1.67 (m, 20H, CH_2 , Cy), 1.31 (m, 1H, CH , c - C_3H_5), 0.77 (m, 2H, CH_2 , c - C_3H_5), 0.60 (m, 2H, CH_2 , c - C_3H_5) ppm.

^{13}C NMR (100.6 MHz, THF- d_8 , 25 °C): δ = 157.0 (NCN), 96.9 (CH-C \equiv C), 69.3 (C \equiv C-C), 67.1 (α -THF), 59.0 (CH, Cy), 38.0 (CH $_2$, Cy), 27.1 (CH $_2$, Cy), 26.3 (β -THF), 9.1 (CH $_2$, *c*-C $_3$ H $_5$), 0.4 (CH, *c*-C $_3$ H $_5$) ppm. MS (EI, 70 eV): m/z (rel. int. %) = 272 (12) [M - Li(THF)] $^+$, 229 (18) [M - Li(THF) - *c*-C $_3$ H $_5$] $^+$, 72 (100) [THF] $^+$.

Preparation of {Li[*c*-C $_3$ H $_5$ -C \equiv C-(N^i Pr) $_2$]} $_4$ (**3**)

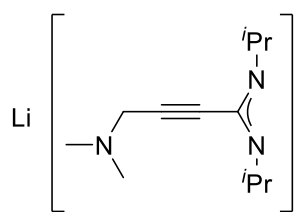
In a fashion similar to the preparation of **1**, but with *n*-pentane as solvent. An analytical sample was obtained by crystallization from *n*-pentane at -25 °C for 2 days to afford **3**



as colorless crystals. Yield: 6.9 g (70%). Elem. anal. calcd. for C $_{48}$ H $_{76}$ Li $_4$ N $_8$ (M = 792.93 g/mol): C 72.71, H 9.66, N 14.13; found: C 69.00, H 10.25, N 13.58%. IR (ATR): ν = 3094 w, 3014 w, 2954 s (ν C-H), 2863 s (ν C-H), 2607 w, 2215 s (ν C \equiv C), 2116 w, 1588 s (ν NCN), 1490 vs, 1461 vs, 1380 s, 1330 vs, 1245 w, 1167 s, 1130 m, 1026 m, 963 s,

871 w, 840 w, 811 m, 727 m, 692 m, 666w cm $^{-1}$. ^1H NMR (400 MHz, THF- d_8 , 25 °C): δ = 3.78 (sept, 2H, CH(CH $_3$) $_2$), 1.37 (m, 1H, CH, *c*-C $_3$ H $_5$), 0.98 (d, 12H, CH(CH $_3$) $_2$), 0.79 (m, 2H, CH $_2$, *c*-C $_3$ H $_5$), 0.65 (m, 2H, CH $_2$, *c*-C $_3$ H $_5$) ppm. ^{13}C NMR (100.6 MHz, THF- d_8 , 25 °C): δ = 157.1 (NCN), 97.2 (CH-C \equiv C), 69.0 (C \equiv C-C), 49.9 (CH(CH $_3$) $_2$), 23.4 (CH(CH $_3$) $_2$), 8.9 (CH $_2$, *c*-C $_3$ H $_5$), 0.4 (CH, *c*-C $_3$ H $_5$) ppm. MS (EI, 70 eV): m/z (rel. int. %) = 793 (100) [M] $^+$.

Preparation of Li[(CH $_3$) $_2$ N-CH $_2$ -C \equiv C-C(N^i Pr) $_2$] (**4**)



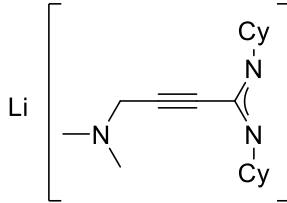
In a fashion similar to the preparation of **1**, but treating 3-dimethylamino-1-propyne (5 g, 59 mmol) with *n*-butyllithium (36.9 mL, 59 mmol, 1.6 M solution in hexanes) in a THF solution. An analytical sample was obtained by crystallization

from THF at -25 °C for 3 days to afford **4** as colorless crystals. Yield: 10.0 g (79%). Mp. 165 °C (dec.). Elem. anal. calcd. for C $_{12}$ H $_{22}$ LiN $_3$ (M = 215.26 g/mol): C 66.96, H

10.30, N 19.52; found: C 66.76, H 10.31, N 18.64%. **IR** (ATR): $\nu = 2956$ vs (ν C–H), 2869 m (ν C–H), 2792 m (ν C–H), 2602 s, 1611 w, 1502 vs (ν NCN), 1466 s, 1437 m, 1405 w, 1368 s, 1355 m, 1316 vs, 1252 w, 1178 m, 1166 m, 1135 w, 1116 m, 1101 w, 1067 m, 1036 w, 1017 m, 978 w, 953 w, 934 w, 868 w, 813 w, 716 s, 686 m, 616 w, 602 w, 512 m, 489 m, 453 s, 439 s, 422 s, 400 m, 359 s, 332 m, 291 w, 233 m, 174 w, 123 m, 95 m, 60 w cm^{-1} . **$^1\text{H NMR}$** (400 MHz, THF- d_8 , 25 °C): $\delta = 3.87$ (sept, 2H, $\text{CH}(\text{CH}_3)_2$), 3.40 (s, 2H, NCH_2C), 2.25 (s, 6H, $(\text{CH}_3)_2\text{N}$), 1.01 (d, 12H, $\text{CH}(\text{CH}_3)_2$) ppm. **$^{13}\text{C NMR}$** (100.6 MHz, THF- d_8 , 25 °C): $\delta = 156.6$ (NCN), 88.5 ($\text{CH}_2\text{-C}\equiv\text{C}$), 78.2 ($\text{C}\equiv\text{C-C}$), 49.9 ($\text{CH}(\text{CH}_3)_2$), 48.7 ($\text{CH}_2\text{-C}\equiv\text{C}$), 44.2 ($(\text{CH}_3)_2\text{N}$), 27.0 ($\text{CH}(\text{CH}_3)_2$) ppm. **MS** (EI, 70 eV): m/z (rel. int. %) = 208 (3) [$M - \text{Li}$] $^+$, 166 (100) [$M - \text{Li} - \text{Pr}$] $^+$, 165 (46) [$M - \text{Li} - (\text{CH}_3)_2\text{N}$] $^+$.

Preparation of $\text{Li}[(\text{CH}_3)_2\text{N-CH}_2\text{-C}\equiv\text{C-C}(\text{NCy})_2]$ (**5**)

In a fashion similar to the preparation of **2**, but treating the 3-dimethylamino-1-propynyl (**5** g, 59 mmol) with *n*-butyllithium (36.9 mL, 59 mmol, 1.6 M solution in hexanes) in

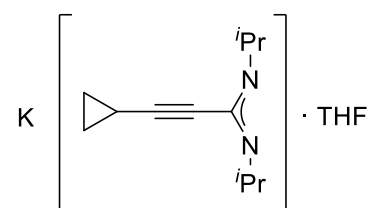
Li  a THF solution. An analytical sample was obtained by crystallization from *n*-pentane at -25 °C for 3 days to afford **5** as colorless crystals. Yield: 15.0 g (86%). Mp. 115 °C (dec.). Elem. anal. calcd. for $\text{C}_{18}\text{H}_{30}\text{LiN}_3$ ($M = 295.39$ g/mol): C 73.19,

H 10.24, N 14.23; found: C 74.05, H 10.27, N 14.48%. **IR** (ATR): $\nu = 3663$ w, 2919 vs (ν C–H), 2848 m (ν C–H), 2791 m (ν C–H), 2664 w, 2588 w, 2121 w, 1618 w, 1585 w, 1506 vs (ν NCN), 1460m, 1445 s, 1404 w, 1364 m, 1328 vs, 1310 m, 1252 m, 1241 m, 1162 m, 1139 m, 1087 w, 1074 m, 1036 m, 1011 m, 979 w, 949 w, 919 w, 889 m, 840 w, 811 w, 755 w, 720 m, 674 w, 649 m, 618 w, 549 m, 494 m, 449 m, 416 m, 368 s, 333 m, 256 m, 225 w, 199 w, 164 w, 136 w, 109 w, 78 w, 60 w cm^{-1} . **$^1\text{H NMR}$** (400 MHz, THF- d_8 , 25 °C): $\delta = 3.46$ (m, 2H, CH, Cy), 3.41 (s, 2H, NCH_2C), 2.28 (s, 6H, $(\text{CH}_3)_2\text{N}$), 1.11 – 1.78 (m, 20H, CH_2 , Cy) ppm. **$^{13}\text{C NMR}$** (100.6 MHz, THF- d_8 , 25 °C): $\delta = 156.5$ (NCN), 87.9 ($\text{CH}_2\text{-C}\equiv\text{C}$), 78.5 ($\text{C}\equiv\text{C-C}$), 58.8 (CH, Cy), 48.7 ($\text{CH}_2\text{-C}\equiv\text{C}$),

44.3 ((CH₃)₂N), 38.4 (CH₂, Cy), 26.3 (CH₂, Cy), ppm. **MS** (EI, 70 eV): m/z (rel. int. %) = 289 (19) [M – Li]⁺, 245 (65) [M – Li – (CH₃)₂N]⁺, 206 (17) [M – Li – Cy]⁺.

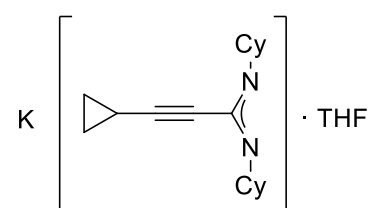
Preparation of K[c-C₃H₅-C≡C-C(N^{*i*}Pr)₂]**·**THF (**6**)

In a fashion similar to the preparation of **1**, but treating a THF (50 mL) solution of potassium hydride (2.0 g, 50 mmol) with a THF (50 mL) solution of



cyclopropylacetylene (4.2 mL, 50 mmol). The THF solvent was removed in vacuum affording **6** as white solid. Yield: 11.8 g (78%). Elem. anal. calcd. for C₁₆H₂₇KN₂O ($M = 302.50$ g/mol): C 63.53, H 9.00, N 9.26; found: C 62.53, H 8.81, N 9.45%. **IR** (ATR): $\nu = 3504$ w, 3093 w, 3013 w, 2957 vs (ν C–H), 2926 s (ν C–H), 2863 s (ν C–H), 2606 w, 2210 w (ν C≡C), 1983 w, 1693 w, 1639 s (ν NCN), 1574 w, 1484 vs, 1370 s, 1326 s, 1241 S, 1161 s, 1124 s, 1033 m, 984 w, 959 s, 871 w, 834 w, 811 w, 778 w, 716 w, 681 m, 629 w, 553 w, 515 m, 450 s, 382 w, 277 w cm⁻¹. **¹H NMR** (400 MHz, THF-*d*₈, 25 °C): $\delta = 3.72$ (sept, 2H, CH(CH₃)₂), 3.67 (m, 4H, α -THF), 1.76 (m, 4H, β -THF), 1.36 (m, 1H, CH, *c*-C₃H₅), 0.96 (d, 12H, CH(CH₃)₂), 0.79 (m, 2H, CH₂, *c*-C₃H₅), 0.65 (m, 2H, CH₂, *c*-C₃H₅) ppm. **¹³C NMR** (100.6 MHz, THF-*d*₈, 25 °C): $\delta = 153.8$ (NCN), 95.1 (CH–C≡C), 70.4 (C≡C–C), 67.8 (α -THF), 49.2 (CH(CH₃)₂), 27.4 (CH(CH₃)₂), 25.3 (β -THF), 8.9 (CH₂, *c*-C₃H₅), 0.5 (CH, *c*-C₃H₅) ppm. **MS** (EI, 70 eV): m/z (rel. int. %) = 192 (33) [M – Li(THF)]⁺, 149 (55) [M – Li(THF) – *c*-C₃H₅]⁺.

Preparation of K[c-C₃H₅-C≡C-C(NCy)₂]**·**THF (**7**)



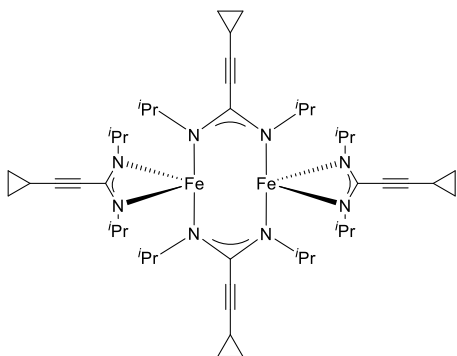
In a fashion similar to the preparation of **2**, but treating a THF (50 mL) solution of potassium hydride (2.0 g, 50 mmol) with a THF (50 mL) solution of cyclopropylacetylene (4.2 mL, 50 mmol). The THF

solvent was removed in vacuum affording **7** as white solid. Yield: 15.3 g (80%). Mp. 261 °C (dec.). Elem. anal. calcd. for C₂₂H₃₅KN₂O ($M = 382.62$ g/mol): C 69.06, H 9.22,

N 7.32; found: C 68.97, H 9.20, N 7.17%. **IR** (ATR): $\nu = 3324$ w, 3092 w, 3009 w, 2920 vs (ν C–H), 2849 s (ν C–H), 2664 w, 2210 w (ν C \equiv C), 1688 w, 1661 w, 1634 s (ν NCN), 1581 w, 1490 vs, 1447 s, 1357 s, 1342 m, 1303 m, 1258 w, 1157 m, 1051 m, 966 s, 942 w, 919 m, 856m, 752 w, 671 m, 619 w, 546 w, 502 w, 448 w, 360 m, 333 w, 263 w, 220 w, 197 m, 136 vs, 74 s, 60 s cm^{-1} . **^1H NMR** (400 MHz, THF- d_8 , 25 °C): $\delta = 3.62$ (m, 4H, α -THF), 3.28 (m, 2H, CH, Cy), 1.75 (m, 4H, β -THF), 1.01 – 1.69 (m, 20H, CH_2 , Cy), 1.30 (m, 1H, CH, c - C_3H_5), 0.77 (m, 2H, CH_2 , c - C_3H_5), 0.60 (m, 2H, CH_2 , c - C_3H_5) ppm. **^{13}C NMR** (100.6 MHz, THF- d_8 , 25 °C): $\delta = 153.6$ (NCN), 94.7 (CH–C \equiv C), 70.5 (C \equiv C–C), 67.9 (α -THF), 59.2 (CH, Cy), 38.5 (CH_2 , Cy), 27.3 (CH_2 , Cy), 25.7 (β -THF), 9.4 (CH_2 , c - C_3H_5), 0.5 (CH, c - C_3H_5) ppm. **MS** (EI, 70 eV): m/z (rel. int. %) = 272 (84) [$M - \text{K}(\text{THF})$] $^+$, 229 (100) [$M - \text{K}(\text{THF}) - c$ - C_3H_5] $^+$, 189 (70) [$M - \text{K}(\text{THF}) - \text{Cy}$] $^+$.

Preparation of $[\text{Fe}_2\{\text{iPrNC}(\text{C}\equiv\text{C}-c\text{-C}_3\text{H}_5)\text{N}^i\text{Pr}\}_4]$ (**8**)

A solution of anhydrous FeCl_2 (0.23 g, 1.8 mmol) in 30 mL of THF was added to a solution of **1** (1.0 g, 3.6 mmol) in 50 mL of THF. The reaction mixture was stirred at



r.t. with a glass-coated stirring bar for 3 hours.

The solvent was then removed in vacuum followed by extraction with *n*-pentane (30 mL).

After a white precipitate (LiCl) was filtered off, a clear, brown solution was obtained and concentrated to a total volume of *ca.* 10 mL. An

analytical sample was isolated by crystallization from *n*-pentane at 5 °C for one week.

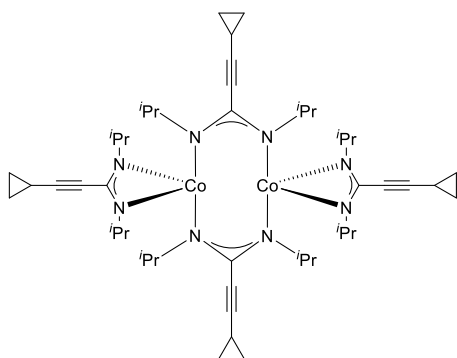
The solvent was decanted with a cannula and the resulting product was dried under reduced pressure to afford **8** as yellow, prism-like crystals. Yield: 0.39 g (49%). Mp.

165 °C (dec.). Elem. anal. calcd. for $\text{C}_{48}\text{H}_{76}\text{Fe}_2\text{N}_8$ ($M = 876.86$ g/mol): C 65.75, H 8.74, N 12.78; found: C 65.70, H 8.67, N 12.79%. **IR** (ATR): $\nu = 3787$ w, 3665 w, 3599 w, 3562 w, 3438 w, 3189 w, 3095 w, 2921 vs (ν C–H), 2848 m (ν C–H), 2662 w, 2225 m (ν C \equiv C), 2075 w, 1606 m (ν NCN), 1461 vs, 1331 vs, 1173 vs, 1131 s, 1040 m, 963 vs,

816 m, 692 s, 535 m, 479 m, 427 m cm^{-1} . **MS** (EI, 70 eV): m/z (rel. int. %) = 877 (1) $[M]^+$, 704 (3) $[M - 4 \text{ }^i\text{Pr}]^+$, 423 (25) $[M - 2(c\text{-C}_3\text{H}_5\text{-C}\equiv\text{C-C}(\text{N}^i\text{Pr})_2) - 2 \text{ }^i\text{Pr} + \text{CH}_3]^+$, 177 (96) $[c\text{-C}_3\text{H}_5\text{-C}\equiv\text{C-C}(\text{N}^i\text{Pr})_2 - \text{CH}_3]^+$.

Preparation of $[\text{Co}_2\{\text{ }^i\text{PrNC}(\text{C}\equiv\text{C-}c\text{-C}_3\text{H}_5)\text{N}^i\text{Pr}\}_4]$ (**9**)

In a fashion similar to the preparation of **8**, compound **9** was made by treatment of **1** (1.0 g, 3.6 mmol) with anhydrous CoCl_2 (0.23 g, 1.8 mmol) afforded **9** in the form of

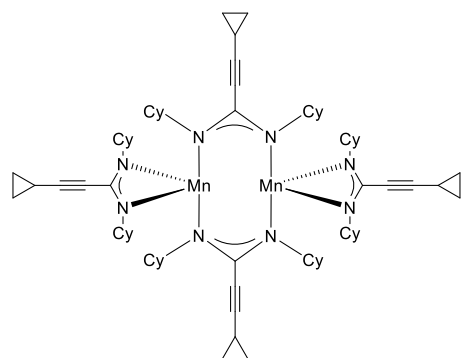


yellow-green, plate-like crystals. Yield: 0.40 g (50%). Mp. 116 °C (dec.). Elem. anal. calcd. for $\text{C}_{48}\text{H}_{76}\text{Co}_2\text{N}_8$ ($M = 883.08$ g/mol): C 65.29, H 8.67, N 12.69; found: C 64.71, H 8.50, N 12.43%. **IR** (ATR): $\nu = 3685$ w, 3096 w, 3014 w, 2962 s (ν C–H), 2920 m (ν C–H), 2863 m (ν C–H), 2602 w, 2219

m (ν $\text{C}\equiv\text{C}$), 1669 w, 1644 w, 1597 m (ν NCN), 1476 vs, 1395 s, 1376 s, 1358 s, 1335 s, 1171 s, 1133 s, 1087 w, 1050 m, 1028 m, 969 s, 876 w, 842 m, 810 m, 719 m, 692 m, 573 m, 527 m, 467 m, 420 m, 353 w, 295 m, 259 m, 239 m, 175 m, 104 m cm^{-1} . **MS** (EI, 70 eV): m/z (rel. int. %) = 899 (2) $[M + \text{CH}_3]^+$, 667 (5) $[M - 5 \text{ }^i\text{Pr}]^+$, 593 (95) $[M - 3 \text{ }^i\text{Pr} - 4(c\text{-C}_3\text{H}_5)]$, 501 (62) $[M - 2(c\text{-C}_3\text{H}_5\text{-C}\equiv\text{C-C}(\text{N}^i\text{Pr})_2)]^+$.

Preparation of $[\text{Mn}_2\{\text{CyNC}(\text{C}\equiv\text{C-}c\text{-C}_3\text{H}_5)\text{NCy}\}_4]$ (**10**)

In a fashion similar to the preparation of **8**, compound **10** was made by treatment of **2** (1.0 g, 2.8 mmol) with anhydrous MnCl_2 (0.18 g, 1.4 mmol) afforded **10** as yellow,

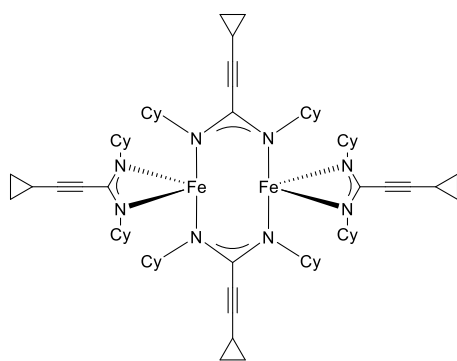


prism-like crystals. Yield: 0.49 g (59%). Mp. 165 °C (dec.). Elem. anal. calcd. for $\text{C}_{72}\text{H}_{108}\text{Mn}_2\text{N}_8$ ($M = 1195.55$ g/mol): C 72.33, H 9.10, N 9.37; found: C 72.27, H 9.36, N 8.70%. **IR** (ATR): $\nu = 3655$ w, 3442 w, 3232 w, 3093 w, 3093 w, 3011 w, 3438 w, 3189 w, 3095 w, 2962 s (ν C–H), 2923 m, 2860 m (ν C–H), 2705 w, 2663 w, 2603 w,

2481 w, 2325 w, 2217 m (ν C \equiv C), 2114 w, 2071 w, 1991 w, 1942 w, 1882 w, 1813 w, 1755 w, 1684 w, 1606 m (ν NCN), 1482 vs, 1447 s, 1419 m, 1358 m, 1343 m, 1303 w, 1255 w, 1212 w, 1175 w, 1119 w, 1070 m, 1052 w, 1028 w, 971 m, 922 w, 888 w, 859 w, 842 w, 809 w, 730 w, 693 m, 624 m, 590 w, 548 w, 504 w, 431 w, 370 m, 324 m, 282 m, 209 m, 164 w, 103 w, 80 m cm^{-1} . **MS** (EI, 70 eV): m/z (rel. int. %) = 925 (3) $[M - (c\text{-C}_3\text{H}_5\text{-C}\equiv\text{C-C}(\text{NCy})_2)]^+$, 899 (37) $[M - 2(c\text{-C}_3\text{H}_5\text{-C}\equiv\text{C}) - 2(\text{Cy})]^+$, 667 (100) $[M - 3(c\text{-C}_3\text{H}_5\text{-C}\equiv\text{C}) - 4(\text{Cy})]^+$.

Preparation of $[\text{Fe}_2\{\text{CyNC}(\text{C}\equiv\text{C-}c\text{-C}_3\text{H}_5)\text{NCy}\}_4]$ (**11**)

In a fashion similar to the preparation of **8**, compound **11** was made by treatment of **7** (1.0 g, 2.6 mmol) with anhydrous FeCl_2 (0.16 g, 1.3 mmol) afforded **11** as orange,

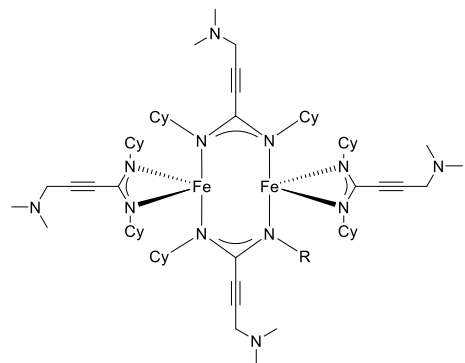


block-like crystals. Yield: 0.30 g (39%). Mp. 165 °C (dec.). Elem. anal. calcd. For $\text{C}_{75}\text{H}_{115}\text{Fe}_2\text{N}_8$ ($M = 1197.37$ g/mol): C 72.22, H 9.09, N 9.36; found: C 72.81, H 9.47, N 9.03%. **IR** (ATR): $\nu = 3437$ w, 3092 w, 3011 w, 2922 vs (ν C–H), 2848 s (ν C–H), 2664 w, 2219 m (ν C \equiv C), 1605 m (ν NCN),

1462 vs, 1446 vs, 1394 m, 1361 vs, 1344 s, 1306 m, 1255 m, 1208 w, 1174 m, 1155 m, 1117 m, 1087 w, 1068 m, 1051 m, 1028 m, 971 s, 923 m, 889 m, 858 m, 843 w, 808 m, 734 m, 717 w, 696 m, 676 m, 611 m, 591 m, 552 w, 505 w, 480 w, 445 w, 431 w, 359 m, 333 w, 281 m, 249 s, 219 m, 185 w, 161 w, 120 w, 89 w, 58 w cm^{-1} . **^1H NMR** (400 MHz, $\text{THF-}d_8$, 25 °C): $\delta = 4.27$ (m, 2H, CH, Cy), 3.21 (m, 2H, CH_2 , Cy), 3.36 – 3.56 (br, 20H, CH_2 , Cy), 1.43 (m, 1H, CH, $c\text{-C}_3\text{H}_5$), 0.80 (m, 2H, CH_2 , $c\text{-C}_3\text{H}_5$) ppm. **^{13}C NMR** (100.6 MHz, $\text{THF-}d_8$, 25 °C): $\delta = 140.8$ (NCN), 94.6 (CH–C \equiv C), 60.4 (C \equiv C–C), 66.7 (CH, Cy), 56.7 (CH_2 , Cy), 52.0 (CH_2 , Cy), 9.2 (CH_2 , $c\text{-C}_3\text{H}_5$), 0.3 (CH, $c\text{-C}_3\text{H}_5$) ppm. **MS** (EI, 70 eV): m/z (rel. int. %) = 899 (1) $[M - 2(c\text{-C}_3\text{H}_5\text{-C}\equiv\text{C}) - 2(\text{Cy})]^+$, 816 (15) $3[c\text{-C}_3\text{H}_5\text{-C}\equiv\text{C-C}(\text{NCy})_2]^+$, 636 (43) $[M - c\text{-C}_3\text{H}_5 - (c\text{-C}_3\text{H}_5\text{-C}\equiv\text{C-C}(\text{NCy})_2) - 3(\text{Cy})]^+$, 569 (75) $[M - 2(c\text{-C}_3\text{H}_5\text{-C}\equiv\text{C-C}(\text{NCy})_2) - \text{Cy}]^+$.

Preparation of $[\text{Fe}_2\{\text{CyNC}(\text{C}\equiv\text{C}-\text{CH}_2-\text{N}(\text{CH}_3)_2\text{NCy})\}_4]$ (**12**)

In a fashion similar to the preparation of **8**, compound **12** was made by treatment of **5** (1.0 g, 2.8 mmol) with anhydrous FeCl_2 (0.18 g, 1.4 mmol) afforded **12** in the form of



brown, block-like crystals. Yield: 0.61 g (69%).

Mp. 166 °C (dec.). Elem. anal. calcd. for

$\text{C}_{72}\text{H}_{120}\text{Fe}_2\text{N}_{12}$ ($M = 1265.49$ g/mol): C 68.33, H

9.56, N 8.83; found: C 68.52, H 9.58, N 8.75%.

IR (ATR): $\nu = 3792$ w, 3685 w, 2922 s (ν C–H),

2848 m (ν C–H), 2781 w (ν C–H), 2664 w, 2593

w, 2218 w (ν C \equiv C), 1603 w (ν NCN), 1463 vs, 1447 vs, 1360 s, 1344 m, 1328 m, 1314

m, 1260 w, 1241 w, 1199 w, 1180 w, 1157 m, 1141 w, 1097 w, 1063 w, 1038 m, 977

w, 945 w, 922 w, 888 m, 843 w, 814 m, 766 w, 750 w, 719 w, 678 w, 642 s, 611 w, 540

w, 494 w, 446 w, 414 w, 384 m, 370 m, 350 w, 319 w, 285 m, 251 m, 219 w, 185 w,

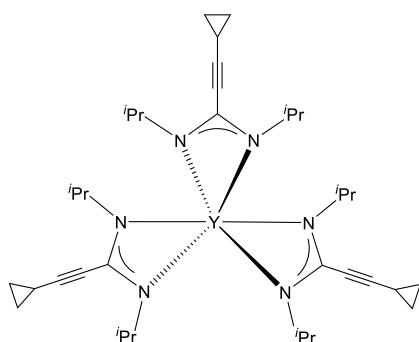
161 w, 144 w, 129 w, 96 w, 82 w, 73 w, 55 w cm^{-1} . **MS** (EI, 70 eV): m/z (rel. int. %) =

976 (10) $[\text{M} - \{(\text{CH}_2)_2\text{N}-\text{CH}_2-\text{C}\equiv\text{C}-\text{C}(\text{NCy})_2\}]^+$, 931 (17) $[\text{M} - 4\text{Cy}]^+$, 717 (86) $[\text{M} -$

$3(\text{CH}_2)_2\text{N} - 5\text{Cy}]^+$.

Preparation of $[\text{Y}\{\text{PrNC}(\text{C}\equiv\text{C}-\text{c}-\text{C}_3\text{H}_5)\text{N}^i\text{Pr}\}_3]$ (**13**):

A solution of anhydrous YCl_3 (0.23 g, 1.2 mmol) in 30 mL of THF was added to a solution of **1** (1.0 g, 3.6 mmol) in 50 mL of THF. The reaction mixture was stirred at



r.t. with a glass-coated stirring bar for 2 hours. The

solvent was then removed in vacuum followed by

extraction with *n*-pentane (30 mL). After a white

precipitate (LiCl) was filtered off, a clear, yellow

solution was obtained and concentrated to a total

volume of *ca.* 10 mL. An analytical sample was

isolated by crystallization from *n*-pentane at 5 °C for two weeks. The solvent was

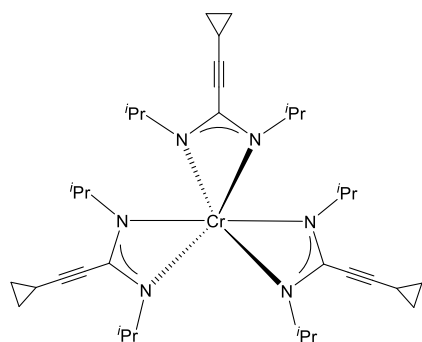
decanted with a cannula and the resulting product was dried under reduced pressure to

afford **13** in the form of colorless, block-like crystals. Yield: 0.21 g (25%). Mp. 117 °C

(dec.). Elem. anal. calcd. for $C_{36}H_{57}YN_6$ ($M = 662.78$ g/mol): C 65.24, H 8.67, N 12.68; found: C 69.11, H 9.27, N 13.54%. **IR** (ATR): $\nu = 3096$ w, 3015 w, 2958 s (ν C–H), 2926 m, 2864 m (ν C–H), 2609 w, 2219 m (ν C \equiv C), 1610 m (ν NCN), 1451 vs, 1404 vs, 1375 s, 1328 vs, 1213 vs, 1186 s, 1168 s, 1140 m, 1122 m, 1085 w, 1052 m, 1027 m, 966 vs, 876 w, 843 m, 810 m, 707 s, 688 s, 657 w, 529 m, 473 m, 438 m, 399 m, 323 w, 268 m, 228 vs, 153 m, 70 s cm^{-1} . **MS** (EI, 70 eV): m/z (rel. int. %) = 637 (2) [$M - c-C_3H_5 + CH_3$] $^+$, 449 (5) [$M - c-C_3H_5 - 4^iPr$] $^+$, 274 (96) [$M - 2(c-C_3H_5-C\equiv C) - 6^iPr$] $^+$, 232 (36) [$M - c-C_3H_5 - 2(c-C_3H_5-C\equiv C) - 6^iPr$] $^+$.

Preparation of [$Cr\{^iPrNC(C\equiv C-c-C_3H_5)N^iPr\}_3$] (**14**)

In a fashion similar to the preparation of **13**, compound **14** was made by treatment of **1** (1.0 g, 3.6 mmol) with anhydrous $CrCl_3$ (0.19 g, 1.2 mmol) afforded **14** in the form of



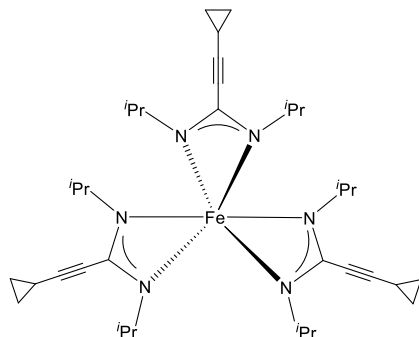
pale pink, block-like crystals. Yield: 0.39 g (52%).

Mp. 135 °C (dec.). Elem. anal. calcd. for $C_{36}H_{57}CrN_6$ ($M = 625.87$ g/mol): C 69.09, H 9.18, N 13.43; found: C 69.11, H 9.27, N 13.54%. **IR** (ATR): $\nu = 3776$ w, 3703 w, 3586 w, 3196 w, 3095 w, 2965 s (ν C–H), 2929 m (ν C–H), 2867 m (ν C–

H), 2702 w, 2608 w, 2472 w, 2286 w, 2221 m (ν C \equiv C), 2068 w, 1988 w, 1941 w, 1889 w, 1817 w, 1769 w, 1604 m (ν NCN), 1480 vs, 1440 vs, 1334 s, 1220 s, 1165 s, 1039 m, 965 s, 813 m, 695 m, 591 w, 533 m, 428 m cm^{-1} . Due to the strongly paramagnetic nature of the Cr^{3+} ion, the 1H NMR resonances could not be assigned. ^{13}C NMR (100.6 MHz, THF- d_8 , 25 °C): $\delta = 139.6$ (NCN), 93.6 (CH–C \equiv C), 67.1 (C \equiv C–C), 52.9 (CH(CH $_3$) $_2$), 42.2 (CH(CH $_3$) $_2$), 25.3 (CH(CH $_3$) $_2$), 22.9 (CH(CH $_3$) $_2$), 8.9 (CH $_2$, $c-C_3H_5$), –0.9 (CH, $c-C_3H_5$) ppm. **MS** (EI, 70 eV): m/z (rel. int. %) = 626 (5) [M] $^+$, 433 (100) [$M - (c-C_3H_5-C\equiv C-C(N^iPr)_2$)] $^+$, 191 (66) [$(c-C_3H_5-C\equiv C-C(N^iPr)_2$)] $^+$, 177 (34) [$(c-C_3H_5-C\equiv C-C(N^iPr)_2 - CH_3$)] $^+$.

Preparation of $[\text{Fe}\{\text{}^i\text{PrNC}(\text{C}\equiv\text{C}-c\text{-C}_3\text{H}_5)\text{N}^i\text{Pr}\}_3]$ (**15**)

In a fashion similar to the preparation of **13**, compound **15** was made by treatment of **1** (1.0 g, 3.6 mmol) with anhydrous FeCl_3 (0.19 g, 1.2 mmol) in 80 mL of THF. The THF



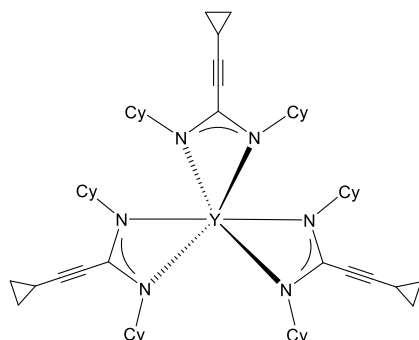
solvent was removed in vacuum followed by extraction with *n*-pentane (2×20 mL) to produce a blue solution. The extract was filtered again and concentrated to a total volume of *ca.* 10 mL.

Crystallization at 5 °C for one week afforded **15** in the form of blue, block-like crystals. Yield: 0.4 g

(53%). Mp. 135 °C (dec.). Elem. anal. calcd. for $\text{C}_{36}\text{H}_{57}\text{FeN}_6$ ($M = 629.72$ g/mol): C 68.66, H 9.12, N 13.35; found: C 68.49, H 9.10, N 13.39%. **IR** (ATR): $\nu = 3098$ w, 3017 w, 2961 s (ν C–H), 2929 m (ν C–H), 2863 m (ν C–H), 2799 w, 2699 w, 2606 w, 2222 m (ν C≡C), 1601 w (ν NCN), 1462 vs, 1431 vs, 1375 m, 1356 m, 1331 vs, 1213 s, 1184 s, 1169 s, 1140 m, 1120 m, 1086 m, 1054 m, 1028 m, 878 w, 843 m, 812 m, 702 m, 689 m, 663 w, 597 w, 531 m, 508 w, 482 m, 432 m, 399 m, 299 s, 257 m, 143 w, 105 m, 59 w cm^{-1} . Due to the strongly paramagnetic nature of the Cr^{3+} ion, the ^1H NMR resonances could not be assigned. ^{13}C NMR (100.6 MHz, $\text{THF-}d_8$, 25 °C): $\delta = 105.1$ (C≡C–C), 90.9 (C≡C–C), 49.0 ($\text{CH}(\text{CH}_3)_2$), 24.5 ($\text{CH}(\text{CH}_3)_2$), 8.8 (CH_2 , *c*- C_3H_5), 0.0 (CH , *c*- C_3H_5) ppm. **MS** (EI, 70 eV): m/z (rel. int. %) = 629 (5) $[\text{M}]^+$, 504 (5) $[\text{M} - 2(\text{c}\text{-C}_3\text{H}_5) - \text{}^i\text{Pr}]^+$, 501 (15) $[\text{M} - 3^i\text{Pr}]^+$, 433 (100) $[\text{M} - 3(\text{c}\text{-C}_3\text{H}_5\text{-C}\equiv\text{C})]^+$.

Preparation of $[\text{Y}\{\text{CyNC}(\text{C}\equiv\text{C}-c\text{-C}_3\text{H}_5)\text{NCy}\}_3]$ (**16**)

In a fashion similar to the preparation of **13**, compound **16** was made by treatment of **2**



(1.0 g, 2.9 mmol) with anhydrous YCl_3 (0.2 g, 1 mmol) afforded **16** as colorless plate-like crystals.

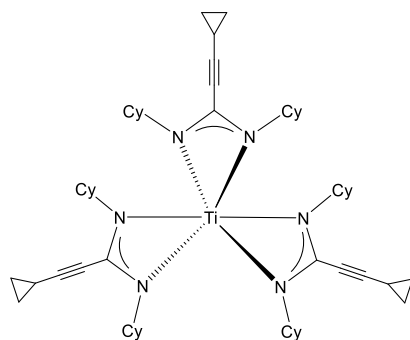
Yield: 0.21 g (22%). Mp. 135 °C (dec.). Elem. anal. calcd. for $\text{C}_{54}\text{H}_{81}\text{YN}_6$ ($M = 903.16$ g/mol): C 71.81, H 9.04, N 9.31; found: C 71.81, H 9.08, N 9.22%.

IR (ATR): $\nu = 3437$ w, 3093 w, 3012 w, 2921 vs (ν

C–H), 2849 s (ν C–H), 2665 w, 2590 w, 2223 m (ν C \equiv C), 1606 m (ν NCN), 1448 vs, 1400 s, 1360 vs, 1343 s, 1309 m, 1255 m, 1209 m, 1177 m, 1121 m, 1074 m, 1052 w, 1028 m, 972 s, 920 w, 888 m, 858 m, 841 w, 807 m, 764 w, 703 m, 676 m, 591 m, 548 w, 503 m, 482 m, 448 m, 432 m, 356 m, 333 w, 270 m, 234 vs, 183 m, 137 w, 105m, 80 w cm^{-1} . **MS** (EI, 70 eV): m/z (rel. int. %) = 902 (95) $[M]^+$, 819 (60) $[M - \text{Cy}]^+$, 631 (100) $[M - (c\text{-C}_3\text{H}_5\text{-C}\equiv\text{C-C}(\text{NCy})_2)]^+$.

Preparation of $[\text{Ti}\{\text{CyNC}(\text{C}\equiv\text{C}\text{-}c\text{-C}_3\text{H}_5)\text{NCy}\}_3]$ (**17**)

In a fashion similar to the preparation of **13**, compound **17** was made by treatment of **2** (1.0 g, 2.9 mmol) with anhydrous $\text{TiCl}_3\cdot(\text{THF})_3$ (0.37 g, 1 mmol) afforded **17** as black,

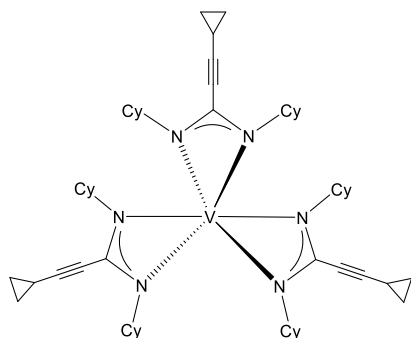


block-like crystals. Yield: 0.59 g (69%). Mp. 129 °C (dec.). **$^1\text{H NMR}$** (400 MHz, $\text{THF-}d_8$, 25 °C): δ = 1.01 – 1.89 (m, 20H, CH_2 , Cy), 1.35 (overlapped, 1H, CH , $c\text{-C}_3\text{H}_5$), 0.83 (m, 2H, CH_2 , $c\text{-C}_3\text{H}_5$), 0.68 (m, 2H, CH_2 , $c\text{-C}_3\text{H}_5$) ppm. **$^{13}\text{C NMR}$** (100.6 MHz, $\text{THF-}d_8$, 25 °C): δ = 94.8 ($\text{CH-C}\equiv\text{C}$), 65.0 ($\text{C}\equiv\text{C-C}$), 28.1

(CH_2 , Cy), 27.6 (CH_2 , Cy), 24.2 (CH_2 , Cy), 8.9 (CH_2 , $c\text{-C}_3\text{H}_5$), 0.0 (CH , $c\text{-C}_3\text{H}_5$) ppm. Elem. anal. calcd. for $\text{C}_{54}\text{H}_{81}\text{TiN}_6$ ($M = 862.12$ g/mol): C 75.23, H 9.47, N 9.75; found: C 75.25, H 9.44, N 9.73%. **IR** (ATR): ν = 3438 w, 3091 w, 3009 w, 2922 vs (ν C–H), 2849 s (ν C–H), 2662 w, 2223 m (ν C \equiv C), 2119 w, 1598 m (ν NCN), 1483 vs, 1447 vs, 1361 s, 1343 s, 1342 s, 1310 m, 1255 m, 1210 w, 1175 m, 1119 w, 1087 w, 1070 m, 1052 w, 1027 w, 972 m, 921 w, 888 m, 858 w, 841 w, 782 s, 718 w, 699 w, 683 w, 649 w, 599 m, 548 w, 489 w, 436 w, 366 m, 332 m, 226 m, 147 w, 123 w, 101 w, 84 w, 74 w, 64w, 53w cm^{-1} . **MS** (EI, 70 eV): m/z (rel. int. %) = 799 (15) $[M - (c\text{-C}_3\text{H}_5\text{-C}\equiv\text{C})]^+$, 612 (100) $[M - 3\text{Cy}]^+$, 529 (43) $[M - 4\text{Cy}]^+$.

Preparation of $[\text{V}\{\text{CyNC}(\text{C}\equiv\text{C}\text{-}c\text{-C}_3\text{H}_5)\text{NCy}\}_3]$ (**18**)

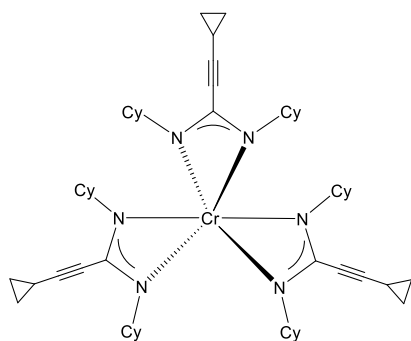
In a fashion similar to the preparation of **13**, compound **18** was made by treatment of **7** (1.0 g, 2.6 mmol) with anhydrous $\text{VCl}_3\cdot(\text{THF})_3$ (0.33 g, 0.9 mmol) afforded **18** as red,



block-like crystals. Yield: 0.35 g (45%). Mp. 110 °C (dec.). Elem. anal. calcd. for $C_{54}H_{81}N_6V$ ($M = 865.20$ g/mol): C 74.96, H 9.44, N 9.71; found: C 75.04, H 9.45, N 9.72%. **IR** (ATR): $\nu = 3094$ w, 3011 w, 2924 vs (ν C–H), 2849 s (ν C–H), 2660 w, 2221 m (ν C≡C), 1689 m (ν NCN), 1629 m, 1578 w, 1473 vs, 1448 vs, 1363 vs, 1343 s, 1309 m, 1255 m, 1207 w, 1175 m, 1150 w, 1119 w, 1076 m, 1051 w, 1029 w, 1005 w, 972 vs, 921 w, 888 m, 859 w, 842 w, 808 m, 754 m, 716 w, 697 m, 679 m, 629 w, 599 m, 522 w, 503w, 487 w, 434 w, 367 m, 306 s, 281 m, 258 m, 226 m, 194 w, 161 w, 123 w, 96 w, 86 w, 74 w, 65w cm^{-1} . **MS** (EI, 70 eV): m/z (rel. int. %) = 861 (4) $[M]^+$, 783 (20) $[M - 2Cy]^+$, 667 (100) $[M - 3(c-C_3H_5-C\equiv C)]^+$.

Preparation of $[Cr\{CyNC(C\equiv C-c-C_3H_5)NCy\}_3]$ (**19**)

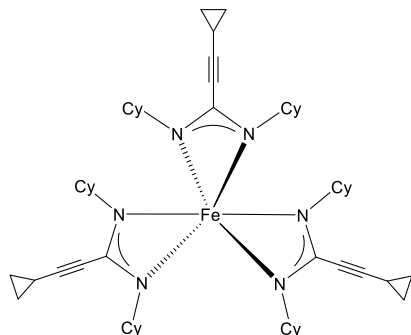
In a fashion similar to the preparation of **13**, compound **19** was made by treatment of **2** (1.0 g, 2.9 mmol) with anhydrous $CrCl_3$ (0.16 g, 1 mmol) afforded **19** as brown, block-



like crystals. Yield: 0.59 g (69%). Mp. 150 °C (dec.). Elem. anal. calcd. for $C_{54}H_{81}CrN_6$ ($M = 866.25$ g/mol): C 74.87, H 9.42, N 9.70; found: C 74.49, H 9.59, N 9.83%. Due to the strongly paramagnetic nature of the Cr^{3+} ion, the 1H NMR resonances could not be assigned. ^{13}C NMR (100.6 MHz, THF- d_8 , 25 °C): $\delta = 95.0$ (CH–C≡C), 65.0 (C≡C–C), 35.9 (CH₂, Cy), 33.8 (CH₂, Cy), 26.3 (CH₂, Cy), 8.9 (CH₂, *c*-C₃H₅), 0.0 (CH, *c*-C₃H₅) ppm. **IR** (ATR): $\nu = 3567$ w, 3013 w, 2923 vs (ν C–H), 2849 s (ν C–H), 2664 w, 2224 m (ν C≡C), 1605 m (ν NCN), 1486 vs, 1447 s, 1362 s, 1343 m, 1311 m, 1254 m, 1212 m, 1177 s, 1121 m, 1084 m, 1051 m, 1029 m, 973 s, 888 m, 860 m, 842 w, 808 m, 762 w, 718 w, 694 w, 633 w, 604 m, 557 w, 489 m, 438 m, 373 s, 331 s, 262 w, 196 w, 174 w, 129 w, 75w, 61 w cm^{-1} . **MS** (EI, 70 eV): m/z (rel. int. %) = 866 (70) $[M]^+$, 593 (100) $[M - (c-C_3H_5-C\equiv C-C(NCy)_2)]^+$, 271 (66) $[c-C_3H_5-C\equiv C-C(NCy)_2]^+$.

Preparation of [Fe{CyNC(C≡C-*c*-C₃H₅)NCy}₃] (**20**)

In a fashion similar to the preparation of **13**, compound **20** was made by treatment of **2** (1.0 g, 2.9 mmol) with anhydrous FeCl₃ (0.16 g, 1 mmol) in 80 mL of THF. The THF

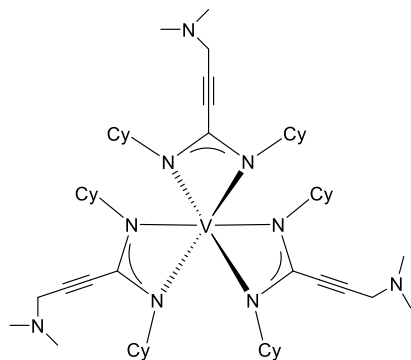


solvent was removed in vacuum, followed by extraction with *n*-pentane (2 × 20 mL) producing a blue solution. The extract was filtered again and concentrated to a total volume of *ca.* 10 mL. Crystallization at 5 °C for 5 days afforded **20** in the form of blue, block-like crystals. Yield: 0.41 g (45%).

Mp. 139 °C (dec.). Elem. anal. calcd. for C₅₄H₈₁FeN₆ (*M* = 870.09 g/mol): C 74.54, H 9.38, N 9.66; found: C 74.51, H 9.36, N %. **IR** (ATR): ν = 3326 w, 3094 w, 3012 w, 2924 vs (ν C–H), 2848 s (ν C–H), 2663 w, 2587 w, 2225 m (ν C≡C), 1890 m, 1605 m (ν NCN), 1462 vs, 1448 vs, 1361 s, 1343 m, 1309 w, 1255 m, 1243 m, 1174 s, 1118 m, 1086 w, 1066 m, 1051 m, 1028 m, 1009 w, 923 w, 887 m, 859 m, 841 w, 809 m, 753 w, 718 w, 699 m, 675 m, 641 w, 617 w, 595 m, 550 w, 504 w, 449 w, 434 m, 364 m, 297 s, 255 m, 190 w, 175 w, 114 w, 86 w cm⁻¹. **MS** (EI, 70 eV): *m/z* (rel. int. %) = 870.1 (1) [*M*]⁺, 831 (7) [*M* - *c*-C₃H₅]⁺, 783 (15) [*M* - 2C₃H₇]⁺, 618 (100) [*M* - *c*-C₃H₅ - 2Cy - C₃H₇]⁺.

Preparation of [V{CyNC(C≡C-CH₂-N(CH₃)₂)NCy}₃] (**21**)

In a fashion similar to the preparation of **13**, compound **21** was made by treatment of **5** (1.0 g, 3.3 mmol) with anhydrous VCl₃(THF)₃ (0.41 g, 1.1 mmol) afforded **21** as red,



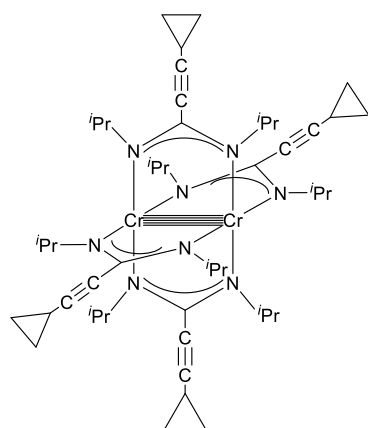
block-like crystals (Crystallization at -30 °C for 10 days). Yield: 0.75 g (75%). Mp. 158 °C (dec.). Elem. anal. calcd. for C₅₄H₉₀N₉V (*M* = 916.29 g/mol): C 70.78, H 9.90, N 5.56; found: C 70.79, H 9.95, N 5.56%. **IR** (ATR): ν = 2923 vs (ν C–H), 2850 s (ν C–H), 2823 m (ν C–H), 2664 w, 2219 w (ν C≡C),

1647 m (ν NCN), 1477 vs, 1448 vs, 1361 vs, 1344 s, 1321 s, 1258 m, 1195 s, 1177 s,

1158 m, 1144 m, 1074 m, 1037 s, 977 m, 922 w, 888 m, 843 w, 817 w, 798 w, 748 w, 697 m, 679 w, 643 s, 543 w, 495 w, 457 w, 438w, 413 w, 365 m, 349 m, 298 s, 212 w, 183 s, 158 w, 124 w, 80 w, 65 cm⁻¹. **MS** (EI, 70 eV): m/z (rel. int. %) = 915 (30) [M]⁺, 739 (55) [M - 3(CH₂-N(CH₃)₂)]⁺, 490 (100) [M - 3Cy - 3(CH₂-N(CH₃)₂)]⁺.

Preparation of [Cr₂{ⁱPrNC(C≡C-*c*-C₃H₅)NⁱPr}₄] (**22**)

A solution of anhydrous CrCl₂ (0.21 g, 1.7 mmol) in 30 mL of THF was added to a solution of **2** (1.0 g, 3.3 mmol) in 50 mL of THF. The reaction mixture was stirred at



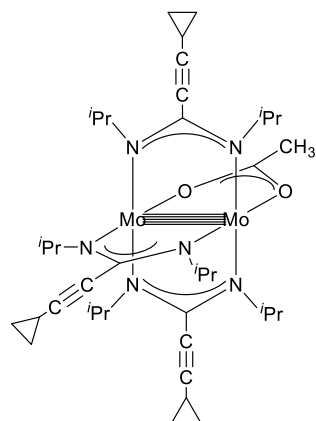
r.t. with a glass-coated stirring bar overnight. The THF solvent was removed in vacuum followed by extraction with *n*-pentane (3 × 20 mL) to produce an orange solution and a white precipitate (LiCl). After filtration and concentration to a total volume of *ca.* 10 mL, an analytical sample was obtained by crystallization from *n*-pentane at 5 °C for 5 days. The solvent was decanted

with a cannula and the resulting product was dried under reduced pressure to afford **22** in the form of orange, rod-like crystals. Yield: 0.43 g (60%). Mp. 146 °C (dec.). Elem. anal. calcd. for C₄₈H₇₆Cr₂N₈ ($M = 869.16$ g/mol): C 66.33, H 8.81, N 12.89; found: C 66.41, H 8.50, N 12.43%. **IR** (ATR): $\nu = 3086$ w, 2964 m (ν C-H), 2921 m, 2867 m (ν C-H), 2609 w, 2220 m (ν C≡C), 1981 w, 1693 w, 1639 w, 1506 vs (ν NCN), 1491 vs, 1447 m, 1414 s, 1373 s, 1354 s, 1318 s, 1246 w, 1223 w, 1199 m, 1179 s, 1163 s, 1145 s, 1110 s, 1051 m, 1027 m, 974 vs, 932 m, 863 m, 845 m, 810 m, 746 m, 697 s, 659 w, 619 m, 597 m, 552 m, 507 m, 463 m, 427 m, 388 w, 324 w, 274 m, 249 w, 206 w, 156 m, 115 w, 86 w, 67 w, 54 w cm⁻¹. **¹H NMR** (400 MHz, THF-*d*₈, 25 °C): $\delta = 3.75$ (s, 2H, CH(CH₃)₂), 1.42 – 1.53 (m, 1H, CH, *c*-C₃H₅), 0.98 (br, 12H, CH(CH₃)₂), 0.76 – 0.89 (m, 4H, CH₂, *c*-C₃H₅) ppm. **¹³C NMR** (100.6 MHz, THF-*d*₈, 25 °C): $\delta = 156.3$ (NCN), 97.1 (CH₂-C≡C), 69.0 (C≡C-C), 67.1 (THF), 49.8 (CH(CH₃)₂), 26.8 (CH(CH₃)₂), 26.3 (THF), 8.9 (CH₂, *c*-C₃H₅), 0.6 (CH, *c*-C₃H₅) ppm. **MS** (EI, 70 eV): m/z (rel. int. %) =

869 (35) $[M]^+$, 626 (50) $[M - 6\text{ }^i\text{Pr} + \text{CH}_3]^+$, 554 (35) $[M - 3(c\text{-C}_3\text{H}_5) - (c\text{-C}_3\text{H}_5\text{-C}\equiv\text{C-C}(\text{N}^i\text{Pr})_2)]$, 478 (100) $[M - 4(c\text{-C}_3\text{H}_5\text{-C}\equiv\text{C}) - 3\text{ }^i\text{Pr}]^+$.

Preparation of $[\text{Mo}_2\{^i\text{PrNC}(\text{C}\equiv\text{C}\text{-}c\text{-C}_3\text{H}_5)\text{N}^i\text{Pr}\}_3(\mu\text{-OAc})]$ (**23**)

In a fashion similar to the preparation of **22**, compound **23** was made by treatment of **1** (1.0 g, 3.6 mmol) with anhydrous $[\text{Mo}_2(\mu\text{-OAc})_4]$ (0.51 g, 1.2 mmol) afforded **23** in the

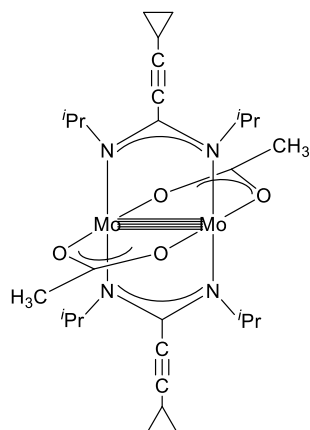


form of yellow, block-like crystals. Yield: 0.31 g (30%). Mp. 185 °C (dec.). Elem. anal. calcd. for $\text{C}_{38}\text{H}_{60}\text{Mo}_2\text{N}_6\text{O}_2$ ($M = 824.80$ g/mol): C 55.34, H 7.33, N 10.19; **IR** (ATR): $\nu = 3190$ w, 3080 w, 3007 w, 2972 m (ν C–H), 2923 w (ν C–H), 2873 w (ν C–H), 2718 w, 2323 w, 2227 m (ν C≡C), 2169 w, 2148 w, 2122 w, 1995 w, 1895 w, 1630 vs (ν NCN), 1570 vs, 1442 m, 1429 m, 1389 m, 1371 m, 1325 m, 1276 m, 1194

w, 1168 m, 1128 s, 1086 w, 1055 w, 1030 w, 978 m, 934 m, 888 s, 869 s, 784 m, 761 m, 736 m, 651 m, 613 w, 606 w, 571 w, 521 w, 450 w, 429 w, 353 w, 314 w, 301 w, 266 w, 196 w, 159 w, 149 w, 122 m, 110 m, 98 w, 81 w, 69 w, 59w cm^{-1} . **^1H NMR** (400 MHz, THF- d_8 , 25 °C): $\delta = 4.57$ (sept, 2H, $\text{CH}(\text{CH}_3)_2$), 1.54 – 1.62 (m, 1H, CH , $c\text{-C}_3\text{H}_5$), 0.76 (d, 12H, $\text{CH}(\text{CH}_3)_2$), 0.83 – 0.94 (m, 4H, CH_2 , $c\text{-C}_3\text{H}_5$) ppm. **^{13}C NMR** (100.6 MHz, THF- d_8 , 25 °C): $\delta = 148.5$ (NCN), 95.6 ($\text{CH-C}\equiv\text{C}$), 68.6 ($\text{C}\equiv\text{C-C}$), 53.4 ($\text{CH}(\text{CH}_3)_2$), 24.8 ($\text{CH}(\text{CH}_3)_2$), 8.7 (CH_2 , $c\text{-C}_3\text{H}_5$), 0.3 (CH , $c\text{-C}_3\text{H}_5$) ppm. **MS** (EI, 70 eV): m/z (rel. int. %) = 822 (100) $[M - 3\text{H}]^+$, 692 (100) $[M - (c\text{-C}_3\text{H}_5\text{-C}\equiv\text{C-C}(\text{N}^i\text{Pr})_2) + \text{OAc}]^+$.

Preparation of $[\text{Mo}_2\{^i\text{PrNC}(\text{C}\equiv\text{C}\text{-}c\text{-C}_3\text{H}_5)\text{N}^i\text{Pr}\}_2(\mu\text{-OAc})_2]$ (**24**)

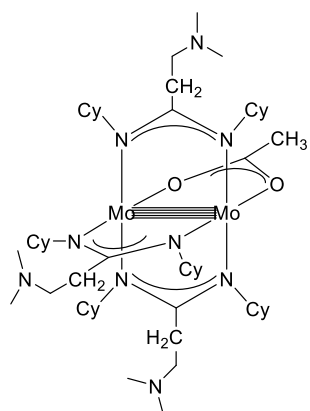
In a fashion similar to the preparation of **22**, compound **24** was made by treatment of **1** (1.0 g, 3.6 mmol) with anhydrous $[\text{Mo}_2(\mu\text{-OAc})_4]$ (0.77 g, 1.8 mmol) afforded **24** in the form of orange, block-like crystals. Yield: 0.81 g (65%). Mp. 191 °C (dec.). Elem. anal. calcd. for $\text{C}_{28}\text{H}_{44}\text{Mo}_2\text{N}_4\text{O}_4$ ($M = 692.55$ g/mol): C 48.56, H 6.40, N 8.09; found: C 48.56, H 6.42, N 8.17%. **IR** (ATR): $\nu = 3093$ w, 2963 m (ν C–H), 2945 m, 2921 m, 2865 m



(ν C–H), 2599 w, 2216 m (ν C \equiv C), 1531 s (ν NCN), 1438 vs, 1427 vs, 1375 s, 1356 m, 1333 m, 1207 w, 1172 m, 1138 m, 1122 m, 1086 w, 1052 w, 1027 m, 968 s, 934 w, 861 w, 847 w, 809 m, 771 w, 721 w, 695 w, 672 s, 622 w, 596 w, 561 w, 532 w, 507 w, 452 w, 416 w, 366w, 346 w, 301 s, 271 m, 222 w, 189 w, 157 w, 145 w, 125 w, 103 w, 86 w, 56 w cm^{-1} . $^1\text{H NMR}$ (400 MHz, THF- d_8 , 25 °C): δ = 4.55 (sept, 2H, CH(CH $_3$) $_2$), 1.55 – 1.59 (m, 1H, CH, c -C $_3$ H $_5$), 0.85 (d, 12H, CH(CH $_3$) $_2$), 0.78 – 0.93 (m, 4H, CH $_2$, c -C $_3$ H $_5$) ppm. $^{13}\text{C NMR}$ (100.6 MHz, THF- d_8 , 25 °C): δ = 148.4 (NCN), 147.6 (NCN), 95.2 (CH–C \equiv C), 94.3 (CH–C \equiv C), 70.5 (C \equiv C–C), 69.7 (C \equiv C–C), 54.2 (CH(CH $_3$) $_2$), 53.8 (CH(CH $_3$) $_2$), 24.0 (CH(CH $_3$) $_2$), 23.2 (CH(CH $_3$) $_2$), 9.1 (CH $_2$, c -C $_3$ H $_5$), 8.8 (CH $_2$, c -C $_3$ H $_5$), 0.5 (CH, c -C $_3$ H $_5$), 0.4 (CH, c -C $_3$ H $_5$) ppm. **MS** (EI, 70 eV): m/z (rel. int. %) = 692 (100) [M] $^+$, 501 (6) [M – (c -C $_3$ H $_5$ –C \equiv C–C(N i Pr) $_2$)] $^+$.

Preparation of [Mo $_2$ {(CH $_3$) $_2$ N–CH $_2$ –(C \equiv C- c -C $_3$ H $_5$) $_3$ (μ -OAc)] (25)

In a fashion similar to the preparation of **22**, compound **25** was made by treatment of **5** (1.0 g, 3.6 mmol) with anhydrous [Mo $_2$ (μ -OAc) $_4$] (0.51 g, 1.2 mmol) afforded **25** in the

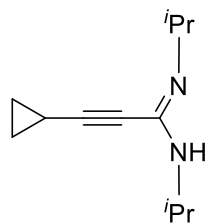


form of yellow, block-like crystals. Yield: 0.51 g (50%). Mp. 180 °C (dec.). Elem. anal. calcd. for C $_{56}$ H $_{93}$ Mo $_2$ N $_9$ O $_2$ (M = 1116.27 g/mol): C 60.25, H 8.4, N 17.19; found: C 48.56, H 6.42, N 8.17%, which was not consistent with the proposed formulation. **IR** (ATR): ν = 2922 m (ν C–H), 2850 m (ν C–H), 2827 w (ν C–H), 2767 w (ν C–H), 1645 w (ν NCN), 1529 w, 1446 vs, 1429 m, 1389 m, 1371 m, 1325 m, 1276 m, 1194 w, 1168 m, 1128 s, 1086 w, 1055 w, 1030 w, 978 m, 934 m, 888 s, 869 s, 784 m, 761 m, 736 m, 651 m, 613 w, 606 w, 571 w, 521 w, 450 w, 429 w, 353 w, 314 w, 301 w, 266 w, 196 w, 159 w, 149 w, 122 m, 110 m, 98 w, 81 w, 69 w, 59w cm^{-1} . $^1\text{H NMR}$ (400 MHz, THF- d_8 , 25 °C): δ = 3.46 (m, 2H, CH, Cy), 3.36 (s, 2H, NCH $_2$ C), 2.36 (s, 6H, (CH $_3$) $_2$ N), 0.85 – 1.75 (m, 20H, CH $_2$, Cy) ppm. $^{13}\text{C NMR}$ (100.6 MHz, THF- d_8 ,

25 °C): δ = 140.5 (N₂CN), 61.2 (CH, Cy), 50.0 (CH₂-C≡C), 48.6 (CH₂-C≡C), 43.3 ((CH₃)₂N), 42.3 ((CH₃)₂N), 34.4 (CH₂, Cy), 26.6 (CH₂, Cy), ppm. **MS** (EI, 70 eV): m/z (rel. int. %) = 998 (10) [M - 2OAc]⁺, 887 (100) [M - 3Cy]⁺, 827 (15) [M - {(CH₂)₂N-CH₂-C≡C-C(NCy)₂}]⁺.

Preparation of [*c*-C₃H₅-C≡C-C(N^{*i*}Pr)(NH^{*i*}Pr)] (**26**)

A THF (80 mL) solution of cyclopropylacetylene (4.2 mL, 50 mmol) was cooled to -20 °C and treated slowly with *n*-butyllithium (50 mmol, 1.6 M solution in *n*-hexane).

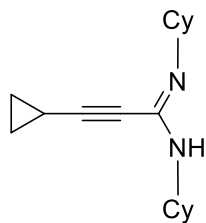


After the reaction mixture was stirred for 30 mins, *N,N'*-diisopropylcarbodiimide (7.8 ml, 50 mmol) was added and stirred for another 30 min at -20 °C. The solution was then warmed to room temperature and stirred for 1 hour. Then 20 mL of distilled water

were added in the reaction mixture, and the color of the solution turned to yellow. The reaction mixture was further stirred for 30 min and separated by the separatory funnel (water phase was removed). To the organic phase was added 3.0 g of anhydrous magnesium sulfate (overnight) to remove the remaining water. The solution was filtered, and the solvent was removed in vacuum to obtain **26** as a yellow oil. Yield: 6.9 g, 72%. Elem. anal. calcd. for C₁₂H₂₀N₂ (*M* = 192.3 g/mol): C, 74.95; H, 10.48; N, 14.57; found C, 74.74; H, 10.46; N, 14.58. **¹H NMR** (400.1 MHz, THF-*d*₈, 25 °C): δ (ppm) 4.71 – 4.78 (s br, 1H, NH, NHCN), 3.72 – 3.88 (s, 2H, CH, ^{*i*}Pr), 1.31 – 1.38 (m, 1H, CH, *c*-C₃H₅), 0.97 – 1.04 (d, 12H, CH₃, ^{*i*}Pr), 0.79 – 0.84 (m, 4H, CH₂, *c*-C₃H₅), 0.66 – 0.69 (m, 4H, CH₂, *c*-C₃H₅). **¹³C NMR** (100.6 MHz, THF-*d*₈, 25 °C): δ (ppm) 140.5 (NHCN), 96.6 (CH-C≡C), 69.2 (C≡C-C), 67.8 (CH, ^{*i*}Pr), 26.8 (CH₃, ^{*i*}Pr), 9.83 (CH₂, *c*-C₃H₅), 0.37 (CH, *c*-C₃H₅). **IR** (ATR): ν = 3440 w (ν N-H), 3415 w (ν N-H), 3096 w, 3014 w, 2963 s (ν C-H), 2931 m, 2867 m (ν C-H), 2614 w, 2226 m, 1606 vs (ν N=C), 1487 m, 1466 m, 1453 m, 1375 m, 1360 m, 1344 m, 1317 m, 1263 m, 1178 m, 1132 m, 1088 w, 1055 w, 1031 w, 970 w, 943 m, 880 w, 849 w, 812 w, 685 m, 616 w, 472 w, 424 w, 254 w, 105 w, 71 w, 60 w cm⁻¹. **MS** (EI, 70 eV): m/z (rel. int. %) = 107 (10) [M - 2^{*i*}Pr]⁺, 149 (68) [M - ^{*i*}Pr]⁺, 164 (47) [M - 2CH₃]⁺, 177 (100) [M - CH₃]⁺, 191 (43) [M]⁺.

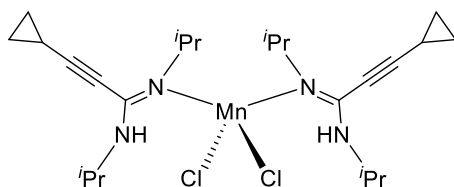
Preparation of [*c*-C₃H₅-C≡C-C(NCy)(NHCy)] (27)

Compound **27** was made in a fashion similar to the preparation of **26**, but adding *N,N'*-dicyclohexylcarbodiimide (10.3 g, 50 mmol) in a THF (80 mL) solution of



cyclopropylacetylene (4.2 mL, 50 mmol) and *n*-butyllithium (31.3 mL, 50 mmol, 1.6 M solution in hexanes). The solution was filtered, and the solvent was removed in vacuum to obtain **27** as a yellow oil. Yield: 10.1 g, 74%. Elem. anal. calcd. for C₁₈H₂₈N₂ (*M* = 272.4

g/mol): C, 79.36; H, 10.36; N, 10.28; found C, 79.36; H, 10.30; N, 10.38. ¹H NMR (400.1 MHz, THF-*d*₈, 25 °C): δ (ppm) 4.87–4.95 (s, 1H, NHCN), 1.69–1.06 (m, 20H, CH₂, Cy), 1.40–1.34 (m, 1H, CH, *c*-C₃H₅), 0.79–0.86 (m, 2H, CH₂, *c*-C₃H₅), 0.61–0.69 (m, 2H, CH₂, *c*-C₃H₅). ¹³C NMR (100.6 MHz, THF-*d*₈, 25 °C): δ (ppm) 141.5 (NHCN), 95.6 (CH–C≡C), 69.2 (C≡C–C), 64.5 (CH, Cy), 25.1–26.8 (CH₂, Cy), 8.83 (CH₂, *c*-C₃H₅), 0.37 (CH, *c*-C₃H₅). IR (ATR): ν = 3351 w (ν N–H), 3062 w, 2960 vs (ν C–H), 2925 s, 2866 m (ν C–H), 2225 w, 2116 w, 1917 w, 1855 w, 1796 w, 1661 w, 1626 m (ν N=C), 1601 m, 1591 m, 1530 w, 1382 m, 1361 m, 1330 m, 1314 m, 1255 s, 1177 m, 1162 m, 1146 m, 1107 m, 1058 m, 1043 m, 972 w, 956 w, 923 m, 888 w, 865 w, 839 w, 819 m, 794 s, 753 vs, 706 w, 678 m, 622 w, 601 w, 577 w, 527 w, 519 w, 465 w, 441 m, 416 m, 326 s, 275 s, 169 m, 152 m, 114 m, 88 m, 57 w cm⁻¹. MS (EI, 70 eV): *m/z* (rel. int. %) = 109 (19) [M – 2Cy]⁺, 189 (75) [M – Cy]⁺, 272 (79) [M]⁺.

Preparation of MnCl₂[*c*-C₃H₅-C≡C-C(N^{*i*}Pr)(NH^{*i*}Pr)]₂ (28)

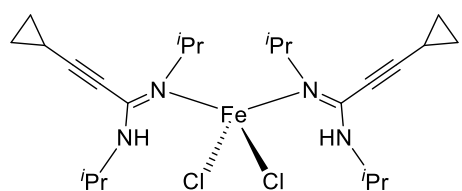
A solution of anhydrous MnCl₂ (0.33 g, 2.6 mmol) in 30 mL of THF was added to a solution of **26** (1.0 g, 5.2 mmol) in 50 mL of THF. The reaction mixture was stirred at r.t. for 3 hours.

The THF solvent was then removed in vacuum followed by extraction with *n*-pentane (30 mL) to give a clear, brown solution. After filtration and concentration to a total volume of *ca.* 10 mL, an analytical sample was obtained by crystallization from *n*-pentane at 5 °C for 3 days. The solvent was decanted with a cannula and the resulting

product was dried under reduced pressure to afford **28** as colorless, block-like crystals. Yield: 0.52 g, 39%. M.p. = 122 °C. Elem. anal. calcd. for C₂₄H₄₀Cl₂MnN₄ (*M* = 510.45 g/mol): C, 56.47; H, 7.90; N, 10.98; found C, 56.49; H, 7.93; N, 10.98. **IR** (ATR): ν = 3411 w (ν N–H), 3239 m (ν N–H), 3129 w (ν N–H), 2967 m, 2930 w, 2872 w, 2217 s, 1628 w, 1571 vs (ν N=C), 1464 s, 1432 vs, 1382 w, 1363 m, 1330 m, 1313 m, 1243 m, 1172 m, 1132 vs, 1061 w, 1032 w, 963 s, 940 w, 879 w, 843 m, 831 m, 705 s, 658 m, 603 w, 520 w, 489 w, 460 w, 387 w, 333 m, 279 vs (ν Mn–Cl), 207 m, 173 m, 128 vs cm⁻¹. **MS** (EI, 70 eV): m/z (rel. int. %) = 425 (50) [M – 2Cl – CH₃]⁺, 433 (2) [M – Cl – ⁱPr]⁺, 498 (100) [M – CH₂ + 2H]⁺.

Preparation of FeCl₂[*c*-C₃H₅-C≡C-C(N^{*i*}Pr)(NH^{*i*}Pr)]₂ (**29**)

In a fashion similar to the preparation of **28**, compound **29** was made by treatment of **26** (1.0 g, 5.2 mmol) with anhydrous FeCl₂ (0.33 g, 2.6 mmol) in 80 mL of THF. The

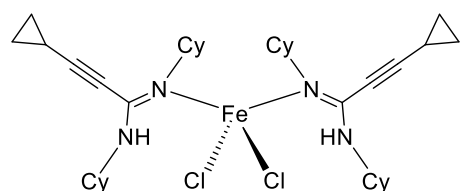


reaction mixture was heated to 60 °C in a water bath and stirred with a glass-coated stirring bar for 1 h. The reaction mixture was then cooled to room temperature and stirred for another 12

hours, resulting in a brown suspension. The suspension was filtered, and the filtrate was extracted by *n*-pentane (30 mL) to give a clear, brown solution. The solution was concentrated in vacuum to ca. 10 mL before it was kept at room temperature to afford **29** as brown crystals. Yield: 0.40 g, 30%. M.p. = 127 °C. Elem. anal. calcd. for C₂₄H₄₀Cl₂FeN₄ (*M* = 511.35 g/mol): C, 56.37; H, 7.88; N, 10.96; found C, 56.34; H, 7.75; N, 10.98%. **IR** (ATR): ν = 3290 (w, N–H), 3222 (w, N–H), 3119 (w, N–H), 2976 (m, C–H), 2933 (w), 2874 (w, C–H), 2225 (m), 1619 (s, N=C), 1568 (m), 1485 (w), 1463 (w), 1429 (w), 1392 (w), 1372 (w), 1309 (w), 1244 (w), 1169 (m), 1129 (m), 1062 (w), 1033 (w), 963 (m), 939 (m), 879 (m), 846 (m), 818 (w), 793 (w), 709 (s), 691 (s), 649 (s), 599 (s), 520 (s), 460 (s), 353 (vs), 313 (vs), 280 (vs), 211 (vs Fe–Cl), 134 (s), 68 (s) cm⁻¹. **MS** (EI, 70 eV): m/z (rel. int. %) = 432 (100) [M – Cl – ⁱPr]⁺, 439 (40) [M – 2Cl]⁺, 475 (63) [M – Cl]⁺, 501 (100) [M – CH₂ + 2H]⁺.

Preparation of $\text{FeCl}_2[\text{c-C}_3\text{H}_5\text{-C}\equiv\text{C-C}(\text{NCy})(\text{NHCy})]_2$ (**30**)

In a fashion similar to the preparation of **28**, compound **30** was made by treatment of **27** (1.0 g, 3.6 mmol) with anhydrous FeCl_2 (0.23 g, 1.8 mmol) afforded **30** in the form

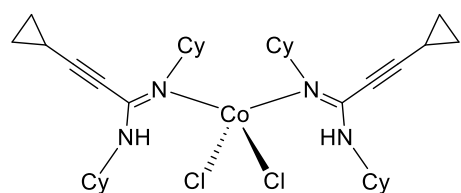


of brown crystals. Yield: 0.45 g, 37%. M.p. = 132 °C. Elem. anal. calcd. for $\text{C}_{24}\text{H}_{40}\text{Cl}_2\text{CoN}_4$ ($M = 671.61$ g/mol): C, 65.66; H, 8.21; N, 8.57; found C, 64.38; H, 8.40; N, 8.34%. **IR** (ATR): $\nu = 3214$ (w, N–H), 2928 (s, C–H), 2852 (s, C–H), 2227 (s), 1573 (vs, N=C), 1448 (s),

1365 (m), 1347 (w), 1308 (w), 1245 (m), 1188 (w), 1154 (w), 1062 (w), 1031 (w), 974 (m), 891 (w), 858 (w), 842 (w), 814 (w), 702 (m), 603 (w), 549 (w), 474 (w), 443 (w), 279 (s), 198 (vs, Fe–Cl), 140 (s), 121 (s), 107 (s), 89 (m) cm^{-1} . **MS** (EI, 70 eV): m/z (rel. int. %) = 363 (24) $[\text{M} - \text{c-C}_3\text{H}_5\text{-C}\equiv\text{C-C}(\text{NCy})(\text{NHCy}) - \text{Cl}]^+$, 457 (74) $[\text{M} - 3\text{C}_3\text{H}_7 - \text{C}_6\text{H}_{11}]^+$, 540 (100) $[\text{M} - 3\text{C}_3\text{H}_7]^+$.

Preparation of $\text{CoCl}_2[\text{c-C}_3\text{H}_5\text{-C}\equiv\text{C-C}(\text{NCy})(\text{NHCy})]_2$ (**31**)

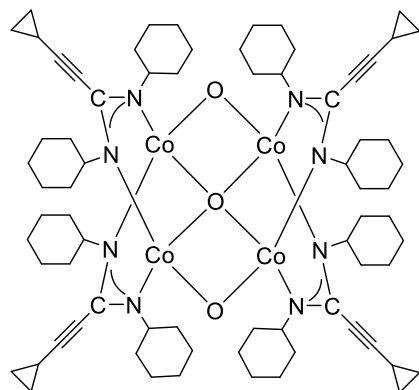
In a fashion similar to the preparation of **28**, treatment of **27** (1.0 g, 3.6 mmol) with anhydrous CoCl_2 (0.23 g, 1.8 mmol) afforded **31** in the form of blue crystals. Yield:



0.45 g, 37%. M.p. = 126 °C. Elem. anal. calcd. for $\text{C}_{24}\text{H}_{40}\text{Cl}_2\text{FeN}_4$ ($M = 674.69$ g/mol): C, 64.09; H, 8.37; N, 8.30; found C, 63.69; H, 8.31; N, 9.26%. **IR** (ATR): $\nu = 3440$ (w, N–H), 3212 (w, N–H), 3128 (w, N–H), 3090 (w), 3008 (w), 2925 (vs, C–H), 2850 (s, C–H), 2662 (w), 2228 (m), 1690 (w), 1635(w), 1605 (m), 1575 (N=C), 1486 (m), 1447 (vs), 1433 (s), 1363 (s), 1346 (m), 1300 (w), 1257 (m), 1221 (w), 1188 (w), 1157 (w), 1090 (w), 1064 (m), 1031 (m), 973 (m), 889 (w), 858 (m), 841 (w), 815 (w), 788 (w), 701 (s), 656 (m), 549 (w), 475 (w), 444 (w), 430 (w), 392 (w), 349 (w), 292 (vs, Co–Cl), 228 (m), 204 (w), 166 (w), 127 (vs), 74 (w) cm^{-1} . **MS** (EI, 70 eV): m/z (rel. int. %) = 402 (24) $[\text{M} - \text{c-C}_3\text{H}_5\text{-C}\equiv\text{C-C}(\text{NCy})(\text{NHCy})]^+$, 461 (89) $[\text{M} - 3\text{C}_3\text{H}_7 - \text{C}_6\text{H}_{11}]^+$, 544 (15) $[\text{M} - 3\text{C}_3\text{H}_7]^+$.

Preparation of $(\mu_4\text{-O})(\mu_2\text{-O})_2\{\text{Co}[c\text{-C}_3\text{H}_5\text{-C}\equiv\text{C-C}(\text{NCy})_2]\}_4$ (**39**)

A solution of anhydrous CoCl_2 (0.34 g, 2.6 mmol) in 30 mL of THF was added to a solution of **7** (1.0 g, 2.6 mmol) in 50 mL of THF in a molar ratio 1:1. The reaction



mixture was stirred at room temperature for 1h and exposed to air for 5 min (opened the cap of the flask).

The THF solvent was then removed in vacuum followed by extraction with n-pentane (30 mL).

After a white precipitate (LiCl) was filtered off, a clear, brown solution was obtained and concentrated

to a total volume of *ca.* 20 mL. An analytical sample

was isolated by crystallization from n-pentane at $-30\text{ }^\circ\text{C}$ for two weeks. The solvent was decanted with a cannula and the resulting product was dried under reduced pressure

to afford **39** as blue crystals. Yield: 0.11 g (12%). Elem. anal. calcd. For

$\text{C}_{72}\text{H}_{108}\text{Co}_4\text{N}_8\text{O}_3$ ($M = 1369.41\text{ g/mol}$): C 63.15, H 7.95, N 8.18; found: C 64.79, H 8.1,

N 8.03%. **IR** (ATR): $\nu = 3439\text{ w}, 3091\text{ w}, 3009\text{ w}, 2922\text{ s}$ ($\nu\text{ C-H}$), 2849 m ($\nu\text{ C-H}$),

$2665\text{ w}, 2223\text{ m}$ ($\nu\text{ C}\equiv\text{C}$), $1638\text{ m}, 1604\text{ s}$ ($\nu\text{ NCN}$), $1487\text{ vs}, 1447\text{ vs}, 1393\text{ m}, 1363\text{ s},$

$1344\text{ s}, 1312\text{ m}, 1255\text{ m}, 1238\text{ m}, 1188\text{ m}, 1156\text{ w}, 1118\text{ w}, 1088\text{ w}, 1066\text{ w}, 1051\text{ w},$

$1027\text{ w}, 973\text{ s}, 921\text{ w}, 889\text{ m}, 860\text{ m}, 842\text{ w}, 808\text{ w}, 716\text{ w}, 685\text{ w}, 638\text{ w}, 601\text{ w}, 566$

$\text{w}, 504\text{ w}, 475\text{ w}, 450\text{ w}, 378\text{ m}, 284\text{ w}, 196\text{ w}, 169\text{ w}, 110\text{ w}, 58\text{ w}$. **MS** (EI, 70 eV):

m/z (rel. int. %) = 544 (70) $[2\{c\text{-C}_3\text{H}_5\text{-C}\equiv\text{C-C}(\text{NCy})_2\}]^+$.

Chapter 5

Crystal data and refinement details

Table 12. Crystal data and structure refinement for $\{\text{Li}[c\text{-C}_3\text{H}_5\text{-C}\equiv\text{C}-(\text{N}^i\text{Pr})_2]\}_4$ (**3**)

Identification code:	ip504
Empirical formula	$\text{C}_{48}\text{H}_{76}\text{Li}_4\text{N}_8$
Formula weight	792.93
Crystal color / shape / size (mm)	Colorless prism, $0.39 \times 0.35 \times 0.31$
Crystal system	Triclinic
Space group	$P\bar{1}$
Unit cell dimensions	
<i>a</i> (Å)	15.818(3)
<i>b</i> (Å)	17.898(4)
<i>c</i> (Å)	19.280(4)
α (deg)	64.99(3)
β (deg)	81.91(3)
γ (deg)	85.50(3)
Unit cell volume <i>V</i> (Å ³)	4896(2)
Molecules per cell <i>z</i>	4
Crystallographic density ρ_{calcd} (g cm ⁻³)	1.076
Absorption coefficient μ (mm ⁻¹)	0.063
Diffractometer	STOE IPDS 2T
Radiation (λ [Å])	Graphite-monochromated Mo-K α (0.71073)
Temperature (°C)	-173(2)
Scan type	ω scan (increment 1.5°, exposure 1 min)
Completeness of dataset	99.5%
θ range of data collection(deg)	2.152 to 26.000
Reflections collected	42287 ($-19 \leq h \leq 19$, $-22 \leq k \leq 22$, $-23 \leq l \leq 23$)
Independent reflections	19166 ($R_{\text{int}} = 0.0598$)
Independent reflections with $I > 2\sigma(I)$	10944
Structure solution method	Dual-space structure solution (SHELXT)
Refinement method	Full-matrix least-squares on F^2 (SHELXL)
Absorption correction method	None
Range of transmission factors	
Data / restraints / parameters	19166 / 1164 / 0
Goodness of fit (goof) [all data]	0.881
Final <i>R</i> values	
<i>R</i> ₁ [all data, $I \geq 2\sigma(I)$]	0.1047, 0.0488
<i>wR</i> ₂ [all data, $I \geq 2\sigma(I)$]	0.1038, 0.0902
Largest diff. peak and hole	0.316 and -0.191 e.Å ⁻³

Table 13. Selected bond lengths (Å) and angles (°) for **3**

N(1)–Li(2)	2.166(4)	N(6)–Li(1)	2.241(4)
N(1)–Li(4)	2.183(3)	N(6)–Li(4)	2.356(4)
N(1)–Li(1)	2.294(3)	N(7)–Li(4)	1.993(3)
N(2)–Li(3)	2.029(4)	N(8)–Li(1)	1.965(3)
N(2)–Li(1)	2.060(3)	N(1)–C(6)	1.339(2)
N(3)–Li(2)	1.968(3)	N(2)–C(6)	1.332(2)
N(4)–Li(3)	1.963(3)	C(3)–C(4)	1.442(3)
N(5)–Li(4)	2.079(3)	C(4)–C(5)	1.195(3)
N(5)–Li(2)	2.094(4)	C(5)–C(6)	1.453(2)
N(6)–Li(3)	2.080(4)		
N(8)–Li(1)–N(2)	143.2 (2)	Li–N(1)–Li(4)	77.1(1)
N(8)–Li(1)–N(6)	117.9(2)	Li–N(1)–Li(1)	101.7(1)
N(2)–Li(1)–N(6)	98.8(1)	Li–N(1)–Li(1)	63.5(1)
N(8)–Li(1)–N(1)	109.9(2)	Li–N(2)–Li(1)	80.3(1)
N(2)–Li(1)–N(1)	63.7(1)	Li–N(5)–Li(2)	81.0(1)
N(6)–Li(1)–N(1)	98.6(1)	Li–N(6)–Li(1)	75.1(1)
N(3)–Li(2)–N(5)	140.8(2)	Li–N(6)–Li(4)	102.2(1)
N(3)–Li(2)–N(1)	117.1(2)	Li–N(6)–Li(4)	61.7(1)
N(5)–Li(2)–N(1)	100.9(1)	C(6)–N(1)–Li(2)	98.3(1)
N(4)–Li(3)–N(2)	119.9(2)	C(6)–N(1)–Li(4)	136.9(1)
N(4)–Li(3)–N(6)	122.8(2)	C(6)–N(1)–Li(1)	76.0(1)
N(2)–Li(3)–N(6)	105.4(1)	C(6)–N(2)–Li(3)	120.7(1)
N(7)–Li(4)–N(5)	142.2(2)	C(6)–N(2)–Li(1)	85.3(1)
N(7)–Li(4)–N(1)	116.9(2)	C(18)–N(3)–Li(2)	104.2(2)
N(5)–Li(4)–N(1)	100.8(1)	C(18)–N(4)–Li(3)	124.2(2)
N(7)–Li(4)–N(6)	106.6(1)	C(30)–N(5)–Li(4)	86.3(1)
N(5)–Li(4)–N(6)	62.4(1)	C(30)–N(5)–Li(2)	112.0(1)
N(1)–Li(4)–N(6)	98.4(1)	C(30)–N(6)–Li(3)	103.9(1)
N(2)–C(6)–N(1)	119.3(2)	C(30)–N(6)–Li(1)	135.1(2)
N(3)–C(18)–N(4)	120.5(2)	C(30)–N(6)–Li(4)	75.2(1)
N(5)–C(30)–N(6)	119.5(2)	C(42)–N(7)–Li(4)	120.8(2)
N(7)–C(42)–N(8)	121.4(2)	C(42)–N(8)–Li(1)	117.5(2)

Table 14. Crystal data and structure refinement for $\{\text{Li}[(\text{CH}_3)_2\text{N}-\text{CH}_2-\text{C}\equiv\text{C}-\text{(N}^i\text{Pr)}_2]\cdot\text{THF}\}_2$ (**4**)

Identification code:	fe0252
Empirical formula	$\text{C}_{32}\text{H}_{60}\text{Li}_2\text{N}_6\text{O}_2$
Formula weight	574.74
Crystal color / shape / size (mm)	Colorless block, $0.20 \times 0.16 \times 0.13$
Crystal system	Triclinic
Space group	$P\bar{1}$
Unit cell dimensions	
<i>a</i> (Å)	9.539(7)
<i>b</i> (Å)	9.738(7)
<i>c</i> (Å)	11.471(7)
α (deg)	95.91(6)
β (deg)	112.34(5)
γ (deg)	109.70(6)
Unit cell volume <i>V</i> (Å ³)	894.6(12)
Molecules per cell <i>z</i>	1
Crystallographic density ρ_{calcd} (g cm ⁻³)	1.067
Absorption coefficient μ (mm ⁻¹)	0.066
Diffractometer	STOE IPDS 2T
Radiation (λ [Å])	Graphite-monochromated Mo-K α (0.71073)
Temperature (°C)	-173(2)
Scan type	ω scan (increment 1.5°, exposure 1 min)
Completeness of dataset	93.6 %
θ range of data collection(deg)	1.991 to 29.183
Reflections collected	8962 ($-12 \leq h \leq 13$, $-13 \leq k \leq 13$, $-15 \leq l \leq 13$)
Independent reflections	4528 ($R_{\text{int}} = 0.0654$)
Independent reflections with $I > 2\sigma(I)$	4295
Structure solution method	Dual-space structure solution (SHELXT)
Refinement method	Full-matrix least-squares on F^2 (SHELXL)
Absorption correction method	None
Range of transmission factors	
Data / restraints / parameters	4528 / 476 / 242
Goodness of fit (goof) [all data]	1.131
Final <i>R</i> values	
<i>R</i> ₁ [all data, $I \geq 2\sigma(I)$]	0.0539, 0.0567
<i>wR</i> ₂ [all data, $I \geq 2\sigma(I)$]	0.1397, 0.1419
Largest diff. peak and hole	0.260 and -0.161 e.Å ⁻³

Table 15. Crystal data and structure refinement for **4**

Li(1)–O(1)	1.920(9)	N(2)–C(1)	1.319(2)
Li(1)–N(1)	2.221(3)	C(1)–C(2)	1.463(2)
Li(1)–N(2)	1.994(3)	C(2)–C(3)	1.190(2)
Li(1)–N(1)#1	2.037(3)	C(3)–C(4)	1.480(2)
N(1)–C(1)	1.335(1)	N(3)–C(4)	1.450(2)
N(1)–C(10)	1.462(2)		
O(1)–Li(1)–N(1)	112.4(3)	C(4)–N(3)–C(6)	111.1(1)
O(1)–Li(1)–N(1)#1	111.5(3)	C(5)–N(3)–C(6)	111.0(1)
O(1)–Li(1)–N(2)	120.4(3)	C(1)–N(1)–C(10)	119.7(1)
N(1)#1–Li(1)–N(1)	109.9(1)	C(1)–N(1)–Li(1)#1	126.1(1)
N(1)#1–Li(1)–N(2)	124.1(1)	C(1)–N(1)–Li(1)	79.5(1)
N(2)–Li(1)–N(1)	65.4(9)	C(1)–N(2)–Li(1)	89.1(1)
N(3)–C(4)–C(3)	115.0(1)	N(1)–C(1)–N(2)	118.8(1)
C(4)–N(3)–C(5)	111.7(1)	Li(1)#1–N(1)–Li(1)	70.0(1)

Symmetry transformations used to generate equivalent atoms:

#1 -x, -y+1, -z+1

Table 16. Crystal data and structure refinement for $\{\text{Li}[(\text{CH}_3)_2\text{N}-\text{CH}_2-\text{C}\equiv\text{C}-(\text{NCy})_2]\cdot\text{THF}\}_2$ (**5**)

Identification code:	fe0092
Empirical formula	$\text{C}_{48}\text{H}_{84}\text{Li}_2\text{N}_6\text{O}_3$
Formula weight	807.09
Crystal color / shape / size (mm)	Colorless block, $0.31 \times 0.25 \times 0.18$
Crystal system	Monoclinic
Space group	$P2_1/c$
Unit cell dimensions	
<i>a</i> (Å)	15.147(5)
<i>b</i> (Å)	13.781(3)
<i>c</i> (Å)	23.355(8)
α (deg)	90
β (deg)	99.17(3)
γ (deg)	90
Unit cell volume <i>V</i> (Å ³)	4813(3)
Molecules per cell <i>z</i>	4
Crystallographic density ρ_{calcd} (g cm ⁻³)	1.114
Absorption coefficient μ (mm ⁻¹)	0.068
Diffractometer	STOE IPDS 2T
Radiation (λ [Å])	Graphite-monochromated Mo-K α (0.71073)
Temperature (°C)	-173(2)
Scan type	ω scan (increment 1.5°, exposure 1 min)
Completeness of dataset	99.4 %
θ range of data collection(deg)	2.010 to 25.349
Reflections collected	30702 ($-18 \leq h \leq 18$, $-16 \leq k \leq 16$, $-27 \leq l \leq 28$)
Independent reflections	8799 ($R_{\text{int}} = 0.1016$)
Independent reflections with $I > 2\sigma(I)$	7047
Structure solution method	Dual-space structure solution (SHELXT)
Refinement method	Full-matrix least-squares on F^2 (SHELXL)
Absorption correction method	None
Range of transmission factors	
Data / restraints / parameters	8799 / 1412 / 628
Goodness of fit (goof) [all data]	1.171
Final <i>R</i> values	
<i>R</i> ₁ [all data, $I \geq 2\sigma(I)$]	0.0656, 0.0879
<i>wR</i> ₂ [all data, $I \geq 2\sigma(I)$]	0.1421, 0.1540
Largest diff. peak and hole	0.223 and -0.248 e.Å ⁻³

Refinement special details: THF moiety disordered over two positions

Table 17. Selected bond lengths (Å) and angles (°) for **5**

Li(1)–O(1)	1.910(4)	N(1)–C(1)	1.326(3)
Li(1)–N(1)	1.993(4)	N(1)–C(7)	1.458(3)
Li(1)–N(2)	2.233(4)	N(2)–C(1)	1.337(3)
Li(1)–N(5)	2.075(4)	C(1)–C(2)	1.473(3)
Li(2)–N(2)	2.048(4)	C(2)–C(3)	1.204(3)
Li(2)–N(4)	2.015(4)	C(3)–C(4)	1.487(3)
Li(1)–N(5)	2.209(4)	N(3)–C(4)	1.457(3)
<hr/>			
O(1)–Li(1)–N(1)	119.2(2)	C(4)–N(3)–C(6)	111.3(2)
O(1)–Li(1)–N(5)	112.5(2)	C(5)–N(3)–C(6)	111.6(2)
O(1)–Li(1)–N(2)	111.2(2)	C(1)–N(1)–C(7)	118.9(2)
N(1)–Li(1)–N(2)	65.3(1)	C(1)–N(1)–Li(1)	88.9(2)
N(1)–Li(1)–N(5)	126.1(2)	C(1)–N(2)–Li(1)	79.0(2)
N(2)–Li(1)–N(5)	109.5(2)	C(1)–N(2)–Li(2)	128.3(1)
N(3)–C(4)–C(3)	115.7(1)	N(1)–C(1)–N(2)	118.6(2)
C(4)–N(3)–C(5)	111.5(2)	Li(1)–N(2)–Li(2)	69.5(1)

Table 18. Crystal data and structure refinement for $[\text{Fe}_2(\mu\text{-}i\text{-C}_3\text{H}_5\text{-C}\equiv\text{C-C}(\text{N}^i\text{Pr})_2)_2\text{-}(\eta^2\text{-}i\text{-C}_3\text{H}_5\text{-C}\equiv\text{C-C}(\text{N}^i\text{Pr})_2)_2]$ (**8**)

Identification code:	li0037
Empirical formula	$\text{C}_{48}\text{H}_{76}\text{FeN}_8$
Formula weight	876.86
Crystal color / shape / size (mm)	Yellow prism, $0.41 \times 0.28 \times 0.14$
Crystal system	Monoclinic
Space group	$C2/c$
Unit cell dimensions	
<i>a</i> (Å)	23.2180(8)
<i>b</i> (Å)	9.5855(4)
<i>c</i> (Å)	22.7357(7)
α (deg)	90
β (deg)	96.321(3)
γ (deg)	90
Unit cell volume <i>V</i> (Å ³)	5029.2(3)
Molecules per cell <i>z</i>	4
Crystallographic density ρ_{calcd} (g cm ⁻³)	1.158
Absorption coefficient μ (mm ⁻¹)	0.615
Diffractometer	STOE IPDS 2T
Radiation (λ [Å])	Graphite-monochromated Mo-K α (0.71073)
Temperature (°C)	-120(2)
Scan type	ω scan (increment 1.5°, exposure 7 min)
Completeness of dataset	99.7%
θ range of data collection(deg)	2.435 to 26.148
Reflections collected	17383 ($-28 \leq h \leq 28$, $-11 \leq k \leq 11$, $-26 \leq l \leq 28$)
Independent reflections	4938 ($R_{\text{int}} = 0.0274$)
Independent reflections with $I > 2\sigma(I)$	4427
Structure solution method	Patterson methods (SHELXL)
Refinement method	Full-matrix least-squares on F^2 (SHELXL)
Absorption correction method	Numerical
Range of transmission factors	0.7987 to 0.9179
Data / restraints / parameters	4938 / 0 / 270
Goodness of fit (goof) [all data]	1.055
Final <i>R</i> values	
<i>R</i> ₁ [all data, $I \geq 2\sigma(I)$]	0.0333, 0.0280
<i>wR</i> ₂ [all data, $I \geq 2\sigma(I)$]	0.0670, 0.0649
Largest diff. peak and hole	0.281 and -0.253 e.Å ⁻³

Table 19. Selected bond lengths (Å) and angles (°) for **8**

Fe–N(2)#1	2.053(1)	C(1)–C(2)	1.445(2)
Fe–N(1)	2.061(1)	C(2)–C(3)	1.194(2)
Fe–N(3)	2.109(1)	C(3)–C(4)	1.438(2)
Fe–N(4)	2.110(1)	C(13)–N(4)	1.326(2)
N(2)–Fe#1	2.053(1)	C(13)–N(3)	1.326(2)
C(1)–N(2)	1.325(2)	Fe–Fe#1	3.001(6)
C(1)–N(1)	1.333(2)		
N(2)–C(1)–N(1)	117.9(1)	N(1)–Fe–N(3)	104.8(5)
N(4)–C(13)–N(3)	114.8(1)	N(2)#1–Fe–N(4)	105.7(5)
C(1)–N(1)–Fe	109.2(9)	N(1)–Fe–N(4)	115.4(5)
C(7)–N(1)–Fe	125.7(9)	N(3)–Fe–N(4)	63.9(5)
C(1)–N(2)–Fe#1	106.9(9)	N(1)–Fe–Fe#1	64.5(4)
C(10)–N(2)–Fe#1	128.4(9)	N(3)–Fe–Fe#1	148.8(5)
C(13)–N(3)–Fe	90.6(8)	N(4)–Fe–Fe#1	147.2(4)
C(19)–N(3)–Fe	147.6(1)	N(2)#1–Fe–Fe#1	68.5(4)
C(13)–N(4)–Fe	90.6(9)	N(1)#1–Fe#1–Fe	64.5(4)
C(22)–N(4)–Fe	147.9(1)	N(3)#1–Fe#1–Fe	148.8(4)
N(2)#1–Fe–N(1)	132.8(5)	N(4)#1–Fe#1–Fe	147.2(4)
N(2)#1–Fe–N(3)	113.7(5)	N(2)–Fe#1–Fe	68.5(4)

Symmetry transformations used to generate equivalent atoms:

#1 -x, y, -z+1/2

Table 20. Crystal data and structure refinement for [Co₂(μ -*c*-C₃H₅-C≡C-C(N^{*i*}Pr)₂)₂-(η^2 -*c*-C₃H₅-C≡C-C(N^{*i*}Pr)₂)₂] (**9**)

Identification code:	li0014
Empirical formula	C ₄₈ H ₇₆ CoN ₈
Formula weight	883.02
Crystal color / shape / size (mm)	Yellow-green plate, 0.37 × 0.18 × 0.15
Crystal system	Monoclinic
Space group	C2/c
Unit cell dimensions	
<i>a</i> (Å)	23.1687(7)
<i>b</i> (Å)	9.5358(2)
<i>c</i> (Å)	22.7158(7)
<i>α</i> (deg)	90
<i>β</i> (deg)	96.107(2)
<i>γ</i> (deg)	90
Unit cell volume <i>V</i> (Å ³)	4990.2(2)
Molecules per cell <i>z</i>	4
Crystallographic density ρ_{calcd} (g cm ⁻³)	1.175
Absorption coefficient μ (mm ⁻¹)	0.703
Diffractometer	STOE IPDS 2T
Radiation (λ [Å])	Graphite-monochromated Mo-K α (0.71073)
Temperature (°C)	-140(2)
Scan type	ω scan (increment 1.5°, exposure 10 min)
Completeness of dataset	99.8%
θ range of data collection(deg)	1.768 to 25.999
Reflections collected	15518 ($-28 \leq h \leq 28$, $-11 \leq k \leq 11$, $-28 \leq l \leq 28$)
Independent reflections	4901 ($R_{\text{int}} = 0.0329$)
Independent reflections with $I > 2\sigma(I)$	4225
Structure solution method	Patterson methods (SHELXL)
Refinement method	Full-matrix least-squares on F^2 (SHELXL)
Absorption correction method	Numerical
Range of transmission factors	0.8275 to 0.9284
Data / restraints / parameters	4901 / 0 / 270
Goodness of fit (goof) [all data]	1.028
Final <i>R</i> values	
<i>R</i> ₁ [all data, $I \geq 2\sigma(I)$]	0.0377, 0.0296
<i>wR</i> ₂ [all data, $I \geq 2\sigma(I)$]	0.0710, 0.0680
Largest diff. peak and hole	0.232 and -0.338 e.Å ⁻³

Refinement special details: Reflection (2 0 0) was omitted for refinement.

Table 21. Selected bond lengths (Å) and angles (°) for **9**

N(1)–Co	2.035(1)	C(1)–C(2)	1.448(2)
N(2)–Co#1	2.018(1)	C(2)–C(3)	1.192(2)
N(3)–Co	2.074(1)	C(3)–C(4)	1.438(2)
N(4)–Co	2.085(1)	C(13)–N(4)	1.323(2)
Co–N(2)#1	2.018(1)	C(13)–N(3)	1.329(2)
C(1)–N(2)	1.326(2)	Co–Co#1	3.057(1)
C(1)–N(1)	1.331(2)		
N(2)–C(1)–N(1)	117.7(1)	N(1)–Co–N(3)	115.8(5)
N(4)–C(13)–N(3)	114.8(1)	N(2)#1–Co–N(4)	113.8(5)
C(1)–N(1)–Co	110.2(1)	N(1)–Co–N(4)	105.4(5)
C(7)–N(1)–Co	124.9(1)	N(3)–Co–N(4)	65.0(5)
C(1)–N(2)–Co#1	107.6(1)	N(1)–Co–Co#1	63.5(1)
C(10)–N(2)–Co#1	127.7(1)	N(3)–Co–Co#1	146.9(1)
C(13)–N(3)–Co	90.2(9)	N(4)–Co–Co#1	148.0(1)
C(19)–N(3)–Co	148.0(1)	N(2)#1–Co–Co#1	67.8(1)
C(13)–N(4)–Co	89.9(9)	N(1)#1–Co#1–Co	63.5(1)
C(22)–N(4)–Co	147.7(1)	N(3)#1–Co#1–Co	146.9(1)
N(2)#1–Co–N(1)	131.1(5)	N(4)#1–Co#1–Co	148.0(1)
N(2)#1–Co–N(3)	106.7(5)	N(2)–Co#1–Co	67.8(1)

Symmetry transformations used to generate equivalent atoms:

#1 -x+1, y, -z+3/2

Table 22. Crystal data and structure refinement for $[\text{Mn}_2(\mu\text{-}i\text{-C}_3\text{H}_5\text{-C}\equiv\text{C-C}(\text{NCy})_2)_2\text{-}(\eta^2\text{-}i\text{-C}_3\text{H}_5\text{-C}\equiv\text{C-C}(\text{NCy})_2)_2]$ (**10**)

Identification code:	li0242
Empirical formula	$\text{C}_{75}\text{H}_{108}\text{MnN}_8, 0.5(\text{C}_6\text{H}_{14})$
Formula weight	1238.62
Crystal color / shape / size (mm)	Yellow prisms, $0.32 \times 0.26 \times 0.16$
Crystal system	Monoclinic
Space group	$C2/c$
Unit cell dimensions	
<i>a</i> (Å)	43.338(1)
<i>b</i> (Å)	16.0374(2)
<i>c</i> (Å)	22.0688(5)
α (deg)	90
β (deg)	113.721(2)
γ (deg)	90
Unit cell volume <i>V</i> (Å ³)	14042.4(5)
Molecules per cell <i>z</i>	4
Crystallographic density ρ_{calcd} (g cm ⁻³)	1.172
Absorption coefficient μ (mm ⁻¹)	0.406
Diffractometer	STOE IPDS 2T
Radiation (λ [Å])	Graphite-monochromated Mo-K α (0.71073)
Temperature (°C)	-120(2)
Scan type	ω scan (increment 1.5°, exposure 15 min)
Completeness of dataset	99.4%
θ range of data collection(deg)	1.996 to 25.097
Reflections collected	39331 ($-51 \leq h \leq 51, -11 \leq k \leq 11, -26 \leq l \leq 28$)
Independent reflections	12443 ($R_{\text{int}} = 0.0416$)
Independent reflections with $I > 2\sigma(I)$	9914
Structure solution method	Patterson methods (SHELXL)
Refinement method	Full-matrix least-squares on F^2 (SHELXL)
Data / restraints / parameters	12443 / 797 / 106
Goodness of fit (goof) [all data]	1.036
Final <i>R</i> values	
<i>R</i> ₁ [all data, $I \geq 2\sigma(I)$]	0.0667, 0.0488
<i>wR</i> ₂ [all data, $I \geq 2\sigma(I)$]	0.1269, 0.1184
Largest diff. peak and hole	0.771 and -0.680 e.Å ⁻³

Refinement special details: Three reflections have been omitted for refinement. One cyclopropyl group (C22–C24) and the *n*-hexane molecule (C73–C75) are disordered over each two positions. ^a Restraints on the disordered atoms (SADI, SIMU, EXYZ, EADP).

Table 23. Selected bond lengths (Å) and angles (°) for **10**

N(1)–Mn(1)	2.137(2)	C(1)–N(1)	1.325(3)
N(2)–Mn(2)	2.107(2)	C(1)–N(2)	1.331(3)
N(3)–Mn(2)	2.149(2)	C(19)–N(3)	1.328(3)
N(4)–Mn(1)	2.164(2)	C(19)–N(4)	1.333(3)
N(5)–Mn(1)	2.164 (2)	C(37)–N(6)	1.320(3)
N(6)–Mn(1)	2.195(2)	C(37)–N(5)	1.330(3)
N(7)–Mn(2)	2.169(2)	C(55)–N(7)	1.325(3)
N(8)–Mn(2)	2.146(2)	C(55)–N(8)	1.325(3)
Mn(1)–Mn(2)	3.162(5)		
N(1)–Mn(1)–N(5)	107.5(8)	N(1)–Mn(1)–Mn(2)	66.7(6)
N(1)–Mn(1)–N(4)	125.5(8)	N(5)–Mn(1)–Mn(2)	152.9(6)
N(5)–Mn(1)–N(4)	114.1(8)	N(4)–Mn(1)–Mn(2)	60.1(5)
N(1)–Mn(1)–N(6)	127.2(8)	N(6)–Mn(1)–Mn(2)	143.5(6)
N(5)–Mn(1)–N(6)	62.1(8)	N(2)–Mn(2)–Mn(1)	68.4(6)
N(4)–Mn(1)–N(6)	103.2(8)	N(8)–Mn(2)–Mn(1)	145.0(6)
N(2)–Mn(2)–N(8)	124.2(8)	N(3)–Mn(2)–Mn(1)	55.8(5)
N(2)–Mn(2)–N(3)	124.0(8)	N(7)–Mn(2)–Mn(1)	150.5(6)
N(8)–Mn(2)–N(3)	105.7(8)	N(1)–C(1)–N(2)	119.3(2)
N(2)–Mn(2)–N(7)	107.2(8)	N(4)–C(19)–N(3)	115.6(2)
N(8)–Mn(2)–N(7)	62.7(8)	N(6)–C(37)–N(5)	116.0(2)
N(3)–Mn(2)–N(7)	118.1(8)	N(7)–C(55)–N(8)	115.9(2)

Symmetry transformations used to generate equivalent atoms:

#1 -x+3/2, -y+1/2, -z+2

Table 24. Crystal data and structure refinement for $[\text{Fe}_2(\mu\text{-}c\text{-C}_3\text{H}_5\text{-C}\equiv\text{C-C}(\text{NCy})_2)_2\text{-}(\eta^2\text{-}c\text{-C}_3\text{H}_5\text{-C}\equiv\text{C-C}(\text{NCy})_2)_2]$ (**11**)

Identification code:	fe0059
Empirical formula	$\text{C}_{72}\text{H}_{108}\text{FeN}_8, 0.501(\text{C}_5\text{H}_{12})$
Formula weight	1233.48
Crystal color / shape / size (mm)	Orange block, $0.20 \times 0.20 \times 0.20$
Crystal system	Monoclinic
Space group	$C2/c$
Unit cell dimensions	
<i>a</i> (Å)	42.779(10)
<i>b</i> (Å)	15.921(2)
<i>c</i> (Å)	21.913(4)
<i>α</i> (deg)	90
<i>β</i> (deg)	113.408(17)
<i>γ</i> (deg)	90
Unit cell volume <i>V</i> (Å ³)	13696(5)
Molecules per cell <i>z</i>	8
Crystallographic density ρ_{calcd} (g cm ⁻³)	1.196
Absorption coefficient μ (mm ⁻¹)	0.471
Diffractometer	STOE IPDS 2T
radiation (λ [Å])	Graphite-monochromated Mo-K α (0.71073)
Temperature (°C)	-173(2)
Scan type	ω scan (increment 1.5°, exposure 15 min)
Completeness of dataset	99.5%
θ range of data collection(deg)	1.830 to 25.350
Reflections collected	37825 ($-51 \leq h \leq 51, -19 \leq k \leq 18, -24 \leq l \leq 26$)
Independent reflections	12504 ($R_{\text{int}} = 0.0420$)
Independent reflections with $I > 2\sigma(I)$	10172
Structure solution method	Dual-space structure solution (SHELXT)
Refinement method	Full-matrix least-squares on F^2 (SHELXL)
Absorption correction method	None
Data / restraints / parameters	12504 / 1520 / 846
Goodness of fit (goof) [all data]	1.030
Final <i>R</i> values	
<i>R</i> ₁ [all data, $I \geq 2\sigma(I)$]	0.0553, 0.0392
<i>wR</i> ₂ [all data, $I \geq 2\sigma(I)$]	0.0824, 0.0779
Largest diff. peak and hole	0.298 and -0.351 e.Å ⁻³

Refinement special details: Pentane disordered on two positions (occupancy 66% and 33%) around inversion center. Minor fraction only modeled isotropically.

Table 25. Selected bond lengths (Å) and angles (°) for **11**

Fe(1)–N(7)	2.047(2)	C(1)–N(1)	1.328(2)
Fe(1)–N(4)	2.068(2)	C(19)–N(3)	1.320(2)
Fe(1)–N(2)	2.115(2)	C(19)–N(4)	1.337(2)
Fe(1)–N(1)	2.122(2)	C(37)–N(6)	1.326(2)
Fe(2)–N(8)	2.062(2)	C(37)–N(5)	1.331(2)
Fe(2)–N(3)	2.076(2)	C(55)–N(8)	1.332(2)
Fe(2)–N(5)	2.125(2)	C(55)–N(7)	1.334(2)
Fe(2)–N(6)	2.150(2)	C(1)–C(2)	1.442(5)
Fe(1)–Fe(2)	3.072(6)	C(2)–C(3)	1.198(5)
C(1)–N(2)	1.323(2)	C(3)–C(4)	1.445(4)
N(7)–Fe(1)–N(4)	127.7(6)	N(11)–Fe(1)–Fe(2)	150.5(5)
N(7)–Fe(1)–N(2)	122.6(6)	N(2)–Fe(1)–Fe(2)	144.4(5)
N(4)–Fe(1)–N(2)	103.7(6)	N(4)–Fe(1)–Fe(2)	57.8(5)
N(7)–Fe(1)–N(1)	105.0(6)	N(7)–Fe(1)–Fe(2)	70.1(4)
N(4)–Fe(1)–N(1)	117.5(6)	N(3)–Fe(2)–Fe(1)	61.5(4)
N(2)–Fe(1)–N(1)	63.5(6)	N(5)–Fe(2)–Fe(1)	152.6(5)
N(8)–Fe(2)–N(3)	127.7(6)	N(6)–Fe(2)–Fe(1)	143.1(5)
N(8)–Fe(2)–N(5)	105.1(6)	N(8)–Fe(2)–Fe(1)	67.6(5)
N(3)–Fe(2)–N(5)	114.3(6)	N(2)–C(1)–N(1)	114.6(2)
N(8)–Fe(2)–N(6)	126.5(6)	N(3)–C(19)–N(4)	115.3(2)
N(3)–Fe(2)–N(6)	102.0(6)	N(6)–C(37)–N(5)	114.9(2)
N(5)–Fe(2)–N(6)	63.2(6)	N(8)–C(55)–N(7)	119.2(2)

Table 26. Crystal data and structure refinement for $[\text{Fe}_2(\mu\text{-(CH}_3)_2\text{N-CH}_2\text{-C}\equiv\text{C-C}(\text{NCy})_2)_2\text{-}(\eta^2\text{-(CH}_3)_2\text{N-CH}_2\text{-C}\equiv\text{C-C}(\text{NCy})_2)]$ (**12**)

Identification code:	fe0227
Empirical formula	$\text{C}_{72}\text{H}_{120}\text{Fe}_2\text{N}_{12}$
Formula weight	1265.49
Crystal color / shape / size (mm)	Brown block, $0.15 \times 0.18 \times 0.23$
Crystal system	Monoclinic
Space group	$P2_1/c$
Unit cell dimensions	
<i>a</i> (Å)	14.405(6)
<i>b</i> (Å)	18.877(5)
<i>c</i> (Å)	26.765(8)
α (deg)	90
β (deg)	93.03(3)
γ (deg)	90
Unit cell volume <i>V</i> (Å ³)	7268(4)
Molecules per cell <i>z</i>	4
Crystallographic density ρ_{calcd} (g cm ⁻³)	1.157
Absorption coefficient μ (mm ⁻¹)	0.447
Diffractometer	STOE IPDS 2T
Radiation (λ [Å])	Graphite-monochromated Mo-K α (0.71073)
Temperature (°C)	-173(2)
Scan type	ω scan (increment 1.5°, exposure 15 min)
Completeness of dataset	99.3%
θ range of data collection(deg)	1.867 to 25.200
Reflections collected	34288 ($-17 \leq h \leq 17$, $-19 \leq k \leq 22$, $-32 \leq l \leq 31$)
Independent reflections	13006 ($R_{\text{int}} = 0.0510$)
Independent reflections with $I > 2\sigma(I)$	10607
Structure solution method	Dual-space structure solution (SHELXL)
Refinement method	Full-matrix least-squares on F^2 (SHELXL)
Absorption correction method	None
Range of transmission factors	
Data / restraints / parameters	13006 / 948 / 2194
Goodness of fit (goof) [all data]	1.079
Final <i>R</i> values	
<i>R</i> ₁ [all data, $I \geq 2\sigma(I)$]	0.0748, 0.0551
<i>wR</i> ₂ [all data, $I \geq 2\sigma(I)$]	0.1617, 0.1507
Largest diff. peak and hole	0.252 and -0.524 e.Å ⁻³

Refinement special details: Disorder of the cyclohexyl moieties

Table 27. Selected bond lengths (Å) and angles (°) for **12**

N(1)–Fe(1)	2.086(3)	C(1)–N(2)	1.325(4)
N(2)–Fe(1)	2.112(3)	C(1)–C(2)	1.444(4)
N(8)–Fe(2)	2.093(3)	C(2)–C(3)	1.198(4)
N(9)–Fe(2)	2.111(3)	C(6)–C(7)	1.476(4)
N(6)–Fe(1)	2.052(2)	C(24)–N(4)	1.331(4)
N(4)–Fe(2)	2.074(2)	C(24)–N(6)	1.322(4)
N(11)–Fe(1)	2.054(2)	C(41)–N(8)	1.324(4)
N(12)–Fe(2)	2.060(3)	C(41)–N(9)	1.325(4)
Fe(1)–Fe(2)	2.939(1)	C(57)–N(11)	1.345(4)
C(1)–N(1)	1.327(4)	C(57)–N(12)	1.322(4)
N(6)–Fe(1)–N(11)	127.4(1)	N(6)–Fe(1)–Fe(2)	64.0(7)
N(6)–Fe(1)–N(1)	103.8(1)	N(11)–Fe(1)–Fe(2)	64.6(7)
N(11)–Fe(1)–N(1)	124.0(1)	N(1)–Fe(1)–Fe(2)	142.9(7)
N(6)–Fe(1)–N(2)	114.8(1)	N(2)–Fe(1)–Fe(2)	152.9(7)
N(11)–Fe(1)–N(2)	105.5(1)	N(12)–Fe(2)–Fe(1)	70.5(8)
N(1)–Fe(1)–N(2)	64.0(1)	N(4)–Fe(2)–Fe(1)	64.1(7)
N(12)–Fe(2)–N(4)	134.4(1)	N(8)–Fe(2)–Fe(1)	148.1(7)
N(12)–Fe(2)–N(8)	103.0(1)	N(9)–Fe(2)–Fe(1)	148.0(7)
N(4)–Fe(2)–N(8)	118.0(1)	N(1)–C(1)–N(2)	114.1(3)
N(12)–Fe(2)–N(9)	109.8(1)	N(4)–C(24)–N(6)	116.9(3)
N(4)–Fe(2)–N(9)	105.9(1)	N(8)–C(41)–N(9)	114.1(3)
N(8)–Fe(2)–N(9)	63.9(1)	N(11)–C(57)–N(12)	117.4(3)

Table 28. Crystal data and structure refinement for $[\text{Y}(\text{c-C}_3\text{H}_5\text{-C}\equiv\text{C-C}(\text{N}^i\text{Pr})_2)_3]$ (**13**)

Identification code:	fe0118
Empirical formula	$\text{C}_{72}\text{H}_{113}\text{Y}_2\text{N}_{12}$
Formula weight	1324.56
Crystal color / shape / size (mm)	Colorless block, $0.19 \times 0.26 \times 0.32$
Crystal system	Triclinic
Space group	$P\bar{1}$
Unit cell dimensions	
<i>a</i> (Å)	9.685(7)
<i>b</i> (Å)	16.943(10)
<i>c</i> (Å)	24.972(14)
α (deg)	71.42(4)
β (deg)	84.91(5)
γ (deg)	75.10(5)
Unit cell volume <i>V</i> (Å ³)	3753(4)
Molecules per cell <i>z</i>	2
Crystallographic density ρ_{calcd} (g cm ⁻³)	1.172
Absorption coefficient μ (mm ⁻¹)	1.584
Diffractometer	STOE IPDS 2T
Radiation (λ [Å])	Graphite-monochromated Mo-K α (0.71073)
Temperature (°C)	-173(2)
Scan type	ω scan (increment 1.5°, exposure 1 min)
Completeness of dataset	98.5%
θ range of data collection(deg)	1.776 to 25.484
Reflections collected	31657 ($-11 \leq h \leq 11$, $-20 \leq k \leq 20$, $-30 \leq l \leq 25$)
Independent reflections	13742 ($R_{\text{int}} = 0.0574$)
Independent reflections with $I > 2\sigma(I)$	10482
Structure solution method	Dual-space structure solution (SHELXT)
Refinement method	Full-matrix least-squares on F^2 (SHELXL)
Absorption correction method	Numerical
Range of transmission factors	0.6764 and 0.5420
Data / restraints / parameters	13742 / 975 / 1857
Goodness of fit (goof) [all data]	0.985
Final <i>R</i> values	
<i>R</i> ₁ [all data, $I \geq 2\sigma(I)$]	0.0626, 0.0439
<i>wR</i> ₂ [all data, $I \geq 2\sigma(I)$]	0.1079, 0.1006
Largest diff. peak and hole	0.584 and -0.591 e.Å ⁻³

Refinement special details: Relatively large residuals near a disordered cyclopropyl group possibly due to additional disorder. Trying to refine additional positions does not improve the model.

Table 29. Selected bond lengths (Å) and angles (°) for **13**

N(1)–Y(1)	2.346(3)	C(13)–N(3)	1.336(4)
N(2)–Y(1)	2.358(3)	C(13)–N(4)	1.327(4)
N(3)–Y(1)	2.336(3)	C(25)–N(5)	1.333(4)
N(4)–Y(1)	2.380(3)	C(25)–N(6)	1.330(4)
N(5)–Y(1)	2.341(3)	C(1)–C(2)	1.445(4)
N(6)–Y(1)	2.340(3)	C(2)–C(3)	1.189(4)
C(1)–N(1)	1.321(4)	C(3)–C(4)	1.439(4)
C(1)–N(2)	1.330(5)		
<hr/>			
N(1)–Y(1)–N(2)	57.5(9)	N(3)–Y(1)–N(4)	57.3(8)
N(1)–Y(1)–N(3)	103.2(9)	N(3)–Y(1)–N(5)	106.6(9)
N(1)–Y(1)–N(4)	155.0(9)	N(3)–Y(1)–N(6)	154.2(9)
N(1)–Y(1)–N(5)	101.8(9)	N(4)–Y(1)–N(5)	99.1(9)
N(1)–Y(1)–N(6)	100.6(1)	N(4)–Y(1)–N(6)	102.2(9)
N(2)–Y(1)–N(3)	97.1(8)	N(5)–Y(1)–N(6)	57.9(9)
N(2)–Y(1)–N(4)	106.2(8)	N(1)–C(1)–N(2)	117.3(3)
N(2)–Y(1)–N(5)	152.2(1)	N(3)–C(13)–N(4)	116.2(3)
N(2)–Y(1)–N(6)	104.3(9)	N(5)–C(25)–N(6)	116.7(3)

Table 30. Crystal data and structure refinement for $[\text{Cr}(c\text{-C}_3\text{H}_5\text{-C}\equiv\text{C-C}(\text{N}^i\text{Pr})_2)_3]$ (**14**)

Identification code:	li0072
Empirical formula	$\text{C}_{36}\text{H}_{57}\text{CrN}_6$
Formula weight	625.87
Crystal color / shape / size (mm)	Pale pink block, $0.40 \times 0.29 \times 0.22$
Crystal system	Monoclinic
Space group	$\text{P2}_1/c$
Unit cell dimensions	
<i>a</i> (Å)	16.451(3)
<i>b</i> (Å)	16.764(3)
<i>c</i> (Å)	26.706(4)
α (deg)	90
β (deg)	94.748(1)
γ (deg)	90
Unit cell volume <i>V</i> (Å ³)	7339.5(2)
Molecules per cell <i>z</i>	8
Crystallographic density ρ_{calcd} (g cm ⁻³)	1.133
Absorption coefficient μ (mm ⁻¹)	0.343
Diffractometer	STOE IPDS 2T
Radiation (λ [Å])	Graphite-monochromated Mo-K α (0.71073)
Temperature (°C)	-120(2)
Scan type	ω scan (increment 1.5°, exposure 1 min)
Completeness of dataset	99.9%
θ range of data collection(deg)	1.857 to 26.000
Reflections collected	49661 ($-20 \leq h \leq 20$, $-20 \leq k \leq 20$, $-32 \leq l \leq 32$)
Independent reflections	14409 ($R_{\text{int}} = 0.0417$)
Independent reflections with $I > 2\sigma(I)$	11021
Structure solution method	Patterson methods (SHELXT 2013)
Refinement method	Full-matrix least-squares on F^2 (SHELXL 2014)
Absorption correction method	Numerical
Range of transmission factors	0.9030 and 0.9371
Data / restraints / parameters	14409 / 799 / 0
Goodness of fit (goof) [all data]	1.022
Final <i>R</i> values	
<i>R</i> ₁ [all data, $I \geq 2\sigma(I)$]	0.0648, 0.0438
<i>wR</i> ₂ [all data, $I \geq 2\sigma(I)$]	0.1074, 0.0997
Largest diff. peak and hole	0.610 and $-0.324 \text{ e.}\text{\AA}^{-3}$

Table 31. Selected bond lengths (Å) and angles (°) for **14**

N(1)–Cr(1)	2.068(2)	C(13)–N(3)	1.321(3)
N(2)–Cr(1)	2.074(2)	C(13)–N(4)	1.328(3)
N(3)–Cr(1)	2.039(2)	C(25)–N(5)	1.320(3)
N(4)–Cr(1)	2.088(2)	C(25)–N(6)	1.327(3)
N(5)–Cr(1)	2.045(2)	C(1)–C(2)	1.452(3)
N(6)–Cr(1)	2.078(2)	C(2)–C(3)	1.195(3)
C(1)–N(1)	1.325(3)	C(3)–C(4)	1.439(3)
C(1)–N(2)	1.323(3)		
N(1)–Cr(1)–N(2)	64.5(6)	N(3)–Cr(1)–N(4)	64.7(7)
N(1)–Cr(1)–N(3)	163.9(7)	N(3)–Cr(1)–N(5)	94.7(7)
N(1)–Cr(1)–N(4)	105.5(7)	N(3)–Cr(1)–N(6)	100.1(7)
N(1)–Cr(1)–N(5)	100.1(7)	N(4)–Cr(1)–N(5)	102.2(6)
N(1)–Cr(1)–N(6)	92.1(7)	N(4)–Cr(1)–N(6)	160.1(7)
N(2)–Cr(1)–N(3)	101.8(7)	N(5)–Cr(1)–N(6)	64.8(7)
N(2)–Cr(1)–N(4)	91.6(6)	N(1)–C(1)–N(2)	113.3(2)
N(2)–Cr(1)–N(5)	161.9(7)	N(3)–C(13)–N(4)	112.9(2)
N(2)–Cr(1)–N(6)	104.6(7)	N(5)–C(25)–N(6)	113.2(2)

Table 32. Crystal data and structure refinement for [Fe(*c*-C₃H₅-C≡C-C(N^{*i*}Pr)₂)₃] (**15**)

Identification code:	fe0196
Empirical formula	C ₃₆ H ₅₇ FeN ₆
Formula weight	629.72
Crystal color / shape / size (mm)	Black block, 0.10 × 0.10 × 0.10
Crystal system	Monoclinic
Space group	P2 ₁ /c
Unit cell dimensions	
<i>a</i> (Å)	16.379(3)
<i>b</i> (Å)	16.785(2)
<i>c</i> (Å)	26.662(4)
α (deg)	90
β (deg)	94.655(14)
γ (deg)	90
Unit cell volume <i>V</i> (Å ³)	7306(2)
Molecules per cell <i>z</i>	8
Crystallographic density ρ _{calcd} (g cm ⁻³)	1.145
Absorption coefficient μ (mm ⁻¹)	0.444
Diffractometer	STOE IPDS 2T
Radiation (λ [Å])	Graphite-monochromated Mo-K _α (0.71073)
Temperature (°C)	-173(2)
Scan type	ω scan (increment 1.5°, exposure 1 min)
Completeness of dataset	98.4%
θ range of data collection(deg)	1.860 to 29.208
Reflections collected	50194 (-22 ≤ <i>h</i> ≤ 22, -20 ≤ <i>k</i> ≤ 22, -31 ≤ <i>l</i> ≤ 36)
Independent reflections	18655 (<i>R</i> _{int} = 0.0360)
Independent reflections with <i>I</i> > 2σ(<i>I</i>)	17229
Structure solution method	Dual-space structure solution (SHELXT)
Refinement method	Full-matrix least-squares on <i>F</i> ² (SHELXL)
Absorption correction method	None
Range of transmission factors	
Data / restraints / parameters	19504 / 856 / 1458
Goodness of fit (goof) [all data]	1.182
Final <i>R</i> values	
<i>R</i> ₁ [all data, <i>I</i> ≥ 2σ(<i>I</i>)	0.0682, 0.0581
<i>wR</i> ₂ [all data, <i>I</i> ≥ 2σ(<i>I</i>)	0.1264, 0.1221
Largest diff. peak and hole	0.299 and -0.755 e.Å ⁻³

Table 33. Selected bond lengths (Å) and angles (°) for **15**

N(1)–Fe	2.119(2)	C(13)–N(3)	1.323(3)
N(2)–Fe	2.107(2)	C(13)–N(4)	1.329(3)
N(3)–Fe	2.125(2)	C(25)–N(5)	1.329(3)
N(4)–Fe	2.068(2)	C(25)–N(6)	1.327(3)
N(5)–Fe	2.114(2)	C(1)–C(2)	1.448(3)
N(6)–Fe	2.093(2)	C(2)–C(3)	1.193(3)
C(1)–N(1)	1.324(2)	C(3)–C(4)	1.434(3)
C(1)–N(2)	1.327(3)		
N(1)–Fe–N(2)	63.5(6)	N(3)–Fe–N(4)	63.9(6)
N(1)–Fe–N(3)	99.4(7)	N(3)–Fe–N(5)	162.7(6)
N(1)–Fe–N(4)	154.6(7)	N(3)–Fe–N(6)	101.5(7)
N(1)–Fe–N(5)	93.5(6)	N(4)–Fe–N(5)	107.2(7)
N(1)–Fe–N(6)	103.9(7)	N(4)–Fe–N(6)	98.4(7)
N(2)–Fe–N(3)	92.9(6)	N(5)–Fe–N(6)	63.9(6)
N(2)–Fe–N(4)	96.9(7)	N(1)–C(1)–N(2)	114.1(2)
N(2)–Fe–N(5)	103.1(6)	N(3)–C(13)–N(4)	113.5(2)
N(2)–Fe–N(6)	162.5(6)	N(5)–C(25)–N(6)	114.1(2)

Table 34. Crystal data and structure refinement for [Y(*c*-C₃H₅-C≡C-C(NCy)₂)₃] (**16**)

Identification code:	fe0123
Empirical formula	C ₂₁₆ H ₃₂₄ Y ₄ N ₂₄
Formula weight	3612.61
Crystal color / shape / size (mm)	Colorless plate, 0.18 × 0.16 × 0.09
Crystal system	Triclinic
Space group	$P\bar{1}$
Unit cell dimensions	
<i>a</i> (Å)	14.977(13)
<i>b</i> (Å)	16.977(10)
<i>c</i> (Å)	20.241(13)
<i>α</i> (deg)	93.17(5)
<i>β</i> (deg)	91.46(6)
<i>γ</i> (deg)	89.88(6)
Unit cell volume <i>V</i> (Å ³)	5137(6)
Molecules per cell <i>z</i>	4
Crystallographic density ρ_{calcd} (g cm ⁻³)	1.168
Absorption coefficient μ (mm ⁻¹)	1.175
Diffractometer	STOE IPDS 2T
Radiation (λ [Å])	Graphite-monochromated Mo-K α (0.71073)
Temperature (°C)	-173(2)
Scan type	ω scan (increment 1.5°, exposure 1 min)
Completeness of dataset	99.8%
θ range of data collection(deg)	1.814 to 25.350
Reflections collected	39004 ($-18 \leq h \leq 18, -20 \leq k \leq 18, -24 \leq l \leq 24$)
Independent reflections	18655 ($R_{\text{int}} = 0.0509$)
Independent reflections with $I > 2\sigma(I)$	14744
Structure solution method	Dual-space structure solution (SHELXT)
Refinement method	Full-matrix least-squares on F^2 (SHELXL)
Absorption correction method	Numerical
Range of transmission factors	0.6929 and 0.8248
Data / restraints / parameters	18757 / 1200 / 2348
Goodness of fit (goof) [all data]	1.006
Final <i>R</i> values	
<i>R</i> ₁ [all data, $I \geq 2\sigma(I)$]	0.0768, 0.0556
<i>wR</i> ₂ [all data, $I \geq 2\sigma(I)$]	0.1292, 0.1199
Largest diff. peak and hole	0.530 and -1.102 e.Å ⁻³

Table 35. Selected bond lengths (Å) and angles (°) for **16**

N(1)–Y	2.330(3)	C(19)–N(3)	1.341(4)
N(2)–Y	2.368(3)	C(19)–N(4)	1.325(4)
N(3)–Y	2.349(3)	C(37)–N(5)	1.330(4)
N(4)–Y	2.350(3)	C(37)–N(6)	1.333(4)
N(5)–Y	2.348(3)	C(1)–C(2)	1.461(5)
N(6)–Y	2.345(3)	C(2)–C(3)	1.192(4)
C(1)–N(1)	1.330(5)	C(3)–C(4)	1.443(4)
C(1)–N(2)	1.319(4)		
N(1)–Y–N(2)	57.3(1)	N(3)–Y–N(4)	57.8(1)
N(1)–Y–N(3)	104.7(1)	N(3)–Y–N(5)	108.2(1)
N(1)–Y–N(4)	152.8(1)	N(3)–Y–N(6)	157.1(1)
N(1)–Y–N(5)	106.8(1)	N(4)–Y–N(5)	99.1(1)
N(1)–Y–N(6)	97.3(1)	N(4)–Y–N(6)	104.1(1)
N(2)–Y–N(3)	95.2(1)	N(5)–Y–N(6)	57.8(9)
N(2)–Y–N(4)	100.9(1)	N(1)–C(1)–N(2)	116.3(3)
N(2)–Y–N(5)	155.3(1)	N(3)–C(19)–N(4)	116.6(3)
N(2)–Y–N(6)	102.7(9)	N(5)–C(25)–N(6)	116.6(3)

Table 36. Crystal data and structure refinement for $[\text{Cr}(c\text{-C}_3\text{H}_5\text{-C}\equiv\text{C-C}(\text{NCy})_2)_3]$ (**17**)

Identification code:	fe0288
Empirical formula	$\text{C}_{54}\text{H}_{81}\text{TiN}_6$
Formula weight	862.14
Crystal color / shape / size (mm)	Black block, $0.13 \times 0.16 \times 0.23$
Crystal system	Triclinic
Space group	$P\bar{1}$
Unit cell dimensions	
<i>a</i> (Å)	14.804(9)
<i>b</i> (Å)	17.049(6)
<i>c</i> (Å)	19.961(7)
α (deg)	83.90(3)
β (deg)	88.06(4)
γ (deg)	88.24(4)
Unit cell volume <i>V</i> (Å ³)	5005(4)
Molecules per cell <i>z</i>	4
Crystallographic density ρ_{calcd} (g cm ⁻³)	1.144
Absorption coefficient μ (mm ⁻¹)	0.212
Diffractometer	STOE IPDS 2T
Radiation (λ [Å])	Graphite-monochromated Mo-K α (0.71073)
Temperature (°C)	-173(2)
Scan type	ω scan (increment 1.5°, exposure 1 min)
Completeness of dataset	99.2%
θ range of data collection(deg)	1.803 to 25.200
Reflections collected	35622 ($-17 \leq h \leq 17, -19 \leq k \leq 20, -23 \leq l \leq 23$)
Independent reflections	17896 ($R_{\text{int}} = 0.0476$)
Independent reflections with $I > 2\sigma(I)$	14854
Structure solution method	Dual-space structure solution (SHELXT)
Refinement method	Full-matrix least-squares on F^2 (SHELXL)
Absorption correction method	None
Range of transmission factors	
Data / restraints / parameters	17896 / 1264 / 2560
Goodness of fit (goof) [all data]	1.105
Final <i>R</i> values	
<i>R</i> ₁ [all data, $I \geq 2\sigma(I)$]	0.0880, 0.0712
<i>wR</i> ₂ [all data, $I \geq 2\sigma(I)$]	0.1767, 0.1667
Largest diff. peak and hole	1.196 and -0.501 e.Å ⁻³

Table 37. Selected bond lengths (Å) and angles (°) for **17**

N(1)–Ti	2.166(3)	C(19)–N(3)	1.331(4)
N(2)–Ti	2.105(3)	C(19)–N(4)	1.323(4)
N(3)–Ti	2.105(3)	C(37)–N(5)	1.322(4)
N(4)–Ti	2.130(3)	C(37)–N(6)	1.322(4)
N(5)–Ti	2.118(3)	C(1)–C(2)	1.446(5)
N(6)–Ti	2.152(3)	C(2)–C(3)	1.191(5)
C(1)–N(1)	1.316(4)	C(3)–C(4)	1.452(7)
C(1)–N(2)	1.330(4)		
N(1)–Ti–N(2)	62.8(1)	N(3)–Ti–N(4)	63.6(1)
N(1)–Ti–N(3)	104.4(9)	N(3)–Ti–N(5)	99.3(1)
N(1)–Ti–N(4)	157.6(9)	N(3)–Ti–N(6)	158.9(1)
N(1)–Ti–N(5)	103.6(1)	N(4)–Ti–N(5)	97.2(1)
N(1)–Ti–N(6)	91.7(1)	N(4)–Ti–N(6)	105.2(1)
N(2)–Ti–N(3)	97.1(1)	N(5)–Ti–N(6)	63.0(1)
N(2)–Ti–N(4)	98.6(1)	N(1)–C(1)–N(2)	114.5(3)
N(2)–Ti–N(5)	160.9(1)	N(3)–C(19)–N(4)	114.5(3)
N(2)–Ti–N(6)	102.4(9)	N(5)–C(25)–N(6)	115.2(3)

Table 38. Crystal data and structure refinement for $[\text{V}(c\text{-C}_3\text{H}_5\text{-C}\equiv\text{C-C}(\text{NCy})_2)_3]$ (**18**)

Identification code:	fe0264
Empirical formula	$\text{C}_{54}\text{H}_{81}\text{VN}_6$
Formula weight	865.18
Crystal color / shape / size (mm)	Red block, $0.14 \times 0.18 \times 0.21$
Crystal system	Monoclinic
Space group	$P2_1/c$
Unit cell dimensions	
<i>a</i> (Å)	14.527(4)
<i>b</i> (Å)	18.878(3)
<i>c</i> (Å)	18.454(4)
α (deg)	90
β (deg)	101.784(19)
γ (deg)	90
Unit cell volume <i>V</i> (Å ³)	4954.1(19)
Molecules per cell <i>z</i>	4
Crystallographic density ρ_{calcd} (g cm ⁻³)	1.160
Absorption coefficient μ (mm ⁻¹)	0.241
Diffractometer	STOE IPDS 2T
Radiation (λ [Å])	Graphite-monochromated Mo-K α (0.71073)
Temperature (°C)	-173(2)
Scan type	ω scan (increment 1.5°, exposure 1 min)
Completeness of dataset	99.4%
θ range of data collection(deg)	1.793 to 25.348
Reflections collected	24240 ($-17 \leq h \leq 17$, $-21 \leq k \leq 22$, $-20 \leq l \leq 22$)
Independent reflections	9025 ($R_{\text{int}} = 0.0681$)
Independent reflections with $I > 2\sigma(I)$	7541
Structure solution method	Dual-space structure solution (SHELXT)
Refinement method	Full-matrix least-squares on F^2 (SHELXL)
Absorption correction method	Integration
Range of transmission factors	0.9690 and 0.9393
Data / restraints / parameters	9025 / 550 / 936
Goodness of fit (goof) [all data]	1.121
Final <i>R</i> values	
<i>R</i> ₁ [all data, $I \geq 2\sigma(I)$]	0.0827, 0.0663
<i>wR</i> ₂ [all data, $I \geq 2\sigma(I)$]	0.1421, 0.1351
Largest diff. peak and hole	0.344 and $-0.333 \text{ e.}\text{\AA}^{-3}$

Table 39. Selected bond lengths (Å) and angles (°) for **18**

N(1)–V	2.063(2)	C(19)–N(3)	1.327(4)
N(2)–V	2.094(2)	C(19)–N(4)	1.325(4)
N(3)–V	2.100(2)	C(37)–N(5)	1.327(4)
N(4)–V	2.099(2)	C(37)–N(6)	1.342(4)
N(5)–V	2.109(2)	C(1)–C(2)	1.445(4)
N(6)–V	2.060(2)	C(2)–C(3)	1.119(4)
C(1)–N(1)	1.331(3)	C(3)–C(4)	1.440(4)
C(1)–N(2)	1.328(3)		
N(1)–V–N(2)	64.5(8)	N(3)–V–N(4)	63.7(9)
N(1)–V–N(3)	102.4(9)	N(3)–V–N(5)	103.2(9)
N(1)–V–N(4)	162.6(9)	N(3)–V–N(6)	161.4(9)
N(1)–V–N(5)	102.7(9)	N(4)–V–N(5)	91.1(9)
N(1)–V–N(6)	94.3(9)	N(4)–V–N(6)	101.2(9)
N(2)–V–N(3)	91.5(9)	N(5)–V–N(6)	64.5(9)
N(2)–V–N(4)	103.9 (8)	N(1)–C(1)–N(2)	113.1(2)
N(2)–V–N(5)	162.5(9)	N(3)–C(19)–N(4)	113.2(2)
N(2)–V–N(6)	103.2(9)	N(5)–C(25)–N(6)	113.1(2)

Table 40. Crystal data and structure refinement for $[\text{Cr}(c\text{-C}_3\text{H}_5\text{-C}\equiv\text{C-C}(\text{NCy})_2)_3]$ (**19**)

Identification code:	li0148
Empirical formula	$\text{C}_{54}\text{H}_{81}\text{CrN}_6$
Formula weight	866.24
Crystal color / shape / size (mm)	Brown block, $0.36 \times 0.21 \times 0.20$
Crystal system	Monoclinic
Space group	$P2_1/c$
Unit cell dimensions	
<i>a</i> (Å)	14.6199(4)
<i>b</i> (Å)	18.8975(6)
<i>c</i> (Å)	18.4895(5)
<i>α</i> (deg)	90
<i>β</i> (deg)	102.140(2)
<i>γ</i> (deg)	90
Unit cell volume <i>V</i> (Å ³)	4994.0(3)
Molecules per cell <i>z</i>	4
Crystallographic density ρ_{calcd} (g cm ⁻³)	1.152
Absorption coefficient μ (mm ⁻¹)	0.270
Diffractometer	STOE IPDS 2T
Radiation (λ [Å])	Graphite-monochromated Mo-K α (0.71073)
Temperature (°C)	-120(2)
Scan type	ω scan (increment 1.5°, exposure 7 min)
Completeness of dataset	99.8%
θ range of data collection(deg)	2.155 to 26.000
Reflections collected	30988 ($-18 \leq h \leq 17$, $-23 \leq k \leq 23$, $-22 \leq l \leq 22$)
Independent reflections	9787 ($R_{\text{int}} = 0.0720$)
Independent reflections with $I > 2\sigma(I)$	7079
Structure solution method	Heavy atom methods (SHELXL)
Refinement method	Full-matrix least-squares on F^2 (SHELXL)
Absorption correction method	None
Range of transmission factors	
Data / restraints / parameters	9787 / 551 / 0
Goodness of fit (goof) [all data]	1.015
Final <i>R</i> values	
<i>R</i> ₁ [all data, $I \geq 2\sigma(I)$]	0.0815, 0.0520
<i>wR</i> ₂ [all data, $I \geq 2\sigma(I)$]	0.1251, 0.1134
Largest diff. peak and hole	0.338 and -0.409 e.Å ⁻³

Refinement special details: The intensities of the reflections (1 1 0) and (-1 1 1) are strongly disagreeing with the structural model and were therefore omitted for refinement.

Table 41. Selected bond lengths (Å) and angles (°) for **19**

N(1)–Cr	2.066(2)	C(19)–N(3)	1.329(3)
N(2)–Cr	2.051(2)	C(19)–N(4)	1.322(3)
N(3)–Cr	2.061(2)	C(37)–N(5)	1.325(3)
N(4)–Cr	2.067(2)	C(37)–N(6)	1.325(3)
N(5)–Cr	2.049(2)	C(1)–C(2)	1.443(3)
N(6)–Cr	2.073(2)	C(2)–C(3)	1.188(4)
C(1)–N(1)	1.330(3)	C(3)–C(4)	1.442(4)
C(1)–N(2)	1.318(3)		
N(1)–Cr–N(2)	64.9(7)	N(3)–Cr–N(4)	64.7(7)
N(1)–Cr–N(3)	92.2(8)	N(3)–Cr–N(5)	161.9(8)
N(1)–Cr–N(4)	103.1(8)	N(3)–Cr–N(6)	102.9(8)
N(1)–Cr–N(5)	102.4(8)	N(4)–Cr–N(5)	101.3(8)
N(1)–Cr–N(6)	162.2(8)	N(4)–Cr–N(6)	91.9 (8)
N(2)–Cr–N(3)	102.4(8)	N(5)–Cr–N(6)	64.8(8)
N(2)–Cr–N(4)	162.9(8)	N(1)–C(1)–N(2)	113.0(2)
N(2)–Cr–N(5)	93.5(8)	N(3)–C(19)–N(4)	112.7(2)
N(2)–Cr–N(6)	102.2(8)	N(5)–C(25)–N(6)	112.9(2)

Table 42. Crystal data and structure refinement for $[\text{Fe}(c\text{-C}_3\text{H}_5\text{-C}\equiv\text{C-C}(\text{NCy})_2)_3]$ (**20**)

Identification code:	fe0248
Empirical formula	$\text{C}_{54}\text{H}_{81}\text{FeN}_6$
Formula weight	870.09
Crystal color / shape / size (mm)	Blue block, $0.23 \times 0.28 \times 0.35$
Crystal system	Monoclinic
Space group	$P2_1/c$
Unit cell dimensions	
<i>a</i> (Å)	14.588(4)
<i>b</i> (Å)	18.909(4)
<i>c</i> (Å)	18.380(5)
α (deg)	90
β (deg)	101.64(2)
γ (deg)	90
Unit cell volume <i>V</i> (Å ³)	4996(2)
Molecules per cell <i>z</i>	4
Crystallographic density ρ_{calcd} (g cm ⁻³)	1.164
Absorption coefficient μ (mm ⁻¹)	0.345
Diffractometer	STOE IPDS 2T
Radiation (λ [Å])	Graphite-monochromated Mo-K α (0.71073)
Temperature (°C)	-173(2)
Scan type	ω scan (increment 1.5°, exposure 1 min)
Completeness of dataset	96.8%
θ range of data collection(deg)	1.786 to 29.433
Reflections collected	36406 ($-20 \leq h \leq 19$, $-25 \leq k \leq 25$, $-25 \leq l \leq 23$)
Independent reflections	13294 ($R_{\text{int}} = 0.0686$)
Independent reflections with $I > 2\sigma(I)$	12011
Structure solution method	Dual-space structure solution (SHELXT)
Refinement method	Full-matrix least-squares on F^2 (SHELXL)
Absorption correction method	None
Range of transmission factors	
Data / restraints / parameters	13294 / 550 / 0
Goodness of fit (goof) [all data]	1.274
Final <i>R</i> values	
<i>R</i> ₁ [all data, $I \geq 2\sigma(I)$]	0.0814, 0.0729
<i>wR</i> ₂ [all data, $I \geq 2\sigma(I)$]	0.1735, 0.1689
Largest diff. peak and hole	0.373 and -0.737 e.Å ⁻³

Table 43. Selected bond lengths (Å) and angles (°) for **20**

N(1)–Fe	2.069(2)	C(19)–N(3)	1.324(3)
N(2)–Fe	2.135(2)	C(19)–N(4)	1.326(3)
N(3)–Fe	2.106(2)	C(37)–N(5)	1.331(3)
N(4)–Fe	2.117(2)	C(37)–N(6)	1.328(3)
N(5)–Fe	2.107(2)	C(1)–C(2)	1.443(3)
N(6)–Fe	2.107(2)	C(2)–C(3)	1.189(3)
C(1)–N(1)	1.330(3)	C(3)–C(4)	1.436(4)
C(1)–N(2)	1.327(3)		
N(1)–Fe–N(2)	63.9(7)	N(3)–Fe–N(4)	63.3(7)
N(1)–Fe–N(3)	101.2(8)	N(3)–Fe–N(5)	160.9(8)
N(1)–Fe–N(4)	159.3(8)	N(3)–Fe–N(6)	104.2(8)
N(1)–Fe–N(5)	96.2(8)	N(4)–Fe–N(5)	101.5(8)
N(1)–Fe–N(6)	103.3(8)	N(4)–Fe–N(6)	94.1(8)
N(2)–Fe–N(3)	93.5(8)	N(5)–Fe–N(6)	63.7(8)
N(2)–Fe–N(4)	101.9 (7)	N(1)–C(1)–N(2)	113.7(2)
N(2)–Fe–N(5)	101.3(8)	N(3)–C(19)–N(4)	113.4(2)
N(2)–Fe–N(6)	160.2(8)	N(5)–C(25)–N(6)	113.5(2)

Table 44. Crystal data and structure refinement for $[\text{Cr}_2(\mu\text{-}c\text{-}\text{C}_3\text{H}_5\text{-}\text{C}\equiv\text{C-C}(\text{N}^i\text{Pr})_2)_4]$
(22)

Identification code:	ip467
Empirical formula	$\text{C}_{48}\text{H}_{76}\text{Cr}_2\text{N}_8$
Formula weight	869.16
Crystal color / shape / size (mm)	Orange prisim, $0.58 \times 0.52 \times 0.34$
Crystal system	Monoclinic
Space group	$\text{P2}_1/\text{c}$
Unit cell dimensions	
<i>a</i> (Å)	11.161(2)
<i>b</i> (Å)	14.170(3)
<i>c</i> (Å)	30.435(6)
<i>α</i> (deg)	90
<i>β</i> (deg)	98.34(3)
<i>γ</i> (deg)	90
Unit cell volume <i>V</i> (Å ³)	4762.7(17)
Molecules per cell <i>z</i>	4
Crystallographic density ρ_{calcd} (g cm ⁻³)	1.212
Absorption coefficient μ (mm ⁻¹)	0.497
Diffractometer	STOE IPDS 2T
Radiation (λ [Å])	Graphite-monochromated Mo-K α (0.71073)
Temperature (°C)	-173(2)
Scan type	ω scan (increment 1.5°, exposure 1 min)
Completeness of dataset	98.0%
θ range of data collection(deg)	1.974 to 24.999
Reflections collected	21939 ($-12 \leq h \leq 13$, $-15 \leq k \leq 16$, $-36 \leq l \leq 36$)
Independent reflections	8239 ($R_{\text{int}} = 0.0499$)
Independent reflections with $I > 2\sigma(I)$	5682
Structure solution method	Dual-space structure solution (SHELXT)
Refinement method	Full-matrix least-squares on F^2 (SHELXL)
Absorption correction method	Sphere
Range of transmission factors	0.845 and 0.801
Data / restraints / parameters	8239 / 568 / 30
Goodness of fit (goof) [all data]	1.145
Final <i>R</i> values	
<i>R</i> ₁ [all data, $I \geq 2\sigma(I)$]	0.0972, 0.0660
<i>wR</i> ₂ [all data, $I \geq 2\sigma(I)$]	0.1576, 0.1497
Largest diff. peak and hole	0.837 and -0.671 e.Å ⁻³

Table 45. Selected bond lengths (Å) and angles (°) for **22**

Cr(1)–Cr(2)	1.889(1)	N(4)–C(21)	1.327(6)
Cr(1)–N(1)	2.078(4)	N(5)–C(41)	1.339(6)
Cr(1)–N(3)	2.043(4)	N(6)–C(41)	1.332(6)
Cr(1)–N(5)	2.070(4)	N(7)–C(61)	1.328(6)
Cr(1)–N(7)	2.046(4)	N(8)–C(61)	1.326(6)
N(1)–C(1)	1.339(6)	C(1)–C(2)	1.457(7)
N(2)–C(1)	1.320(6)	C(2)–C(3)	1.191(7)
N(3)–C(21)	1.344(6)	C(3)–C(4)	1.454(8)
<hr/>			
N(1)–C(1)–N(2)	120.1(4)	N(2)–Cr(2)–N(4)	91.5(2)
N(3)–C(21)–N(4)	117.5(4)	N(2)–Cr(2)–N(6)	171.1(1)
N(5)–C(41)–N(6)	118.3(4)	N(2)–Cr(2)–N(8)	87.8(2)
N(7)–C(61)–N(8)	119.4(4)	Cr(2)–Cr(1)–N(1)	93.9(1)
N(1)–Cr(1)–N(3)	91.9(2)	Cr(2)–Cr(1)–N(3)	94.6(1)
N(1)–Cr(1)–N(5)	171.1(1)	Cr(2)–Cr(1)–N(5)	95.0(1)
N(1)–Cr(1)–N(7)	87.9(2)	Cr(2)–Cr(1)–N(7)	94.3(1)

Table 46. Crystal data and structure refinement for $[\text{Mo}_2(\mu\text{-OAc})_2(\mu\text{-}C_3H_5\text{-}C\equiv C\text{-}C(\text{N}^i\text{Pr})_2)_2]$ (**23**)

Identification code:	fe0243
Empirical formula	$C_{28}H_{44}Mo_2N_4O_4$
Formula weight	692.55
Crystal color / shape / size (mm)	Orange block, $0.19 \times 0.16 \times 0.09$
Crystal system	Triclinic
Space group	$P\bar{1}$
Unit cell dimensions	
<i>a</i> (Å)	8.881(4)
<i>b</i> (Å)	11.638(4)
<i>c</i> (Å)	15.952(6)
α (deg)	85.63(3)
β (deg)	85.84(4)
γ (deg)	68.22(3)
Unit cell volume <i>V</i> (Å ³)	1524.7(11)
Molecules per cell <i>z</i>	2
Crystallographic density ρ_{calcd} (g cm ⁻³)	1.508
Absorption coefficient μ (mm ⁻¹)	0.860
Diffractometer	STOE IPDS 2T
Radiation (λ [Å])	Graphite-monochromated Mo-K α (0.71073)
Temperature (°C)	-173(2)
Scan type	ω scan (increment 1.5°, exposure 1 min)
Completeness of dataset	98.2%
θ range of data collection(deg)	1.887 to 29.171
Reflections collected	16158 ($-12 \leq h \leq 12, -15 \leq k \leq 15, -17 \leq l \leq 21$)
Independent reflections	8087 ($R_{\text{int}} = 0.0589$)
Independent reflections with $I > 2\sigma(I)$	7539
Structure solution method	Dual-space structure solution (SHELXT)
Refinement method	Full-matrix least-squares on F^2 (SHELXL)
Absorption correction method	Numerical
Range of transmission factors	0.8991 and 0.8143
Data / restraints / parameters	8087 / 399 / 612
Goodness of fit (goof) [all data]	1.167
Final <i>R</i> values	
<i>R</i> ₁ [all data, $I \geq 2\sigma(I)$]	0.0481, 0.0439
<i>wR</i> ₂ [all data, $I \geq 2\sigma(I)$]	0.1033, 0.1012
Largest diff. peak and hole	0.710 and $-1.125 \text{ e.}\text{\AA}^{-3}$

Table 47. Selected bond lengths (Å) and angles (°) for **23**

Mo(01)–Mo(01) #1	2.076(1)	N(3)–C(15)	1.334(4)
Mo(01)–N(3)	2.123(3)	N(3)–C(21)	1.467(4)
Mo(01)–N(4)#1	2.127(3)	N(4)–C(15)	1.336(4)
Mo(01)–O(3)	2.105(2)	N(4)–C(24)	1.469(4)
Mo(01)–O(4)#1	2.121(2)	C(15)–C(16)	1.451(4)
O(3)–C(27)	1.264(4)	C(16)–C(17)	1.190(5)
O(4)–C(27)	1.271(4)	C(17)–C(18)	1.435(5)
Mo(01)#1–Mo(01)–O(3)	93.2(7)	O(4)#1–Mo(01)–N(3)	90.9(1)
Mo(01)#1–Mo(01)–O(4)#1	90.9(7)	O(4)#1–Mo(01)–N(4)#1	91.4(9)
Mo(01)#1–Mo(01)–N(4)#1	93.4(8)	N(3)–Mo(01)–N(4)#1	173.4(1)
Mo(01)#1–Mo(01)–N(3)	92.8(8)	N(3)–C(15)–N(4)	119.4(3)
O(3)–Mo(01)–N(3)	88.9(1)	O(3)–C(27)–O(4)	122.9(3)
O(3)–Mo(01)–N(4)#1	88.3(9)	O(3)–C(27)–C(28)	118.1(3)
O(3)–Mo(01)–O(4)#1	175.9(8)	O(4)–C(27)–C(28)	119.0(3)

Symmetry transformations used to generate equivalent atoms:

#1 -x+1, -y+1, -z+1 #2 -x+2, -y, -z

Table 48. Crystal data and structure refinement for $[\text{Mo}_2(\mu\text{-OAc})(\mu\text{-}c\text{-C}_3\text{H}_5\text{-C}\equiv\text{C-C}(\text{N}^i\text{Pr})_2)_3]$ (**24**)

Identification code:	fe0245
Empirical formula	$\text{C}_{38}\text{H}_{60}\text{Mo}_2\text{N}_6\text{O}_2$
Formula weight	824.80
Crystal color / shape / size (mm)	Yellow block, $0.15 \times 0.13 \times 0.09$
Crystal system	Monoclinic
Space group	$\text{P2}_1/c$
Unit cell dimensions	
<i>a</i> (Å)	14.472(4)
<i>b</i> (Å)	16.917(5)
<i>c</i> (Å)	16.261(4)
<i>α</i> (deg)	90
<i>β</i> (deg)	97.969(19)
<i>γ</i> (deg)	90
Unit cell volume <i>V</i> (Å ³)	3942.4(17)
Molecules per cell <i>z</i>	4
Crystallographic density ρ_{calcd} (g cm ⁻³)	1.390
Absorption coefficient μ (mm ⁻¹)	0.675
Diffractometer	STOE IPDS 2T
Radiation (λ [Å])	Graphite-monochromated Mo-K α (0.71073)
Temperature (°C)	-173(2)
Scan type	ω scan (increment 1.5°, exposure 1 min)
Completeness of dataset	98.5%
θ range of data collection(deg)	1.862 to 29.181
Reflections collected	27512 ($-19 \leq h \leq 19, -19 \leq k \leq 23, -22 \leq l \leq 22$)
Independent reflections	10502 ($R_{\text{int}} = 0.0589$)
Independent reflections with $I > 2\sigma(I)$	9090
Structure solution method	Dual-space structure solution (SHELXT)
Refinement method	Full-matrix least-squares on F^2 (SHELXL)
Absorption correction method	Numerical
Range of transmission factors	0.9260 and 0.8784
Data / restraints / parameters	10502 / 646 / 1751
Goodness of fit (goof) [all data]	1.148
<i>R</i> ₁ [all data, $I \geq 2\sigma(I)$]	0.0993, 0.0851
<i>wR</i> ₂ [all data, $I \geq 2\sigma(I)$]	0.1523, 0.1462
Largest diff. peak and hole	2.825 and -2.225 e.Å ⁻³

Refinement special details: Poor data quality. High residual density is probably due to inefficient absorption correction.

Table 49. Selected bond lengths (Å) and angles (°) for **24**

Mo(1)–Mo(2)	2.076(8)	O(1)–C(37)	1.267(6)
Mo(1)–N(5)	2.103(5)	O(2)–C(37)	1.263(7)
Mo(1)–N(2)	2.122(5)	N(1)–C(1)	1.337(7)
Mo(1)–N(3)	2.137(4)	N(2)–C(1)	1.343(6)
Mo(2)–N(6)	2.099(5)	C(1)–C(2)	1.415(9)
Mo(2)–N(1)	2.131(5)	C(2)–C(3)	1.156(9)
Mo(2)–N(4)	2.137(4)	C(3)–C(4)	1.430(1)
Mo(1)–O(2)	2.157(4)	C(37)–C(38)	1.489(9)
Mo(2)–O(1)	2.177(4)		
C(37)–O(1)–Mo(2)	116.0(4)	C(37)–O(2)–Mo(1)	116.6(4)
Mo(2)–Mo(1)–N(5)	92.81(1)	C(1)–N(1)–C(10)	122.8(8)
Mo(2)–Mo(1)–N(2)	92.92(1)	C(1)–N(1)–Mo(2)	117.1(3)
Mo(2)–Mo(1)–N(3)	93.08(1)	C(10)–N(1)–Mo(2)	118.5(7)
N(5)–Mo(1)–N(2)	96.30(2)	N(1)–C(1)–N(2)	118.5(5)
N(5)–Mo(1)–N(3)	96.22(2)	N(1)–C(1)–C(2)	117.4(8)
N(2)–Mo(1)–N(3)	165.82(2)	N(2)–C(1)–C(2)	124.0(8)
Mo(2)–Mo(1)–O(2)	92.32(1)	O(2)–C(37)–O(1)	123.4(6)
N(5)–Mo(1)–O(2)	174.86(1)	O(2)–C(37)–C(38)	118.8(5)
N(2)–Mo(1)–O(2)	83.75(2)	O(1)–C(37)–C(38)	117.8(5)
N(3)–Mo(1)–O(2)	83.18(2)		

Table 50. Crystal data and structure refinement for $[\text{Mo}_2(\mu\text{-OAc})((\text{CH}_3)_2\text{N-CH}_2\text{-C}\equiv\text{C-C}(\text{NCy})_2)_3]$ (**25**)

Identification code:	li0308
Empirical formula	$\text{C}_{61}\text{H}_{105}\text{Mo}_2\text{N}_9\text{O}_2$
Formula weight	1188.41
Crystal color / shape / size (mm)	Yellow plate, $0.23 \times 0.18 \times 0.04$
Crystal system	Triclinic
Space group	$P\bar{1}$
Unit cell dimensions	
<i>a</i> (Å)	12.5924(6)
<i>b</i> (Å)	14.3188(7)
<i>c</i> (Å)	20.1356(8)
α (deg)	70.493(3)
β (deg)	74.843(3)
γ (deg)	66.464(3)
Unit cell volume <i>V</i> (Å ³)	3102.8(3)
Molecules per cell <i>z</i>	2
Crystallographic density ρ_{calcd} (g cm ⁻³)	1.272
Absorption coefficient μ (mm ⁻¹)	0.452
Diffractometer	STOE IPDS 2T
Radiation (λ [Å])	Graphite-monochromated Mo-K α (0.71073)
Temperature (°C)	-173(2)
Scan type	ω scan (increment 1.5°, exposure 1 min)
Completeness of dataset	99.4%
θ range of data collection(deg)	4.318 to 52
Reflections collected	24567 ($-15 \leq h \leq 15, -16 \leq k \leq 17, -24 \leq l \leq 24$)
Independent reflections	12137 ($R_{\text{int}} = 0.0627$)
Independent reflections with $I > 2\sigma(I)$	8905
Structure solution method	Dual-space structure solution (SHELXT)
Refinement method	Full-matrix least-squares on F^2 (SHELXL)
Absorption correction method	
Range of transmission factors	
Data / restraints / parameters	12137 / 60 / 721
Goodness of fit (goof) [all data]	1.148
Final <i>R</i> values	
<i>R</i> ₁ [all data, $I \geq 2\sigma(I)$]	0.0504, 0.0852
<i>wR</i> ₂ [all data, $I \geq 2\sigma(I)$]	0.0894, 0.1084
Largest diff. peak and hole	0.58 and -0.71 e.Å ⁻³

Table 51. Selected bond lengths (Å) and angles (°) for **25**

Mo(1)–Mo(2)	2.086(5)	O(2)–C(55)	1.272(5)
Mo(1)–O(1)	2.156(3)	N(1)–C(1)	1.350(5)
Mo(1)–N(1)	2.098(3)	N(2)–C(1)	1.334(5)
Mo(1)–N(4)	2.134(4)	N(3)–C(4)	1.458(6)
Mo(1)–N(7)	2.136(4)	N(3)–C(5)	1.463(6)
Mo(2)–O(2)	2.167(3)	N(3)–C(6)	1.456(6)
Mo(2)–N(2)	2.114(3)	C(1)–C(2)	1.449(6)
Mo(2)–N(5)	2.141(3)	C(2)–C(3)	1.194(6)
Mo(2)–N(8)	2.144(3)	C(3)–C(4)	1.466(6)
O(1)–C(55)	1.262(5)	C(55)–C(56)	1.504(6)
Mo(2)–Mo(1)–O(1)	92.6(8)	C(55)–O(2)–Mo(2)	116.2(3)
Mo(2)–Mo(1)–N(1)	92.9(9)	C(1)–N(1)–Mo(1)	118.6(3)
Mo(2)–Mo(1)–N(4)	93.6(1)	C(1)–N(1)–C(7)	122.5(3)
Mo(2)–Mo(1)–N(7)	93.2(1)	C(7)–N(1)–Mo(1)	118.8(3)
N(1)–Mo(1)–O(1)	174.5(1)	C(5)–N(3)–C(4)	108.3(4)
N(1)–Mo(1)–N(4)	94.2(1)	C(6)–N(3)–C(4)	111.5(4)
N(1)–Mo(1)–N(7)	94.6(1)	C(6)–N(3)–C(5)	109.8(4)
N(4)–Mo(1)–O(1)	85.6(1)	N(2)–C(1)–N(1)	117.3(4)
N(4)–Mo(1)–N(7)	168.6(1)	N(1)–C(1)–C(2)	120.1(4)
N(7)–Mo(1)–O(1)	84.9(1)	N(2)–C(1)–C(2)	122.5(4)
C(55)–O(1)–Mo(1)	115.9(3)		

Symmetry transformations used to generate equivalent atoms:

#1 -x, -y+1, -z+1 #2 -x, -y+1, -z+2

Table 52. Crystal data and structure refinement for $\text{MnCl}_2[\text{c-C}_3\text{H}_5\text{-C}\equiv\text{C-C}(\text{N}^i\text{Pr})(\text{NH}^i\text{Pr})]_2$ (**28**)

Identification code:	li0135
Empirical formula	$\text{C}_{24}\text{H}_{40}\text{Cl}_2\text{MnN}_2$
Formula weight	510.44
Crystal color / shape / size (mm)	Colorless plates, $0.32 \times 0.24 \times 0.10$
Crystal system	Orthorhombic
Space group	<i>Fdd2</i>
Unit cell dimensions	
<i>a</i> (Å)	17.670(1)
<i>b</i> (Å)	30.981(2)
<i>c</i> (Å)	10.145(1)
α (deg)	90
β (deg)	90
γ (deg)	90
Unit cell volume <i>V</i> (Å ³)	5553.8(5)
Molecules per cell <i>z</i>	8
Crystallographic density ρ_{calcd} (g cm ⁻³)	1.221
Absorption coefficient μ (mm ⁻¹)	0.685
Diffractometer	STOE IPDS 2T
Radiation (λ [Å])	Graphite-monochromated Mo-K α (0.71073)
Temperature (°C)	-120(2)
Scan type	ω scan (increment 1.5°, exposure 3 min)
Completeness of dataset	100%
θ range of data collection(deg)	2.406 to 25.990
Reflections collected	5371 ($-21 \leq h \leq 19, -38 \leq k \leq 36, -10 \leq l \leq 12$)
Independent reflections	2432 ($R_{\text{int}} = 0.0295$)
Independent reflections with $I > 2\sigma(I)$	2203
Structure solution method	Heavy atom methods (SHELXT 2014/5)
Refinement method	Full-matrix least-squares on F^2 (SHELXL 2016/4)
Absorption correction method	Numerical
Range of transmission factors	0.8508 and 0.9315
Data / restraints / parameters	2432 / 145 / 1
Goodness of fit (goof) [all data]	0.982
Final <i>R</i> values	
<i>R</i> ₁ [all data, $I \geq 2\sigma(I)$]	0.0312, 0.0261
<i>wR</i> ₂ [all data, $I \geq 2\sigma(I)$]	0.0542, 0.0531
Largest diff. peak and hole	0.174 and -0.164 e.Å ⁻³

Table 53. Selected bond lengths (Å) and angles (°) for **28**

C(1)–N(1)	1.311(3)	C(10)–N(2)	1.466(3)
C(1)–N(2)	1.337(4)	C(10)–C(11)	1.488(5)
C(1)–C(2)	1.444(4)	C(10)–C(12)	1.494(4)
C(2)–C(3)	1.191(4)	Cl–Mn	2.356(8)
C(3)–C(4)	1.428(4)	N(1)–Mn	2.160(2)
C(7)–N(1)	1.473(3)	Mn–N(1)#1	2.160(2)
C(7)–C(9)	1.511(4)	Mn–Cl#1	2.356(8)
C(7)–C(8)	1.520(5)	N(2)–H(2)	0.850(2)
<hr/>			
N(1)–C(1)–N(2)	122.1(2)	C(1)–N(1)–C(7)	117.6(2)
N(1)–C(1)–C(2)	122.1(2)	C(1)–N(1)–Mn	125.9(2)
N(2)–C(1)–C(2)	115.8(2)	C(7)–N(1)–Mn	116.5(2)
C(3)–C(2)–C(1)	177.2(3)	N(1)#1–Mn–N(1)	113.1(1)
C(2)–C(3)–C(4)	177.5(3)	N(1)#1–Mn–Cl	112.8(6)
C(3)–C(4)–C(5)	120.8(3)	N(1)–Mn–Cl	106.6(6)
C(3)–C(4)–C(6)	120.1(3)	N(1)#1–Mn–Cl#1	106.6(6)
C(5)–C(4)–C(6)	58.4(2)	N(1)–Mn–Cl#1	112.8(6)
C(6)–C(5)–C(4)	60.8(2)	Cl–Mn–Cl#1	104.7(5)
C(5)–C(6)–C(4)	60.8(2)		

Symmetry transformations used to generate equivalent atoms:

#1 -x+1, -y+1, z

Table 54. Crystal data and structure refinement for $\text{FeCl}_2[\text{c-C}_3\text{H}_5\text{-C}\equiv\text{C-C}(\text{N}^i\text{Pr})(\text{NH}^i\text{Pr})]_2$ (**29**)

Identification code:	li0140
Empirical formula	$\text{C}_{24}\text{H}_{40}\text{Cl}_2\text{FeN}_2$
Formula weight	511.35
Crystal color / shape / size (mm)	Colorless blocks, $0.27 \times 0.25 \times 0.25$
Crystal system	Orthorhombic
Space group	<i>Fdd2</i>
Unit cell dimensions	
<i>a</i> (Å)	17.570(1)
<i>b</i> (Å)	30.917(1)
<i>c</i> (Å)	10.111(1)
α (deg)	90
β (deg)	90
γ (deg)	90
Unit cell volume <i>V</i> (Å ³)	5492.5(5)
Molecules per cell <i>z</i>	8
Crystallographic density ρ_{calcd} (g cm ⁻³)	1.237
Absorption coefficient μ (mm ⁻¹)	0.761
Diffractometer	STOE IPDS 2T
Radiation (λ [Å])	Graphite-monochromated Mo-K α (0.71073)
Temperature (°C)	-120(2)
Scan type	ω scan (increment 1.5°, exposure 3 min)
Completeness of dataset	99.9%
θ range of data collection(deg)	2.416 to 25.987
Reflections collected	5377 ($-20 \leq h \leq 21$, $-38 \leq k \leq 36$, $-10 \leq l \leq 12$)
Independent reflections	2495 ($R_{\text{int}} = 0.0369$)
Independent reflections with $I > 2\sigma(I)$	2239
Structure solution method	Heavy atom methods (SHELXT 2014/5)
Refinement method	Full-matrix least-squares on F^2 (SHELXL 2016/4)
Absorption correction method	Numerical
Range of transmission factors	0.8366 to 0.8876
Data / restraints / parameters	2495 / 145 / 1
Goodness of fit (goof) [all data]	1.013
Final <i>R</i> values	
<i>R</i> ₁ [all data, $I \geq 2\sigma(I)$]	0.0395, 0.0332
<i>wR</i> ₂ [all data, $I \geq 2\sigma(I)$]	0.0744, 0.0725
Largest diff. peak and hole	0.206 and -0.426 e.Å ⁻³

Table 55. Selected bond lengths (Å) and angles (°) for **29**

C(1)–N(1)	1.315(4)	C(10)–N(2)	1.471(4)
C(1)–N(2)	1.337(5)	C(10)–C(11)	1.492(6)
C(1)–C(2)	1.436(5)	C(10)–C(12)	1.496(6)
C(2)–C(3)	1.194(5)	Cl–Fe	2.314(1)
C(3)–C(4)	1.428(5)	N(1)–Fe	2.087(3)
C(7)–N(1)	1.477(5)	Fe–N(1)#1	2.087(3)
C(7)–C(9)	1.513(6)	Fe–Cl#1	2.314(1)
C(7)–C(8)	1.514(6)	N(2)–H(1)	0.87(2)
<hr/>			
N(1)–C(1)–N(2)	121.8(3)	C(1)–N(1)–C(7)	116.9(3)
N(1)–C(1)–C(2)	122.1(3)	C(1)–N(1)–Fe	125.7(2)
N(2)–C(1)–C(2)	116.1(3)	C(7)–N(1)–Fe	117.4(2)
C(3)–C(2)–C(1)	177.6(4)	N(1)#1–Fe–N(1)	112.1(2)
C(2)–C(3)–C(4)	177.3(4)	N(1)#1–Fe–Cl	113.1(9)
C(3)–C(4)–C(5)	120.6(4)	N(1)–Fe–Cl	108.4(8)
C(3)–C(4)–C(6)	120.3(4)	N(1)#1–Fe–Cl#1	108.4(8)
C(5)–C(4)–C(6)	58.6(4)	N(1)–Fe–Cl#1	113.1(9)
C(6)–C(5)–C(4)	60.7(3)	Cl–Fe–Cl#1	101.3(6)
C(5)–C(6)–C(4)	60.7(3)		

Symmetry transformations used to generate equivalent atoms:

#1 -x+1, -y+1, z

Table 56. Crystal data and structure refinement for $\text{FeCl}_2[\text{c-C}_3\text{H}_5\text{-C}\equiv\text{C-C}(\text{NCy})(\text{NHCy})]_2$ (**30**)

Identification code:	fe0085
Empirical formula	$\text{C}_{36}\text{H}_{56}\text{Cl}_2\text{FeN}_2$
Formula weight	671.59
Crystal color / shape / size (mm)	Colorless plate, $0.26 \times 0.19 \times 0.12$
Crystal system	Monoclinic
Space group	$\text{P2}_1/\text{c}$
Unit cell dimensions	
<i>a</i> (Å)	13.905(7)
<i>b</i> (Å)	12.500(6)
<i>c</i> (Å)	20.742(11)
α (deg)	90
β (deg)	92.24(4)
γ (deg)	90
Unit cell volume <i>V</i> (Å ³)	3603(3)
Molecules per cell <i>z</i>	4
Crystallographic density ρ_{calcd} (g cm ⁻³)	1.238
Absorption coefficient μ (mm ⁻¹)	0.597
Diffractometer	STOE IPDS 2T
Radiation (λ [Å])	Graphite-monochromated Mo-K α (0.71073)
Temperature (°C)	-173(2)
Scan type	ω scan (increment 1.5°, exposure 1 min)
Completeness of dataset	99.4%
θ range of data collection(deg)	1.903 to 25.349
Reflections collected	17648 ($-16 \leq h \leq 16$, $-14 \leq k \leq 15$, $-24 \leq l \leq 24$)
Independent reflections	6560 ($R_{\text{int}} = 0.0283$)
Independent reflections with $I > 2\sigma(I)$	5935
Structure solution method	Dual-space structure solution (SHELXT)
Refinement method	Full-matrix least-squares on F^2 (SHELXL)
Absorption correction method	Numerical
Range of transmission factors	0.9078 and 0.8383
Data / restraints / parameters	6560 / 391 / 1
Goodness of fit (goof) [all data]	1.119
Final <i>R</i> values	
<i>R</i> ₁ [all data, $I \geq 2\sigma(I)$]	0.0374, 0.0315
<i>wR</i> ₂ [all data, $I \geq 2\sigma(I)$]	0.0719, 0.0697
Largest diff. peak and hole	0.357 and -0.349 e.Å ⁻³

Table 57. Selected bond lengths (Å) and angles (°) for **30**

C(1)–N(1)	1.309(2)	C(13)–N(2)	1.462(2)
C(1)–N(2)	1.340(2)	C(13)–C(14)	1.520(2)
C(1)–C(2)	1.442(2)	C(13)–C(18)	1.526(2)
C(2)–C(3)	1.192(2)	Cl(1)–Fe(1)	2.315(9)
C(3)–C(4)	1.432(2)	N(1)–Fe(1)	2.073(1)
C(7)–N(1)	1.480(2)	Fe(1)–N(3)	2.080(1)
C(7)–C(12)	1.518(2)	Fe(1)–Cl(2)	2.301(1)
C(7)–C(8)	1.526(2)	N(2)–H(1)	0.844(1)
N(1)–C(1)–N(2)	122.6(1)	C(19)–N(3)–C(25)	117.1(1)
N(1)–C(1)–C(2)	121.7(1)	C(19)–N(3)–Fe(1)	123.8(1)
N(2)–C(1)–C(2)	115.7(1)	C(25)–N(3)–Fe(1)	119.0(1)
C(3)–C(2)–C(1)	179.1(2)	N(3)–Fe(1)–N(1)	108.6(6)
C(2)–C(3)–C(4)	179.0(2)	N(1)–Fe(1)–Cl(2)	114.8(5)
C(3)–C(4)–C(5)	119.1(1)	N(3)–Fe(1)–Cl(2)	106.7(5)
C(3)–C(4)–C(6)	118.7(1)	N(1)–Fe(1)–Cl(1)	105.7(5)
C(1)–N(1)–C(7)	116.7(1)	N(3)–Fe(1)–Cl(1)	114.7(5)
C(1)–N(1)–Fe(1)	124.0(1)	Cl(1)–Fe(1)–Cl(2)	106.6(4)
C(7)–N(1)–Fe(1)	119.3(1)		

Table 58. Crystal data and structure refinement for $\text{CoCl}_2[\text{C}-\text{C}_3\text{H}_5-\text{C}\equiv\text{C}-\text{C}(\text{NCy})(\text{NHCy})]_2$ (**31**)

Identification code:	li0056
Empirical formula	$\text{C}_{36}\text{H}_{56}\text{Cl}_2\text{CoN}_4$
Formula weight	674.67
Crystal color / shape / size (mm)	Blue rod, $0.39 \times 0.19 \times 0.10$
Crystal system	Monoclinic
Space group	$P2_1/c$
Unit cell dimensions	
<i>a</i> (Å)	18.8898(3)
<i>b</i> (Å)	12.5574(3)
<i>c</i> (Å)	20.8394(5)
<i>α</i> (deg)	90
<i>β</i> (deg)	91.717(2)
<i>γ</i> (deg)	90
Unit cell volume <i>V</i> (Å ³)	3633.2(12)
Molecules per cell <i>z</i>	4
Crystallographic density ρ_{calcd} (g cm ⁻³)	1.233
Absorption coefficient μ (mm ⁻¹)	0.649
Diffractometer	STOE IPDS 2T
Radiation (λ [Å])	Graphite-monochromated Mo-K α (0.71073)
Temperature (°C)	-120(2)
Scan type	ω scan (increment 1.5°, exposure 1 min)
Completeness of dataset	99.9%
θ range of data collection(deg)	1.894 to 25.997
Reflections collected	22020 ($-15 \leq h \leq 17$, $-15 \leq k \leq 15$, $-25 \leq l \leq 25$)
Independent reflections	7126 ($R_{\text{int}} = 0.0417$)
Independent reflections with $I > 2\sigma(I)$	5923
Structure solution method	Patterson methods (SHELXT)
Refinement method	Full-matrix least-squares on F^2 (SHELXL)
Absorption correction method	Numerical
Range of transmission factors	0.8074 and 0.9379
Data / restraints / parameters	7126 / 388 / 0
Goodness of fit (goof) [all data]	1.035
Final <i>R</i> values	
<i>R</i> ₁ [all data, $I \geq 2\sigma(I)$]	0.0478, 0.0355
<i>wR</i> ₂ [all data, $I \geq 2\sigma(I)$]	0.0845, 0.0794
Largest diff. peak and hole	0.660 and -0366 e.Å ⁻³

Table 59. Selected bond lengths (Å) and angles (°) for **31**

C(1)–N(1)	1.311(2)	C(13)–N(2)	1.465(2)
C(1)–N(2)	1.339(2)	C(13)–C(14)	1.517(3)
C(1)–C(2)	1.447(2)	C(13)–C(18)	1.520(3)
C(2)–C(3)	1.191(3)	Cl(1)–Co	2.273(5)
C(3)–C(4)	1.435(5)	N(1)–Co	2.041(1)
C(7)–N(1)	1.483(2)	Co–N(3)	2.042(1)
C(7)–C(12)	1.523(2)	Co–Cl(2)	2.283(5)
C(7)–C(8)	1.517(2)	N(2)–H(1)	0.848(1)
N(1)–C(1)–N(2)	122.6(2)	C(19)–N(3)–C(25)	116.6(1)
N(1)–C(1)–C(2)	121.6(2)	C(19)–N(3)–Co	125.6(1)
N(2)–C(1)–C(2)	115.9(2)	C(25)–N(3)–Co	117.8(1)
C(3)–C(2)–C(1)	179.0(2)	N(3)–Co–N(1)	111.1(6)
C(2)–C(3)–C(4)	179.4(2)	N(1)–Co–Cl(2)	112.4(4)
C(3)–C(4)–C(5)	119.3(2)	N(3)–Co–Cl(2)	107.9(4)
C(3)–C(4)–C(6)	118.6(2)	N(1)–Co–Cl(1)	107.1(4)
C(1)–N(1)–C(7)	116.5(1)	N(3)–Co–Cl(1)	112.5(4)
C(1)–N(1)–Co	125.8(1)	Cl(1)–Co–Cl(2)	105.8(2)
C(7)–N(1)–Co	117.7(1)		

Table 60. Crystal data and structure refinement for $(\mu_4\text{-O})\{\text{Mn}[\text{C}_3\text{H}_5\text{-C}\equiv\text{C-C}(\text{NCy})_2]\}_4\text{Cl}_2$ (**37**)

Identification code:	fe0129
Empirical formula	$\text{C}_{72}\text{H}_{108}\text{Cl}_2\text{Mn}_4\text{N}_8\text{O}$
Formula weight	1392.32
Crystal color / shape / size (mm)	Yellow block, $0.23 \times 0.18 \times 0.13$
Crystal system	Monoclinic
Space group	$C2/c$
Unit cell dimensions	
<i>a</i> (Å)	13.457(5)
<i>b</i> (Å)	22.508(5)
<i>c</i> (Å)	23.650(9)
α (deg)	90
β (deg)	101.08(3)
γ (deg)	90
Unit cell volume <i>V</i> (Å ³)	7030(4)
Molecules per cell <i>z</i>	4
Crystallographic density ρ_{calcd} (g cm ⁻³)	1.316
Absorption coefficient μ (mm ⁻¹)	0.826
Diffractometer	STOE IPDS 2T
Radiation (λ [Å])	Graphite-monochromated Mo-K α (0.71073)
Temperature (°C)	-173(2)
Scan type	ω scan (increment 1.5°, exposure 1 min)
Completeness of dataset	99.7%
θ range of data collection(deg)	1.809 to 25.350
Reflections collected	23488 ($-16 \leq h \leq 16, -27 \leq k \leq 26, -28 \leq l \leq 28$)
Independent reflections	6426 ($R_{\text{int}} = 0.0524$)
Independent reflections with $I > 2\sigma(I)$	5895
Structure solution method	Dual-space structure solution (SHELXT)
Refinement method	Full-matrix least-squares on F^2 (SHELXL)
Absorption correction method	integration
Range of transmission factors	0.8914 and 0.7846
Data / restraints / parameters	6426 / 394 / 387
Goodness of fit (goof) [all data]	1.124
<i>R</i> ₁ [all data, $I \geq 2\sigma(I)$]	0.0484, 0.0431
<i>wR</i> ₂ [all data, $I \geq 2\sigma(I)$]	0.1012, 0.0988
Largest diff. peak and hole	1.566 and -0.482 e.Å ⁻³

Refinement special details: Large residual density peaks probably due to inefficient absorption correction.

Table 61. Selected bond lengths (Å) and angles (°) for **37**

Mn(1)–O(1)	2.019(2)	Mn(2)–Mn(2)#1	2.964(1)
Mn(1)–N2_2	2.098(2)	C1_1–N1_1	1.309(3)
Mn(1)–N2_1	2.(11)9(2)	C1_1–N2_1	1.347(3)
Mn(1)–Cl(2)	2.450(9)	C1_1–C2_1	1.458(3)
Mn(1)–Mn(2)	2.750(8)	C2_1–C3_1	1.195(4)
Mn(1)–Mn(1)#1	3.028(1)	C3_1–C4_1	1.435(4)
Mn(2)–O(1)	2.015(2)	C4_1–C6_1	1.499(4)
Mn(2)–N1_1	2.088(2)	C4_1–C5_1	1.502(4)
Mn(2)–N1_2	2.094(2)	C5_1–C6_1	1.457(4)
Mn(2)–Cl(1)	2.454(9)		
O(1)–Mn(1)–N2_2	102.5(7)	Mn(2)–O(1)–Mn(2)#1	94.7(1)
O(1)–Mn(1)–N(21)	106.8(6)	Mn(2)–O(1)–Mn(1)#1	165.2(2)
N(22)–Mn(1)–N(21)	(11)6.7(8)	Mn(2)#1–O(1)–Mn(1)#1	86.0(3)
O(1)–Mn(1)–Cl(2)	93.3(6)	Mn(2)–O(1)–Mn(1)	86.0(3)
N(22)–Mn(1)–Cl(2)	(11)9.8(6)	Mn(2)#1–O(1)–Mn(1)	165.2(2)
N(21)–Mn(1)–Cl(2)	(11)3.5(6)	Mn(1)#1–O(1)–Mn(1)	97.2(1)
O(1)–Mn(2)–N(11)	98.0(7)	Mn(2)#1–Cl(1)–Mn(2)	74.3(4)
O(1)–Mn(2)–N(12)	(11)0.5(7)	Mn(1)–Cl(2)–Mn(1)#1	76.4(4)
N(11)–Mn(2)–N(12)	(11)8.9(8)	N(11)–C(11)–N(21)	(12)0.8(2)
O(1)–Mn(2)–Cl(1)	95.5(6)	N(11)–C(11)–C(21)	(12)0.8(2)
N(11)–Mn(2)–Cl(1)	(11)4.9(6)	N(21)–C(11)–C(21)	(11)8.4(2)
N(12)–Mn(2)–Cl(1)	(11)4.6(6)		

Symmetry transformations used to generate equivalent atoms:

#1 $-x+1, y, -z+1/2$

Table 62. Crystal data and structure refinement for $(\mu_4\text{-O})(\mu_2\text{-O})_2\{\text{Mn}[c\text{-C}_3\text{H}_5\text{-C}\equiv\text{C-C}(\text{NCy})_2]\}_4$ (**39**)

Identification code:	fe0076
Empirical formula	$\text{C}_{72}\text{H}_{108}\text{Co}_4\text{N}_8\text{O}_3, 0.51(\text{C}_{18}\text{H}_{25}\text{N}_2), 0.40(\text{C}_5\text{H}_{11})$
Formula weight	1551.67
Crystal color / shape / size (mm)	Blue block, $0.42 \times 0.33 \times 0.19$
Crystal system	Triclinic
Space group	$P\bar{1}$
Unit cell dimensions	
<i>a</i> (Å)	15.133(10)
<i>b</i> (Å)	15.300(9)
<i>c</i> (Å)	19.392(13)
<i>α</i> (deg)	100.55(5)
<i>β</i> (deg)	108.79(5)
<i>γ</i> (deg)	90.45(5)
Unit cell volume <i>V</i> (Å ³)	4168(5)
Molecules per cell <i>z</i>	2
Crystallographic density ρ_{calcd} (g cm ⁻³)	1.236
Absorption coefficient μ (mm ⁻¹)	0.849
Diffractometer	STOE IPDS 2T
Radiation (λ [Å])	Graphite-monochromated Mo-K α (0.71073)
Temperature (°C)	-173(2)
Scan type	ω scan (increment 1.5°, exposure 1 min)
Completeness of dataset	97.3%
θ range of data collection(deg)	1.930 to 25.348
Reflections collected	32383 ($-18 \leq h \leq 18, -18 \leq k \leq 17, -23 \leq l \leq 23$)
Independent reflections	14839 ($R_{\text{int}} = 0.1256$)
Independent reflections with $I > 2\sigma(I)$	11572
Structure solution method	Dual-space structure solution (SHELXT)
Refinement method	Full-matrix least-squares on F^2 (SHELXL)
Absorption correction method	Numerical
Range of transmission factors	0.6981 to 0.8197
Data / restraints / parameters	14839 / 1069 / 1990
Goodness of fit (goof) [all data]	1.058
Final <i>R</i> values	
<i>R</i> ₁ [all data, $I \geq 2\sigma(I)$]	0.0893, 0.0711
<i>wR</i> ₂ [all data, $I \geq 2\sigma(I)$]	0.2066, 0.1922
Largest diff. peak and hole	0.735 and -1.021 e.Å ⁻³

Refinement special details: Additional to the Cobalt complex, there is also free ligand within the unit cell. The free ligand molecule is positioned on an inversion center. Therefore, it is only 50% occupied. Furthermore, a partially occupied solvent molecule (pentane) could be found and refined.

Table 63. Selected bond lengths (Å) and angles (°) for **39**

Co(1)–O(2)	1.956(3)	Co(3)–N(5)	2.007(4)
Co(1)–N(1)	1.991(4)	Co(3)–O(3)	2.017(3)
Co(1)–N(3)	2.001(4)	Co(3)–Co(4)	2.659(2)
Co(1)–O(3)	2.003(3)	Co(4)–O(2)	1.953(3)
Co(1)–Co(2)	2.646(2)	Co(4)–N(8)	1.986(4)
Co(1)–Co(3)	2.883(2)	Co(4)–N(6)	1.994(4)
Co(2)–O(2)	1.958(3)	Co(4)–O(4)	2.005(4)
Co(2)–N(2)	1.988(4)	C(1)–N(1)	1.335(5)
Co(2)–N(4)	1.994(4)	C(1)–N(2)	1.336(6)
Co(2)–O(4)	2.011(3)	C(1)–C(2)	1.458(6)
Co(2)–Co(4)	2.890(2)	C(2)–C(3)	1.186(6)
Co(3)–O(2)	1.950(3)	C(3)–C(4)	1.32(4)
Co(3)–N(7)	2.000(4)		
O(2)–Co(1)–N(1)	102.8(1)	N(4)–Co(2)–O(4)	114.5(1)
O(2)–Co(1)–N(3)	108.4(2)	O(2)–Co(3)–N(7)	104.8(2)
N(1)–Co(1)–N(3)	123.6(2)	O(2)–Co(3)–N(5)	111.1(1)
O(2)–Co(1)–O(3)	86.7(1)	N(7)–Co(3)–N(5)	116.4(2)
N(1)–Co(1)–O(3)	113.61(2)	O(2)–Co(3)–O(3)	86.5(1)
N(3)–Co(1)–O(3)	113.9(1)	N(7)–Co(3)–O(3)	115.8(1)
O(2)–Co(2)–N(2)	109.4(1)	N(5)–Co(3)–O(3)	117.1(1)
O(2)–Co(2)–N(4)	102.7(1)	O(2)–Co(4)–N(8)	110.4(1)
N(2)–Co(2)–N(4)	121.5(1)	O(2)–Co(4)–N(6)	105.3(1)
O(2)–Co(2)–O(4)	86.2(3)	N(8)–Co(4)–N(6)	115.1(1)
N(2)–Co(2)–O(4)	115.2(2)		

Reference

1. T. J. Kealy, P. L. Pauson, *Nature*. **1951**, *168*, 1039-1040.
2. A. F. Hill, M. J. Fink, *Advances in Organometallic Chemistry*: Elsevier Science; 2011.
3. J. Barker, M. Kilner, *Coord. Chem. Rev.* **1994**, *133*, 219-300.
4. F. T. Edelman, *Coord. Chem. Rev.* **1994**, *137*, 403-481.
5. C. Gerhardt, *Ann. Chem. Pharmacie*. **1858**, *108*, 214-223.
6. V. F. Roche, *Am. J. Pharm. Educ.* **2007**, *71*, 122.
7. J. Clayden, N. Greeves, S. Warren, *Organic Chemistry*: OUP Oxford; 2012.
8. C. M. Eulitz, S. Scheuermann, H. J. Thier, *Brockhaus ABC Chemie*: F.A. Brockhaus; **1965**.
9. P. B. Hitchcock, M. F. Lappert, P. G. Merle, *Dalton Trans.* **2007**, 585-594.
10. R. L. Shriner, F. W. Neumann, *Chem. Rev.* **1944**, *35*, 351-425.
11. H. Usui, Y. Watanabe, M. Kanao, *J. Heterocycl. Chem.* **1993**, *30*, 551-552.
12. J. V. Greenhill, P. Lue. 5 Amidines and Guanidines in Medicinal Chemistry. In: Ellis GP, Luscombe DK, *Progress in Medicinal Chemistry*. 30: Elsevier; **1993**, 203-326.
13. S. M. Sondhi, M. Dinodia, A. Kumar, *Bioorg. Med. Chem.* **2006**, *14*, 4657-4663.
14. P. M. Bedi, M. P. Mahajan, V. K. Kapoor, *Bioorg. Med. Chem. Lett.* **2004**, *14*, 3821-3824.
15. A. Pinner, F. Klein, *Ber. Dtsch. Chem. Ges.* **1877**, *10*, 1889-1897.
16. Z. Wang, Pinner Reaction. *Comprehensive Organic Name Reactions and Reagents* Wiley; **2010**.
17. R. Roger, D. G. Neilson, *Chem. Rev.* **1961**, *61*, 179-211.

18. A. R. Sanger, *Inorg. Nucl. Chem. Lett.* **1973**, *9*, 351-354.
19. S. Anga, I. Banerjee, T. K. Panda, *J. Chem. Sci.* **2016**, *128*, 867-873.
20. A. F. Hill, M. j. Fink, *Adv. Organomet. Chem.* **2008**, *57*, 183-352.
21. F. T. Edelmann, *New J. Chem.* **1995**, *19*, 535-550.
22. F. M. Sroor, C. G. Hrib, L. Hilfert, S. Busse, F. T. Edelmann, *New J. Chem.* **2015**, *39*, 7595-7601.
23. F. M. Sroor, C. G. Hrib, L. Hilfert, F. T. Edelmann, *Z. Anorg. Allg. Chem.* **2015**, *641*, 2042-2046.
24. F. M. Sroor, C. G. Hrib, L. Hilfert, L. Hartenstein, P. W. Roesky, F. T. Edelmann, *J. Organomet. Chem.* **2015**, *799-800*, 160-165.
25. F. M. Sroor, C. G. Hrib, L. Hilfert, P. G. Jones, F. T. Edelmann, *J. Organomet. Chem.* **2015**, *785*, 1-10.
26. F. M. Sroor, C. G. Hrib, F. T. Edelmann, *Inorganics* **2015**, *3*, 429-447.
27. J. M. Sundermeyer, S. Wolf, K. Ralf; U.S. Patent 0051878, **2014**.
28. D. Abeysekera, K. N. Robertson, T. S. Cameron, J. A. C. Clyburne, *Organometallics* **2001**, *20*, 5532-5536.
29. L. Cabrera, E. Hollink, J. C. Stewart, P. Wei, D. W. Stephan, *Organometallics* **2005**, *24*, 1091-1098.
30. F. A. Cotton, L. M. Daniels, C. A. Murillo, *Inorg. Chim. Acta* **1994**, *224*, 5-9.
31. F. A. Cotton, L. M. Daniels, C. A. Murillo, P. Schooler, *J. Chem. Soc., Dalton Trans.* **2000**, 2001-2005.
32. F. A. Cotton, W. H. Ilsley, W. Kaim, *Inorg. Chem.* **1981**, *20*, 930-934.
33. L. R. Sita, J. R. Babcock, *Organometallics* **1998**, *17*, 5228-5230.
34. A. F. Hill, M. J. Fink, *Advances in Organometallic Chemistry*: Elsevier Science; **2013**.

35. J. A. R. Schmidt, J. Arnold, *Chem. Commun.* **1999**, 2149-2150.
36. J. Baldamus, C. Berghof, M. L. Cole, D. J. Evans, E. Hey-Hawkins, P. C. Junk, *J. Chem. Soc., Dalton Trans.* **2002**, 2802-2804.
37. F. A. Cotton, L. M. Daniels, D. J. Maloney, J. H. Matonic, C. A. Murillo, *Polyhedron* **1994**, *13*, 815-23.
38. S. R. Foley, C. Bensimon, D. S. Richeson, *J. Am. Chem. Soc.* **1997**, *119*, 10359-10363.
39. D. M. Grove, G. van Koten, H. J. C. Ubbels, K. Vrieze, L. C. Niemann, C. H. Stam, *J. Chem. Soc., Dalton Trans.* **1986**, 717-724.
40. J. A. R. Schmidt, J. Arnold, *J. Chem. Soc., Dalton Trans.* **2002**, 2890-2899.
41. Y. Yamaguchi, K. Ogata, K. Kobayashi, T. Ito, *Dalton Trans.* **2004**, 3982-3990.
42. Y.-C. Tsai, C.-W. Hsu, J.-S. K. Yu, G.-H. Lee, Y. Wang, T.-S. Kuo, *Angew. Chem. Int. Ed.* **2008**, *120*, 7360-7363.
43. F. A. Cotton, L. M. Daniels, J. H. Matonic, C. A. Murillo, *Inorg. Chim. Acta* **1997**, *256*, 277-282.
44. F. A. Cotton, X. Feng, C. A. Murillo, *Inorg. Chim. Acta* **1997**, *256*, 303-308.
45. F. A. Cotton, L. M. Daniels, L. R. Falvello, J. H. Matonic, C. A. Murillo, *Inorg. Chim. Acta* **1997**, *256*, 269-275.
46. F. A. Cotton, L. M. Daniels, X. Feng, D. J. Maloney, J. H. Matonic, C. A. Murillo, *Inorg. Chim. Acta* **1997**, *256*, 291-301.
47. F. A. Cotton, L. M. Daniels, D. J. Maloney, J. H. Matonic, C. A. Murillo, *Inorg. Chim. Acta* **1997**, *256*, 283-289.
48. F. A. Cotton, L. M. Daniels, D. J. Maloney, C. A. Murillo, *Inorg. Chim. Acta* **1996**, *249*, 9-11.
49. F. A. Cotton, L. M. Daniels, C. A. Murillo, *Angew. Chem. Int. Ed. Engl.* **1992**, *31*, 737-738.
50. F. A. Cotton, L. M. Daniels, C. A. Murillo, *Inorg. Chem.* **1993**, *32*, 2881-2885.

-
51. F. A. Cotton, L. M. Daniels, C. A. Murillo, I. Pascual, H.-C. Zhou, *J. Am. Chem. Soc.* **1999**, *121*, 6856-6861.
52. F. A. Cotton, J. P. Donahue, C. Lin, C. A. Murillo, *Inorg. Chem.* **2001**, *40*, 1234-1244.
53. F. A. Cotton, C. Lin, C. A. Murillo, *Inorg. Chem.* **2001**, *40*, 472-477.
54. F. A. Cotton, C. Lin, C. A. Murillo, *Inorg. Chem.* **2001**, *40*, 478-484.
55. F. A. Cotton, C. Lin, C. A. Murillo, *Inorg. Chem.* **2001**, *40*, 6413-6417.
56. F. A. Cotton, C. Y. Liu, C. A. Murillo, *Inorg. Chem.* **2004**, *43*, 2267-2276.
57. F. A. Cotton, C. A. Murillo, I. Pascual, *Inorg. Chem.* **1999**, *38*, 2182-2187.
58. H. Shoukang, S. Gambarotta, C. Bensimon, J. J. H. Edema, *Inorg. Chim. Acta* **1993**, *213*, 65-74.
59. A. Kasani, R. P. Kamalesh Babu, K. Feghali, S. Gambarotta, G. P. A. Yap, L. K. Thompson, *Chem.- Eur. J.* **1999**, *5*, 577-586.
60. B. S. Lim, A. Rahtu, J. S. Park, R. G. Gordon, *Inorg. Chem.* **2003**, *42*, 7951-7958.
61. A. R. Sadique, M. J. Heeg, C. H. Winter, *Inorg. Chem.* **2001**, *40*, 6349-6355.
62. S. Aharonovich, M. Kapon, M. Botoshanski, M. S. Eisen, *Organometallics* **2008**, *27*, 1869-1877.
63. D. J. Brown, M. H. Chisholm, J. C. Gallucci, *Dalton Trans.* **2008**, 1615-1624.
64. S. Dagorne, R. F. Jordan, V. G. Young, *Organometallics* **1999**, *18*, 4619-4623.
65. W. W. Schoeller, A. Sundermann, M. Reiher, *Inorg. Chem.* **1999**, *38*, 29-37.
66. R. Schlund, L. Martin, F. Edelmann, U. Reissmann, W. Rohde; U.S. Patent 5707913, **1998**.
67. C. Chen, L. Rees, A. Cowley, M. Green, *J. Chem. Soc., Dalton Trans.* **2001**, 1761-1767.

68. C. Janiak, K. C. H. Lange, T. G. Scharmann, *Appl. Organomet. Chem.* **2000**, *14*, 316-324.
69. W. P. Kretschmer, B. Hessen, A. Noor, N. M. Scott, R. Kempe, *J. Organomet. Chem.* **2007**, *692*, 4569-4579.
70. A. Littke, N. Sleiman, C. Bensimon, D. S. Richeson, G. P. A. Yap, S. J. Brown, *Organometallics* **1998**, *17*, 446-451.
71. A. Noor, W. P. Kretschmer, G. Glatz, A. Meetsma, R. Kempe, *Eur. J. Inorg. Chem.* **2008**, 5088-5098.
72. M. Talja, M. Klinga, M. Polamo, E. Aitola, M. Leskelä, *Inorg. Chim. Acta* **2005**, *358*, 1061-1067.
73. M. Talja, T. Luhtanen, M. Polamo, M. Klinga, T. A. Pakkanen, M. Leskelä, *Inorg. Chim. Acta* **2008**, *361*, 2195-2202.
74. M. Zhou, H. Tong, X. Wei, D. Liu, *J. Organomet. Chem.* **2007**, *692*, 5195-5202.
75. S. Collins, *Coord. Chem. Rev.* **2011**, *255*, 118-138.
76. D. M. Lyubov, G. K. Fukin, A. A. Trifonov, *Inorg. Chem.* **2007**, *46*, 11450-11456.
77. A. A. Trifonov, G. G. Skvortsov, D. M. Lyubov, N. A. Skorodumova, G. K. Fukin, E. V. Baranov, *Chem.-Eur. J.* **2006**, *12*, 5320-5327.
78. S. Bamberra, M. W. Bouwkamp, A. Meetsma, B. Hessen, *J. Am. Chem. Soc.* **2004**, *126*, 9182-9183.
79. S. Bamberra, E. Otten, D. van Leusen, A. Meetsma, B. Hessen, *Z. Anorg. Allg. Chem.* **2006**, *632*, 1950-1952.
80. S. Bamberra, D. van Leusen, A. Meetsma, B. Hessen, J. H. Teuben, *Chem. Commun.* **2003**, 522-523.
81. R. Kempe, H. Noss, H. Fuhrmann, *Chem.-Eur. J.* **2001**, *7*, 1630-1636.
82. F.-S. Liu, H.-Y. Gao, K.-M. Song, Y. Zhao, J.-M. Long, L. Zhang, *Polyhedron* **2009**, *28*, 673-678.
83. K. Shibayama, S. W. Seidel, B. M. Novak, *Macromolecules* **1997**, *30*, 3159-3163.

-
84. A. Goodwin, B. M. Novak, *Macromolecules* **1994**, *27*, 5520-5522.
85. K. B. Aubrecht, K. Chang, M. A. Hillmyer, W. B. Tolman, *J. Polym. Sci., Part A: Polym. Chem.* **2001**, *39*, 284-293.
86. B. J. O'Keefe, L. E. Breyfogle, M. A. Hillmyer, W. B. Tolman, *J. Am. Chem. Soc.* **2002**, *124*, 4384-4393.
87. Z. Li, S. T. Barry, R. G. Gordon, *Inorg. Chem.* **2005**, *44*, 1728-1735.
88. A. Purniawan, P. J. French, G. Pandraud, P. M. Sarro, *Procedia Engineering* **2010**, *5*, 1131-1135.
89. R. Rosenberg, D. C. Edelstein, C. K. Hu, K. P. Rodbell, *Annu. Rev. Mater. Sci.* **2000**, *30*, 229-262.
90. R. G. Gordon, J. Becker, D. Hausmann, S. Suh, *Chem. Mater.* **2001**, *13*, 2463-2464.
91. H. Kim, *J. Vac. Sci. Technol. B* **2003**, *21*, 2231-2261.
92. B. S. Lim, A. Rahtu, R. G. Gordon, *Nat. Mater.* **2003**, *2*, 749-754.
93. K. Xu, A. P. Milanov, M. Winter, D. Barreca, A. Gasparotto, H.-W. Becker, *Eur. J. Inorg. Chem.* **2010**, 1679-1688.
94. V. Krisyuk, A. N. Gleizes, L. Aloui, A. Turgambaeva, B. Sarapata, N. P. Homme, *J. Electrochem. Soc.* **2010**, *157*, D454-D461.
95. S. M. George, *Chem. Rev.* **2010**, *110*, 111-131.
96. M. Leskela, M. Ritala, *Angew. Chem. Int. Ed. Engl.* **2003**, *42*, 5548-5554.
97. F. M. A. Sroor, C. G. Hrib, L. Hilfert, F. T. Edelmann, *Z. Anorg. Allg. Chem.* **2013**, *639*, 2390-2394.
98. C. N. Rowley, G. A. DiLabio, S. T. Barry, *Inorg. Chem.* **2005**, *44*, 1983-1991.
99. P. Sienkiewicz, K. Bielawski, A. Bielawska, J. Palka, *Environ. Toxicol. Pharmacol.* **2005**, *20*, 118-124.
100. T.-G. Ong, J. S. O'Brien, I. Korobkov, D. S. Richeson, *Organometallics* **2006**, *25*, 4728-4730.

-
101. X. Xu, J. Gao, D. Cheng, J. Li, G. Qiang, H. Guo, *Adv. Synth. Catal.* **2008**, *350*, 61-64.
102. W. Weingärtner, G. Maas, *Eur. J. Org. Chem.* **2012**, *2012*, 6372-6382.
103. P. Dröse, C. G. Hrib, F. T. Edelmann, *J. Organomet. Chem.* **2010**, *695*, 1953-1956.
104. V. Lorenz, P. Liebing, L. Hilfert, S. Busse, F. T. Edelmann, *Acta Crystallogr. E.* **2018**, *74*, 1795-1799.
105. W. Clegg, E. K. Cope, A. J. Edwards, F. S. Mair, *Inorg. Chem.* **1998**, *37*, 2317-2319.
106. F. Feil, S. Harder, *Organometallics* **2000**, *19*, 5010-5015.
107. P. C. Junk, M. L. Cole, *Chem. Commun.* **2007**, 1579-1590.
108. F. T. Edelmann, *Chem. Soc. Rev.* **2012**, *41*, 7657-7672.
109. J. R. Hagadorn, J. Arnold, *Inorg. Chem.* **1997**, *36*, 132-133.
110. J. Richter, J. Feiling, H.-G. Schmidt, M. Noltemeyer, W. Brüser, F. T. Edelmann, *Z. Anorg. Allg. Chem.* **2004**, *630*, 1269-1275.
111. J. Barker, D. Barr, N. D. R. Barnett, W. Clegg, I. Cragg-Hine, M. G. Davidson, *J. Chem. Soc., Dalton Trans.* **1997**, 951-956.
112. G. R. Giesbrecht, A. Shafir, J. Arnold, *J. Chem. Soc., Dalton Trans.* **1999**, 3601-3604.
113. C. Knapp, E. Lork, P. G. Watson, R. Mews, *Inorg. Chem.* **2002**, *41*, 2014-2025.
114. W. W. Seidel, W. Dachtler, T. Pape, *Z. Anorg. Allg. Chem.* **2012**, *638*, 116-121.
115. X. Zhang, W. Z. Zhang, X. Ren, L. L. Zhang, X. B. Lu, *Org. Lett.* **2011**, *13*, 2402-2405.
116. C. F. Caro, P. B. Hitchcock, M. F. Lappert, M. Layh, *Chem. Commun.* **1998**, 1297-8.
117. C. L. Boyd, B. R. Tyrrell, P. Mountford, *Acta Crystallogr. E.* **2002**, *58*, 597-598.

118. J. Nevoralová, T. Chlupatý, Z. Padělková, A. Růžička, *J. Organomet. Chem.* **2013**, 745-746, 186-189.
119. J. Hong, L. Zhang, K. Wang, Z. Chen, L. Wu, X. Zhou, *Organometallics* **2013**, 32, 7312-7322.
120. P. Benndorf, C. Preuß, P. W. Roesky, *J. Organomet. Chem.* **2011**, 696, 1150-1155.
121. J. J. Novoa, P. Lafuente, R. E. Del Sesto, J. S. Miller, *Angew. Chem. Int. Ed.* **2001**, 40, 2540-2545.
122. J.-M. Lü, S. V. Rosokha, J. K. Kochi, *J. Am. Chem. Soc.* **2003**, 125, 12161-12171.
123. F. A. Cottona, L. M. Daniels, D. J. Maloney, C. A. Murillo, *Inorg. Chim. Acta* **1996**, 242, 31-42.
124. L. Xu, Y. C. Wang, W. X. Zhang, Z. Xi, *Dalton Trans.* **2013**, 42, 16466-16469.
125. G. Frenking, R. Tonner, *Nature* **2007**, 446, 276-277.
126. F. Hein, D. Tille, *Z. Anorg. Allg. Chem.* **1964**, 329, 72-82.
127. F. A. Cotton, L. M. Daniels, E. A. Hillard, C. A. Murillo, *Inorg. Chem.* **2002**, 41, 2466-2470.
128. F. A. Cotton, S. A. Koch, M. Millar, *Inorg. Chem.* **1978**, 17, 2084-2086.
129. F. A. Cotton, W. H. Ilsley, W. Kaim, *J. Am. Chem. Soc.* **1980**, 102, 3464-3474.
130. A. R. Sadique, M. J. Heeg, C. H. Winter, *J. Am. Chem. Soc.* **2003**, 125, 7774-7775.
131. F. A. Cotton, W. H. Ilsley, *Inorg. Chem.* **1981**, 20, 572-578.
132. F. A. Cotton, G. N. Mott, *Inorg. Chem.* **1981**, 20, 3896-3899.
133. Y. Yamaguchi, S. Ozaki, H. Hinago, K. Kobayashi, T. Ito, *Inorg. Chim. Acta* **2005**, 358, 2363-2370.
134. G. Zou, T. Ren, *Inorg. Chim. Acta* **2000**, 304, 305-308.
135. M. P. Coles, *Dalton Trans.* **2006**, 985-1001.

136. R. J. H. Clark, C. S. Williams, *Inorg. Chem.* **1965**, *4*, 350-357.
137. J. H. Takemoto, B. Streusand, B. Hutchinson, *Spectrochim. Acta A* **1974**, *30*, 827-834.
138. D. A. Handley, P. B. Hitchcock, T. H. Lee, G. J. Leigh, *Inorg. Chim. Acta* **2001**, *314*, 14-21.
139. X. Wang, *Acta Crystallogr. E* **2009**, *65*, m1659.
140. R. Batcup, V. T. Annibale, D. Song, *Dalton Trans.* **2014**, *43*, 8951-8958.
141. T. Xiao, S. Zhang, G. Kehr, X. Hao, G. Erker, W.-H. Sun, *Organometallics* **2011**, *30*, 3658-3665.
142. E. E. Benson, A. L. Rheingold, C. P. Kubiak, *Inorg. Chem.* **2010**, *49*, 1458-1464.
143. I. Riggio, G. A. van Albada, D. D. Ellis, I. Mutikainen, A. L. Spek, U. Turpeinen, *Polyhedron* **2001**, *20*, 2659-2666.
144. P. Drose, C. G. Hrib, S. Blaurock, F. T. Edelmann, *Acta Crystallogr. E* **2010**, *66*, m1474.
145. N. Harmgarth, D. Grasing, P. Drose, C. G. Hrib, P. G. Jones, V. Lorenz, *Dalton Trans.* **2014**, *43*, 5001-5013.
146. N. Harmgarth, P. Liebing, A. Förster, L. Hilfert, S. Busse, F. T. Edelmann, *Eur. J. Inorg. Chem.* **2017**, *2017*, 4473-4479.
147. N. Harmgarth, P. Liebing, P. Hillebrand, S. Busse, F. T. Edelmann, *Acta Crystallogr. E* **2017**, *73*, 1443-1448.
148. P. Hillebrand, C. G. Hrib, N. Harmgarth, P. G. Jones, V. Lorenz, M. Kühling, *Inorg. Chem. Commun.* **2014**, *46*, 127-129.
149. A. R. Kennedy, R. E. Mulvey, R. B. Rowlings, *J. Am. Chem. Soc.* **1998**, *120*, 7816-7824.
150. R. H. Holm, *Chem. Rev.* **1987**, *87*, 1401-1449.
151. B. Meunier, S. P. de Visser, S. Shaik, *Chem. Rev.* **2004**, *104*, 3947-3980.

152. D. A. Kissounko, M. V. Zabalov, G. P. Brusova, D. A. Lemenovskii, *Russ. Chem. Rev.* **2006**, 75, 351-374.